T.R.
NİĞDE ÖMER HALİSDEMİR UNIVERSITY
GRADUATE SCHOOL OF NATURAL AND APPLIED SCIENCES
DEPARTMENT OF ELECTRICAL AND ELECTRONIC ENGINEERING

DELAY-DEPENDENT STABILITY ANALYSIS OF LOAD FREQUENCY CONTROL SYSTEMS WITH ELECTRIC VEHICLES AND ROBUST CONTROLLER DESIGN

AUSNAIN NAVEED

April 2021

T.R.
NİĞDE ÖMER HALİSDEMİR UNIVERSITY
GRADUATE SCHOOL OF NATURAL AND APPLIED SCIENCES
DEPARTMENT OF ELECTRICAL AND ELECTRONIC ENGINEERING

DELAY-DEPENDENT STABILITY ANALYSIS OF LOAD FREQUENCY CONTROL SYSTEMS WITH ELECTRIC VEHICLES AND ROBUST CONTROLLER DESIGN

AUSNAIN NAVEED

Doctor of Philosophy Thesis

Supervisor

Prof. Dr. Saffet AYASUN

April 2021

Ausnain NAVEED tarafından **Prof. Dr. Saffet AYASUN** danışmanlığında hazırlanan "**Delay-Dependent Stability Analysis of Load Frequency Control Systems with Electric Vehicles and Robust Controller Design**" adlı bu çalışma jürimiz tarafından Niğde Ömer Halisdemir Üniversitesi Fen Bilimleri Enstitüsü **Elektrik Elektronik Mühendisliği Anabilim Dalı**'nda Doktora (İngilizce) tezi olarak kabul edilmiştir.

Başkan : Prof. Dr. Müslüm Cengiz TAPLAMACIOĞLU, Gazi Üniversitesi, Mühendislik Fakültesi, Elektrik Elektronik Mühendisliği Bölümü

Üye : Prof. Dr. Saffet AYASUN, Gazi Üniversitesi, Mühendislik Fakültesi, Elektrik Elektronik Mühendisliği Bölümü

Üye : Prof. Dr., Ersan KABALCI, Nevşehir Hacı Bektaş Veli Üniversitesi, Mühendislik-Mimarlık Fakültesi, Elektrik Elektronik Mühendisliği Bölümü

Üye : Doç. Dr., Emrah ZERDALİ, Niğde Ömer Halisdemir Üniversitesi, Mühendislik Fakültesi, Elektrik Elektronik Mühendisliği Bölümü

Üye : Dr. Öğr Uyesi, Kamil Fatih DILAVER, Niğde Ömer Halisdemir Üniversitesi, Mühendislik Fakültesi, Elektrik Elektronik Mühendisliği Bölümü

ONAY:

Bu tez, Fen Bilimleri Enstitüsü Yönetim Kurulunca belirlenmiş olan yukarıdaki jüri üyeleri tarafından 12/04/2020 tarihinde uygun görülmüş ve Enstitü Yönetim Kurulu'nun …./…./2021 tarih ve …..... sayılı kararıyla kabul edilmiştir.

...../...../2021

Prof. Dr. Murat BARUT

MÜDÜR

THESIS CERTIFICATION

I solemnly declare that the thesis has been written and composed by myself and this work has not been previously submitted as a thesis or dissertation to this or any other institution for a degree. All information presented as part of this thesis is scientific and in accordance with the academic rules. Any help that I have received in preparing this thesis and all the used sources have been acknowledged in the thesis.

Ausnain NAVEED

SUMMARY

DELAY-DEPENDENT STABILITY ANALYSIS OF LOAD FREQUENCY CONTROL SYSTEMS WITH ELECTRIC VEHICLES AND ROBUST CONTROLLER DESIGN

NAVEED, Ausnain
Niğde Ömer Halisdemir University
Graduate School of Natural and Applied Sciences
Department of Electrical and Electronics Engineering

Supervisor :Prof. Dr. Saffet AYASUN

April 2021, 143 pages

Electric Vehicles (EVs) have become a promising tool for frequency regulation Load Frequency Control (LFC) in an interconnected system with one or more independently controlled areas. This is due to increasing environmental concerns, gradual depletion of fossils resources and increased penetration of highly variable renewable energy (RE) power generation. Batteries in EVs can increase or decrease faster power output than conventional generators. This fast response characteristic enhances dynamic performance of LFC system. EVs can be used as generators or loads and hence reduce generation/demand fluctuations, and improve frequency response. The integration of EVs into LFC system requires a communication network to transcieve information to/from EVs aggregators. In this respect, an open distributed communication network is usually used. However, uncertain communication time delays are observed in such a network. These delays can cause instability in power system despite the fact that EVs have fast-response characteristics, which can improve the LFC performance. Hence, it is important to investigate delay-dependent stability of LFC system enhanced by EVs (LFC-EVs) and to develop robust controller design techniques in the presence of uncertainties in system parameters and time delays.

Keywords: Communication time delay, Electric vehicles, Kharitonov Theorem, Load frequency control, Robust PI controller design, Smart grid, Stability delay margin

ÖZET

ELEKTRİKLİ ARAÇ GRUPLARI İÇEREN YÜK FREKANS KONTROL SİSTEMLERİNİN ZAMAN GECİKMESİNE BAĞLI KARARLILIK ANALİZİ VE GÜRBÜZ DENETLEYİCİ TASARIMI

NAVEED, Ausnain
Niğde Ömer Halisdemir Üniversitesi
Fen Bilimleri Enstitüsü
Elektrik Elektronik Mühendisliği Anabilim Dalı

Danışman :Prof. Dr. Saffet AYASUN

Nisan 2021, 143 sayfa

Elektrikli Elektrikli araçlar (EA) frekans regülasyonu için çok bölgeli yük frekans kontrol (YFK) sistemi içeren enterkonnekte güç sistemlerinde umut verici önemli bir üretim birimi haline gelmektedir. Bunun temel nedeni çevre konusundaki artan endişeler, fosil yakıtların hızla tükeniyor olması ve değişken çıkış gücü verebilen yenilenebilir enerji kaynaklarının (YEK) enerji üretiminde yaygın olarak kullanılmasıdır. EA bataryaları klasik jeneratörlere göre hızlı güç çıkışına sahip olduğundan dolayı, YFK sistemlerinin dinamik performansını arttırırlar. Bu süreçte, EA jenerator veya yük grubu olarak frekans düzenlenme servisine katkıda bulunurlar. YFK sistemlerinde EA gruplarının EA toplayıcıları aracılığıyla entegre edilmesi bilgi alış verişi için bir haberleşme ağı gerektirmektedir. EA gruplarının güç şebekesi üzerindeki olumlu dinamik etksine rağmen, haberleşme ağları sistemin dinamik performansını ve kararlılığını olumsuz etkileyen zaman gecikmelerine neden olur. Dolayısıyla, EA gruplarının dahil edildiği YFK sistemlerinin (YFK-EA) gecikmeye bağlı kararlılık analizi incelemek ve sistem parametrleri ile birlikte zaman gecikmelerinde meydana gelen belirsiklerden dolayı gürbüz denetleyici parametre tasarım tekniklerini geliştirmek önemlidir.

Anahtar Sözcükler: Akıllı şebeke, Elektrikli araçlar, Gürbüz PI denetleyici tasarımı, Haberleşme ağı, Kararlılık gecikme payı, Kharitonov Teoremi, Yük frekans kontrolü, Zaman gecikmesi

ACKNOWLEDGEMENT

All praise and thanks to the Almighty for giving me the strength to achieve this goal. First and foremost, I am extremely grateful to my supervisor Prof. Dr. Saffet AYASUN for his invaluable advice, continuous support and patience during my PhD study. His immense knowledge and plentiful experience have encouraged me in all the time of my academic research. I extend my heartfelt and sincere gratitude to Assoc. Prof. Dr. Şahin SÖNMEZ for his technical support and assistance. I would also like to thank members of my PhD Advisory Committee and/or PhD Thesis Defense Jury, Prof. Müslüm Cengiz TAPLAMACIOĞLU, Prof. Dr. Ersan KABALCI, Assoc. Prof. Dr. Emrah ZERDALİ and Assist. Prof. Dr. Kamil Fatih DILAVER for their guidance, insightful comments, and direction.

My special appreciation goes to Scientific and Technological Research Council of Turkey (TÜBİTAK) for providing funds for this study under the Project No. 118E744. I would like to express my sincere gratitude and appreciation to the Council of Higher Education of Turkey (YÖK) for providing fellowship during my doctoral study and allowing me to accomplish my dream of obtaining PhD degree. I am grateful to the University of Azad Jammu & Kashmir (UAJ&K) for granting me a paid leave for a period of five years to complete my PhD degree.

Finally, I would like to express my gratitude to my loving family, particularly my dear parents and my two beautiful children, Shahveer and Shanzay for always standing by my side. Without their tremendous understanding and encouragement in the past few years, it would be impossible for me to complete my study. I am deeply indebted to my wife for her dedicated and tireless moral support all along my study. Without her presence, I would have been lost in the abyss of loneliness.

TABLE OF CONTENTS

LIST OF TABLES

LIST OF FIGURES

SYMBOLS AND ABBREVIATIONS

Symbols	Description
ΔP_L	: Load disturbance
Δf	: Frequency deviation
ΔX_g	: Change in valve position
ΔP_m	: Mechanical power output
ΔP_g	: Generator power output
ΔP_{EV}	: EVs aggregator power output
$x(t)$	: State variables
$u(t)$	: Input signal
$y(t)$	: Output signal
M_i	: Inertia constant of generator in i^{th} area
D_i	: Damping coefficient of generator in i^{th} area
T_{gi}	: Time constant of governor in i^{th} area
T_{ci}	: Time constant of turbine in i^{th} area
T_{ri}	: Time constant of reheat in i^{th} area
F_{pi}	: Fraction of the total turbine power in i^{th} area
β_i	: Frequency bias factor in i^{th} area
R_i	: Speed Regulation in i^{th} area
ACE	: Area Control Error
T_{ij}	: Tie-line synchronizing coefficient between i^{th} and j^{th} control areas
τ_i	: Time delay value in i^{th} area
K_{Pi}	: Proportional controller gain in i^{th} area
K_{Ii}	: Integral controller gain in i^{th} area
ω_c	: Root crossing the imaginary axis

τ^*	: Maximum allowable delay / stability delay margin
$K_{EV,i}$	: Battery coefficient of i^{th} EV
$T_{EV,i}$	: Time constant of battery of i^{th} EV

Abbreviations	**Descriptions**
LFC	: Load Frequency Control
NLDC	: National Load Dispatch Centre
ENTSO-E	: European Network of Transmission System Operators for Electricity
EPDK	: Enerji Piyasası Düzenleme Kurumu (Energy Market Regulatory Authority of Turkey)
TSO	: Transmission System Operator
ISO	: Independent System Operator
TEİAŞ	: Türkiye Elektrik İletim Anonim Şirketi (Turkish Electricity Transmission Corporation)
EVs	: Electric Vehicles
SCADA	: Supervisory Control And Data Acquisition
AGC	: Automatic Generation Control
PMU	: Phasor Measurement Units
WAMS	: Wide Area Monitoring System
CPU	: Central Processing Unit
RAM	: Random Access Memory
PI	: Proportional-Integral
RE	: Renewable Energy
LFC-EVs	: Load Frequency Control system with Electric Vehicles
QPmR	: Quasi Polynomial Mapping based Root finder
LMI	: Linear Matrix Inequalities
PID	: Proportional-Integral-Derivative
RRB	: Real Root Boundary
CRB	: Complex Root Boundary
RT	: Root Tendency

CHAPTER I

INTRODUCTION

The Load Frequency Control (LFC) systems have been widely used in the control of electrical power systems for many years to provide the balance between load demand and generation in each control region and thus to eliminate changes in system frequency (Kundur, 1994; Saadat, 1999). The stability and reliability of electrical power systems may get worse due to unbalance or sudden power changes occurring between power generation and load demand during the daily operation of the electrical grid. In recent years, the frequency control problem of the interconnected network has been seen as an important issue in terms of the stability of the power systems and the studies in this area are continuously increasing. The imbalance between the power generated and load demand in the interconnected network directly affects the frequency of the electrical network and causes a rapid deviation of the nominal frequency value that should be within a certain range for the stable and reliable operation of the system. For this purpose, LFC systems system in an interconnected power system consisting of one or more areas are responsible for maintaining power-sharing at an already planned level between the areas and thereby controlling the frequency of the power grid.

In general, the balance between the generated power and the load demanded by the user requires a three-level control process known as primary, secondary and tertiary frequency control. When load demand rises, the synchronous generator's rotor slows down resulting in a drop in grid's frequency. Nonetheless, the governor comes into action and tries to retrieve the frequency to the normal value. Such a frequency control by the governor is known as "primary frequency control". Governor may control the frequency by providing more water or steam to the turbine, but, at times this alone is not sufficient and secondary frequency control is needed. In "secondary frequency control" the loading on various plants of different areas in the interconnected network is changed as directed by the National Load Dispatch Centre (NLDC). Tertiary frequency control is a standby manual service to ensure the continuity of the secondary frequency control. In case the secondary control is inadequate, the system operator ensures the power balance by switching on the power reserves.

The frequency stability requirements that are determined by European Network of Transmission System Operators for Electricity (ENTSO-E, 2009) and the Energy Market Regulatory Authority of Turkey (EPDK, 2020) must be fulfilled because the electricity network of Turkey is connected to the Continental Europe synchronous area since 2010. Both the standards propose utilization of a hierarchical control structure in the form of primary, secondary and tertiary control levels shown in Figure 1.1.

With the help of a governor, the primary frequency control reserve is locally employed to provide an additional capacity to eliminate the imbalance between supply and demand in the grid within a few seconds. Since, the purpose of primary control reserves is to quickly create a balance between the demand and generation in the power system, therefore, primary frequency control tries to keeps the frequency at its nominal value. Primary control should be used in the system until the power deviation is fully zero by the secondary or tertiary control reserves.

The secondary frequency control is activated by releasing the primary reserves. Secondary control reserves restore the frequency of the system to the acceptable range and set active power exchange between control areas to reference value. The secondary frequency control is activated by the Transmission System Operator (TSO) by changing the active power set points of the generating units in each relevant control area (Díaz-González *et al.*, 2014). Different secondary control methods are widely used at present in the world. Therefore, each country including Turkey that is connected to European interconnected network has its own Independent System Operator (ISO) (Aziz *et al.*, 2018).

The purpose of tertiary frequency control is to bring the frequency to its nominal value if the secondary control is not sufficient. Also, this level is used for economic power dispatch taking into account system constraints such as current limits of transmission lines. The tertiary control reserves are activated manually and centrally by the ISO (Díaz-González *et al.*, 2014). The frequency criteria and special cases given in EPDK (2020) are as follows:

- The nominal frequency of the system (50 Hz) is controlled by Turkish Electricity Transmission Corporation (TEİAŞ) in the range of 49.8 - 50.2 Hz.

- Considering the unstable operating conditions of the system frequency of 52.5 Hz and 47.5 Hz, the frequency ranges provided by interconnected network of Turkey are given as following:

1) Targeted operating conditions: **49.8 Hz ≤ f ≤50.2 Hz**
2) Acceptable operating conditions: **49.5 Hz ≤ f < 49.8 Hz** and **50.2 Hz < f ≤ 50.5 Hz**
3) Critical operating conditions: **47.5 Hz ≤ f < 49.5 Hz** and **50.5 Hz < f ≤ 52.5 Hz**
4) Unstable operating conditions: **f < 47.5 Hz** and **52.5 Hz < f**

It can be seen from the abovementioned standards that the distributed generation units must be connected to the system at an operating frequency within 49.5 Hz and 50.5 Hz. However, if these generation units are outside this frequency range, they must be disconnected from the network. It should be mentioned here that the operating frequency range is wider for traditional generation units and should be between 47.5 Hz and 52.5 Hz (Hartmann *et al.*, 2019).

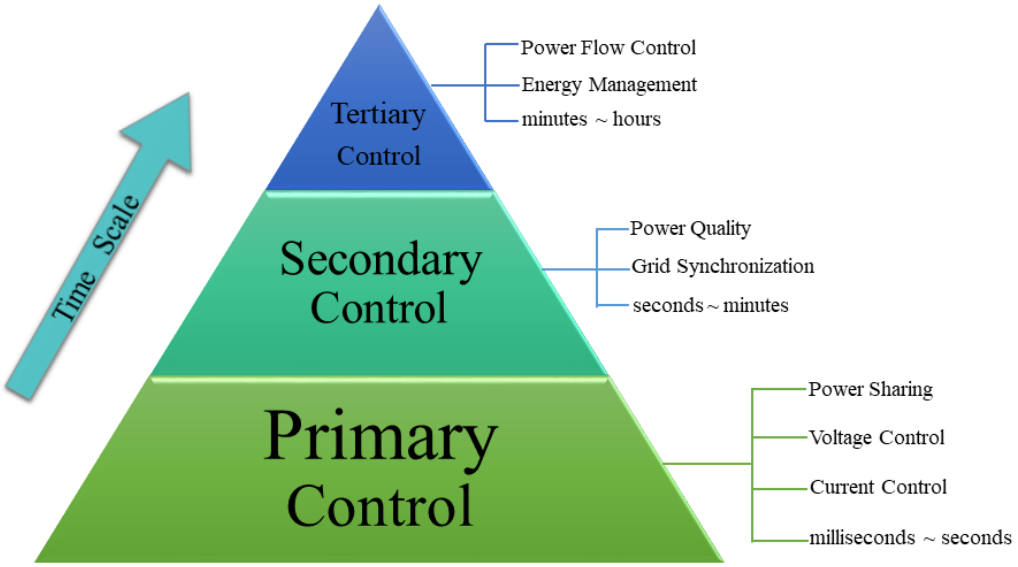

Figure 1.1. Hierarchal structure of load frequency control

The use of alternative energy sources that can provide energy to the system in the long term have gained attention because of the rapid decrease in the reserves of non-renewable fossil resources and the emerging energy crises. In order to reduce the harmful effects of the conventional electricity generation plants on the environment and to contribute to the

sustainable economy and make the social life more reliable, renewable energy based power plants have been intensively incorporated into interconnected power systems; as they utilize energy sources such as wind, solar and geothermal energy (Datta *et al.*, 2011; Delille *et al.*, 2012; Hund *et al.*, 2010; Wang *et al.*, 2011; Yang *et al.*, 2008).

Although, renewable power plants have the characteristics of responding rapidly to the changes in power demand in the interconnected system, the power fluctuations in wind power and solar energy can negatively affect the dynamic behavior and operational performance of the system resulting in large load changes and short circuit faults (Ahn *et al.*, 2011; Falahati *et al.*, 2016; Liu *et al.*, 2016; Luo *et al.*, 2014; Masuta and Yokoyama, 2012; Pillai and Bak-Jensen, 2011; Sekyung *et al.*, 2010). Since, the system frequency control at the desired level has become more challenging, the need for ancillary services to improve frequency stability in modern power systems has increased. Another disadvantage of renewable power plants is the use of converter based devices like photovoltaic or wind inverters which reduce the total mechanical inertial of the system (Li *et al.*, 2015).

The collapse of the interconnected system across Turkey on March 31st, 2015 and recently in Pakistan on January 9th, 2021 has made it clear that the conventional load frequency control or automatic generation control operations performed only by load shedding or controlling the power generation are inadequate. For this reason, there is a need for new tools in load frequency control systems that will ensure system integration and keep system frequency at desired values.

In order to avoid these shortcomings and increase the stability of the power system, battery systems in Electric Vehicles (EVs) can be used in smart grids' LFC systems both as a load group and a generator. Moreover, EVs are seen as an important solution because of the mobile energy storage capacity of their batteries and also in terms of reducing the cost of electric power networks as a replacement for the high cost energy storage devices (Luo *et al.*, 2014; Masuta and Yokoyama, 2012; Mu *et al.*, 2013; Shimizu *et al.*, 2010). Thus, EVs in power systems have a significant impact on the operation and planning of large-scale interconnected power systems network (Green *et al.*, 2011; Li and Zhang, 2012; Richardson *et al.*, 2012). If there is any change in power demand of the electric grid, the frequency change signal is sent to the EVs aggregator by the LFC system. The

battery banks of the electric vehicles connected to the grid will then participate in the frequency regulation service. EVs will perform the charging process if they are acting as a load or they will perform discharging process if they are acting as a generator. This is ensured by the fact that battery banks will serve as generating unit according to the real-time price information sent to the EVs' users at peak times when the power consumption is high and whenever the power demand decreases, battery banks will carry out the charging process by serving as a load. Since, charging or discharging in EVs is an electrical and chemical process, they minimize the constant changes in the power states of large power plants and assure the power balance in lesser time (Jia *et al.*, 2018; Ko and Sung, 2017a; Liu *et al.*, 2016). In addition, EVs can provide additional financial benefits to their owners being a part of Power Balancing Market.

A mechanism is required for aggregating and regulating substantial number of EVs from different makers to practically participate in frequency regulation market. Therefore, an entity known EVs Aggregator is used to fulfill the regulation criteria. In many electricity markets of the world, different energy sources need to have a minimum power generation capacity that determines their ability to participate in the power balancing market. For example, the minimum criteria for an energy source to participate in power balancing market by North-East ISO in the United States is at least 1 MW. This means that if an EV supplies 2 kW power, the EVs aggregator has to put 500 EVs together to join the Power Balancing Market. In Turkey, balancing units that can independently receive or deliver at least 10 MW within 15 minutes can participate in Balancing Power Market. In addition to the minimum capacity requirement, EVs Aggregators must have an Automatic Generation Control (AGC) system to increase or decrease the output power of EVs in real time.

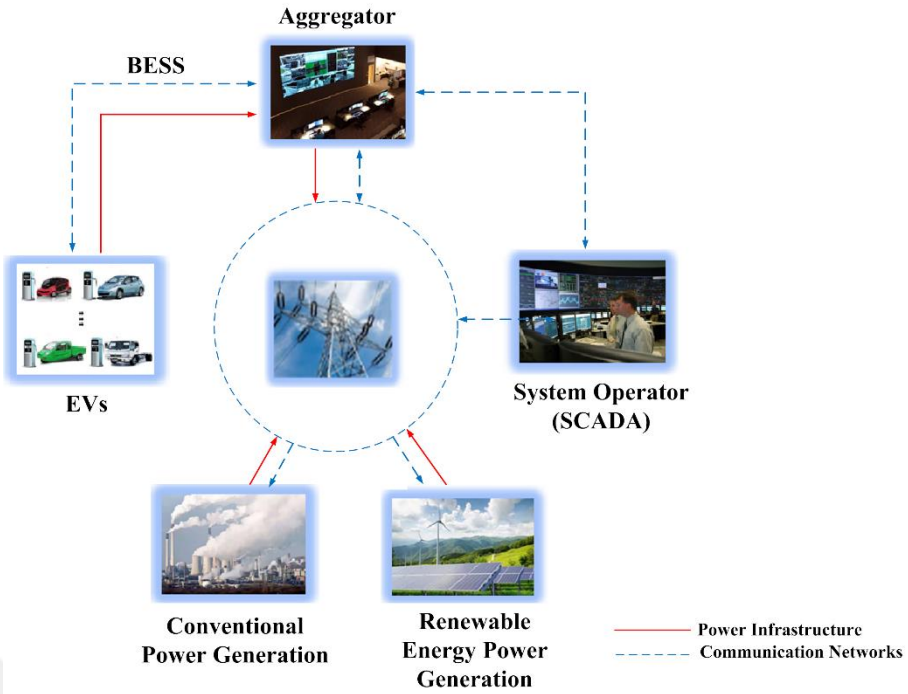

Figure 1.2. Functioning of EVs through Aggregator in Smart Grid

Figure 1.2 shows the electrical power system including conventional power plants, Renewable Energy (RE) sources, EVs aggregator and communication network. The conventional power plants contribute to frequency control with primary and secondary frequency control. In primary frequency control, all plants with speed regulators respond to changes in frequency by increasing or decreasing their generation automatically. The plants that are included in the secondary frequency control contribute to the frequency to reach the nominal value by making changes in their generation according to the frequency regulation signal coming from the system operator.

Similarly, based on the control signal received from the control center, the EVs aggregator controls the output power by decreasing or increasing the power of EVs group. In this interconnected power system, Supervisory Control And Data Acquisition (SCADA) is responsible for two main tasks: the first one is to gather the information, such as predicted load, number of EVs participating, battery status of EVs etc., and the other task is to make a schedule for the EVs to consume/generate power from/to the electric grid.

Since, EVs require a communication network to communicate with the AGC, wide area communication networks are preferred because of the large number of control loops and the complex communication devices. Such a communication network is represented by

dashed lines in Figure 1.2. Wide area communication networks play an important role in the interconnected power systems by linking the smaller area networks operating at different points and the central control unit. Since, the control center is at point far from switchgears, power generation units and users, real-time electrical measurements taken from the interconnected network must be transmitted to the control center or control commands from the control center must be transmitted to various network systems to control electrical devices. In this way, remote protection, control and monitoring tasks in power systems are performed using this information. In order to perform status estimation, protection, monitoring and control operations in the interconnected system, the real-time power data, current and voltage phasor information must be transmitted to the control center by means of wide area network system using Phasor Measurement Units (PMUs) in switchgears and transmission systems (Gungor *et al.*, 2013; Wang *et al.*, 2011; Yan *et al.*, 2013).

In the electric power system, communication links used by Wide Area Monitoring System (WAMS) to transmit data from one point to another can be both wired and wireless networks (Naduvathuparambil *et al.*, 2002). Generally, wired communication networks allocated for the measurement controls and signals transmission are created separately from electrical power lines. Since, these dedicated networks are separate from the power line, they require extra cost of investment for installation. However, it provides higher communication capacity and lesser communication delays. Another type of communication networks is wireless network. These networks communicate wirelessly between devices in the system and do not require any cost of cable installation. However, these networks cannot be used for long distance communications and the low data transmission speed is also a significant shortcoming of these networks (Wang *et al.*, 2011).

In order to maintain the stable operation of the system, the communication infrastructure should ensure security of the transmitted and received messages between the communication devices in the electricity grid. For example, excessive delay in response to control commands can negatively affect the reliability of the system like; a physical fault in the communication lines, noise in the communication network, cyber-attack or physical intervention from outside may badly effect the messages to be transmitted in a timely and successful manner (Wang *et al.*, 2011; Yan *et al.*, 2013). In electrical power

systems, inevitable communication time delays are observed while sending the measured electrical data to the central control unit using the communication networks. In the same way, time delays are observed when the control signals are sent to the power plants and EVs aggregators participating in the frequency control from the central control unit. The magnitude of these time delays varies depending on; the nature of the communication network used, the packet size of the information or control signal to be transmitted, the communication protocol used and the traffic load on the communication network (Naduvathuparambil *et al.*, 2002).

Transfer of energy to/from the LFC is bidirectional when EVs are integrated into the system. Therefore, it is necessary to evaluate the control signals transmitted from the central controller to the EVs and also to take into account the time delays experienced during the participation of the battery groups in the LFC system. Speed of Central Processing Unit (CPU), the size of Random Access Memory (RAM) on EV module side, signal intensity in communication network, activation of necessary algorithms in charging/discharge processes and loading of data are some of the important factors that may cause communication delay in the system (Fan *et al.*, 2016; Jia *et al.*, 2018; Zhou *et al.*, 2016).

Although, the controllable loads within the scope of EVs have the ability to react quickly, but communication time delays varying within a certain range may cause instability in electrical power system. For this reason, it is imperative that delays occurring in the system because of the information signals transmitted should be taken into account for the modeling of power systems. Likewise, the possible negative effects of these delays on the system dynamics and frequency control should be analyzed in order to ensure optimal operation of electrical power systems and to increase their stability and improve their dynamic performance. In particular, it is important to know the maximum communication time delay value for given system parameters and Proportional-Integral (PI) controller gains that the system can tolerate without losing its stability.

Furthermore, electrical power systems can experience many uncertainties because of system modelling, changes in load and system parameters. Especially, power generation, transmission and distribution activities carried out by different companies together with the restructuring of the electricity energy market and lack of coordination in terms of

planning, control and expansion of the system among these companies can further increase these uncertainties (Bervani, 2014). Another reason for the uncertainty is the changes in working conditions of the electric power system throughout the day. In power system with plugged in EVs groups, the transmission of measurement information and control signals over the open and distributed communication network causes communication time delays that vary within a certain range. Since, PI controller gains are adjustable parameters, a controller can be designed considering the uncertainties of the system parameters and time delay to achieve the desired dynamic performance and frequency control for the different operating conditions and load change scenarios of the power system. However, if the uncertainties in the system parameters and time delay are taken into account, it is necessary to determine the robust PI controller gain values that will guarantee the stability of the power system.

1.1 Aims and Objectives

EVs integrated to the LFC system have become a promising tool for frequency regulation in an interconnected system comprising of one or more independently controlled areas. This is attributable to the waxed penetration of RE based power generation that is highly variable. Also, gradual depletion of fossils resources and other environmental concerns have become the reasons behind finding a way out for stable operation of a power system. Moreover, the increase or decrease in the power output of the batteries in EVs is faster than conventional generators. Owing to this fast response characteristic of EVs, the dynamic performance of LFC system can be enhanced. EVs can be used as loads or generators and hence improve frequency response by reducing fluctuations in demand/generation. On the other hand, uncertain time delays can be instigated during the communication between the EVs aggregators and central controller. These delays can cause instability of power system against an expectation that EVs having fast-response characteristics can improve the LFC performance. For that reason, it is essential to examine delay-dependent stability of LFC-EVs system and to develop robust controller design techniques in the presence of uncertainties in system parameters and time delays. This work aims to investigate the delay-dependent stability of single and two-area LFC-EVs systems and to design robust PI controller. To achieve this goal, the following three main studies will be conducted:

1) Computation of stability delay margins for given system parameters and PI controller gains by using two different frequency-domain exact methods (Direct and Rekasius Substitution Methods) and investigation of the effect of PI controller gains on stability delay margins
2) Computation of robust PI controller gains that assure stability of LFC system integrated with EVs in presence of parametric uncertainties and time delays. Such robust PI controller gains are obtained by using a graphical method known as Stability Boundary Locus and Complex Kharitonov's Theorem
3) Verification of theoretical delay margins and robust stability regions by simulation studies and Quasi Polynomial Mapping based Root finder (QPmR) algorithm

The integration of EVs into the classic LFC system and stability analysis are the unique aspects of this work. With the help of stability delay margin results, it will be possible to tune PI controller gains properly and to design communication network such that observed time delays will be less than stability delay margin. Robust stability regions enable us to design robust PI controller for stable operation while taking into account uncertainties in system parameters and time delays.

CHAPTER II

LITERATURE REVIEW

The LFC systems aim to regulate the frequency, to share the load between the generators and to keep the scheduled tie-line power exchange in an interconnected power system with independently controlled multiple areas (Kundur, 1994). Due to the increasing environmental concerns, gradual depletion of fossils resources and increased penetration of highly variable RE power generation, the frequency control and stability are becoming more and more important issue (Bevrani *et al.*, 2010). EVs with a Vehicle-to-Grid technology have become a promising tool that can mitigate the intermittent effects of the RE sources and regulate the system frequency. for load frequency regulation (Yang *et al.*, 2019). This is due to the fact that batteries in EVs can quickly enhance or reduce power output as compared with the conventional generators. This quick response characteristic increases the dynamic performance of LFC systems. EVs can be operated as loads or generators and therefore, they reduce generation/demand fluctuations and improve frequency response (Guille and Gross, 2009; Kempton and Letendre, 1997; Mu *et al.*, 2013; Pillai and Bak-Jensen, 2011). In order to practical participate in frequency regulation market, EVs require an entity known as aggregator. The aggregator aggregates and controls large number of EVs to fulfill the frequency regulation criteria (Bessa and Matos, 2010; Bessa *et al.*, 2014; Carreiroa *et al.*, 2017; Han *et al.*, 2010). The main function of EVs aggregator is to send and receive information regarding the charging status of EVs and their available electrical power and energy capacities to LFC center and to rearrange the control signals dispersing EVs in order to adjust their power output using an AGC.

For the AGC system, EVs aggregator require a dedicated or an open communication network to transfer control commands to EVs. Owing to its low cost, the latter is preferred. However, such a communication network is prone to time delays (Ko and Sung, 2017b; Mak and Holland, 2002; Quinn *et al.*, 2010). These delays can have adverse effects on the dynamics and stability of the LFC system despite the fact that EVs are capable of enhancing the dynamic performance of the system (Jia *et al.*, 2018; Khalil and Peng, 2018; Ko and Sung, 2017a; Naveed *et al.*, 2020). The response time to the regulation command by ISO is imperative in frequency regulation service. Normally, ISO

transmits the commands every 2-6 seconds to the aggregator (Yao *et al.*, 2016). In order to respond to regulation signals, ISOs usually have their own specific protocols for allowing maximum communication delay like; ISO of California allows a communication time delay limit of 4 seconds between EVs and the aggregator (Bilh *et al.*, 2017). Therefore, it is important to investigate the delay-dependent stability of LFC system enhanced by EVs which is denoted as LFC-EVs and to compute the stability delay margins defined as the allowable upper bound on the communication time delay. Besides, the determination of all stabilizing PI controller parameters is required for guaranteeing the stability of LFC-EVs in the presence of communication delay.

In the existing literature, numerous approaches are available to determine stability delay margins of time-delayed dynamical systems. A large share of those studies intended to compute the stability delay margin for a given set of PI controller gains where the LFC system without EVs is marginally stable. These might be categorized into two core groups: i) Direct methods based on frequency-domain computation and ii) Indirect methods based on time-domain computation. The former group intends to compute complex roots of the characteristic polynomial on the imaginary axis. This type of methods includes Schur-Cohn method (Chen *et al.*, 1995), exclusion of the transcendental terms of characteristic polynomial (Walton and Marshall, 1987), Matrix pencil method (Chen *et al.*, 1995; Fu *et al.*, 2006; Gu *et al.*, 2003; Su, 1995), Kronecker product and basic conversion method (Chen *et al.*,1995; Louisell, 2001), Rekasius substitution (Fazelinia, 2007; Naveed *et al.*, 2019; Olgaç and Sipahi, 2002; Olgaç and Sipahi, 2004; Rekasius, 1980; Sipahi and Olgaç, 2005; Sönmez *et al.*, 2014; Yuan *et al.*, 2020), delay space re-scaling approach (Dong *et al.*, 2017), the argument principle or contour integral method (Xu *et al.*, 2016) and frequency sweeping test (Chen and Latchman, 1995; Gu *et al.*, 2017). The direct methods based on frequency domain computation are capable of exact calculation of delay margins with great accuracy. But, the drawback of such methods is that these can only be utilized for the determination of time-constant delays. A thorough study on the approaches for delay margin estimation of continuous linear time-invariant systems experiencing constant communication delays is conferred in (Pekař and Gao, 2018). Among these methods, the direct method based on the removal of transcendental terms (Walton and Marshall, 1987) has been effectively used by computing single and two area LFC systems delay margins (Sönmez *et al.*, 2016). Likewise, the same method is used for computing delay margins of micro-grid frequency

control systems in (Gündüz *et al.*, 2017). Delay margins for a single-area LFC system are computed by Rekasius substitution in (Sönmez *et al.*, 2014). The delay space re-scaling method has been proposed for estimating the stability margin of hybrid energy storage system having hierarchical control in DC micro-grids and undergoing more than one delay (Dong *et al.*, 2017). Finally, the frequency sweeping test is employed to compute the delay margin of single-area LFC system in (Khalil and Peng, 2018).

The other group of methods uses Linear Matrix Inequalities (LMIs) alongside Lyapunov stability theory for stability studies. These methods have been used in calculation of delay margin for LFC systems (Jiang *et al.*, 2012; Jin *et al.*, 2019; Zhang *et al.*, 2013) and micro-grids not including EVs aggregator (Thangaiah and Parthasarathy, 2016). Numerous inequalities have been proposed in recent years such as; free-matrix based inequality (Zeng *et al.*, 2019) and Bessel-Legendre inequality (Seuret and Gouaisbaut, 2015). Indirect methods can be employed for time-varying as well as time-constant delay scenarios. However, this group of methods can only determine the sufficient conditions for the system stability and there exist various studies focusing on the reduction of the conservativeness (Liu *et al.*, 2019; Zeng *et al.*, 2020; Zhang *et al.*, 2015; Zhang *et al.*, 2020).

Even though the EVs are becoming widely used technologies in the future smart power system grid, the reported research work that studies the impact of both the communication delay and the integration of EVs on the frequency regulation is very limited. For example, in (Ko and Sung, 2017a), a direct method based on Lyapunov stability theory with LMIs has been implemented to calculate stability margins in a single-area LFC-EVs. In (Khalil and Peng, 2018), a combination of the frequency sweeping test and the binary iteration algorithm is used to compute the delay margins of single-area LFC-EVs system for different load sharing scenarios between the conventional generator and EVs aggregator. In (Jia *et al.*, 2018), the particle swarm optimization and the LMIs techniques have been utilized to design a robust PI controller so as to handle the inertia uncertainty and the communication delay for the LFC system with multiple EVs aggregators. Last but not the least, for the LFC system in micro-grid dominated by EVs, stability delay margin computation using the time-domain method has been reported in (Khalil *et al.*, 2017).

The stability delay margins can be efficiently computed for any chosen PI controller gains of LFC-EVs system by both frequency and time-domain methods. However, the actual limitation of these methods is that stability needs to be determined every time by computing the delay margin when the controller gains are re-tuned or changed. This causes arduous stability checks. Therefore, computation of all possible controller gains for a given finite time delay is required to ensure the stable operation of LFC-EVs systems.

Since, delay-dependent stability analysis and controller design to assure stability of the LFC-EVs system are the unique aspects of this work, it is necessary to present an efficient analytical method for identifying stability regions that comprise of all stabilizing PI controller gains. Söylemez *et al.* (2003) proposed a technique that relies on the stability boundary locus which can be obtained by equating imaginary and real parts of the characteristic equation of the LFC-EVs system to zero. The method has been effectively applied to single and two-area LFC system containing single delay without having EVs in (Sönmez and Ayasun, 2016; Sönmez and Ayasun, 2018), also to the traditional PI controller design (Hamamcı and Tan, 2006), the fractional-order proportional-derivative controller (Hamamcı and Köksal, 2010), fractional-order controllers (Alomoush, 2010), PI controller synthesis of large wind turbine systems (Wang *et al.*, 2011) and isolated microgrid integrated with EVs (Khalil *et al.*, 2017). With the help of stability regions, one can easily adjust The controller can be easily tuned using the stability regions that comprise of PI controller gains which assure the stability of LFC-EVs system and reduce the adverse effect of time delays on frequency regulation. Time-domain simulations (Simulink, 2000) along with QPmR algorithm presented in (Vyhlídal and Zítek, 2009) can be used to validate the accuracy of the boundaries of stability regions and the stability delay margins obtained by the proposed methods. This root finder algorithm is a mathematical approach for calculating the spectrum of zeros of quasi-polynomials along the complex plane.

Today's rapidly modernizing world is continuously posing a great demand for electric power. It is necessary to have an efficient LFC system that has a capability of disturbance rejection even working under uncertain conditions (Sondhi & Hote, 2016). Changes in power system parameters include many parametric uncertainties due to various reasons. It is obvious that the mathematical representation of the system dynamics may suffer from

uncertainties due to modelling errors, nonlinearities, manufacturing tolerances and operating conditions (Tan *et al.*, 2009). Moreover, lack of coordination in terms of the functioning of power generation, transmission and distribution by different companies and the planning, control and expansion of the system among these firms could also be a reason for the increase in these uncertainties (Bervani, 2014). Therefore, the parametric robust control is very important for the stability analysis and design of real control systems.

In classic control systems, PI or Proportinal-Integral-Derivative (PID) controllers are widely used in frequency control because of their robust operation and practical design. There are many studies in the literature that provide robust PI design methods for LFC systems encompassing the uncertainties in system parameters because the PI controllers designed according to nominal system parameters are not sufficient to provide the desired system frequency performance. Yazdizadeh *et al.* (2012) proposed a robust controller design method using the eigenvalues of the system matrix. Golshannavaz *et al.* (2018) presented a two-stage robust-intelligent controller design for frequency regulation based on Kharitonov theorem and fuzzy logic. Tan *et al.* (2012) proposed an integrated model control method with two degrees of freedom, which allows optimum adjustment of PI controller gains. Khodabakhshian *et al.* (2012) performed robust PI design using sequential quadratic programming. Toulabi *et al.* (2014) presented a graphical method using Kharitonov Theorem (Kharitonov, 1978a, 1978b) for calculating the maximum uncertainty limit of the system parameters that would guarantee the stability of multi area LFC system. In a similar study, Saxena and Hote (2016) determined a set of controller gains in the PI controller parametric space ensuring the robust operation of the system despite the uncertainties in the system parameters. Though, none of the aforementioned studies considered the time delays because of EVs aggregator and communication network in robust PI controller design despite the fact that they are important frequency regulation tools of today's smart grids. However, robust PI design techniques have been presented in some recent studies for LFC systems addressing these problems. Krishnan *et al.* (2017) conducted robust stability analysis for a two area LFC system with communication time delay using Lyapunov-Krasovskii functional approach. Jia *et al.* (2018) proposed a coordinated control method between EVs groups and power plants for LFC system by taking into account the communication time delay caused by the EVs groups.

The robust stability analysis problem for a system having parametric uncertainties is to determine whether the characteristic polynomial of the system remains stable or not when the coefficients of the system are subjected to some perturbations. A significant achievement in the field of robust stability of systems with parametric uncertainty is the Kharitonov's theorem (Kharitonov, 1978a; Kharitonov, 1978b). According to the theorem, an interval polynomial family having an infinite number of members, is Hurwitz stable if and only if a finite small subset of vertex polynomials known as the Kharitonov polynomials of the family are Hurwitz stable. The method can be used to analyze the stability of a system whose real or complex coefficients vary within a certain range, known as interval polynomials in the literature (Rigatos and Siano, 2011; Xu *et al.*, 1993). The theorem states that four vertex polynomials are obtained from an interval polynomial whose real coefficients vary within a certain range by making use of the lower and upper bounds of the given parametric intervals (Bhattacharyya *et al.*, 1995; Lamba *et al.*, 2019; Nazari *et al.*, 2018; Tan *et al.*, 2009). However, the complex coefficients interval polynomial whose coefficients vary within a specific range requires eight vertex polynomials to check the stability of the system (Bhattacharyya *et al.*, 1995; Ho *et al.*, 1998; Wang, 2011). The coefficients of the vertex polynomial have linear dependencies on the uncertain parameters and the adjustable PI controller gains. These parametric uncertainties are not adjustable but independently vary within known intervals. However, the PI controller can be designed according to the robustness considerations. Since, uncertain parameters, communication time delay and adjustable PI controller gains form the coefficients of the vertex polynomials, therefore, the aim of this technique is to identify all the PI controller gains that will stabilize all the vertex polynomials at the same time (Kumar & Shreesha, 2016; Liang *et al.*, 2013; Wang, 2011). Stability Boundary Locus method can be used to achieve this goal (Söylemez *et al.*, 2003; Tan *et al.*, 2006). The stability regions in the parameter space of all stabilizing PI controller gains for each vertex polynomial can be calculated with the help of Stability Boundary Locus method and the intersection of these regions will represent the robust stability region of the LFC system integrated with EVs. This robust stability region yields all the controller gains for the stable operation of the system, thereby, significantly contributing in the controller design specification.

CHAPTER III

TIME DELAYED LFC SYSTEM INTEGRATED WITH EVs AGGREGATORS

The dynamics of LFC systems experiencing any communication delays are usually described by nonlinear differential or/and differential-algebraic equations (Ayasun, 2009; Jia *et al.*, 2008). Those nonlinear equations are linearized around an equilibrium point when the LFC system is subjected to a small disturbance. This linearization of those nonlinear equations then yields a linear state-space equation model, which helps to analyze the small-signal or steady-state stability of the system (Jiang *et al.*, 2012; Kundur, 1994; Yu and Tomsovic, 2004). As explained in the previous sections, EVs are integrated into the LFC system due to their fast response characteristic that helps in improving the dynamic performance of the LFC system. However, this integration of EVs into the LFC requires a communication network for the frequency regulation services. Usually, preference is given to open communication networks because of their low cost but those are susceptible to communication delays.

A fleet of EVs is required to be plugged into the power grid so that they can be utilized in frequency regulation. The control center of these EVs is the aggregator that manages the charging and discharging of each EV integrated into the grid. The dynamic model of the i^{th} EV in the EVs aggregator can be presented by the following first-order transfer function (Fan *et al.*, 2016; Ko and Sung, 2017a; Zhou *et al.*, 2020):

$$G_{EV,i}(s) = \frac{K_{EV,i}}{1 + sT_{EV,i}} \tag{3.1}$$

In general, a transfer function of $e^{-s\tau_i}$ is used to lump and model the communication delay from the EVs aggregator to the EVs and the scheduling delay in the EVs aggregator. It should be mentioned here that τ_i is the delay time taken by the EVs aggregator of i^{th} area to send the control signals. The time constants $T_{EV,i}$ and the delay τ_i for all EVs are assumed to be equal in an average sense. With this assumption, an aggregated model of several EVs comprising of single delay function along with EV dynamics is obtained. The use of an aggregated model of EVs fleet appears to be reasonable as a cluster of

numerous EVs as well as conventional generation sources are controlled together for changing their power injection to follow the load disturbances (Ko and Sung, 2017a).

It should be mentioned here that multiple time-varying or constant delays can occur in multi-area LFC systems. These delays can arise during: 1) transmitting *ACE* signals from the central controller to the generation units and 2) transmitting the telemetry signals to the controller (Bhowmik *et al.*, 2004; Sönmez *et al.*, 2016; Yu and Tomsovic, 2004). Each delay case can be analyzed in a similar fashion if it is assumed that the controller waits until all telemetered values are received. Consequently, all the delays can be aggregated as single time-varying or constant delay (Sönmez *et al.*, 2016).

However, most of the recent studies involving the integration of EVs into the LFC system considered only the communication delays from EVs aggregators to EVs only because the delays observed in the transmission of regulation signal from ISO to the conventional generators are less significant (Khalil and Peng, 2018; Ko and Sung, 2017a; Ko and Sung, 2017b; Naveed *et al.*,2019; Zhou *et al.*, 2020). The primary reason for this assumption is that ISOs usually deploy the communication link between conventional generators and ISOs, independently. Also, communication delay requirements of the link are ensured by the ISOs themselves. The other reason is the utilization of open communication links between EVs aggregator and EVs. Depending on the geographical distribution of EVs, these links can be wireless mobile communication networks, internet, WiFi, power line communication (PLC) or ZigBee. Such communication networks cause relatively more significant delays than those observed between power plants and ISOs. Moreover, there exist scheduling delays since EVs aggregators have to control both charging and regulation of EVs fleet (Ko and Sung, 2017b). Additionally, Ko and Sung (2017a) showed that the participation of fast-response resources such as EVs with communication delays in frequency regulation service severely affects the stability and frequency regulation of LFC systems when compared with conventional generators.

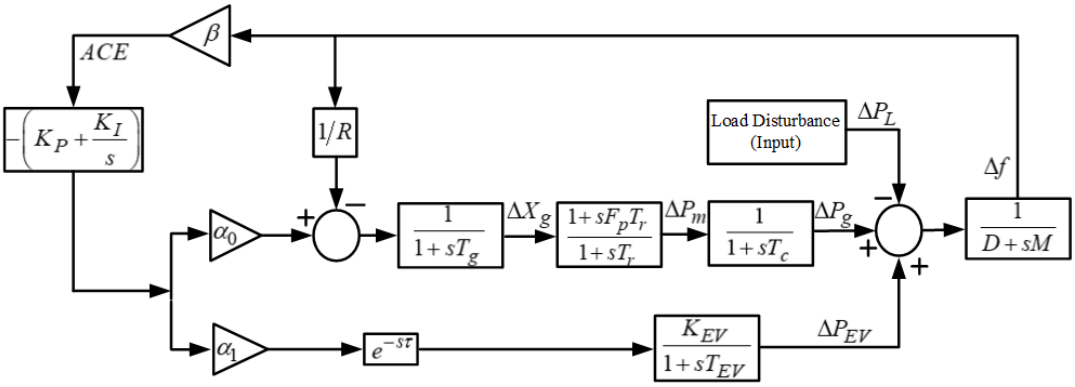

Figure 3.1. Model of single-area LFC system integrated with EVs aggregator

3.1 Single-Area LFC-EVs System

The model of time delayed single-area LFC-EVs system is illustrated in Figure 3.1. It should be observed that a PI controller is adopted as the load frequency controller that is commonly used in the industry. Also, all the delays in EVs are lumped as single constant delay. With the integration of the EVs aggregators into the single-area LFC system, the required control effort called Ω is shared between EVs and the conventional generators in each control area as following (Ko and Sung, 2017a):

$$\begin{aligned} \Delta P_g(s) &= \alpha_0 \Omega \\ \Delta P_{EV}(s) &= \alpha_1 \Omega \end{aligned} \tag{3.2}$$

It should be noted that the sum of power-sharing factor of the conventional generator α_0 and EVs aggregator α_1 should be equal to one. The state-space equation model describing the dynamics of time delayed single-area LFC-EVs system is given as following:

$$\begin{aligned} \dot{x}(t) &= A_o x(t) + A_d x(t-\tau) + F\Delta P_L \\ y(t) &= Cx(t) \end{aligned} \tag{3.3}$$

where

$$x(t) = \begin{bmatrix} \Delta f & \Delta P_g & \Delta P_m & \Delta X_g & \Delta P_{EV} \end{bmatrix}^T,$$

$$y(t) = ACE,$$

$$C = \begin{bmatrix} 1 & 0 & 0 & 0 & 0 & 0 \end{bmatrix},$$

$$F = \begin{bmatrix} -\frac{1}{M} & 0 & 0 & 0 & 0 & K_P\left(\frac{\beta}{M}\right) \end{bmatrix},$$

$$A_0 = \begin{bmatrix} -\frac{D}{M} & \frac{1}{M} & 0 & 0 & \frac{1}{M} & 0 \\ 0 & -\frac{1}{T_c} & \frac{1}{T_c} & 0 & 0 & 0 \\ -\frac{F_P}{T_g R} & 0 & -\frac{1}{T_r} & \left(\frac{1}{T_r} - \frac{F_P}{T_g}\right) & 0 & \frac{\alpha_0 F_P}{T_g} \\ -\frac{1}{T_g R} & 0 & 0 & -\frac{1}{T_g} & 0 & \frac{\alpha_0}{T_g} \\ 0 & 0 & 0 & 0 & -\frac{1}{T_{EV}} & 0 \\ K_P\left(\frac{\beta D}{M}\right) - K_I\beta & -\frac{K_P\beta}{M} & 0 & 0 & -\frac{K_P\beta}{M} & 0 \end{bmatrix},$$

$$A_d = \begin{bmatrix} 0 & 0 & 0 & 0 & 0 & 0 \\ 0 & 0 & 0 & 0 & 0 & 0 \\ 0 & 0 & 0 & 0 & 0 & 0 \\ 0 & 0 & 0 & 0 & 0 & 0 \\ 0 & 0 & 0 & 0 & 0 & \frac{\alpha_{1i} K_{EVi}}{T_{EVi}} \\ 0 & 0 & 0 & 0 & 0 & 0 \end{bmatrix}.$$

In case of any sudden changes in load demand, PI controller receives *ACE* as a control signal after which the output signal from the controller is transmitted to the EVs aggregator and the reheat steam turbine based on their power sharing factors. The *ACE* of single-area LFC-EVs system is the product of frequency deviation and the bias factor that can be shown as follows:

$$ACE = \beta \Delta f \tag{3.4}$$

Whereas, the characteristic equation of the time delayed single-area LFC-EVs system can simply be obtained from Equation (3.3) as:

$$\begin{aligned} \Delta(s,\tau) &= \det\left[sI - A_o - A_d e^{-\tau s} \right] = 0 \\ \Delta(s,\tau) &= a_0(s) + a_1(s) e^{-\tau s} = 0 \end{aligned} \tag{3.5}$$

The degrees of $a_0(s)$ and $a_1(s)$ polynomials are 6 and 4, respectively. The coefficients of these polynomials completely rely on LFC-EVs system parameters. Those coefficients in terms of system parameters are presented in Appendix A1.

3.2. Two-Area LFC System Integrated with EVs Aggregators

The block diagram of a time delayed two-area LFC-EVs system is shown in Figure 3.2. Similar to single-area LFC-EVs system, a PI controller is adopted as the load frequency controller. Moreover, generation units are assumed to be equivalent in each control area, The tie-line synchronization coefficient shown as T_{12} in Figure 3.2 is responsible for the schedule power exchange between both the control areas. Whereas, the ACE signal for each control area is the sum of frequency deviation weighted by a bias factor and the tie-line power exchange between the areas. The ACE of two-area LFC-EVs system is given as:

$$ACE_i = \beta_i \Delta f_i + \Delta P_{tie-i} \tag{3.6}$$

Where, $i = 1, 2$ and the sum of the net tie-line power exchange between all control areas should be zero.

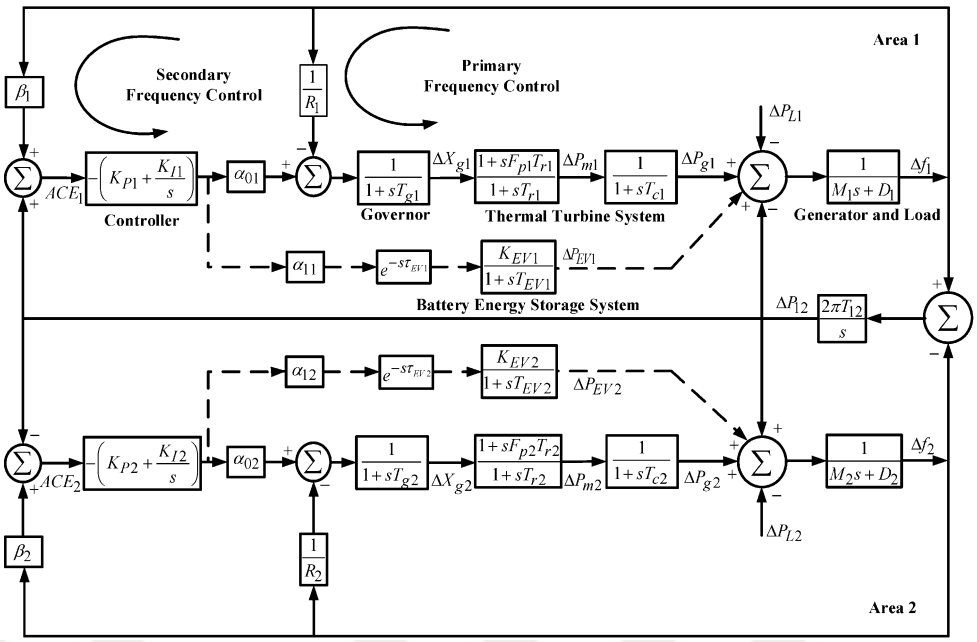

Figure 3.2. Model of two-area LFC-EVs system

Like single-area LFC-EVs system, ACE_i as a control signal is sent to the PI controller as a result of any sudden changes in load demand in the *i*-th control area. The PI controller's output signal is then sent to the reheat steam turbine and the EVs aggregator depending upon their load-sharing factors α_{0i} and α_{1i} so that the system frequency can be regulated. The control signals sent through a communication network to the EVs aggregator enables the EVs fleet to participate in frequency regulation service. The power-sharing factors of conventional generators and EVs aggregators for both areas are assumed to be equal, $\alpha_{01} = \alpha_{02} = \alpha_0$ and $\alpha_{11} = \alpha_{12} = \alpha_1$, respectively (Ko and Sung, 2017a). The closed-loop state-space model of the two-area LFC-EVs system with time delays in Figure 3.2 can also be expressed using Equation (3.3) where the state and output variables, inputs and outputs are defined as follows:

$$x_i(t) = \left[\Delta f_i \quad \Delta P_{gi} \quad \Delta P_{mi} \quad \Delta X_{gi} \quad \Delta P_{EVi} \quad \int ACE_i \right]^T,$$

$$y_i(t) = \left[ACE_i \quad \int ACE_i \right]^T, \quad i = 1, 2$$

$$x(t) = \left[x_1^T(t) \quad x_2^T(t) \quad \Delta P_{12} \right]^T,$$

$$y(t) = \left[y_1^T(t) \quad y_2^T(t) \right]^T,$$

$$\Delta P_L = \left[\Delta P_{L1} \quad \Delta P_{L2} \right]^T.$$

The system, input and output matrices, $A_o, A_d, F,$ and C for $i = 1, 2$ are presented as

following:

$$[A_o]_{13x13} = \left[\begin{array}{c|c|c} [A_{o11}]_{6x6} & [A_{o12}]_{6x6} & [A_{o13}]_{6x1} \\ \hline [A_{o21}]_{6x6} & [A_{o22}]_{6x6} & [A_{o23}]_{6x1} \\ \hline [A_{o31}]_{1x6} & [A_{o32}]_{1x6} & [A_{o33}]_{1x1} \end{array}\right],$$

$$A_{oii} = \begin{bmatrix} -\frac{D_i}{M_i} & \frac{1}{M_i} & 0 & 0 & \frac{1}{M_i} & 0 \\ 0 & -\frac{1}{T_{ci}} & \frac{1}{T_{ci}} & 0 & 0 & 0 \\ -\frac{F_{Pi}}{T_{gi}R_i} & 0 & -\frac{1}{T_{ri}} & \left(\frac{1}{T_{ri}} - \frac{F_{Pi}}{T_{gi}}\right) & 0 & \frac{\alpha_{0i}F_{Pi}}{T_{gi}} \\ -\frac{1}{T_{gi}R_i} & 0 & 0 & -\frac{1}{T_{gi}} & 0 & \frac{\alpha_{0i}}{T_{gi}} \\ 0 & 0 & 0 & 0 & -\frac{1}{T_{EVi}} & 0 \\ K_{Pi}\left(\frac{\beta_i D_i}{M_i} - 2\pi T_{12}\right) - K_{Ii}\beta_i & -\frac{K_{Pi}\beta_i}{M_i} & 0 & 0 & -\frac{K_{Pi}\beta_i}{M_i} & 0 \end{bmatrix}$$

$$A_{o12} = \begin{bmatrix} 0_{5x1} & 0_{5x5} \\ 2\pi T_{12}K_{P1} & 0_{1x5} \end{bmatrix}, A_{o21} = \begin{bmatrix} 0_{5x1} & 0_{5x5} \\ 2\pi T_{12}K_{P2} & 0_{1x5} \end{bmatrix},$$

$$A_{o13} = \begin{bmatrix} -\frac{1}{M_1} & 0_{1x4} & \frac{K_{P1}\beta_1}{M_1} - K_{I1} \end{bmatrix}^T,$$

$$A_{o23} = \begin{bmatrix} \frac{1}{M_2} & 0_{1x4} & \frac{K_{P2}\beta_2}{M_2} - K_{I2} \end{bmatrix}^T,$$

$$A_{o31} = -A_{o32} = \begin{bmatrix} 2\pi T_{12} & 0_{1x5} \end{bmatrix}, A_{o33} = 0,$$

$$[A_d]_{13x13} = \left[\begin{array}{c|c} [A_{d11}]_{6x6} & [A_{d12}]_{6x7} \\ \hline [A_{d21}]_{7x6} & [A_{d22}]_{7x7} \end{array}\right],$$

$$A_{d11} = \begin{bmatrix} 0_{4x5} & 0_{4x1} \\ 0_{1x5} & \frac{\alpha_{11}K_{EV1}}{T_{EV1}} \\ 0_{1x5} & 0 \end{bmatrix}, A_{d22} = \begin{bmatrix} 0_{4x6} & 0_{4x1} \\ 0_{1x6} & \frac{\alpha_{12}K_{EV2}}{T_{EV2}} \\ 0_{2x6} & 0_{2x1} \end{bmatrix}, A_{d12} = \begin{bmatrix} 0_{6x7} \end{bmatrix}, A_{d21} = \begin{bmatrix} 0_{7x6} \end{bmatrix},$$

$$F=\begin{bmatrix}F_1\\F_2\end{bmatrix}^T, F_1=\begin{bmatrix}-\frac{1}{M_1} & 0_{1x12}\end{bmatrix}^T, F_2=\begin{bmatrix}0_{1x6} & -\frac{1}{M_2} & 0_{1x6}\end{bmatrix}^T,$$
$$C=\begin{bmatrix}C_1\\C_2\end{bmatrix}, C_1=\begin{bmatrix}1 & 0_{1x11} & 1\\0_{1x5} & 1 & 0_{1x7}\end{bmatrix}, C_2=\begin{bmatrix}0_{1x6} & 1 & 0_{1x4} & 0 & -1\\0_{1x6} & 0 & 0_{1x4} & 1 & 0\end{bmatrix}.$$

The characteristic equation of the two-area LFC-EVs system can simply be obtained from Equation (3.3) as:

$$\begin{aligned}&\Delta(s,\tau)=\det\left[sI-A_o-A_d e^{-\tau s}\right]=0\\&\Delta(s,\tau)=a_0(s)+a_1(s)e^{-\tau s}+a_2(s)e^{-2\tau s}=0\end{aligned} \tag{3.7}$$

The degree of $a_0(s)$ polynomial is 13. Whereas, the degrees of $a_1(s)$ and $a_2(s)$ polynomials are 11 and 9, respectively. The coefficients of these polynomials completely rely on LFC-EVs system parameters and they are presented in terms of system parameters in Appendix A2.

Likewise, the characteristic equation of a multi-area LFV-EVs system having *n* control areas with equal communication delays in each area will have a similar structure to Equation (3.7) as given in the following:

$$\Delta(s,\tau)=\sum_{k=0}^{n} a_k(s)\, e^{-k\tau s}=0 \tag{3.8}$$

Where, $a_k(s),\ k=0,1,...,n$ are polynomials in *s* having real coefficients and these coefficients totally depend upon system parameters. Also, the characteristic equation given in Equation (3.8) contains ‘n’ exponential terms representing ‘n’ commensurate time delays.

CHAPTER IV

DELAY DEPENDENT STABILITY ANALYSIS OF LFC-EVs SYSTEM

One of the main purpose of this work is to perform a stability analysis for a time delayed single and two-area LFC-EVs systems. The prime objective of the stability analysis is to analytically calculate maximum time delay margin values for given parameters of the LFC system and the PI controller at which the system is marginally stable. In order to perform the stability analysis of single or two-area LFC-EVs system, a more generic form of characteristic equation (3.8) for multi-area LFC-EVs system having n control areas can be utilized. The stability analysis can be performed by determining the change in location of the roots of the characteristic equation (3.8) due to the time delay. However, the identification of roots' location is quite complicated because of the exponential terms $\left(e^{-k\tau s}\right)$ in the characteristic equation due to the time delay. The existence of those exponential term results in infinite number of roots in the characteristic equation. Thus, it is difficult to evaluate those infinite many roots and the change in their location when the time delay value (τ) changes. Though, it is not essential to determine all roots for the stability analysis. Identifying the roots changing their location because of the time delay and determining the location of those roots is sufficient for the analysis. All the roots should reside in the left half of the complex plane for stable operation of the LFC-EVs system.

In time-delayed systems, identification of delay conditions for any given set of system parameters and the maximum delay margin value that will guarantee the stability of the system is the paramount of stability studies. The position of some of the roots may change with the change in the total time delay (τ). Figure 4.1 shows that how the roots can change with respect to the time delay and how a stable system can become unstable due to increase in the time delay value (τ). It can be observed from Figure 4.1 that initially the roots are in the stable left half of the complex plane when there is no time delay in the system $(\tau = 0)$. However, a pair of complex roots begins to move from the stable left half plane to the unstable right half plane when the time delay (τ) is getting increased.

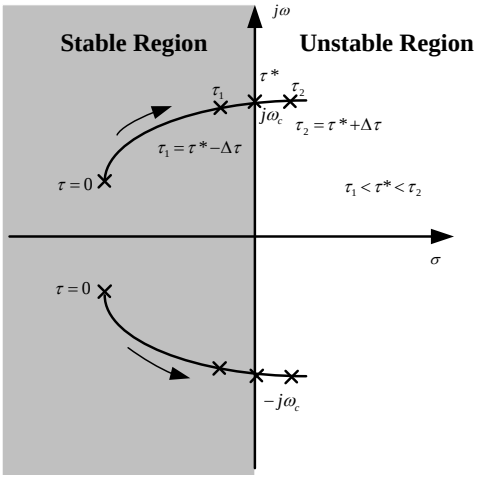

Figure 4.1. Illustration of the roots movement along with the time delay

The roots can pass to the right half of the complex plane by cutting the points $s = \pm j\omega_c$ on imaginary axis at a finite time delay $\left(\tau = \tau^*\right)$. The system is stable up to the points at which the roots crossed the imaginary axis for a given time delay value $\left(\tau^*\right)$. Therefore, in order to perform the stability analysis, it is sufficient to determine the time delay value at which the roots of the characteristic polynomial will be on the imaginary axis. This time delay value is defined as the maximum time delay (Stability Delay Margin) that the system can tolerate without losing its stability and represents the stability limit for the time delay of the system.

Two different stability conditions may occur for the characteristic equation (3.8) depending on the operating conditions and parameters of the LFC-EVs system:

1) **Delay-independent Stability:** For all finite time delay values, the LFC-EVs system will always remain stable independent of the time delay if the roots of the characteristic equation (3.8) does not move from the stable left half plane to the unstable right half plane with an increase in the time delay $\left(\tau\right)$.
2) **Delay-dependent Stability:** If the roots of the characteristic equation (3.8) move from the stable left half plane to the unstable right half plane with the increase in time delay and at least one pair of complex conjugate $\left(s = \pm j\omega_c\right)$ roots will be present on the imaginary axis at a finite time delay value $\tau = \tau*$. The stability of

the LFC-EVs system varies depending on the time delay and the system will be marginally stable at the maximum time delay value $\tau = \tau^*$. However, if $\tau > \tau^*$ the system will become unstable.

As already explained in the previous sections, there are several methods in the literature that have been used for calculating the maximum time delay in time-delayed LFC systems. However, this work includes frequency domain methods; 1) Elimination of exponential terms by an exact method and 2) Rekasius substitution method for the delay-dependent stability analysis of single and two-area LFC-EVs systems. These methods calculate the maximum delay margin value for which the LFC-EVs system will be marginally stable. The main reason for using these methods is that these methods have been used effectively in the previous studies for the stability analysis of single and two area LFC systems without EVs aggregators (Sönmez *et al.*, 2014; Sönmez *et al.*, 2016), micro-grid systems (Gündüz *et al.*, 2017) and generator excitation control systems (Ayasun, 2009; Sönmez *et al.*, 2015). Besides, these methods give quite accurate results when compared with the results obtained from the simulation studies.

4.1 Elimination of Exponential Terms by Direct Method

The direct method analytically calculates the maximum time delay value for which the system is marginally stable. The method removes the exponential terms present in the characteristic equation (3.8) of the LFC-EVs system without any approximation (Ayasun, 2009; Sönmez *et al.*, 2016; Walton and Marshall, 1987). The method converts the characteristic polynomial (4.8) into a regular polynomial which does not contain any exponential terms representing the commensurate time delays. With help of the new polynomial, it is determined that whether the stability of the system depends on the time delay or not. If stability of the system is delay dependent, then the maximum time delay value at which the system is marginally stable is analytically calculated. The method computes the maximum time delay value τ^* at which the roots of the characteristic polynomial lie on the imaginary axis $(s = j\omega_c)$. Since, the complex roots will be present in the form of conjugates at $\tau = \tau^*$, therefore, both $s = j\omega_c$ and $s = -j\omega_c$ roots will yield the characteristic equation (3.8). In other words, the $s = j\omega_c$ root will also be a root of the equation $\Delta(-s, \tau) = 0$, i.e.;

$$\Delta(-s,\tau)=\sum_{k=0}^{n}a_k(-s)e^{k\tau s} \tag{4.1}$$

In order to eliminate the n^{th} exponential term $e^{-n\tau s}$ in the characteristic equation (3.8), a new characteristic equation can be defined as;

$$\Delta^{(1)}(s,\tau)=a_0(-s)\Delta(s,\tau)-a_n(s)e^{-n\tau s}\Delta(-s,\tau)=\sum_{k=0}^{n-1}[a_0(-s)a_k(s)-a_n(s)a_{n-k}(-s)]e^{-k\tau s} \tag{4.2}$$

$$\Delta^{(1)}(-s,\tau)=a_0(s)\Delta(-s,\tau)-a_n(-s)e^{n\tau s}\Delta(s,\tau)=\sum_{k=0}^{n-1}[a_0(s)a_k(-s)-a_n(-s)a_{n-k}(s)]e^{k\tau s} \tag{4.3}$$

It can be observed from Equation (4.2) and Equation (4.3) that the root $s=j\omega_c$ of Equation (3.8) and Equation (4.1) is also a root of the following new characteristic equations;

$$\Delta^{(1)}(s,\tau)=\sum_{k=0}^{n-1}a_k^{(1)}(s)e^{-k\tau s}=0 \tag{4.4}$$

$$\Delta^{(1)}(-s,\tau)=\sum_{k=0}^{n-1}a_k^{(1)}(-s)e^{k\tau s}=0 \tag{4.5}$$

where,

$$a_k^{(1)}(s)=a_0(-s)a_k(s)-a_n(s)a_{n-k}(-s)$$

When compared with the characteristic equation (3.8), it can be observed from Equation (4.4) and Equation (4.5) that the degree of commensuracy is reduced from *n* to *n-1*. In other words, the term $e^{-n\tau s}$ in Equation (3.8) is eliminated and the new characteristic equation given in (4.2) or (4.4) contains the exponential term $e^{-(n-1)\tau s}$. The

aforementioned iterative method of eliminating the exponential term can be easily used to eliminate exponential terms with the help of the new characteristic polynomial equation described below:

$$a_k^{(r+1)}(s) = a_0^{(r)}(-s)a_0^{(r)}(s) - a_{n-r}^{(r)}(s)a_{n-r-k}^{(r)}(-s) \tag{4.6}$$

or given in a more compact form as:

$$\Delta^{(r)}(s,\tau) = \sum_{k=0}^{n-r} a_k^{(r)}(s)e^{-k\tau s} = 0 \tag{4.7}$$

If this elimination of exponential terms is repeated for *n* times, then starting from the term $e^{-n\tau s}$, all exponential terms given in Equation (3.8) can be removed. Therefore, the characteristic equation (3.8) will be converted into a real polynomial without any exponential terms having the following real coefficients (Walton and Marshall, 1987; Ayasun, 2009; Sönmez *et al.*, 2016);

$$\Delta^{(n)}(s) = a_0^{(n)}(s) = a_0^{(n-1)}(-s)a_0^{(n-1)}(s) - a_1^{(n-1)}(s)a_1^{(n-1)}(-s) = 0 \tag{4.8}$$

It should be noticed that the roots of Equation (3.8) for some τ are also roots of Equation (4.8) because the elimination procedure preserves the imaginary roots of the original characteristic equation (3.8). The substitution of $s = j\omega_c$ into Equation (4.8) yields the following polynomial in ${\omega_c}^2$;

$$\mathrm{W}(\omega_c^2) = a_0^{(n-1)}(-j\omega_c)a_0^{(n-1)}(j\omega_c) - a_1^{(n-1)}(j\omega_c)a_1^{(n-1)}(-j\omega_c) = 0 \tag{4.9}$$

The positive real roots $(\omega_c > 0)$ of the regular polynomial Equation (4.9) exactly correspond to the magnitude of purely imaginary roots $(s = \pm j\omega_c)$ of the original characteristic equation (3.8). The calculation of positive real roots of Equation (4.9) is much simpler than that of purely imaginary roots of Equation (3.8). Subjected to the nature of the roots of Equation (3.8), the following two different stability phenomena may be observed (Walton and Marshall, 1987; Sönmez *et al.*, 2016):

1) The LFC-EVs system is ***delay-independent stable*** if the augmented characteristic equation of (4.9) does not have any positive real roots for all finite delays $\tau \geq 0$. The non-existence of such roots implies that the roots of Equation (3.8) remain in the stable left-half of complex plane for all finite delays $\tau \geq 0$.
2) The LFC-EVs system is ***delay-dependent stable*** if the augmented characteristic equation of (4.9) has at least one positive real root. The existence of such roots implies that the roots of (3.8) have crossed the imaginary axis at $s = \pm j\omega_c$ for a finite delay τ^*.

The maximum time delay value $\tau = \tau^*$, corresponding to each positive real root of the characteristic equation (4.9) can be calculated by the following equation (Walton and Marshall, 1987; Ayasun, 2009; Sönmez *et al.*, 2016);

$$\tau^* = \frac{1}{\omega_c} Tan^{-1}\left(\frac{\mathrm{Im}\left[\frac{a_0^{(n-1)}(j\omega_c)}{a_1^{(n-1)}(j\omega_c)} \right]}{\mathrm{Re}\left[\frac{-a_0^{(n-1)}(j\omega_c)}{a_1^{(n-1)}(j\omega_c)} \right]} \right) + \frac{2k\pi}{\omega_c}; \quad k = 0,1,2,\ldots,\infty \tag{4.10}$$

Where, $\mathrm{Im}(\bullet)$ and $\mathrm{Re}(\bullet)$ refer to the imaginary and real parts of (4.10). For a positive root of (4.9), the crossing of roots of Equation (3.8) through the imaginary axis at $s = \pm j\omega_c$ with respect to increase in τ needs to be investigated. This can be done by identifying the roots which cross the imaginary axis with non-zero velocity. The necessary condition for such a roots-crossing can be show as follows:

$$Re\left[\frac{ds}{d\tau} \right]_{s=j\omega_c} \neq 0 \tag{4.11}$$

The real part of a complex variable is shown by $\mathrm{Re}(\bullet)$ in (4.11). The sign of root sensitivity is defined as Root Tendency (*RT*) (Walton and Marshall, 1987; Ayasun, 2009);

$$RT\big|_{s=j\omega_c} = sgn\left\{ \mathrm{Re}\left[\frac{ds}{d\tau} \right]_{s=j\omega_c} \right\} = RT\big|_{s=j\omega_c} = sgn\left[\alpha W'(\omega_c^2) \right] \tag{4.12}$$

Where, α is given as:

$$\alpha = a_0^{(1)}(s)a_0^{(2)}(s)...a_0^{(n-1)}(s)\Big|_{s=j\omega_c} \tag{4.13}$$

Also, the prime $W'(\omega_c^2)$ denotes the derivative of Equation (4.9) with respect to ω_c^2. One of the most prominent features of this method is that not only it can determine the change of the roots across the imaginary axis with respect to the change in time delay, but it can also give the direction of their movement in a simple expression given in Equation (4.12). Therefore, it can be observed from Figure 4.1 that the "RT" expression given in Equation (4.12) provides a practical tool to evaluate the direction of transition of the roots at $s = j\omega_c$ when τ increases from $\tau_1 = \tau^* - \Delta\tau$ to $\tau_2 = \tau^* + \Delta\tau,\ 0 < \Delta\tau << 1$. The root $s = j\omega_c$ crosses the imaginary axis either to unstable right half plane when $RT = +1$, or to stable left half plane when $RT = -1$. The polynomial given in Equation (4.9) can have more than one positive real roots. The set of positive real roots having 'q' number of roots, can be defined as follows:

$$\{\omega_c\} = \{\omega_{c1}, \omega_{c2}, ..., \omega_{cq}\} \tag{4.14}$$

For each of the positive real roots, the corresponding maximum time delay value can be easily calculated using the analytical expression given in Equation (4.10) and the expression for the root tendency given in Equation (4.12). These delay values are defined by the set given below;

$$\{\tau_m^*\} = \{\tau_{m1}^*, \tau_{m2}^*, ..., \tau_{m,\infty}^*\}, m = 1, 2, ..., q \tag{4.15}$$

Where, $\tau_{m,k+1} - \tau_{m,k} = \dfrac{2\pi}{\omega_c}$ is defined as the repetition period of the maximum time delay.

The maximum delay margin value for the system to be marginally stable should be the smallest value among the set of maximum time delay values given in Equation (4.15). The maximum delay margin value of the LFC-EVs system using Direct Method is shown as following:

$$\tau^* = \min(\tau_m^*) \tag{4.16}$$

4.2 Rekasius Substitution Method

The method first converts the characteristic equation (3.8) containing commensurate exponential terms into a regular polynomial having no exponential terms with the help of Rekasius Substitution without using any approximation. Then, the roots of the new polynomial on the imaginary axis and their corresponding maximum time delay values are calculated by the Routh-Hurwitz method that is commonly used in the stability analysis of control systems (Rekasius, 1980; Olgaç and Sipahi, 2002). Rekasius proposed an exact substitution to eliminate the exponential terms present in the characteristic equation (3.8). The substitution is given as follows (Rekasius, 1980);

$$e^{-s\tau} = \frac{1-Ts}{1+Ts} \quad \tau \in \Re^+, \quad T \in \Re \tag{4.17}$$

This substitution is valid only for $s = j\omega_c$ and does not use any approximation for the case of roots on the imaginary axis. Substituting the expression given in Equation (4.17) into the characteristic equation (3.8) yields a new characteristic equation that is given as;

$$\Delta(s,T) = \sum_{k=0}^{p} a_k(s)\left(\frac{1-Ts}{1+Ts}\right)^k = 0 \tag{4.18}$$

Where, p refers to the degree of commensurability of time delay term. When both sides of this equation are multiplied by the expression $(1+Ts)^p$ and the terms are arranged according to the degree of s, the following equations are obtained;

$$\begin{aligned} &\Delta(s,T) = \sum_{k=0}^{p} a_k(s)(1+Ts)^{p-k}(1-Ts)^k = \sum_{k=0}^{m=n+p} b_k(T)s^k = 0 \\ &\Delta(s,T) = b_m(T)s^m + b_{m-1}(T)s^{m-1} + b_{m-2}(T)s^{m-2} + \ldots + b_2(T)s^2 + b_1(T)s + b_0(T) = 0 \end{aligned} \tag{4.19}$$

Where, n is the highest order of the polynomial among $a_k(s)$ polynomials that are dependent on s given by Equation (4.18). The $a_0(s)$ polynomial has the highest (n)

order among $a_k(s)$ polynomials. It is clear from Equation (4.19) that the characteristic equation (3.8) is now converted into a regular polynomial having the parameterized coefficients $b_k(T)$ only and this new polynomial does not contain any delay terms. The new parameter $T \in \Re$ can be positive or negative. It is to be observed from Equation (4.19) that the n^{th} order characteristic polynomial (3.8) having delay terms is now transformed into $(m = n + p)^{th}$ order regular polynomial (4.19) without any delay terms. Both $\Delta(s,\tau)$ and $\Delta(s,T)$ have exactly similar roots that are purely imaginary whereas the remaining roots are not of any concern. Therefore, instead of calculating the roots $\left(s = \pm j\omega_c\right)$ and the corresponding maximum time delay value $\left(\tau = \tau^*\right)$ on the imaginary axis of $\Delta(s,\tau) = 0$ characteristic equation, it is easier to calculate the time delay value of $\Delta(s,T) = 0$ given in Equation (4.19) for the roots located on the virtual axis and the corresponding $T \in \Re$ parameters. The prime objective here is to determine all $T \in \Re$ values that result in imaginary roots of $\Delta(s,T) = 0$. Such $T \in \Re$ values can be easily calculated by Routh-Hurwitz criterion. For this reason, the following Routh's Array is required to be created for the new characteristic equation (4.19);

$$RA(T) = \begin{array}{ccccc} s^m & b_m(T) & b_{m-2}(T) & \dots & b_0 \\ s^{m-1} & b_{m-1}(T) & b_{m-3}(T) & \dots & \\ \vdots & \vdots & \vdots & \vdots & \\ s^2 & R_{21}(T) & R_{22}(T) & & \\ s^1 & R_{11}(T) & & & \\ s^0 & R_{01}(T) & & & \end{array} \tag{4.20}$$

Elements of the Routh's Array can be determined as following:

$$RA(i,\ j) = RA(i-2,\ j+1) - \frac{RA(i-1,\ j+1)RA(i-2,1)}{RA(i-1,1)} \tag{4.21}$$

Where, $RA(i, j)$ denotes the ij^{th} element of Routh's Array. The total number of sign changes in the first column shows the number of unstable roots. It should be noticed that all the $b_k(T)$ coefficients of Equation (4.19) and the elements in first column of Routh's table are all rational functions of *T*. The values of *T* that cause imaginary roots of Equation

(4.19) can be determined from a polynomial of *T* which is obtained by equating the only non-zero term in s^1 row to zero:

$$R_{11}(T) = 0 \tag{4.22}$$

The polynomial in equation (4.22) has degree of $n.p$ and only the determination of its real roots is required (Olgaç and Sipahi, 2002; Rekasius, 1980). Once those real roots are calculated, the corresponding imaginary roots representing the crossing frequencies can be computed by the auxiliary equation obtain from s^2 row as:

$$R_{21}(T)s^2 + R_{22}(T) = 0 \Rightarrow s = \pm j\omega_c = \pm j\sqrt{\frac{R_{22}(T)}{R_{21}(T)}} \tag{4.23}$$

It should be noticed that the auxiliary equation (4.23) consists of the coefficients $R_{21}(T)$ and $R_{22}(T)$ that depend upon the *T* parameter. These two coefficients must have the same signs $R_{21}(T)R_{22}(T) > 0$ for (4.23) to have roots on the imaginary axis. In other words, while determining the roots on the imaginary axis, the only *T* values from the real roots of (4.22) which meet $R_{21}(T)R_{22}(T) > 0$ criteria should be taken into account. If it is assumed that there are '*q*' such *T* values which satisfy this criteria, then the following expression can be obtained:

$$\{T\} = \{T_1, T_2, \cdots, T_q\} \tag{4.24}$$

With the help of Equation (4.23), the roots $(s = \pm j\omega_c)$ of the auxiliary equation and the characteristic equation (3.8) on the imaginary axis can be calculated for each value of this $\{T\}$ set. The roots are given as:

$$\{s = \pm j\omega_c\} = \{\pm j\omega_{c1}, \pm j\omega_{c2}, \cdots, \pm j\omega_{cq}\} \tag{4.25}$$

For each $\{T, \omega_c\}$ given in Equation (4.24) and Equation (4.25), if the maximum time delay values given that Equation (3.8) will have roots on the imaginary axis are written

instead of $s = j\omega_c$ in Equation (4.17), the following analytical expression can be obtained:

$$\tau^* = \frac{2}{\omega_c}\left[Tan^{-1}(\omega_c T) \pm \ell\pi \right], \quad \ell = 0,1,2,\ldots \tag{4.26}$$

Similar to Equation (4.16), the minimum of those calculated time delays will be the maximum delay margin value at which the LFC-EVs system is marginally stable.

CHAPTER V

METHODS FOR OBTAINING ROBUST STABILITY REGIONS

The methods used for the analysis of delay-dependent stability require difficult stability checks every time the PI controller gains are changed. Therefore, all the possible PI controller gains that assure stable operation of the LFC-EVs system in presence of finite time delays are required to be identified. However, knowing the all stabilizing controller parameters will not always guarantee the desired dynamical performance and the stability of LFC-EVs system due to variations in RE source, communication delays and particularly parametric uncertainties. In order to overcome these stability concerns, computation of robust stability regions using Stability Boundary Locus method and Kharitonov Theorem is required.

5.1 Stability Boundary Locus Method

As explained in the reviewed literature, PI controller gain values that assure stable operation of the LFC-EVs system are defined as the stability region in the PI controller parameter space ($(K_P, K_I)-$ plane). In order to compute these regions, it is necessary to obtain the characteristic equation of time-delayed LFC-EVs system in the form of Equation (3.8). The coefficients of $a_k(s)$ polynomials in Equation (3.8) depend upon the system parameters.

The stability regions are then obtained by using a graphical method based on stability boundary locus proposed by (Söylemez *et al.*, 2003; Tan *et al.*, 2006). This method calculates the PI controller parameter values in $(K_P, K_I)-$ plane in the smallest possible frequency range for any specified time delay value of the system. This can be easily achieved by equalizing the real and imaginary parts of the system's characteristic equation to zero. In order to determine the (K_P, K_I) values for which the LFC-EVs system is marginally stable, the following equation is obtained by substituting $s = j\omega_c$ and $e^{-j\omega_c k\tau} = \cos(\omega_c k\tau) - j\sin(\omega_c k\tau)$ in $\Delta(s,\tau) = 0$ of the characteristic equation (3.8):

$$\Delta(j\omega_c,\tau)=\sum_{k=0}^{n}a_k(j\omega_c)e^{-j\omega_c k\tau}=\sum_{k=0}^{n}a_k(j\omega_c)\left[\cos(\omega_c k\tau)-j\sin(\omega_c k\tau)\right]=0 \tag{5.1}$$

Then, the new characteristic equation (5.1) is rearranged so that it can be divided into real and imaginary parts. This new form is expressed in the following equation in terms of K_P and K_I parameters:

$$\begin{aligned}
&\Delta(j\omega_c,\tau)=\sum_{k=0}^{n}R_k(j\omega_c)\cos(\omega_c k\tau)-j\sum_{k=0}^{n}I_k(j\omega_c)\sin(\omega_c k\tau)=R_\Delta+jI_\Delta=0\\
&\Delta(j\omega_c,\tau)=\sum_{k=0}^{n}\left[K_P R_k'(\omega_c)+K_I R_k''(\omega_c)+R_k'''(\omega_c)\right]\cos(\omega k\tau)\\
&\qquad -j\sum_{k=0}^{n}\left[K_P I_k'(\omega_c)+K_I I_k''(\omega_c)+I_k'''(\omega_c)\right]\sin(\omega_c k\tau)=0
\end{aligned} \tag{5.2}$$

It should be noted that $R_k'(\omega)$ and $I_k'(\omega)$ coefficients corresponds to the terms of $R_k(\omega_c)$ and $I_k(\omega_c)$ after K_P being extracted from them while $R_k''(\omega_c)$ and $I_k''(\omega_c)$ coefficients corresponds to the terms of $R_k(\omega_c)$ and $I_k(\omega_c)$ after K_I being extracted from them. Also, $R_k'''(\omega_c)$ and $I_k'''(\omega_c)$ coefficients corresponds to the terms of $R_k(\omega_c)$ and $I_k(\omega_c)$ that neither contain K_P nor K_I controller gains.

For Equation (3.8) and Equation (5.2) to have $s=\pm j\omega_c$ roots on the imaginary axis at any given time delay value τ, the real and imaginary parts of Equation (5.3) must be equal to zero. This can be shown as follows:

$$\begin{aligned}
&K_P\sum_{k=0}^{n}R_k'(\omega_c)\cos(\omega_c k\tau)+K_I\sum_{k=0}^{n}R_k''(\omega_c)\cos(\omega_c k\tau)+\sum_{k=0}^{n}R_k'''(\omega_c)\cos(\omega_c k\tau)=0\\
&K_P\sum_{k=0}^{n}I_k'(\omega_c)\sin(\omega_c k\tau)+K_I\sum_{k=0}^{n}I_k''(\omega_c)\sin(\omega_c k\tau)+\sum_{k=0}^{n}I_k'''(\omega_c)\sin(\omega_c k\tau)=0
\end{aligned} \tag{5.3}$$

Rearranging Equation (5.3) yields the following expression in terms of K_P, K_I and ω_c:

$$\begin{aligned}
&K_P A_1(\omega_c)+K_I B_1(\omega_c)+C_1(\omega_c)=0\\
&K_P A_2(\omega_c)+K_I B_2(\omega_c)+C_2(\omega_c)=0
\end{aligned} \tag{5.4}$$

Where,

$$A_1(\omega_c)=\sum_{k=0}^{n}R_k'(\omega_c)\cos(\omega_c k\tau);\ B_1(\omega_c)=\sum_{k=0}^{n}R_k''(\omega_c)\cos(\omega_c k\tau);$$
$$C_1(\omega_c)=\sum_{k=0}^{n}R_k'''(\omega_c)\cos(\omega_c k\tau);\ A_2(\omega_c)=\sum_{k=0}^{n}I_k'(\omega_c)\sin(\omega_c k\tau); \quad (5.5)$$
$$B_2(\omega_c)=\sum_{k=0}^{n}I_k''(\omega_c)\sin(\omega_c k\tau);\ C_2(\omega_c)=\sum_{k=0}^{n}I_k'''(\omega_c)\sin(\omega_c k\tau);$$

For any selected $\omega_c \neq 0$, the roots of Equation (5.3) on imaginary axis can be calculated by solving for K_P and K_I gains given in Equation (5.4) as:

$$K_P=\frac{B_1(\omega_c)C_2(\omega_c)-B_2(\omega_c)C_1(\omega_c)}{A_1(\omega_c)B_2(\omega_c)-B_1(\omega_c)A_2(\omega_c)},\quad K_I=\frac{A_2(\omega_c)C_1(\omega_c)-A_1(\omega_c)C_2(\omega_c)}{A_1(\omega_c)B_2(\omega_c)-B_1(\omega_c)A_2(\omega_c)} \quad (5.6)$$

For a selected range of ω_c values, the K_P and K_I gains can be calculated by Equation (5.6). Using this proportional-integral gains set, the stability boundary locus $\ell(K_P,K_I,\omega_c)$ in the $(K_P,K_I)-$plane can be identified. The stability boundary locus on the stability region $\ell(K_P,K_I,\omega_c)$ obtained from Equation (5.6) is defined as the Complex Root Boundary (CRB). It should be noticed that the real roots of $\Delta(s,\tau)=0$ when $s=0$ or in other words $\omega_c=0$ may cross the imaginary axis at origin together with the complex roots. By substituting the $\omega_c=0$ value in Equation (5.4), following relationship between K_P and K_I can be obtained:

$$K_I=-\left[\left.\frac{K_P A_1(\omega_c)+C_1(\omega_c)}{B_1(\omega_c)}\right|_{\omega_c=0}\right] \quad (5.7)$$

Equation (5.7) can be defined as the Real Root Boundary (RRB) of the stability region. In this way, the CRB locus $\ell(K_P,K_I,\omega_c)$ computed from Equation (5.6) and the RRB locus obtained from Equation (5.7) divide the $(K_P,K_I)-$plane into stable and unstable regions (Söylemez *et al.*, 2003; Tan *et al.*, 2006). In order to compute the K_P and K_I

parameters at which the LFC-EVs system is stable, the test points (K_P, K_I) can be selected from inside the obtained stability regions.

5.2 Robust Stability Regions Obtained using Kharitonov Theorem

The characteristic polynomial having perturbed coefficients described as an interval polynomial can be represented in general form as shown in Equation (3.8). The coefficients of the characteristic equation (3.8) are originally real in nature. However, substituting $e^{-s\tau} = \cos(\omega\tau) - j\sin(\omega\tau)$ for each $s = j\omega$ in the characteristic polynomial given in Equation (3.8) yields the following equations:

$$\begin{aligned}\Delta(s,\tau) &= \sum_{k=0}^{n} a_k(s)e^{-jk\tau\omega} = a_0(s) + a_1(s)e^{-j\omega\tau} + a_2(s)e^{-j2\omega\tau} + \ldots + a_p(s)e^{-jn\omega\tau} = 0 \\ \Delta(s,\tau) &= \sum_{k=0}^{n} a_k(s)\left[\cos(k\tau\omega) - j\sin(k\tau\omega)\right] = a_0(s) + a_1(s)\left[\cos(\tau\omega) - j\sin(\tau\omega)\right] + \\ &\quad a_2(s)\left[\cos(2\tau\omega) - j\sin(2\tau\omega)\right] + \ldots + a_p(s)\left[\cos(p\tau\omega) - j\sin(n\tau\omega)\right] = 0\end{aligned} \tag{5.8}$$

After some algebraic operations performed on this equation and by separating the real and imaginary parts of the coefficients, a new characteristic polynomial is obtained as:

$$\Delta(s,\alpha,\beta) = \sum_{\ell=0}^{n} (\alpha_\ell + j\beta_\ell)s^\ell = 0 \tag{5.9}$$

Where, $\alpha_\ell \in \Re$, and $\beta_\ell \in \Re$ show the real and imaginary parts of s^ℓ, respectively. Given boxes Q and R as the uncertain bounding sets for α and β, respectively, $\Gamma = \left\{\Delta(\mathrm{s},\alpha,\beta) \middle| \alpha \in \mathrm{Q}; \beta \in \mathrm{R}\right\}$ represents the coefficients of interval polynomial. This can be shown as follows:

$$\begin{aligned}\mathrm{Q} &\triangleq \left\{\alpha = \begin{bmatrix}\alpha_0 & \alpha_1 & \alpha_2 & \ldots & \alpha_\mathrm{n}\end{bmatrix}^\mathrm{T}; \underline{\alpha}_\ell \le \alpha_\ell \le \bar{\alpha}_\ell; \ell = 0,1,2,\ldots,\mathrm{n}\right\} \\ \mathrm{R} &\triangleq \left\{\beta = \begin{bmatrix}\beta_0 & \beta_1 & \beta_2 & \ldots & \beta_\mathrm{n}\end{bmatrix}^\mathrm{T}; \underline{\beta}_\ell \le \beta_\ell \le \bar{\beta}_\ell; \ell = 0,1,2,\ldots,\mathrm{n}\right\}\end{aligned} \tag{5.10}$$

The coefficients $\underline{\alpha}_\ell$ and $\overline{\alpha}_\ell$ given in Equation (5.10) represent the minimum and maximum values (lower and upper limits of the range) of ℓ^{th} component of the vector α. Whereas, $\underline{\beta}_\ell$ and $\overline{\beta}_\ell$ coefficients represent the minimum and maximum values of the ℓ^{th} component of the vector β. Limit values $\underline{\alpha}_\ell$, $\overline{\alpha}_\ell$, $\underline{\beta}_\ell$ and $\overline{\beta}_\ell$ are the functions of the system parameters, PI controller gains $\left(K_P, K_I\right)$ and time delay τ. Using Equation (5.10), the new characteristic polynomial given in Equation (5.9) can be expressed as the following interval polynomial:

$$\Delta(s,\alpha,\beta) = \sum_{\ell=0}^{n} \left(\left[\underline{\alpha}_\ell \quad \overline{\alpha}_\ell \right] + j \left[\underline{\beta}_\ell \quad \overline{\beta}_\ell \right] \right) s^\ell = 0 \tag{5.11}$$

According to the Kharitonov's Theorem, stability analysis of the four vertex Kharitonov polynomials given in Equation (5.12) is required to be done in order to do the stability analysis of the $\Delta(s,\alpha,\beta) \subseteq \Gamma$ interval polynomial given in Equation (5.11) (Bhattacharyya *et al.*, 1995):

$$\begin{aligned}
\Delta_1(s) &= \underline{\alpha}_0 + \underline{\alpha}_1 s + \overline{\alpha}_2 s^2 + \overline{\alpha}_3 s^3 + \underline{\alpha}_4 s^4 + \underline{\alpha}_5 s^5 + \ldots + \\
&\quad j(\underline{\beta}_0 + \underline{\beta}_1 s + \overline{\beta}_2 s^2 + \overline{\beta}_3 s^3 + \underline{\beta}_4 s^4 + \underline{\beta}_5 s^5 + \ldots) \\
\Delta_2(s) &= \overline{\alpha}_0 + \overline{\alpha}_1 s + \underline{\alpha}_2 s^2 + \underline{\alpha}_3 s^3 + \overline{\alpha}_4 s^4 + \overline{\alpha}_5 s^5 + \ldots + \\
&\quad j(\overline{\beta}_0 + \overline{\beta}_1 s + \underline{\beta}_2 s^2 + \underline{\beta}_3 s^3 + \overline{\beta}_4 s^4 + \overline{\beta}_5 s^5 + \ldots) \\
\Delta_3(s) &= \overline{\alpha}_0 + \underline{\alpha}_1 s + \underline{\alpha}_2 s^2 + \overline{\alpha}_3 s^3 + \overline{\alpha}_4 s^4 + \underline{\alpha}_5 s^5 + \ldots + \\
&\quad j(\overline{\beta}_0 + \underline{\beta}_1 s + \underline{\beta}_2 s^2 + \overline{\beta}_3 s^3 + \overline{\beta}_4 s^4 + \underline{\beta}_5 s^5 + \ldots) \\
\Delta_4(s) &= \underline{\alpha}_0 + \overline{\alpha}_1 s + \overline{\alpha}_2 s^2 + \underline{\alpha}_3 s^3 + \underline{\alpha}_4 s^4 + \overline{a}_5 s^5 + \ldots + \\
&\quad j(\underline{\beta}_0 + \overline{\beta}_1 s + \overline{\beta}_2 s^2 + \underline{\beta}_3 s^3 + \underline{\beta}_4 s^4 + \overline{\beta}_5 s^5 + \ldots)
\end{aligned} \tag{5.12}$$

The necessary and sufficient condition for stability of the interval polynomial given in Equation (5.11) is that all the four vertex polynomials given in Equation (5.12) are stable. It should be noticed that the coefficients of the four vertex polynomials given in Equation (5.12) depend upon system parameters, communication time delays and adjustable PI controller gains. Therefore, the PI controller gains that will make these vertex polynomials stable are required to be determined using Stability Boundary Locus method.

Implementing the Stability Boundary Locus method presented in section 5.1 to each vertex polynomial $\eta = 1,2,3,4$ will yield four different stability regions defined by $\Delta_\eta(s = j\omega, \alpha, \beta)$ and $G_{c\eta}(s = j\omega, K_P, K_I)$. The intersection of these four stability regions will be the robust stability region $G_c(\omega, K_P, K_I) = \bigcap_{\eta=1}^{4} G_{c\eta}(\omega, K_P, K_I)$ in the parameter space of PI controller gains that ensure the stability of the system in spite of the parametric uncertainties and communication time delay.

CHAPTER VI

COMPUTATION OF STABILITY DELAY MARGIN

In this chapter, stability delay margin computations are presented for single and two-area LFC-EVs systems using removal of exponential terms by direct method and Rekasius substitution method. The system parameters used by Ko and Sung (2017a) are adopted for the computations. For a given set of PI controller gains, participation factor of EVs and system parameters, maximum allowable time delay is computed by the proposed methods and the obtained results are compared for the validation. Moreover, those obtained results are then verified by an independent technique known as QPmR algorithm along with simulation studies using Matlab/Simulink program.

6.1 Computation of Stability Margin by Direct Method

A general recursive procedure used for eliminating the exponential terms from the characteristic equation has been presented in section 4.1. However, the computation of stability margin in both single and two-area LFC-EVs system for given system parameters, PI controller gains and participation factors are presented in this section.

6.1.1 Stability margin computation in single-area LFC-EVs system

A step-by-step implementation of the proposed method for identifying the maximum allowable time delay or stability delay margin in single-area LFC-EVs system is given below:

Step 1: In order to identify the stability margin, it is necessary to obtain the characteristic equation of single-area LFC-EVs system. The characteristic equation given in the form of Equation (3.5) can be easily obtained from the system model shown in Figure 3.1.

Step 2: The characteristic equation of the system for the given parameters ($M = 8.8$, $D = 1$, $T_g = 0.2s$, $T_c = 0.3s$, $T_r = 12s$, $F_P = 1/6$, $\mathrm{R} = 1/11$, $\beta = 21$, $K_{EV} = 1$,

$T_{EV} = 0.1s$), PI controller gains $(K_P = 0.3,\ K_I = 0.6)$ `and participation factors $(\alpha_0 = 0.8,\ \alpha_1 = 0.2)$ is as follows:

$$\Delta(s,\tau) = a_0(s) + a_1(s)e^{-s\tau} = \begin{pmatrix} 0.0576s^6 + 1.0673s^5 + 5.9685s^4 + 11.0362s^3 + \\ 5.1909s^2 + 3.4735s + 0.9162 \end{pmatrix} + \left(0.0825s^4 + 0.8591s^3 + 2.8201s^2 + 2.9782s + 0.2291\right)e^{-s\tau} = 0 \quad (6.1)$$

Step 3: Using Equations (4.2) - (4.9), the exponential term in Equation (6.1) has been eliminated as given below:

$$\begin{aligned} \Delta(j\omega_c,\tau) &= a_0(j\omega_c) + a_1(j\omega_c)e^{-j\omega_c\tau} = 0 \\ \Delta(-j\omega_c,\tau) &= a_0(-j\omega_c) + a_1(-j\omega_c)e^{j\omega_c\tau} = 0 \end{aligned} \quad (6.2)$$

$$W(\omega_c^2) = a_0(-j\omega_c) - a_1(-j\omega_c)\frac{a_1(j\omega_c)}{a_0(j\omega_c)} = 0 \quad (6.3)$$

$$W(\omega_c^2) = a_0(j\omega_c)a_0(-j\omega_c) - a_1(j\omega_c)a_1(-j\omega_c) = 0 \quad (6.4)$$

The two positive real roots of the system crossing the imaginary axis are calculated as $\omega_{c1} = 0.7964\ rad/s$ and $\omega_{c2} = 0.3071\ rad/s$ by the solution of the following Equation (6.5):

$$W(\omega_c^2) = 0.0033\omega_c^{12} + 0.4516\omega_c^{10} + 12.6559\omega_c^8 + 66.8693\omega_c^6 - 41.6568\omega_c^4 - 5.0261\omega_c^2 + 0.7872 = 0 \quad (6.5)$$

Step 4: Using Equation (4.10), the corresponding time delay values for both the real positive roots $\omega_{c1} = 0.7964\ rad/s$ and $\omega_{c2} = 0.3071\ rad/s$ can simply be obtained as following:

$$\tau_i = \frac{1}{\omega_{ci}} \text{Tan}^{-1}\left(\frac{0.0385\omega_{ci}^9 + 1.3789\omega_{ci}^7 + 9.4193\omega_{ci}^5 + 2.3484\omega_{ci}^3 - 1.9334\omega_{ci}}{-0.0048\omega_{ci}^{10} - 0.2623\omega_{ci}^8 - 4.6134\omega_{ci}^6 - 21.1373\omega_{ci}^4 + 6.5711\omega_{ci}^2 + 0.2099} \right) \tag{6.6}$$

Where, $i = 1, 2$ and the corresponding time delay values are $\tau_1 = 0.8325s$ and $\tau_2 = 12.2167s,$ respectively.

Step 5: Using Equation (4.12), the root tendencies of the positive real roots are obtained by substituting $\omega_{c1} = 0.7964\ rad/s$ and $\omega_{c2} = 0.3071\ rad/s$ for $i = 1, 2$ in Equation (6.7):

$$\begin{aligned} W'(\omega_{ci}^2) &= 0.0199{\omega_{ci}}^{10} + 2.2582{\omega_{ci}}^{8} + 50.6236{\omega_{ci}}^{6} \\ &\quad + 200.6078{\omega_{ci}}^{4} - 83.3137{\omega_{ci}}^{2} - 5.0261 = 0 \end{aligned} \tag{6.7}$$

The root crossing of $\omega_{c1} = 0.7964\ rad/s$ yields $RT = +1$ inferring that the complex conjugate roots move from the stable left half-plane to the unstable right half-plane cutting the imaginary axis at $\tau_1 = 0.8325s.$ Whereas, the root crossing of $\omega_{c2} = 0.3071\ rad/s$ yields $RT = -1$ showing that the complex conjugate roots move back from the unstable right half-plane to the stable left half-plane cutting the imaginary axis at $\tau_2 = 12.2167s.$ Since, the system is getting unstable right after $\tau_1 = 0.8325s,$ therefore, the maximum allowable delay or the stability margin in the single-area LFC-EVs system is computed as $\tau_1 = \tau^* = 0.8325s.$

Stability delay margins are computed for a wide range of PI controller gains. The theoretical delay margins are presented in Table 6.1, Table 6.2 and Table 6.3 for the EVs participation factor of $\alpha_1 = 0.1,\ 0.2$ and 0.3, respectively. Results in all these three tables indicate that for a fixed value of K_P, the stability delay margin decreases when K_I is increased inferring a less stable system. It is should be observed that the delay margins are not computed for the values of K_P and K_I such that the delay-free system $(\tau = 0)$ is not stable. The corresponding locations are marked by (*) in Table.1. However, the

system is observed to be delay-independent stable for the K_P and K_I values marked by (∞) in Table 6.1, Table 6.2 and Table 6.3. Moreover, the stability delay margin increases with increasing K_P for nearly all values of K_I. The impact of EVs participation factor on the stability delay margin is also investigated for different values of K_P and K_I. As shown in Figure 6.1, stability margins decrease with an increase in the EVs participation factor α_1 when $K_P = 0.3$ and $K_I = 0.6$.

Table 6.1. Stability delay margins in single-area LFC-EVs for $(\alpha_0 = 0.9,\ \alpha_1 = 0.1)$

τ^*	K_I									
K_p	**0.1**	**0.2**	**0.3**	**0.4**	**0.5**	**0.6**	**0.7**	**0.8**	**0.9**	**1.0**
0.1	∞	∞	2.0473	1.0325	0.5308	0.2264	0.0216	*	*	*
0.2	∞	∞	3.0999	1.6598	1.0155	0.6299	0.3707	0.1841	0.0432	*
0.3	∞	∞	∞	2.2690	1.4712	1.0077	0.6977	0.4743	0.3051	0.1725
0.4	∞	∞	∞	2.8813	1.8952	1.3560	0.9997	0.7432	0.5488	0.3959
0.5	∞	∞	∞	3.5966	2.2905	1.6732	1.2745	0.9891	0.7726	0.6020
0.6	∞	∞	∞	∞	2.6691	1.9606	1.5217	1.2108	0.9756	0.7901
0.7	∞	∞	∞	∞	3.0597	2.2221	1.7422	1.4085	1.1574	0.9597
0.8	∞	∞	∞	∞	3.5589	2.4646	1.9382	1.5831	1.3185	1.1107
0.9	∞	∞	∞	∞	∞	2.6988	2.1129	1.7362	1.4596	1.2436
1.0	∞	∞	∞	∞	∞	2.9439	2.2702	1.8697	1.5822	1.3594
1.5	∞	∞	∞	∞	∞	∞	3.0656	2.3177	1.9652	1.7190
2.0	∞	∞	∞	∞	∞	∞	∞	2.5729	2.0572	1.7978

Table 6.2. Stability delay margin in single-area LFC-EVs for $(\alpha_0 = 0.8,\ \alpha_1 = 0.2)$

τ^*	K_I									
K_p	**0.1**	**0.2**	**0.3**	**0.4**	**0.5**	**0.6**	**0.7**	**0.8**	**0.9**	**1.0**
0.1	∞	2.7435	1.3678	0.8269	0.5333	0.3494	0.2241	0.1338	0.0658	0.0131
0.2	∞	3.5876	1.8631	1.2000	0.8341	0.6015	0.4410	0.3239	0.2349	0.1653
0.3	∞	4.2535	2.2633	1.5212	1.1030	0.8325	0.6429	0.5031	0.3958	0.3111
0.4	∞	4.6984	2.5513	1.7766	1.3297	1.0342	0.8238	0.6665	0.5445	0.4474
0.5	∞	4.8590	2.7273	1.9627	1.5088	1.2018	0.9793	0.8104	0.6779	0.5713
0.6	∞	4.6807	2.8033	2.0821	1.6398	1.3332	1.1068	0.9322	0.7936	0.6808
0.7	∞	4.3114	2.7976	2.1423	1.7255	1.4292	1.2060	1.0311	0.8904	0.7746
0.8	∞	3.9029	2.7309	2.1533	1.7713	1.4926	1.2780	1.1074	0.9680	0.8522
0.9	∞	3.5170	2.6227	2.1258	1.7834	1.5266	1.3252	1.1621	1.0272	0.9137
1.0	∞	3.1714	2.4897	2.0700	1.7685	1.5363	1.3504	1.1974	1.0692	0.9600
1.5	2.2180	1.9741	1.7801	1.6193	1.4826	1.3642	1.2603	1.1682	1.0859	1.0118
2.0	1.4071	1.3332	1.2651	1.2020	1.1435	1.0889	1.0379	0.9901	0.9451	0.9029

Table 6.3. Stability delay margins in single-area LFC-EVs for $(\alpha_0 = 0.7,\ \alpha_1 = 0.3)$

τ^*	K_I									
K_p	**0.1**	**0.2**	**0.3**	**0.4**	**0.5**	**0.6**	**0.7**	**0.8**	**0.9**	**1.0**
0.1	∞	1.9963	1.1029	0.7100	0.4887	0.3473	0.2495	0.1782	0.1240	0.0816
0.2	∞	2.4989	1.4766	1.0043	0.7302	0.5514	0.4259	0.3333	0.2623	0.2063
0.3	∞	2.7733	1.7519	1.2449	0.9385	0.7334	0.5868	0.4771	0.3920	0.3243
0.4	∞	2.8374	1.9189	1.4207	1.1046	0.8862	0.7264	0.6048	0.5093	0.4325
0.5	4.5639	2.7512	1.9872	1.5306	1.2246	1.0053	0.8408	0.7131	0.6112	0.5283
0.6	3.6590	2.5810	1.9776	1.5809	1.2996	1.0900	0.9282	0.7999	0.6958	0.6098
0.7	3.0680	2.3769	1.9146	1.5831	1.3346	1.1421	0.9891	0.8649	0.7623	0.6762
0.8	2.6330	2.1692	1.8196	1.5499	1.3370	1.1658	1.0256	0.9090	0.8109	0.7273
0.9	2.2956	1.9730	1.7092	1.4931	1.3148	1.1661	1.0409	0.9344	0.8429	0.7637
1.0	2.0257	1.7944	1.5943	1.4226	1.2753	1.1485	1.0389	0.9436	0.8602	0.7868
1.5	1.2253	1.1646	1.1056	1.0489	0.9947	0.9431	0.8943	0.8481	0.8046	0.7637
2.0	0.8497	0.8266	0.8036	0.7808	0.7582	0.7360	0.7141	0.6926	0.6715	0.6510

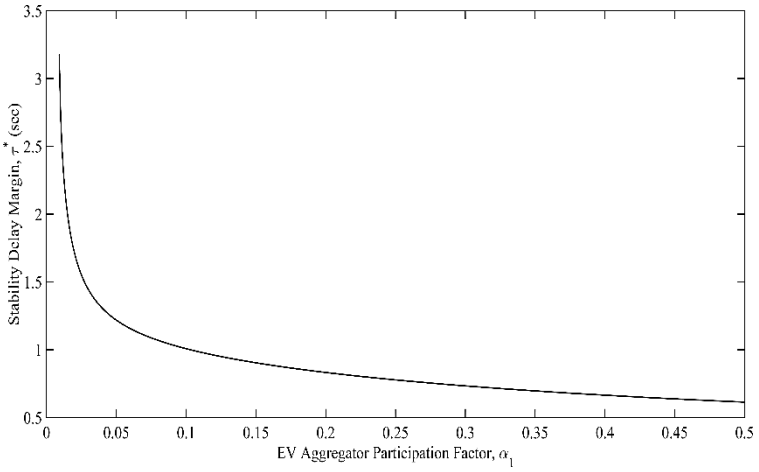

Figure 6.1. Variation in stability margins against EVs participation factor for $(K_P = 0.3, K_I = 0.6)$

6.1.2 Stability margin computation in two-area LFC-EVs system

The procedure for stability margin computation in two-area LFC-EVs system is based on the following steps:

Step 1: Primarily, the characteristic equation of two-area LFC-EVs system is required to be obtained for identifying the stability margin. The characteristic equation given in the form of Equation (3.7) can be easily obtained from the system model shown in Figure 3.2.

Step 2: The characteristic equation of the system for the given parameters $(M_1 = M_2 = 8.8,\quad D_1 = D_2 = 1,\quad T_{g1} = T_{g2} = 0.2s,\quad T_{c1} = T_{c2} = 0.3s,\quad T_{r1} = T_{r2} = 12s,$ $T_{12} = 0.1,\quad F_{P1} = F_{P2} = 1/6,\quad \mathrm{R}_1 = \mathrm{R}_2 = 1/11,\quad \beta_1 = \beta_2 = 21,\quad K_{EV1} = K_{EV2} = 1,$ $T_{EV1} = T_{EV2} = 0.1s)$, PI controller gains $(K_P = 0.6,\ K_I = 0.7)$ and participation factors $(\alpha_{01} = \alpha_{02} = 0.7,\ \alpha_{11} = \alpha_{12} = 0.3)$ is as follows:

$$\begin{aligned}\Delta(s,\tau) &= a_0(s)+a_1(s)e^{-\tau s}+a_2(s)e^{-2\tau s}\\ &= \begin{pmatrix}0.003s^{13}+0.123s^{12}+1.83s^{11}+14.04s^{10}+60.27s^9+\\ 147.62s^8+210.73s^7+199.31s^6+156.38s^5+\\ 82.44s^4+34.998s^3+10.08s^2+1.353s+0.0524\end{pmatrix}\\ &+\begin{pmatrix}0.0285s^{11}+0.8022s^{10}+8.816s^9+49.092s^8+\\ 149.43s^7+251.96s^6+239.595s^5+150.92s^4+\\ 73.144s^3+17.363s^2+1.5543s+0.0449\end{pmatrix}e^{-\tau s}\\ &+\begin{pmatrix}0.0612s^9+1.177s^8+9.02s^7+35.076s^6+72.885s^5+\\ 78.16s^4+38.49s^3+6.33s^2+0.418s+0.0096\end{pmatrix}e^{-2\tau s}=0\end{aligned} \tag{6.8}$$

Step 3: Using Equations (4.2) - (4.9), the exponential terms in Equation (6.8) has been eliminated as given below:

$$\begin{aligned}\Delta^{(1)}(s,\tau) &= a_0(-s)\Delta(s,\tau)-a_2(s)e^{-2\tau s}\Delta(-s,\tau)\\ &= \sum_{k=0}^{1}\left[a_0(-s)a_k(s)-a_2(s)a_{2-k}(-s)\right]e^{-k\tau s}\end{aligned} \tag{6.9}$$

$$\begin{aligned}\Delta^{(1)}(-s,\tau) &= a_0(s)\Delta(-s,\tau)-a_2(-s)e^{2\tau s}\Delta(s,\tau)\\ &= \sum_{k=0}^{1}\left[a_0(s)a_k(-s)-a_2(s)a_{2-k}(-s)\right]e^{k\tau s}\end{aligned} \tag{6.10}$$

$$\Delta^{(1)}(s,\tau)=a_0^{(1)}(s)+a_1^{(1)}(s)e^{-s\tau}=0 \tag{6.11}$$

$$\Delta^{(2)}(s)=a_0^{(2)}(s)=0 \tag{6.12}$$

$$a_0^{(2)}(s)=a_0^{(1)}(-s)a_0^{(1)}(s)-a_1^{(1)}(s)a_1^{(1)}(-s) \tag{6.13}$$

$$W(\omega_c^2)=a_0^{(1)}(-j\omega_c)a_0^{(1)}(j\omega_c)-a_1^{(1)}(j\omega_c)a_1^{(1)}(-j\omega_c)=0 \tag{6.14}$$

The four positive real roots of the system crossing the imaginary axis are calculated as $\omega_{c1}=1.1165\ rad/s$, $\omega_{c2}=1.0324 rad/s$, $\omega_{c3}=0.2257 rad/s$ and $\omega_{c4}=0.1827 rad/s$ by the solution of the following Equation (6.15):

$$W(\omega_c^2) = 1.21\times10^{-10}\omega_c^{52} + 6.59\times10^{-8}\omega_c^{50} + ... \\ -4.83\times10^{7}\omega_c^{22} + ... + 0.0015\omega_c^{2} + 3.34\times10^{-6} = 0 \quad (6.15)$$

Step 4: Using Equation (4.10), the corresponding time delay values for all the four real positive roots $\omega_{c1} = 1.1165\ rad/s,\ \omega_{c2} = 1.0324\ rad/s,\ \omega_{c3} = 0.2257\ rad/s$ and $\omega_{c4} = 0.1827\ rad/s$ are obtained as $\tau_1 = 0.8353s,\ \tau_2 = 0.9282s,\ \tau_3 = 16.1359s$ and $\tau_4 = 20.9243s$ respectively.

Step 5: Using Equation (4.12), the root tendencies of the positive real roots are obtained for $\omega_{c1} = 1.1165\ rad/s,\ \omega_{c2} = 1.0324\ rad/s,\ \omega_{c3} = 0.2257\ rad/s$ and $\omega_{c4} = 0.1827\ rad/s.$

The root crossing of $\omega_{c1} = 1.1165\ rad/s$ and $\omega_{c2} = 1.0324\ rad/s$ yields $RT = +1$ inferring that the complex conjugate roots move from the stable left half-plane to the unstable right half-plane cutting the imaginary axis at $\tau_1 = 0.8353s,$ and $\tau_2 = 0.9282s,$ respectively. However, the root crossing of $\omega_{c3} = 0.2257\ rad/s$ and $\omega_{c4} = 0.1827\ rad/s$ yields $RT = -1$ showing that the complex conjugate roots move back from the unstable right half-plane to the stable left half-plane cutting the imaginary axis at $\tau_3 = 16.1359s$ and $\tau_4 = 20.9243s,$ respectively. Since, the system is getting unstable right after $\tau_1 = 0.8353s,$ therefore, the maximum allowable delay or the stability margin in the two-area LFC-EVs system is computed as $\tau_1 = \tau^* = 0.8353s.$

Stability delay margins are computed for a wide range of PI controller gains. The theoretical delay margins are presented in Table 6.4, Table 6.5 and Table 6.6 for the EVs participation factor of $\alpha_{01} = \alpha_{11} = 0.1,\ 0.2$ and 0.3, respectively. Results in all these three tables indicate that for a fixed value of K_P, the stability delay margin decreases when K_I is increased inferring a less stable system. Similar to the single-area LFC-EVs system, the stability margins are not computed for the values of K_P and K_I such that the delay-free system $(\tau = 0)$ is not stable. The corresponding locations are denoted as (*) in Table 6.4 and Table 6.5. However, the system is observed to be delay-independent stable for

some K_P and K_I values. For such a scenario, the stability margin is marked as (∞) in Table 6.4, Table 6.5 and Table 6.6. Moreover, the stability margin increases with increasing K_P for almost all values of K_I. The effect of EVs participation factor on stability margin is also investigated for different values of K_P and K_I values. As shown in Figure 6.2, stability margin decreases with an increase in the EVs participation factors α_{11} and α_{12} for $(K_P = 0.5,\ K_I = 0.7)$. Also, it is imperative to study the impact of tie-lie power exchange between the two areas on stability delay margins. As shown in Figure 6.3, the stability delay margins decrease with an increase in the tie-lie power coefficient T_{12} for $K_P = 0.5$ and $K_I = 0.7$.

Table 6.4. Stability margins in two-area LFC-EVs for $(\alpha_{01} = \alpha_{02} = 0.9,\ \alpha_{11} = \alpha_{12} = 0.1)$

τ^*	K_I									
K_p	**0.1**	**0.2**	**0.3**	**0.4**	**0.5**	**0.6**	**0.7**	**0.8**	**0.9**	**1.0**
0.1	∞	∞	2.0473	1.0325	0.5308	0.2264	0.0216	*	*	*
0.2	∞	∞	3.0999	1.6598	1.0155	0.6192	0.3479	0.1538	0.0077	*
0.3	∞	∞	∞	2.2691	1.4466	0.9624	0.6476	0.4225	0.2524	0.1190
0.4	∞	∞	∞	2.8813	1.8274	1.2737	0.9211	0.6695	0.4788	0.3288
0.5	∞	∞	∞	3.5966	2.1788	1.5504	1.1655	0.8922	0.6848	0.5209
0.6	∞	∞	∞	∞	2.5190	1.7934	1.3797	1.0892	0.8689	0.6943
0.7	∞	∞	∞	∞	2.9106	2.0062	1.5648	1.2607	1.0308	0.8484
0.8	∞	∞	∞	∞	3.5589	2.1939	1.7228	1.4077	1.1710	0.9832
0.9	∞	∞	∞	∞	∞	2.3636	1.8564	1.5319	1.2906	1.0995
1.0	∞	∞	∞	∞	∞	2.5248	1.9683	1.6352	1.3909	1.1982
1.5	∞	∞	∞	∞	∞	∞	2.2814	1.9015	1.6585	1.4743
2.0	∞	∞	∞	∞	∞	∞	2.2302	1.8549	1.6448	1.4901

Table 6.5. Stability margins in two-area LFC-EVs for $(\alpha_{01} = \alpha_{02} = 0.8,\ \alpha_{11} = \alpha_{12} = 0.2)$

τ^*	K_I									
K_p	**0.1**	**0.2**	**0.3**	**0.4**	**0.5**	**0.6**	**0.7**	**0.8**	**0.9**	**1.0**
0.1	∞	2.7426	1.3615	0.7779	0.4760	0.2907	0.1659	0.0769	0.0106	*
0.2	∞	3.5866	1.8058	1.1214	0.7586	0.5307	0.3743	0.2607	0.1750	0.1082
0.3	∞	4.2528	2.1240	1.4014	1.0037	0.7463	0.5659	0.4326	0.3305	0.2500
0.4	∞	4.6976	2.3116	1.6084	1.2019	0.9300	0.7346	0.5875	0.4730	0.3816
0.5	∞	4.8539	2.3884	1.7443	1.3506	1.0777	0.8764	0.7217	0.5993	0.5003
0.6	∞	3.9200	2.3840	1.8190	1.4526	1.1894	0.9899	0.8334	0.7074	0.6041
0.7	∞	3.2397	2.3268	1.8447	1.5137	1.2674	1.0757	0.9222	0.7966	0.6920
0.8	∞	2.8917	2.2383	1.8338	1.5411	1.3158	1.1361	0.9893	0.8671	0.7639
0.9	∞	2.6220	2.1332	1.7969	1.5420	1.3395	1.1742	1.0365	0.9200	0.8203
1.0	∞	2.3963	2.0210	1.7426	1.5228	1.3433	1.1934	1.0663	0.9571	0.8624
1.5	1.7583	1.6180	1.4942	1.3840	1.2850	1.1957	1.1146	1.0408	0.9733	0.9113
2.0	1.2158	1.1628	1.1124	1.0645	1.0190	0.9757	0.9345	0.8953	0.8579	0.8223

Table 6.6. Stability margins in two-area LFC-EVs for $(\alpha_{01} = \alpha_{02} = 0.7,\ \alpha_{11} = \alpha_{12} = 0.3)$

τ^*	K_I									
K_p	**0.1**	**0.2**	**0.3**	**0.4**	**0.5**	**0.6**	**0.7**	**0.8**	**0.9**	**1.0**
0.1	∞	1.9830	1.0194	0.6299	0.4153	0.2801	0.1876	0.1208	0.0706	0.0316
0.2	∞	2.3553	1.3531	0.9057	0.6465	0.4779	0.3599	0.2731	0.2068	0.1548
0.3	∞	2.4588	1.5732	1.1202	0.8406	0.6514	0.5153	0.4132	0.3340	0.2709
0.4	∞	2.3986	1.6862	1.2672	0.9899	0.7936	0.6481	0.5363	0.4481	0.3768
0.5	3.2164	2.2643	1.7161	1.3517	1.0933	0.9018	0.7550	0.6394	0.5463	0.4700
0.6	2.6931	2.1048	1.6895	1.3851	1.1550	0.9767	0.8353	0.7210	0.6270	0.5487
0.7	2.3407	1.9431	1.6288	1.3803	1.1820	1.0217	0.8903	0.7814	0.6899	0.6123
0.8	2.0713	1.7891	1.5499	1.3495	1.1821	1.0416	0.9231	0.8222	0.7358	0.6611
0.9	1.8539	1.6470	1.4630	1.3022	1.1627	1.0419	0.9371	0.8459	0.7661	0.6960
1.0	1.6734	1.5176	1.3747	1.2456	1.1302	1.0276	0.9363	0.8552	0.7829	0.7184
1.5	1.0916	1.0430	0.9952	0.9487	0.9036	0.8602	0.8187	0.7790	0.7411	0.7052
2.0	0.7869	0.7666	0.7464	0.7263	0.7063	0.6865	0.6669	0.6477	0.6288	0.6102

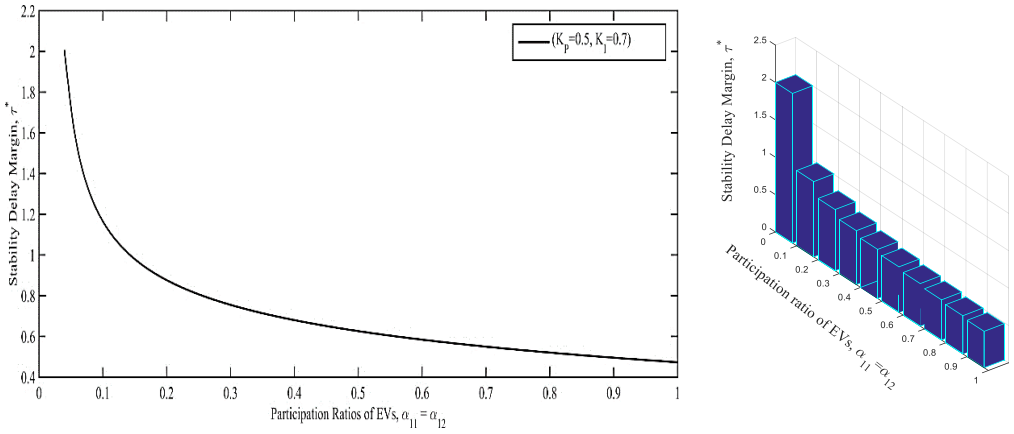

Figure 6.2. Variation of stability margin against the EVs participation factors for $(K_P = 0.5, K_I = 0.7)$

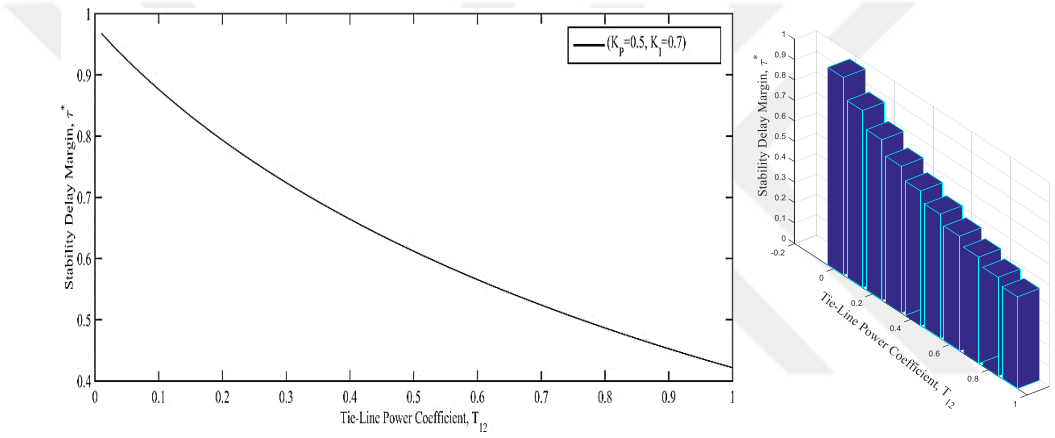

Figure 6.3. Variation of stability margin against the Tie-line Power for $(K_P = 0.5, K_I = 0.7)$

6.2 Computation of Stability Margin by Rekasius Substitution Method

The characteristic equation of a time delayed LFC-EVs system has exponential transcendentality feature. This results in infinitely many finite roots, which makes the determination of the roots and delay margin a difficult task. However, this problem can be easily overcome by using Rekasius substitution for the transcendental term shown in Equation (4.17). This substitution is defined only for the roots on the imaginary axis, $s = \pm j\omega_c$. It should be mentioned here that the Equation (4.17) is not an approximation but an exact substitution when the characteristic equation of the system has roots on the imaginary axis.

6.2.1 Stability margin computation in single-area LFC-EVs system

A step-by-step implementation of the proposed method for identifying the maximum allowable time delay or stability delay margin in single-area LFC-EVs system is given below:

Step 1: The characteristic equation of single-area LFC-EVs system given in the form of Equation (3.5) can be easily obtained from the system model shown in Figure 3.1.

Step 2: The characteristic equation of the system for the given parameters ($M = 8.8$, $D = 1$, $T_g = 0.2s$, $T_c = 0.3s$, $T_r = 12s$, $F_P = 1/6$, $R = 1/11$, $\beta = 21$, $K_{EV} = 1$, $T_{EV} = 0.1s$), PI controller gains ($K_P = 0.4$, $K_I = 0.9$) and participation factors ($\alpha_0 = 0.9$, $\alpha_1 = 0.1$) is as follows:

$$\Delta(s,\tau) = a_0(s) + a_1(s)e^{-s\tau} = \begin{pmatrix} 0.0576s^6 + 1.0674s^5 + 5.9686s^4 + 11.082s^3 + \\ 5.798s^2 + 5.0256s + 1.5464 \end{pmatrix} + \left(0.05498s^4 + 0.587s^3 + 1.996s^2 + 2.224s + 0.1718\right)e^{-s\tau} = 0 \tag{6.16}$$

Step 3: Using Equations (4.17), the exponential term in Equation (6.16) has been eliminated as given below:

$$\Delta(s,\tau) = a_0(s) + a_1(s)\left(\frac{1-Ts}{1+Ts}\right) = 0 \tag{6.17}$$

After some simplifications, the augmented characteristic equation is obtained in a simpler form as:

$$\Delta(s,T) = b_7s^7 + b_6s^6 + b_5s^5 + b_4s^4 + b_3s^3 + b_2s^2 + b_1s + b_0 = 0 \tag{6.18}$$

where,

$$b_7 = 0.0576T,\ b_6 = 1.0674T + 0.0576,\ b_5 = 5.9136T + 1.0674,$$
$$b_4 = 10.496T + 6.024,\ b_3 = 3.802T + 11.6685,\ b_2 = 2.802T + 7.7938,$$
$$b_1 = 1.3746T + 7.2496,\ b_0 = 1.7182.$$

Step 4: It is necessary to determine the roots of the system that cross the imaginary axis by calculating the values of augmented polynomial T obtained in Equation (6.18). Therefore, using Equations (4.20) and (4.21) along with Equation (6.18), the Routh array is obtained as follows:

$$\begin{array}{ccccc} s^7 & b_7 & b_5 & b_3 & b_1 \\ s^6 & b_6 & b_4 & b_2 & b_0 \\ s^5 & R_{51} & R_{52} & R_{53} & 0 \\ s^4 & R_{41} & R_{42} & R_{43} & 0 \\ s^3 & R_{31} & R_{32} & 0 & 0 \\ s^2 & R_{21} & R_{22} & 0 & 0 \\ s^1 & R_{11} & 0 & 0 & 0 \\ s^0 & b_0 & & & \end{array} \tag{6.19}$$

Where, the elements of Routh table are given as:

$$R_{51}(T) = \frac{b_6 b_5 - b_7 b_4}{b_6},\ R_{52}(T) = \frac{b_6 b_3 - b_7 b_2}{b_6},\ R_{53}(T) = \frac{b_6 b_1 - b_7 b_0}{b_6};$$

$$R_{41}(T) = \frac{R_{51} b_4 - b_6 R_{52}}{R_{51}},\ R_{42}(T) = \frac{R_{51} b_2 - b_6 R_{53}}{R_{51}},\ R_{43}(T) = b_0 = 1.7182;$$

$$R_{31}(T) = \frac{R_{41} R_{52} - R_{51} R_{42}}{R_{41}},\ R_{32}(T) = \frac{R_{41} R_{53} - R_{51} R_{43}}{R_{41}};$$

$$R_{21}(T) = \frac{R_{42} R_{31} - R_{41} R_{32}}{R_{31}},\ R_{22}(T) = b_0 = 1.7182;\ R_{11}(T) = \frac{R_{32} R_{21} - R_{31} R_{22}}{R_{21}}.$$

Step 5: An 18th order T polynomial given in the form of Equation (6.20) is obtained by setting $R_{11}(T)$ in the s^1 row to zero:

$$R_{11}(T) = t_{18}T^{18} + ... + t_6T^6 + t_5T^5 + ... + t_1T + t_0 = 0 \tag{6.20}$$

The polynomial shown in Equation (51) has 12 real roots; $T_1 = -3.474$, $T_2 = -0.054$, $T_3 = -0.105$, $T_4 = -0.209$, $T_5 = -0.3995$, $T_6 = -0.394$, $T_7 = -0.192$, $T_8 = -0.189$, $T_9 = -5.306$, $T_{10} = -0.282$, $T_{11} = -4.270$ and $T_{12} = 0.2793$.

Step 6: For each real root $T_i \in T_c$ $(i = 1, 2, ..., 12)$,, the corresponding crossing frequencies $s = \pm j\omega_c$ can be obtained using the auxiliary equation from the s^2 row of the Routh's array that is given in the form of Equation (4.23). It must be mentioned here that the following additional sign agreement condition given in Equation (6.21) must be satisfied for Equation (4.23) to yield imaginary roots $s = \pm j\omega_c$:

$$R_{21}(T_i)R_{22}(T_i) > 0 \tag{6.21}$$

It should be noticed that the coefficient R_{21} is a function of $T_i \in T_c$ $(i = 1, 2, ..., 12)$. Whereas, R_{22} is a positive constant given as $R_{22}(T) = 1.7182$. For this reason, the auxiliary equation will yield imaginary roots for positive $R_{21}(T)$ only. The crossing frequencies for each $T_i \in T_c$ $(i = 1, 2, ..., 12)$. roots are obtained from Equation (6.22) as following:

$$\omega_c = \sqrt{\frac{R_{22}(T_i)}{R_{21}(T_i)}} \tag{6.22}$$

12 different crossing frequencies $\{\omega_{c1}, \omega_{c2}, ..., \omega_{c12}\}$ corresponding to $T_c = \{T_1, T_2, ..., T_{12}\}$ are determined. However, only $T_{12} = 0.2793$ with $s = \pm j\omega_c = \pm j0.8399$ as the corresponding root crossing the imaginary axis, satisfy the sign agreement condition show in Equation (6.21).

Step 7: Substituting $\omega_c = 0.8399\ rad/s$ and $T = T_{12} = 0.2793$ into the Equation (4.26), the corresponding stability margin for the given system parameters, PI controller gains and participation factors is obtained as $\tau = \tau^* = 0.5487s$.

Stability margins are computed for an extensive range of PI controller gains. These results are exactly the same as obtained by Time Domain Direct Method. The theoretical delay margin values are presented in Table 6.7, Table 6.8 and Table 6.9 for the EVs participation factor of $\alpha_1 = 0.1,\ 0.2$ and 0.3, respectively. Results in all these three tables indicate that for a fixed value of K_P, the stability delay margin decreases when K_I is increased inferring a less stable system. It is to be observed that the delay margins are not computed for the values of K_P and K_I such that the delay-free system $(\tau = 0)$ is not stable. The corresponding locations are marked by (*) in Table 6.7. However, the system is observed to be delay-independent stable for the K_P and K_I values marked by (∞) in Table 6.7, Table 6.8 and Table 6.9. Moreover, the stability delay margin increases with an increase in K_P for almost all values of K_I.

Table 6.7. Stability margins in single-area LFC-EVs system for $(\alpha_0 = 0.9,\ \alpha_1 = 0.1)$

τ^*	K_I									
K_p	**0.1**	**0.2**	**0.3**	**0.4**	**0.5**	**0.6**	**0.7**	**0.8**	**0.9**	**1.0**
0.1	∞	∞	2.0473	1.0325	0.5308	0.2264	0.0216	*	*	*
0.2	∞	∞	3.0999	1.6598	1.0155	0.6299	0.3707	0.1841	0.0432	*
0.3	∞	∞	∞	2.2690	1.4712	1.0077	0.6977	0.4743	0.3051	0.1725
0.4	∞	∞	∞	2.8813	1.8952	1.3560	0.9997	0.7432	0.5488	0.3959
0.5	∞	∞	∞	3.5966	2.2905	1.6732	1.2745	0.9891	0.7726	0.6020
0.6	∞	∞	∞	∞	2.6691	1.9606	1.5217	1.2108	0.9756	0.7901
0.7	∞	∞	∞	∞	3.0597	2.2221	1.7422	1.4085	1.1574	0.9597
0.8	∞	∞	∞	∞	3.5589	2.4646	1.9382	1.5831	1.3185	1.1107
0.9	∞	∞	∞	∞	∞	2.6988	2.1129	1.7362	1.4596	1.2436
1.0	∞	∞	∞	∞	∞	2.9439	2.2702	1.8697	1.5822	1.3594
1.5	∞	∞	∞	∞	∞	∞	3.0656	2.3177	1.9652	1.7190
2.0	∞	∞	∞	∞	∞	∞	∞	2.5729	2.0572	1.7978

Table 6.8. Stability margins in single-area LFC-EVs for $(\alpha_0 = 0.8,\ \alpha_1 = 0.2)$

τ^*	K_I									
K_p	**0.1**	**0.2**	**0.3**	**0.4**	**0.5**	**0.6**	**0.7**	**0.8**	**0.9**	**1.0**
0.1	∞	2.7435	1.3678	0.8269	0.5333	0.3494	0.2241	0.1338	0.0658	0.0131
0.2	∞	3.5876	1.8631	1.2000	0.8341	0.6015	0.4410	0.3239	0.2349	0.1653
0.3	∞	4.2535	2.2633	1.5212	1.1030	0.8330	0.6429	0.5031	0.3958	0.3111
0.4	∞	4.6984	2.5513	1.7766	1.3297	1.0342	0.8238	0.6665	0.5445	0.4474
0.5	∞	4.8590	2.7273	1.9627	1.5088	1.2018	0.9793	0.8104	0.6779	0.5713
0.6	∞	4.6807	2.8033	2.0821	1.6398	1.3332	1.1068	0.9322	0.7936	0.6808
0.7	∞	4.3114	2.7976	2.1423	1.7255	1.4292	1.2060	1.0311	0.8904	0.7746
0.8	∞	3.9029	2.7309	2.1533	1.7713	1.4926	1.2780	1.1074	0.9680	0.8522
0.9	∞	3.5170	2.6227	2.1258	1.7834	1.5266	1.3252	1.1621	1.0272	0.9137
1.0	∞	3.1714	2.4897	2.0700	1.7685	1.5363	1.3504	1.1974	1.0692	0.9600
1.5	2.2180	1.9741	1.7801	1.6193	1.4826	1.3642	1.2603	1.1682	1.0859	1.0118
2.0	1.4071	1.3332	1.2651	1.2020	1.1435	1.0889	1.0379	0.9901	0.9451	0.9029

Table 6.9. Stability margins in single-area LFC-EVs system for $(\alpha_0 = 0.7,\ \alpha_1 = 0.3)$

τ^*	K_I									
K_p	**0.1**	**0.2**	**0.3**	**0.4**	**0.5**	**0.6**	**0.7**	**0.8**	**0.9**	**1.0**
0.1	∞	1.9963	1.1029	0.7100	0.4887	0.3473	0.2495	0.1782	0.1240	0.0816
0.2	∞	2.4989	1.4766	1.0043	0.7302	0.5514	0.4259	0.3333	0.2623	0.2063
0.3	∞	2.7733	1.7519	1.2449	0.9385	0.7334	0.5868	0.4771	0.3920	0.3243
0.4	∞	2.8374	1.9189	1.4207	1.1046	0.8862	0.7264	0.6048	0.5093	0.4325
0.5	4.5639	2.7512	1.9872	1.5306	1.2246	1.0053	0.8408	0.7131	0.6112	0.5283
0.6	3.6590	2.5810	1.9776	1.5809	1.2996	1.0900	0.9282	0.7999	0.6958	0.6098
0.7	3.0680	2.3769	1.9146	1.5831	1.3346	1.1421	0.9891	0.8649	0.7623	0.6762
0.8	2.6330	2.1692	1.8196	1.5499	1.3370	1.1658	1.0256	0.9090	0.8109	0.7273
0.9	2.2956	1.9730	1.7092	1.4931	1.3148	1.1661	1.0409	0.9344	0.8429	0.7637
1.0	2.0257	1.7944	1.5943	1.4226	1.2753	1.1485	1.0389	0.9436	0.8602	0.7868
1.5	1.2253	1.1646	1.1056	1.0489	0.9947	0.9431	0.8943	0.8481	0.8046	0.7637
2.0	0.8497	0.8266	0.8036	0.7808	0.7582	0.7360	0.7141	0.6926	0.6715	0.6510

6.2.2 Stability margin computation in two-area LFC-EVs system

The procedure for stability margin computation in two-area LFC-EVs system is based on the following steps:

Step 1: The characteristic equation of two-area LFC-EVs system given in the form of Equation (3.7).is obtained from the system model shown in Figure 3.2.

Step 2: The characteristic equation of the system for the given parameters $(M_1 = M_2 = 8.8,\quad D_1 = D_2 = 1,\quad T_{g1} = T_{g2} = 0.2s,\quad T_{c1} = T_{c2} = 0.3s,\quad T_{r1} = T_{r2} = 12s,$ $T_{12} = 0.1,\quad F_{P1} = F_{P2} = 1/6,\quad \mathrm{R}_1 = \mathrm{R}_2 = 1/11,\quad \beta_1 = \beta_2 = 21,\quad K_{EV1} = K_{EV2} = 1,$ $T_{EV1} = T_{EV2} = 0.1s)$, PI controller gains $(K_P = 0.8,\ K_I = 0.8)$ and participation factors $(\alpha_{01} = \alpha_{02} = 0.8,\ \alpha_{11} = \alpha_{12} = 0.2)$ is as follows:

$$\begin{aligned}\Delta(s,\tau) &= a_0(s) + a_1(s)e^{-\tau s} + a_2(s)e^{-2\tau s} \\ &= \begin{pmatrix} 0.003s^{13} + 0.123s^{12} + 1.83s^{11} + 14.048s^{10} + 60.56s^9 + \\ 150.76s^8 + 226.14s^7 + 234.81s^6 + 197.43s^5 + \\ 113.84s^4 + 52.58s^3 + 16.05s^2 + 2.266s + 0.0893 \end{pmatrix} \\ &+ \begin{pmatrix} 0.0254s^{11} + 0.709s^{10} + 7.722s^9 + 42.5s^8 + 127.68s^7 + \\ 214.06s^6 + 209.45s^5 + 42.95s^4 + 70.95s^3 + 17.11s^2 + \\ 1.543s + 0.0447 \end{pmatrix} e^{-\tau s} \\ &+ \begin{pmatrix} 0.0484s^9 + 0.914s^8 + 6.837s^7 + 25.70s^6 + 50.868s^5 + \\ 50.97s^4 + 23.34s^3 + 3.744s^2 + 0.244s + 0.0056 \end{pmatrix} e^{-2\tau s} = 0\end{aligned} \tag{6.23}$$

Step 3: Using Equations (4.17), the exponential term in Equation (6.23) has been eliminated as given below:

$$\Delta(s,\tau) = P(s) + Q(s)\left(\frac{1-Ts}{1+Ts}\right) + R(s)\left(\frac{1-Ts}{1+Ts}\right)^2 = 0 \tag{6.24}$$

After some simplifications, the augmented characteristic equation is obtained in a simpler form as:

$$\begin{aligned}\Delta(s,T) = {} & b_{15}s^{15} + b_{14}s^{14} + b_{13}s^{13} + b_{12}s^{12} + b_{11}s^{11} + b_{10}s^{10} + b_9s^9 + b_8s^8 \\ & + b_7s^7 + b_6s^6 + b_5s^5 + b_4s^4 + b_3s^3 + b_2s^2 + b_1s + b_0 = 0\end{aligned} \tag{6.25}$$

where

$$b_{15} = 0.0033T^2,\ b_{14} = 0.123T^2 + 0.0066T,\ b_{13} = 1.802T^2 + 0.2459T + 0.0033$$
$$b_{12} = 13.34T^2 + 3.655T + 0.123,\ b_{11} = 52.88T^2 + 28.09T + 1.853$$
$$b_{10} = 109.2T^2 + 121.0T + 14.76,\ b_9 = 105.3T^2 + 299.7T + 68.33$$
$$b_8 = 46.45T^2 + 438.6T + 194.2,\ b_7 = 38.85T^2 + 418.2T + 360.7$$
$$b_6 = 21.85T^2 + 293.1T + 474.6,\ b_5 = 4.978T^2 + 125.7T + 457.7$$
$$b_4 = 2.682T^2 + 58.5T + 307.8,\ b_3 = 0.967T^2 + 24.61T + 146.9$$
$$b_2 = 0.0503T^2 + 4.044T + 36.91,\ b_1 = 0.1675T + 4.053,\ b_0 = 0.1396$$

Step 4: The roots of the system that cross the imaginary axis are required to be determine by calculating the values of augmented polynomial T obtained in Equation (6.25). Therefore, using Equations (4.20) and (4.21) along with Equation (6.25), the Routh array is obtained as follows:

$$\begin{array}{cccccccccc}
s^{15} & b_{15} & b_{13} & b_{11} & b_9 & b_7 & b_5 & b_3 & b_1 \\
s^{14} & b_{14} & b_{12} & b_{10} & b_8 & b_6 & b_4 & b_2 & b_0 \\
s^{13} & R_{131} & R_{132} & R_{133} & R_{134} & R_{135} & R_{136} & R_{137} & 0 \\
\vdots & \vdots & \vdots & \vdots & \vdots & \vdots & \vdots & \vdots & \vdots \\
\vdots & \vdots & \vdots & \vdots & \vdots & \vdots & \vdots & \vdots & \vdots \\
s^2 & R_{21} & b_0 & 0 & 0 & 0 & 0 & 0 & 0 \\
s^1 & R_{11} & 0 & 0 & 0 & 0 & 0 & 0 & 0 \\
s^0 & b_0 & & & & & & &
\end{array} \tag{6.26}$$

where

$$R_{131}(T) = \frac{b_{14}b_{13} - b_{15}b_{12}}{b_{14}},\ R_{132}(T) = \frac{b_{14}b_{11} - b_{15}b_{10}}{b_{14}},\ R_{133}(T) = \frac{b_{14}b_9 - b_{15}b_8}{b_{14}},$$
$$R_{134}(T) = \frac{b_{14}b_7 - b_{15}b_6}{b_{14}},\ R_{135}(T) = \frac{b_{14}b_5 - b_{15}b_4}{b_{14}},\ R_{136}(T) = \frac{b_{14}b_3 - b_{15}b_2}{b_{14}},$$
$$R_{137}(T) = \frac{b_{14}b_1 - b_{15}b_0}{b_{14}};$$

$$R_{121}(T)=\frac{R_{131}b_{12}-b_{14}R_{132}}{R_{131}},\ R_{122}(T)=\frac{R_{131}b_{10}-b_{14}R_{133}}{R_{131}},\ R_{123}(T)=\frac{R_{131}b_{8}-b_{14}R_{134}}{R_{131}},$$
$$R_{124}(T)=\frac{R_{131}b_{6}-b_{14}R_{135}}{R_{131}},\ R_{125}(T)=\frac{R_{131}b_{4}-b_{14}R_{136}}{R_{131}},\ R_{126}(T)=\frac{R_{131}b_{2}-b_{14}R_{137}}{R_{131}};$$

$$R_{111}(T)=\frac{R_{121}R_{132}-R_{131}R_{122}}{R_{121}},\ R_{112}(T)=\frac{R_{121}R_{133}-R_{131}R_{123}}{R_{121}},$$
$$R_{113}(T)=\frac{R_{121}R_{134}-R_{131}R_{124}}{R_{121}},\ R_{114}(T)=\frac{R_{121}R_{135}-R_{131}R_{125}}{R_{121}},$$
$$R_{115}(T)=\frac{R_{121}R_{136}-R_{131}R_{126}}{R_{121}},\ R_{116}(T)=\frac{R_{121}R_{137}-R_{131}b_{0}}{R_{121}};$$

$$R_{101}(T)=\frac{R_{111}R_{122}-R_{121}R_{112}}{R_{111}},\ R_{102}(T)=\frac{R_{111}R_{123}-R_{121}R_{113}}{R_{111}},$$
$$R_{103}(T)=\frac{R_{111}R_{124}-R_{121}R_{114}}{R_{111}},\ R_{104}(T)=\frac{R_{111}R_{125}-R_{121}R_{115}}{R_{111}},$$
$$R_{105}(T)=\frac{R_{111}R_{126}-R_{121}R_{116}}{R_{111}};$$

$$R_{91}(T)=\frac{R_{101}R_{112}-R_{111}R_{102}}{R_{101}},\ R_{92}(T)=\frac{R_{101}R_{113}-R_{111}R_{103}}{R_{101}},$$
$$R_{93}(T)=\frac{R_{101}R_{114}-R_{111}R_{104}}{R_{101}},\ R_{94}(T)=\frac{R_{101}R_{115}-R_{111}R_{105}}{R_{101}},$$
$$R_{95}(T)=\frac{R_{101}R_{116}-R_{111}b_{0}}{R_{101}};$$

$$R_{81}(T)=\frac{R_{91}R_{102}-R_{101}R_{92}}{R_{91}},\ R_{82}(T)=\frac{R_{91}R_{103}-R_{101}R_{93}}{R_{91}},\ R_{83}(T)=\frac{R_{91}R_{104}-R_{101}R_{94}}{R_{91}},$$
$$R_{84}(T)=\frac{R_{91}R_{105}-R_{101}R_{95}}{R_{91}};$$

$$R_{71}(T)=\frac{R_{81}R_{92}-R_{91}R_{82}}{R_{81}},\ R_{72}(T)=\frac{R_{81}R_{93}-R_{91}R_{83}}{R_{81}},R_{73}(T)=\frac{R_{81}R_{94}-R_{91}R_{84}}{R_{81}},$$
$$R_{74}(T)=\frac{R_{81}R_{95}-R_{91}b_{0}}{R_{81}};$$

$$R_{61}(T)=\frac{R_{71}R_{82}-R_{81}R_{72}}{R_{71}},\ R_{62}(T)=\frac{R_{71}R_{83}-R_{81}R_{73}}{R_{71}},\ R_{63}(T)=\frac{R_{71}R_{84}-R_{81}R_{74}}{R_{71}};$$

$$R_{51}(T)=\frac{R_{61}R_{72}-R_{71}R_{62}}{R_{61}},\ R_{52}(T)=\frac{R_{61}R_{73}-R_{71}R_{63}}{R_{61}},\ R_{53}(T)=\frac{R_{61}R_{74}-R_{71}b_0}{R_{61}};$$

$$R_{41}(T)=\frac{R_{51}R_{62}-R_{61}R_{52}}{R_{51}},\ \ R_{42}(T)=\frac{R_{51}R_{63}-R_{61}R_{53}}{R_{51}};$$

$$R_{31}(T)=\frac{R_{41}R_{52}-R_{51}R_{42}}{R_{41}},\ \ R_{32}(T)=\frac{R_{41}R_{53}-R_{51}b_0}{R_{41}};$$

$$R_{21}(T)=\frac{R_{42}R_{31}-R_{41}R_{32}}{R_{31}};\ R_{11}(T)=\frac{R_{32}R_{21}-R_{31}b_0}{R_{21}}.$$

Step 5: A 32nd order T polynomial given in the form of Equation (6.27) is obtained by setting $R_{11}(T)$ in the s^1 row to zero:

$$R_{11}(T)=t_{32}T^{32}+...+t_6T^6+t_5T^5+...+t_1T+t_0=0 \qquad (6.27)$$

The polynomial shown in Equation (6.27) has 16 real roots; $T_1=0.621$ $T_2=-7.622$, $T_3=-0.110$, $T_4=-0.206$, $T_5=-0.099$, $T_6=-0.194$, $T_7=-12.121$, $T_8=-10.690$, $T_9=-9.420$, $T_{10}=-35.776$, $T_{11}=-8.862$, $T_{12}=-34.598$, $T_{13}=-0.538$, $T_{14}=-8.538$, $T_{15}=-0.529$ and $T_{16}=0.551$

Step 6: For each real root $T_i\in T_c$ $(i=1,2,...,16),$, the corresponding crossing frequencies $s=\pm j\omega_c$ can be obtained using the auxiliary equation from the s^2 row of the Routh's array that is given in the form of Equation (4.23). However, the sign agreement condition $R_{21}(T_i)R_{22}(T_i)>0$ must be fulfilled to yield imaginary roots $s=\pm j\omega_c$. As explained in Section 6.2.1, the coefficient R_{21} is a function of $T_i\in T_c$ $(i=1,2,...,16)$. Whereas, R_{22} is a positive constant given as $R_{22}(T)=0.1396.$ For this reason, the auxiliary equation will

yield imaginary roots for positive $R_{21}(T)$ only. The crossing frequencies for each $T_i \in T_c$ $(i = 1,2,...,16)$. roots are obtained using Equation (6.22). Where, 16 different crossing frequencies $\{\omega_{c1}, \omega_{c2}, ..., \omega_{c16}\}$ corresponding to $T_c = \{T_1, T_2, ..., T_{16}\}$ are determined. However, only $T_1 = 0.621$ with $s = \pm j\omega_c = \pm j1.0187$ and $T_{16} = 0.551$ with $s = \pm j\omega_c = \pm j1.1065$ as the corresponding roots crossing the imaginary axis, satisfy the sign agreement condition.

Step 7: Substituting the values of both $T_1 = 0.621$ and $T_{16} = 0.551$ along with their corresponding roots $\omega_{c1} = 1.0187\ rad/s$ and $\omega_{c2} = 1.1065\ rad/s$ into the Equation (4.26), will result in two different values of time delays; $\tau_1 = 1.1074s$ and $\tau_2 = 0.9893s$. However, the minimum of these two time delays, $\tau^* = \tau_2 = 0.9893s$ is the stability margin of the two-area LFC-EVs system.

Stability delay margins are computed for a wide range of PI controller gains. These results are similar to the results obtained by Time Domain Direct Method. The theoretical delay margin values are presented in Table 6.10, Table 6.11 and Table 6.12 for the EVs participation factor of $\alpha_{01} = \alpha_{11} = 0.1,\ 0.2$ and 0.3, respectively. Results in all these three tables indicate that for a fixed value of K_P, the stability delay margin decreases when K_I is increased inferring a less stable system. It is to be observed that the delay margins are not computed for the values of K_P and K_I such that the delay-free system $(\tau = 0)$ is not stable. The corresponding locations are marked by (*) in Table 6.10 and Table 6.11. However, the system is observed to be delay-independent stable for the K_P and K_I values marked by (∞) in Table 6.10, Table 6.11 and Table 6.12. Moreover, the stability delay margin increases with an increase in K_P for almost all values of K_I.

Table 6.10. Stability margins in two-area LFC-EVs for $(\alpha_{01} = \alpha_{02} = 0.9,\ \alpha_{11} = \alpha_{12} = 0.1)$

τ^*	-K_I									
K_p	**0.1**	**0.2**	**0.3**	**0.4**	**0.5**	**0.6**	**0.7**	**0.8**	**0.9**	**1.0**
0.1	∞	∞	2.0473	1.0325	0.5308	0.2264	0.0216	*	*	*
0.2	∞	∞	3.0999	1.6598	1.0155	0.6192	0.3479	0.1538	0.0077	*
0.3	∞	∞	∞	2.2691	1.4466	0.9624	0.6476	0.4225	0.2524	0.1190
0.4	∞	∞	∞	2.8813	1.8274	1.2737	0.9211	0.6695	0.4788	0.3288
0.5	∞	∞	∞	3.5966	2.1788	1.5504	1.1655	0.8922	0.6848	0.5209
0.6	∞	∞	∞	∞	2.5190	1.7934	1.3797	1.0892	0.8689	0.6943
0.7	∞	∞	∞	∞	2.9106	2.0062	1.5648	1.2607	1.0308	0.8484
0.8	∞	∞	∞	∞	3.5589	2.1939	1.7228	1.4077	1.1710	0.9832
0.9	∞	∞	∞	∞	∞	2.3636	1.8564	1.5319	1.2906	1.0995
1.0	∞	∞	∞	∞	∞	2.5248	1.9683	1.6352	1.3909	1.1982
1.5	∞	∞	∞	∞	∞	∞	2.2814	1.9015	1.6585	1.4743
2.0	∞	∞	∞	∞	∞	∞	2.2302	1.8549	1.6448	1.4901

Table 6.11. Stability margin in two-area LFC-EVs for $(\alpha_{01} = \alpha_{02} = 0.8,\ \alpha_{11} = \alpha_{12} = 0.2)$

τ^*	K_I									
K_p	**0.1**	**0.2**	**0.3**	**0.4**	**0.5**	**0.6**	**0.7**	**0.8**	**0.9**	**1.0**
0.1	∞	2.7426	1.3615	0.7779	0.4760	0.2907	0.1659	0.0769	0.0106	*
0.2	∞	3.5866	1.8058	1.1214	0.7586	0.5307	0.3743	0.2607	0.1750	0.1082
0.3	∞	4.2528	2.1240	1.4014	1.0037	0.7463	0.5659	0.4326	0.3305	0.2500
0.4	∞	4.6976	2.3116	1.6084	1.2019	0.9300	0.7346	0.5875	0.4730	0.3816
0.5	∞	4.8539	2.3884	1.7443	1.3506	1.0777	0.8764	0.7217	0.5993	0.5003
0.6	∞	3.9200	2.3840	1.8190	1.4526	1.1894	0.9899	0.8334	0.7074	0.6041
0.7	∞	3.2397	2.3268	1.8447	1.5137	1.2674	1.0757	0.9222	0.7966	0.6920
0.8	∞	2.8917	2.2383	1.8338	1.5411	1.3158	1.1361	0.9893	0.8671	0.7639
0.9	∞	2.6220	2.1332	1.7969	1.5420	1.3395	1.1742	1.0365	0.9200	0.8203
1.0	∞	2.3963	2.0210	1.7426	1.5228	1.3433	1.1934	1.0663	0.9571	0.8624
1.5	1.7583	1.6180	1.4942	1.3840	1.2850	1.1957	1.1146	1.0408	0.9733	0.9113
2.0	1.2158	1.1628	1.1124	1.0645	1.0190	0.9757	0.9345	0.8953	0.8579	0.8223

Table 6.12. Stability margins in two-area LFC-EVs for $(\alpha_{01} = \alpha_{02} = 0.7,\ \alpha_{11} = \alpha_{12} = 0.3)$

τ^*	K_I									
K_p	**0.1**	**0.2**	**0.3**	**0.4**	**0.5**	**0.6**	**0.7**	**0.8**	**0.9**	**1.0**
0.1	∞	1.9830	1.0194	0.6299	0.4153	0.2801	0.1876	0.1208	0.0706	0.0316
0.2	∞	2.3553	1.3531	0.9057	0.6465	0.4779	0.3599	0.2731	0.2068	0.1548
0.3	∞	2.4588	1.5732	1.1202	0.8406	0.6514	0.5153	0.4132	0.3340	0.2709
0.4	∞	2.3986	1.6862	1.2672	0.9899	0.7936	0.6481	0.5363	0.4481	0.3768
0.5	3.2164	2.2643	1.7161	1.3517	1.0933	0.9018	0.7550	0.6394	0.5463	0.4700
0.6	2.6931	2.1048	1.6895	1.3851	1.1550	0.9767	0.8353	0.7210	0.6270	0.5487
0.7	2.3407	1.9431	1.6288	1.3803	1.1820	1.0217	0.8903	0.7814	0.6899	0.6123
0.8	2.0713	1.7891	1.5499	1.3495	1.1821	1.0416	0.9231	0.8222	0.7358	0.6611
0.9	1.8539	1.6470	1.4630	1.3022	1.1627	1.0419	0.9371	0.8459	0.7661	0.6960
1.0	1.6734	1.5176	1.3747	1.2456	1.1302	1.0276	0.9363	0.8552	0.7829	0.7184
1.5	1.0916	1.0430	0.9952	0.9487	0.9036	0.8602	0.8187	0.7790	0.7411	0.7052
2.0	0.7869	0.7666	0.7464	0.7263	0.7063	0.6865	0.6669	0.6477	0.6288	0.6102

6.3 Verification of Theoretical Results

In this section, the verification studies for theoretically computed stability margins in single and two-area LFC system by the proposed methods are shown. It can be observed from the tables that stability margins computed using elimination of exponential terms by direct method are almost similar to the stability margins computed by Rekasius substitution method. Therefore, verification studies provided for any of the two methods would be sufficient to validate the theoretically computed stability margins in single and two-area LFC-EVs system.

6.3.1 Verification of single-area LFC-EVs system

The theoretical delay margins are verified using time-domain simulations and QPmR algorithm. The controller gains are chosen as $(K_P = 0.3, K_I = 0.6)$ and the EVs participation factor is selected as $\alpha_1 = 0.2$. It is clear from Table 6.2 that the stability delay margin is computed as $\tau^* = 0.8325s$ for this case. Therefore, Figure 6.4 illustrates that for $\tau = 0.785s,$ which is a smaller value when compared with the calculated stability margin $\tau^* = 0.8325s,$ all roots are located in the left half of the complex plane and the

frequency response has decaying oscillations indicating the LFC-EVs system to be stable. Whereas, the dominant roots distribution of Equation (6.1) and frequency response of the LFC-EVs system for $\tau^* = 0.8325s$ is shown in Figure 6.5. It should be noticed that the system has a pair of complex roots on the imaginary axis and the frequency response exhibits sustained oscillations indicating the marginal stability of LFC-EVs system. If the time delay exceeds the stability delay margin, the system will become unstable due to the growing oscillations in the frequency response. The results shown in Figure 6.5 clearly prove the accuracy of the theoretically computed stability margins. Whereas, a pair of complex roots in the unstable right half of the $s-$plane and growing oscillations in the frequency response in Figure 6.6 clearly show that the LFC-EVs system becomes unstable at $\tau = 0.875s$.

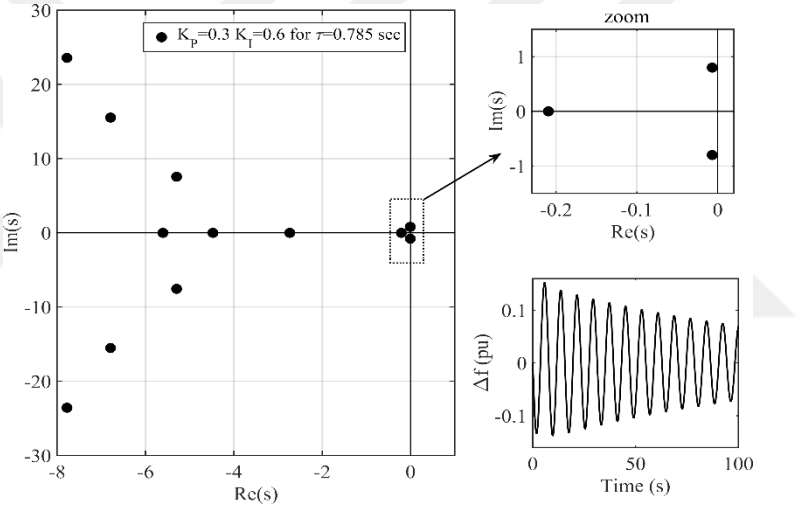

Figure 6.4. Dominant roots distribution by QPmR algorithm and frequency response for $\tau = 0.785\ s$

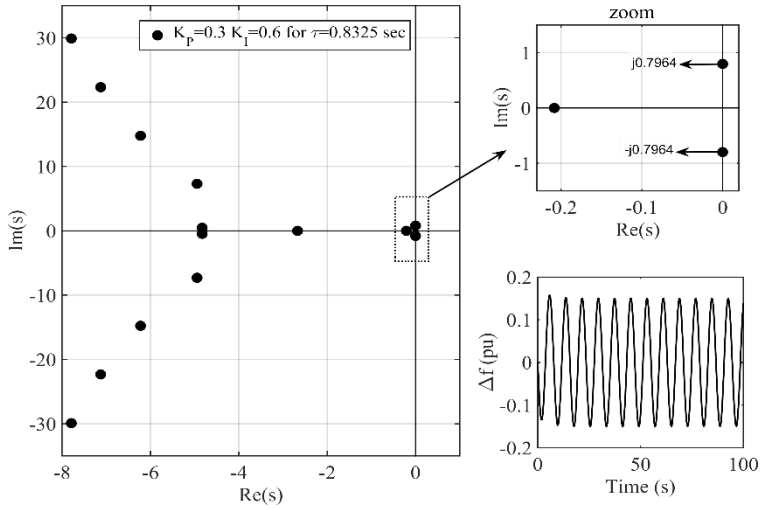

Figure 6.5. Dominant roots distribution by QPmR algorithm and frequency response for $\tau^* = 0.8325\ s$

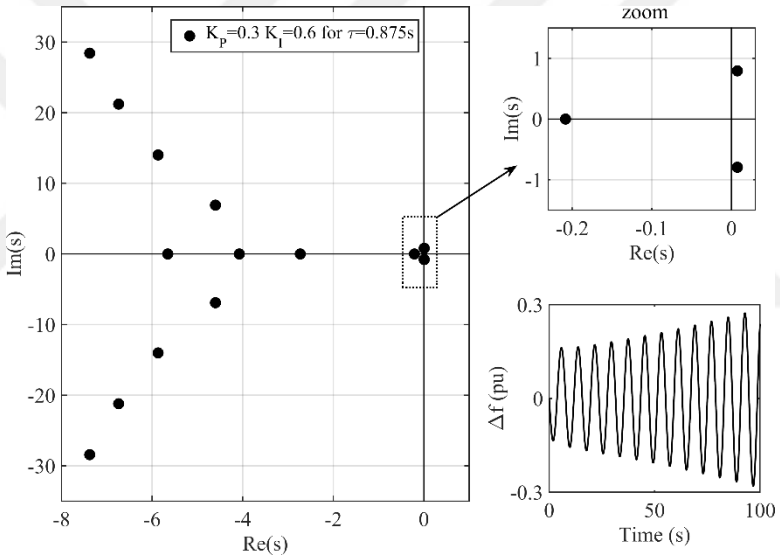

Figure 6.6. Dominant roots distribution by QPmR algorithm and frequency response for $\tau = 0.875\ s$

6.3.2 Verification of two-area LFC-EVs system

The theoretical delay margins computed in two-area LFC-EVs system are verified using time-domain simulations and QPmR algorithm. The controller gains are chosen as $\left(K_P = 0.6,\ K_I = 0.7\right)$ and the EVs participation factor is selected as $\alpha_{01} = \alpha_{11} = 0.3$. It is clear from Table 6.6 that the stability delay margin is computed as $\tau^* = 0.8353s$ for this case. Therefore, Figure 6.7 illustrates that for $\tau = 0.7853\ s,$ which is a smaller value when

compared with the calculated stability margin $\tau^* = 0.8353s,$ all roots are located in the left half of the complex plane and the frequency response has decaying oscillations indicating the LFC-EVs system to be stable. Whereas, the dominant roots distribution of Equation (6.8) and frequency response of the LFC-EVs system for $\tau^* = 0.8353\ s$ is shown in Figure 6.8. It should be noticed that the system has a pair of complex roots on the imaginary axis and the frequency response exhibits sustained oscillations indicating the LFC-EVs system to be marginal stable. If the time delay exceeds the stability delay margin, the system will become unstable due to the growing oscillations in the frequency response. The results shown in Figure 6.8 clearly prove the accuracy of the theoretical stability delay margin. Furthermore, the LFC-EVs system becomes unstable right after the calculated delay margin value. As depicted in Figure 6.9, LFC-EVs system becomes unstable for $\tau = 0.8853s$ due to a pair of complex roots located in the right half of the complex plane and growing oscillations can be observed in the frequency response.

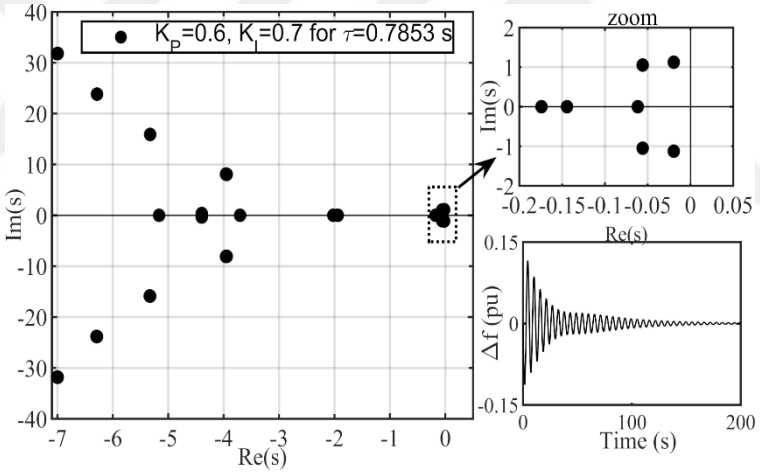

Figure 6.7. Dominant roots distribution by QPmR algorithm and frequency response for $\tau = 0.7853s$

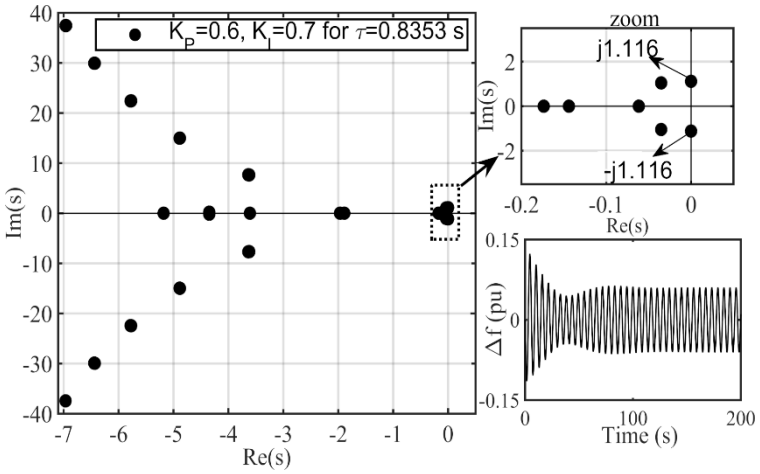

Figure 6.8. Dominant roots distribution by QPmR algorithm and frequency response for $\tau^* = 0.8353s$

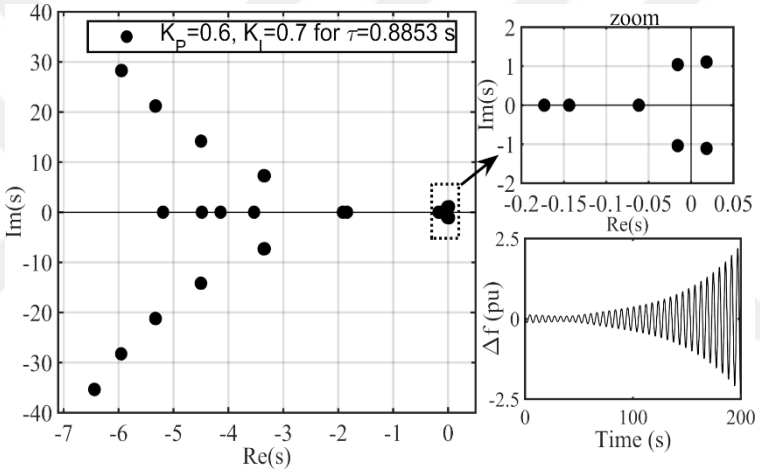

Figure 6.9. Dominant roots distribution by QPmR algorithm and frequency response for $\tau = 0.8853s$

CHAPTER VII

COMPUTATION OF ROBUST STABILITY REGIONS

In this chapter, robust controller design for single and two-area LFC-EVs systems using stability boundary locus method and Kharitonov Theorem is presented. For a given delay, participation factor of EVs and system parameters, stability regions are computed in the parameters space of PI controller gains. Moreover, robust stability regions in the presence of parametric uncertainties are also computed for the system. Furthermore, the obtained results are verified by an independent technique known as QPmR algorithm and simulation studies using Matlab/Simulink program.

7.1 Computation of Stability Regions by Stability Boundary Locus Method

A general procedure used computing stability regions in the controller parameters space has been presented in section 5.1. However, the computation of stability regions assuring the stable operation of single and two-area LFC-EVs system for a given time delay, system parameters and participation factors are presented in this section.

7.1.1 Stability region computation in single-area LFC-EVs system

A step-by-step implementation of the proposed method for identifying the stability regions in the parametric space of controller gains for single-area LFC-EVs system is given below:

Step 1: In order to identify the stability region, it is necessary to obtain the characteristic equation of single-area LFC-EVs system. The characteristic equation given in the form of Equation (3.5) can be easily obtained from the system model shown in Figure 3.1.

Step 2: The characteristic equation of the system for the given parameters ($M = 8.8$, $D = 1$, $T_g = 0.2s$, $T_c = 0.3s$, $T_r = 12s$, $F_P = 1/6$, $\mathrm{R} = 1/11$, $\beta = 21$, $K_{EV} = 1$, $T_{EV} = 0.1s$) is as follows:

$$\Delta(s,\tau) = a_0(s) + a_1(s)e^{-s\tau} = \begin{pmatrix} p_6 s^6 + p_5 s^5 + p_4 s^4 + p_3 s^3 + \\ p_2 s^2 + p_1 s + p_0 \end{pmatrix} + \left(q_4 s^4 + q_3 s^3 + q_2 s^2 + q_1 s + q_0\right)e^{-s\tau} = 0 \tag{7.1}$$

Where,

$$\begin{aligned}
p_6 &= MRT_gT_rT_cT_{EV} \\
p_5 &= DRT_gT_rT_cT_{EV} + MR(T_gT_rT_c + T_rT_cT_{EV} + T_gT_cT_{EV} + T_gT_rT_{EV}) \\
p_4 &= DR(T_gT_rT_c + T_rT_cT_{EV} + T_gT_cT_{EV} + T_gT_rT_{EV}) \\
&\quad + MR(T_rT_c + T_gT_c + T_gT_r + T_cT_{EV} + T_rT_{EV} + T_gT_{EV}) \\
p_3 &= DR(T_rT_c + T_gT_c + T_gT_r + T_cT_{EV} + T_rT_{EV} + T_gT_{EV}) + MR(T_c + T_r + T_g + T_{EV}) \\
&\quad + F_pT_rT_{EV} + K_p[\alpha_0\beta RF_pT_rT_{EV}] \\
p_2 &= DR(T_c + T_r + T_g + T_{EV}) + MR + F_pT_r + T_{EV} \\
&\quad + K_p[\alpha_0\beta R(T_{EV} + F_pT_r)] + K_I[\alpha_0\beta RF_pT_rT_{EV}] \\
p_1 &= DR + 1 + K_p[\alpha_0\beta R] + K_I[\alpha_0\beta R(T_{EV} + F_pT_r)] \\
p_0 &= K_I[\alpha_0\beta R] \\
q_4 &= K_p[\alpha_1\beta RK_{EV}T_gT_rT_c] \\
q_3 &= K_p[\alpha_1\beta RK_{EV}(T_rT_c + T_gT_c + T_gT_r)] + K_I[\alpha_1\beta RK_{EV}T_gT_rT_c] \\
q_2 &= K_p[\alpha_1\beta RK_{EV}(T_c + T_r + T_g)] + K_I[\alpha_1\beta RK_{EV}(T_rT_c + T_gT_c + T_gT_r)] \\
q_1 &= K_p[\alpha_1\beta RK_{EV}] + K_I[\alpha_1\beta RK_{EV}(T_c + T_r + T_g)] \\
q_0 &= K_I[\alpha_1\beta RK_{EV}]
\end{aligned}$$

Step 3: In order to identify boundary of the stability region in $(K_P, K_I)-$plane for a given time delay τ, $s = j\omega_c$ when $\omega_c > 0$ is substituted into Equation (7.1) and a new characteristic equation is obtained as following:

$$\begin{aligned}
\Delta(\mathrm{j}\omega_c,\tau) &= p_6(\mathrm{j}\omega_c)^6 + p_5(\mathrm{j}\omega_c)^5 + p_4(\mathrm{j}\omega_c)^4 + p_3'''(\mathrm{j}\omega_c)^3 + p_2'''(\mathrm{j}\omega_c)^2 + p_1'''(\mathrm{j}\omega_c) \\
&\quad + K_P\left[p_3'(\mathrm{j}\omega_c)^3 + p_2'(\mathrm{j}\omega_c)^2 + p_1'(\mathrm{j}\omega_c)\right] + K_P\left[\begin{pmatrix} q_4'(\mathrm{j}\omega_c)^4 + q_3'(\mathrm{j}\omega_c)^3 \\ +q_2'(\mathrm{j}\omega_c)^2 + q_1'(\mathrm{j}\omega_c) \end{pmatrix}\mathrm{e}^{-\mathrm{j}\omega_c\tau}\right] \\
&\quad + K_I\left[p_2''(\mathrm{j}\omega_c)^2 + p_1''(\mathrm{j}\omega_c) + p_0''\right] + K_I\left[\begin{pmatrix} q_3''(\mathrm{j}\omega_c)^3 + q_2''(\mathrm{j}\omega_c)^2 \\ +q_1''(\mathrm{j}\omega_c) + q_0'' \end{pmatrix}\mathrm{e}^{-\mathrm{j}\omega_c\tau}\right] = 0
\end{aligned} \tag{7.2}$$

It should be noticed that p_6, p_5 and p_4 coefficients in Equation (7.2) are similar to the coefficients given in Equation (7.1). Whereas, the coefficients $p_1^{'''}$, $p_2^{'''}$ and $p_3^{'''}$ in Equation (7.2) represent the terms of p_1, p_2 and p_3 given in Equation (7.1) that neither contain K_P nor K_I terms. On the other hand, p' and q' coefficients in Equation (7.2) corresponds to the terms of p and q terms of Equation (7.1) after K_P is excluded from them. Moreover, p'' and q'' coefficients in Equation (7.2) corresponds to the terms of p and q in Equation (7.1) after K_I is excluded from them.

Step 4: Substituting $e^{-j\omega_c\tau} = \cos(\omega_c\tau) - j\sin(\omega_c\tau)$ into (7.2) and separating the imaginary and real parts, a more compact form of Equation (7.2) is obtained as:

$$\begin{aligned}\Delta(j\omega_c,\tau) &= K_P A_1(\omega_c) + K_I B_1(\omega_c) + C_1(\omega_c) \\ &\quad + j\left[K_P A_2(\omega_c) + K_I B_2(\omega_c) + C_2(\omega_c)\right] = \Re\left\{\Delta(j\omega_c,\tau)\right\} + j\Im\left\{\Delta(j\omega_c,\tau)\right\} = 0\end{aligned} \tag{7.3}$$

where $\Re\{.\}$ represent the real part and $\Im\{.\}$ represent the imaginary part of the new characteristic equation. Whereas, the expressions for A_1, B_1, C_1, A_2, B_2 and C_2 are given as following:

$$\begin{aligned}A_1(\omega_c) &= -p_2'\omega_c^2 + q_4'\omega_c^4\cos(\omega_c\tau) - q_2'\omega_c^2\cos(\omega_c\tau) - q_3'\omega_c^3\sin(\omega_c\tau) + q_1'\omega_c\sin(\omega_c\tau) \\ B_1(\omega_c) &= -p_2''\omega_c^2 + p_0'' - q_2''\omega_c^2\cos(\omega_c\tau) + q_0''\cos(\omega_c\tau) - q_3''\omega_c^3\sin(\omega_c\tau) \\ &\quad + q_1''\omega_c\sin(\omega_c\tau) \\ C_1(\omega_c) &= -p_6\omega_c^6 + p_4\omega_c^4 - p_2\omega_c^2 \\ A_2(\omega_c) &= -p_3'\omega_c^3 + p_1'\omega_c - q_3'\omega_c^3\cos(\omega_c\tau) + q_1'\omega_c\cos(\omega_c\tau) - q_4'\omega_c^4\sin(\omega_c\tau) \\ &\quad + q_2'\omega_c^2\sin(\omega_c\tau) \\ B_2(\omega_c) &= p_1''\omega_c - q_3''\omega_c^3\cos(\omega_c\tau) + q_1''\omega_c\cos(\omega_c\tau) + q_2''\omega_c^2\sin(\omega_c\tau) - q_0''\sin(\omega_c\tau) \\ C_2(\omega_c) &= p_5\omega_c^5 - p_3\omega_c^3 + p_1\omega_c\end{aligned}$$

Step 5: Setting both the real part and imaginary part of $\Delta(j\omega_c,\tau) = 0$ in (7.3) to zero, an equation in the form of (5.6) is obtained. This equation is then solved for (K_P, K_I) to identify the stability boundary locus $\ell(K_P, K_I, \omega_c)$ in the (K_P, K_I) – plane similar to the

one shown in (5.6).This stability boundary is the CRB of the single-area LFC-EVs system. However, a real root of Equation (7.1) may cross the imaginary axis through the origin. It can be observed from Equation (7.3) that such a stability change occurs only for $K_I = 0$ constituting the (RRB) locus of the system. As a result, the $(K_P, K_I) - \text{plane}$ is divided into stable and unstable regions by the RRB locus $K_I = 0$ and the CRB locus $\ell(K_P, K_I, \omega_c)$.

The impact of EVs aggregator participation factor α_1 and the communication time delay τ on the stability region is investigated. For this purpose, the stability region in the $(K_P, K_I) - \text{plane}$ is first obtained without EVs aggregator ($\alpha_1 = 0$). This scheme corresponds to the case where all required control efforts for frequency regulation are provided by the conventional generator $(\alpha_0 = 1)$ and the communication time delay is zero $(\tau = 0)$. The corresponding stability region is illustrated in Figure 7.1.

Then, in order to investigate the impact of EVs aggregator participation factor on the stability region, three different EVs aggregator participation factors are selected, i.e., $\alpha_1 = 0.1,\ 0.2$ and $0.3,$ whereas the time delay is fixed at $\tau = 0.5 \text{ sec}$. These participation factors imply that 10%, 20% and 30% of the required control effort are provided by the EVs aggregator with a time delay of $\tau = 0.5 \text{ sec}$. Figure 7.1 compares the corresponding stability regions. It is observed that the largest region is computed when EVs participation is not considered ($\alpha_1 = 0$). More importantly, the size of stability regions decreases as the EVs participation factor increases, whereas the shape of the regions is unchanged. Figure 7.1 clearly illustrates that the stability regions get smaller as the contribution of EVs aggregator to the frequency regulation increases due to the presence of the communication time delay.

Furthermore, the impact of time delay is investigated for a selected EVs participation factor. Figure 7.2 illustrates the stability regions for $\tau = 0.25s,\ 0.5s,\ 0.75s$ and $1.0s$ when participation factors are chosen as $\alpha_0 = 0.8$ and $\alpha_1 = 0.2,$ respectively. Figure 7.2 clearly shows that the stability regions shrink as the time delay increases from $\tau = 0.25s$ to $\tau = 1.0s.$ Whereas, the shapes of those regions remain unchanged. The stability regions

in Figure 7.1 and Figure 7.2 illustrate that both EVs participation factor and the time delay associated with EVs aggregator have significant adverse effect on the stability regions. These stability regions represent a set of all stabilizing PI controller gains which ensure a stable operation of the LFC-EVs system.

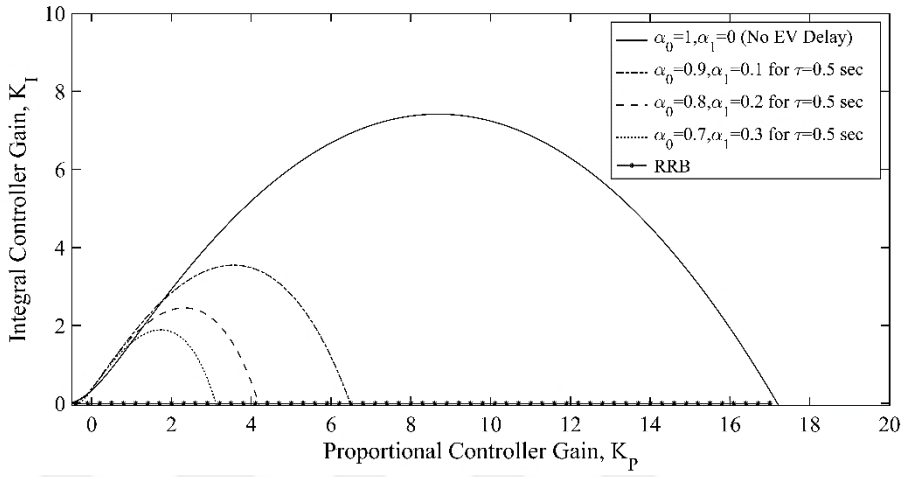

Figure 7.1. Stability regions for different values of EVs aggregator participation factors when $\tau = 0.5s$

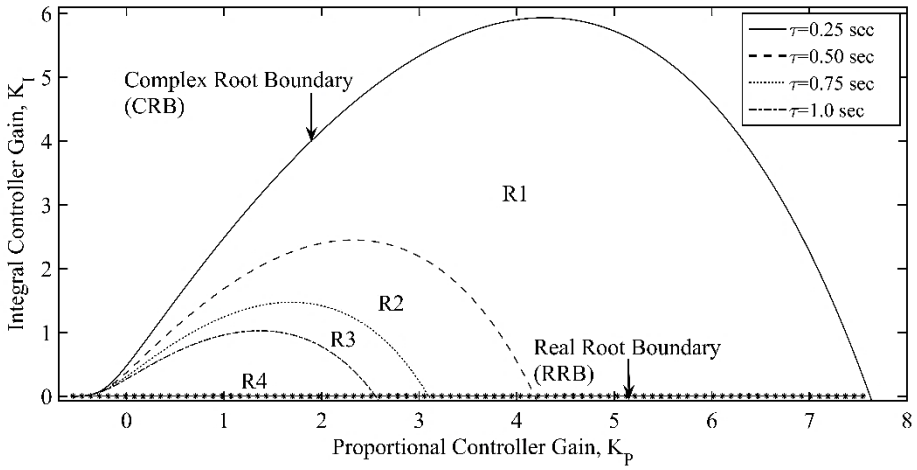

Figure 7.2. Stability region for different communication delays for $\alpha_1 = 0.2$

7.1.2 Verification of stability regions computed for single-area LFC-EVs system

The accuracy of stability boundary locus, CRB and RRB loci, is validated by the time-domain simulations and QPmR algorithm. As shown in Figure 7.3, different values of (K_P, K_I) around the CRB and RRB are selected from the stability region R2 illustrated

by dashed-line in Figure 7.2. Primarily, three different points are selected by fixing the $K_I = 2.0$ controller gain value around the CRB; inside the region R2, on the marginally stable CRB locus and outside the region R2. Then, value of K_P is fixed at 2.0 and on the stable RRB locus and below the RRB locus. The time-domain simulation along with the QPmR algorithm based dominant roots distribution and their zoom picture are shown for $(K_P = 3.0, K_I = 2.0)$ inside R2 in Figure 7.4. It should be observed that the dominant roots are present in stable left half of the $s-$plane and oscillations in the frequency deviations are decaying. Such a scenario indicates asymptotic stability of the single-area LFC-EVs system. Figure 7.5 shows that the LFC-EVs system is marginally stable due to undamped frequency response because of a complex conjugate roots pair present on the imaginary axis for a point $(K_P = 3.203, K_I = 2.0)$ selected on the CRB locus. However, the LFC-EVs becomes unstable for any controller gains outside the region. This happens because of a complex roots pair is located in right half of the $s-$plane. Growing oscillations in frequency response for such a scenario are depicted by Figure 7.6 when $(K_P = 3.406, K_I = 2.0)$.

Figure 7.7 shows a stable operation of the LFC-EVs system for all PI controller gains like; $(K_P = 2.0, K_I = 0.0)$ selected on the RRB locus where Equation (7.1) has a root situated on origin while the remaining roots are present in stable left half of the $s-$plane. Such a scenario infers that characteristic equation (7.1) has a positive real root and the system will become exponentially (non-oscillatory) unstable if PI controller gains are selected below the $K_P - axis$ as depicted in Figure 7.8 for $(K_P = 2.0, K_I = -0.2)$.

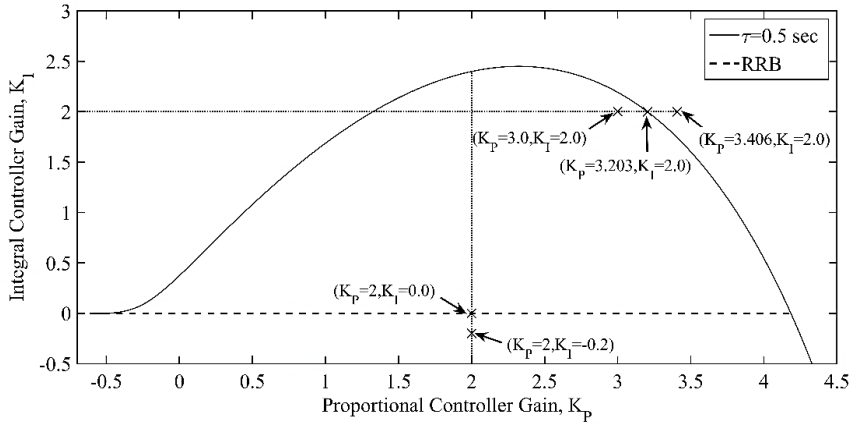

Figure 7.3. Demonstrating the CRB and RRB loci for the region R2

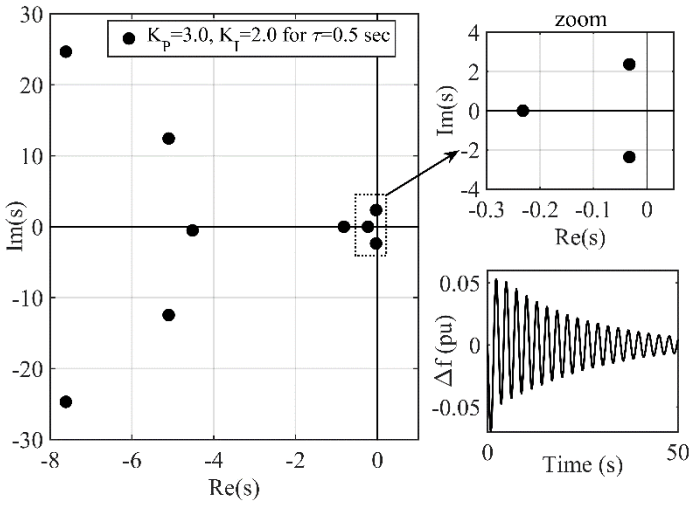

Figure 7.4. Dominant roots distribution inside the stability region and frequency response for stable case

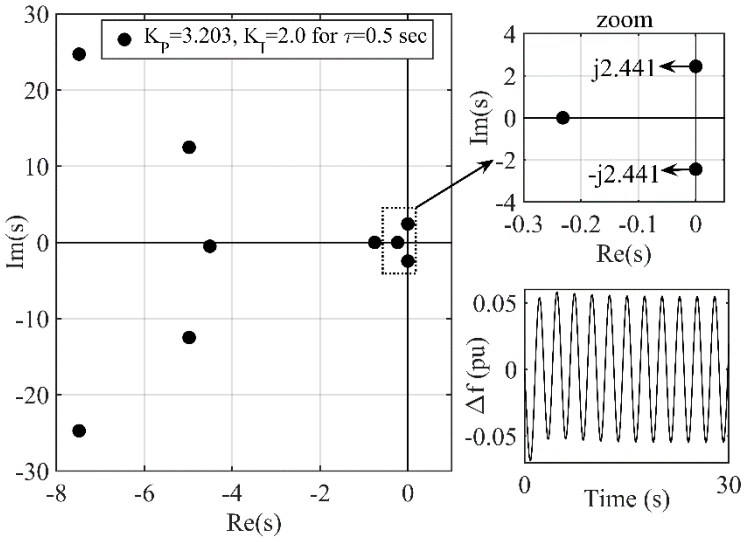

Figure 7.5. Dominant roots distribution on the CRB locus and frequency response for marginally stable case

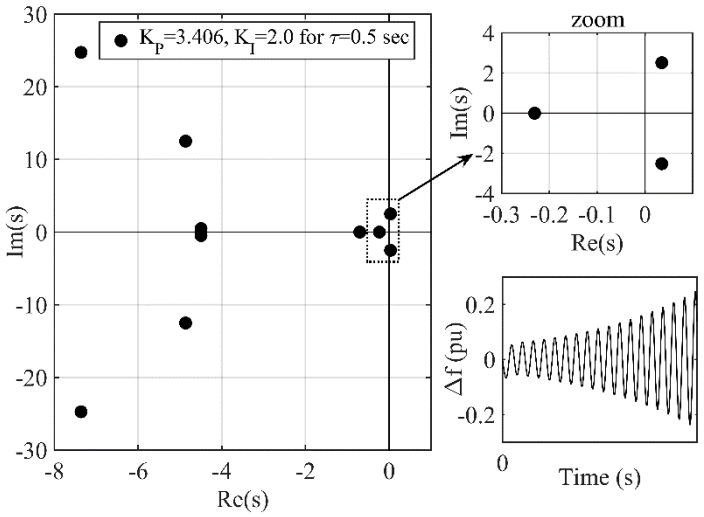

Figure 7.6. Dominant roots distribution outside the stability region and frequency response for unstable case

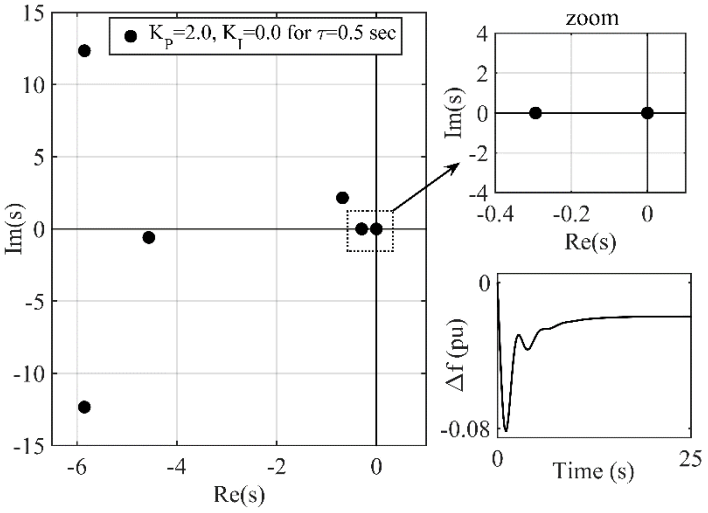

Figure 7.7. Dominant roots distribution on the RRB locus and the frequency response for stable case

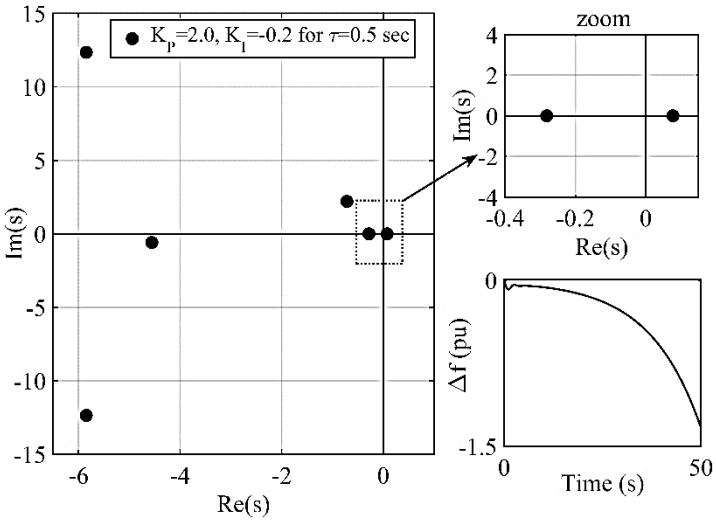

Figure 7.8. Dominant roots distribution below the RRB locus and the frequency response for unstable case

7.1.3 Stability regions in single-area LFC-EVs system with incommensurate delays

In this section, stability regions are obtained by considering incommensurate (not integer multiple of eachother) delays from PI controller to generator and EVs aggregator. The communication time delay from the controller to the conventional generator is represented by τ_1 and to the EVs is represented by τ_2. Figure 7.9 illustrates that both the delays are modelled as exponential transfer functions $e^{-s\tau_1}$ and $e^{-s\tau_2}$.

The incommensurate time delays τ_1 and τ_2 are represented in polar coordinate $(|\tau|,\theta)$ as shown in Figure 7.10. All points are defined as $T(\tau_1,\tau_2)$ on a boundary depending on $(|\tau|,\theta)$ in $(\tau_1,\tau_2)-$space. Angle θ and magnitude $|\tau|$ are defined as $\theta=\tan^{-1}\tau_2/\tau_1$ and $|\tau|=\sqrt{\tau_1^2+\tau_2^2}$. Changing the angle in a range of $\theta\in[0^0-90^0]$ when the magnitude $|\tau|$ is fixed, such a representation allows to investigate the effect of different delay scenarios on the stability regions like; $\tau_1>\tau_2$, $\tau_1=\tau_2$ and $\tau_1<\tau_2$.

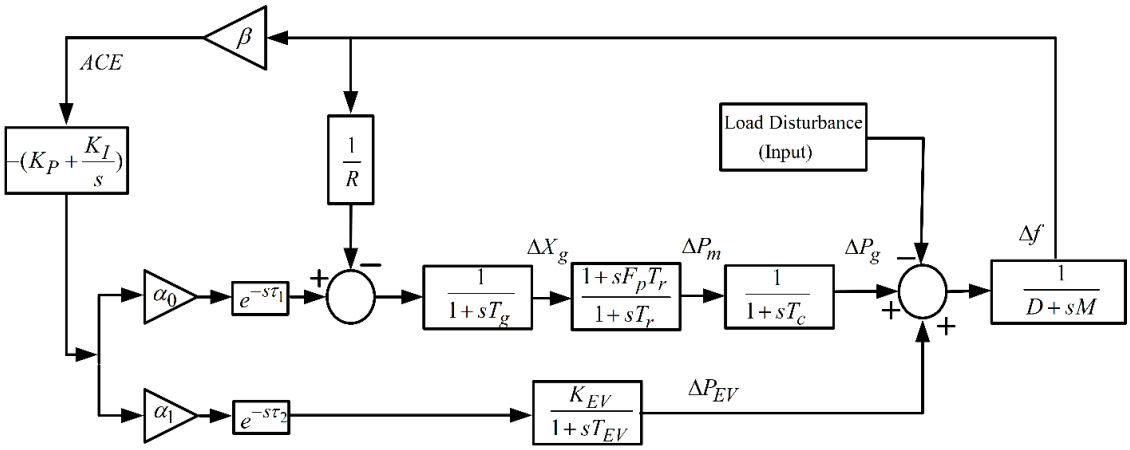

Figure 7.9. Block diagram of a single-area LFC-EVs system with multiple incommensurate delays

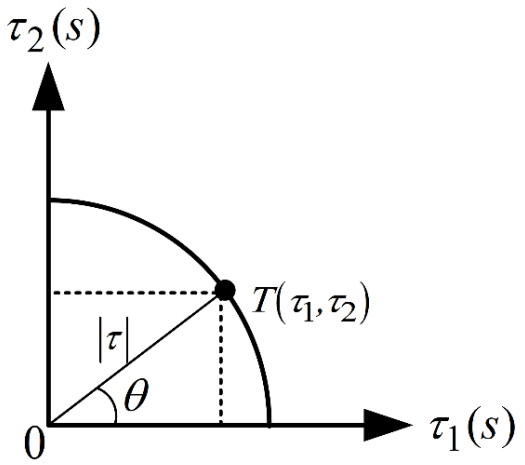

Figure 7.10. Changing of τ_1 and τ_2 time delay values in a direction

A step-by-step implementation of the proposed method for identifying the stability regions in the parametric space of controller gains for single-area LFC-EVs system with incommensurate time delays is given below:

Step 1: The characteristic equation of single-area LFC-EVs system with incommensurate delays can be easily obtained from the system model shown in Figure 7.9.

Step 2: The characteristic equation of the system for the given parameters $(M=8.8,\ D=1,\ T_g=0.2s,\ T_c=0.3s,\ T_r=12s,\ F_P=1/6,\ \mathrm{R}=1/11,\ \beta=21,\ K_{EV}=1,\ T_{EV}=0.1s)$ is as follows:

$$\Delta(s,\tau_1,\tau_2) = a_0(s) + a_1(s)e^{-s\tau_1} + a_2(s)e^{-s\tau_2} = \begin{pmatrix} p_6 s^6 + p_5 s^5 + p_4 s^4 + \\ p_3 s^3 + p_2 s^2 + p_1 s \end{pmatrix} + \left(q_3 s^3 + q_2 s^2 + q_1 s + q_0\right)e^{-s\tau_1} + \left(r_4 s^4 + r_3 s^3 + r_2 s^2 + r_1 s + r_0\right)e^{-s\tau_2} = 0 \quad (7.4)$$

Where,

$$p_6 = MRT_g T_r T_c T_{EV}$$
$$p_5 = DRT_g T_r T_c T_{EV} + MRT_g T_r T_c + MRT_r T_c T_{EV} + MRT_g T_c T_{EV} + MRT_g T_r T_{EV}$$
$$p_4 = DRT_g T_r T_c + DRT_r T_c T_{EV} + DRT_g T_c T_{EV} + DRT_g T_r T_{EV} + MRT_r T_c + MRT_g T_c + MRT_g T_r + MRT_c T_{EV} + MRT_r T_{EV} + MRT_g T_{EV}$$
$$p_3 = DRT_r T_c + DRT_g T_c + DRT_g T_r + DRT_c T_{EV} + DRT_r T_{EV} + DRT_g T_{EV} + MRT_c + MRT_r + MRT_g + MRT_{EV} + F_p T_r T_{EV}$$
$$p_2 = DRT_c + DRT_r + DRT_g + DRT_{EV} + MR + F_p T_r + T_{EV}$$
$$p_1 = DR + 1$$
$$q_3 = K_p[\alpha_0 \beta R F_p T_r T_{EV}]$$
$$q_2 = K_p[\alpha_0 \beta R(T_{EV} + F_p T_r)] + K_I[\alpha_0 \beta R F_p T_r T_{EV}]$$
$$q_1 = K_p[\alpha_0 \beta R] + K_I[\alpha_0 \beta R(T_{EV} + F_p T_r)]$$
$$q_0 = K_I[\alpha_0 \beta R]$$
$$r_4 = K_p[\alpha_1 \beta R K_{EV} T_g T_r T_c]$$
$$r_3 = K_p[\alpha_1 \beta R K_{EV}(T_r T_c + T_g T_c + T_g T_r)] + K_I[\alpha_1 \beta R K_{EV} T_g T_r T_c]$$
$$r_2 = K_p[\alpha_1 \beta R K_{EV}(T_c + T_r + T_g)] + K_I[\alpha_1 \beta R K_{EV}(T_r T_c + T_g T_c + T_g T_r)]$$
$$r_1 = K_p[\alpha_1 \beta R K_{EV}] + K_I[\alpha_1 \beta R K_{EV}(T_c + T_r + T_g)]$$
$$r_0 = K_I[\alpha_1 \beta R K_{EV}]$$

Step 3: The identification of the stability region boundary for given time delays (τ_1, τ_2) or $(|\tau|, \theta)$ is done by substituting $s = j\omega_c$ when $\omega_c > 0$ into the characteristic equation (7.4) as follows:

$$\Delta(j\omega_c, \tau_1, \tau_2) = a_0(j\omega_c) + a_1(j\omega_c)e^{-j\omega_c\tau_1} + a_2(j\omega_c)e^{-j\omega_c\tau_2} = 0 \quad (7.5)$$

Step 4: The coefficients of Equation (7.5) are re-written and the controller gains are extracted to obtain a new equation given as follows:

$$\begin{aligned}\Delta(j\omega_c,\tau_1,\tau_2) &= p_6(j\omega_c)^6 + p_5(j\omega_c)^5 + p_4(j\omega_c)^4 + p_3(j\omega_c)^3 + p_2(j\omega_c)^2 + p_1(j\omega_c) \\ &+ K_P\begin{bmatrix}\{r_4'(j\omega_c)^4 + r_3'(j\omega_c)^3 + r_2'(j\omega_c)^2 + r_1'(j\omega_c)\}e^{-j\omega_c\tau_2} \\ +\{q_3'(j\omega_c)^3 + q_2'(j\omega_c)^2 + q_1'(j\omega_c)\}e^{-j\omega_c\tau_1}\end{bmatrix} \\ &+ K_I\begin{bmatrix}\{r_3''(j\omega_c)^3 + r_2''(j\omega_c)^2 + r_1''(j\omega_c) + r_0''\}e^{-j\omega_c\tau_2} \\ +\{q_2''(j\omega_c)^2 + q_1''(j\omega_c) + q_0''\}e^{-j\omega_c\tau_1}\end{bmatrix} = 0\end{aligned} \tag{7.6}$$

It should be noticed that q' and r' coefficients in (7.6) corresponds to the terms q and r in (7.4) excluding K_P. Whereas, q'' and r'' coefficients in (7.6) represent the q and r terms in Equation (18) excluding K_I.

Step 5: A set of two equations in the form of (5.6) is obtained by simplifying (7.6) further and equating both its imaginary and real parts to zero. The coefficients of $A_1(\omega_c)$, $B_1(\omega_c)$, $C_1(\omega_c)$, $A_2(\omega_c)$, $B_2(\omega_c)$ and $C_2(\omega_c)$ are given as:

$$\begin{aligned}A_1(\omega_c) &= r_4'\omega_c^4\cos(\omega_c\tau_2) - r_2'\omega_c^2\cos(\omega_c\tau_2) - r_3'\omega_c^3\sin(\omega_c\tau_2) + r_1'\omega_c\sin(\omega_c\tau_2) \\ &\quad - q_2'\omega_c^2\cos(\omega_c\tau_1) - q_3'\omega_c^3\sin(\omega_c\tau_1) + q_1'\omega_c\sin(\omega_c\tau_1) \\ B_1(\omega_c) &= -r_2''\omega_c^2\cos(\omega_c\tau_2) + r_0''\cos(\omega_c\tau_2) - r_3''\omega_c^3\sin(\omega_c\tau_2) + r_1''\omega_c\sin(\omega_c\tau_2) \\ &\quad - q_2''\omega_c^2\sin(\omega_c\tau_1) + q_0''\cos(\omega_c\tau_1) + q_1''\omega_c\sin(\omega_c\tau_1) \\ C_1(\omega_c) &= -p_6\omega_c^6 + p_4\omega_c^4 + p_2\omega_c^2 \\ A_2(\omega_c) &= -r_3'\omega_c^3\cos(\omega_c\tau_2) + r_1'\omega_c\cos(\omega_c\tau_2) - r_4'\omega_c^4\sin(\omega_c\tau_2) + r_2'\omega_c^2\sin(\omega_c\tau_2) \\ &\quad - q_3'\omega_c^3\cos(\omega_c\tau_1) + q_1'\omega_c\cos(\omega_c\tau_1) + q_2'\omega_c^2\sin(\omega_c\tau_1) \\ B_2(\omega_c) &= -r_3''\omega_c^3\cos(\omega_c\tau_2) + r_1''\omega_c\cos(\omega_c\tau_2) + r_2''\omega_c^2\sin(\omega_c\tau_2) + r_0''\sin(\omega_c\tau_2) \\ &\quad + q_1''\omega_c\cos(\omega_c\tau_1) + q_2''\omega_c^2\sin(\omega_c\tau_1) - q_0''\sin(\omega_c\tau_1) \\ C_2(\omega_c) &= p_5\omega_c^5 - p_3\omega_c^3 + p_1\omega_c\end{aligned} \tag{7.7}$$

Step 6: In order to identify the CRB locus $\ell(K_P,K_I,\omega_c)$ in the $(K_P,K_I)-$plane, a set of two equations in the form of Equation (5.7) is solved for (K_P,K_I). Also, the RRB $(K_I=0)$, which is the K_P-axis in $(K_P,K_I)-$plane is part of the stability boundary locus because a real root of $\Delta(j\omega_c,\tau_1,\tau_2)=0$ in (7.4) could cross the imaginary axis at

$s = j\omega_c = 0$ only for $K_I = 0$. Consequently, the CRB locus $\ell(K_P, K_I, \omega_c)$ and the RRB locus divide the $(K_P, K_I)-$plane into stable and unstable regions. The stable region yields PI controller gains for which (7.4) has all its roots present in stable left half of the $s-$plane. This indicate that the system is stable for the selected incommensurate time delays (τ_1, τ_2).

The selection of incommensurate delays (τ_1, τ_2) is done by using the polar coordinates and specifying the values of (τ_1, τ_2) by choosing $|\tau|$ and θ. At first, the angle is fixed at $\theta = 30^0$ and stability regions for four different $|\tau|$ values, $|\tau| = 0.5s$, $|\tau| = 0.8s$, $|\tau| = 1.0s$ and $|\tau| = 1.2s$ are obtained for investigate the impact of different values of (τ_1, τ_2). Table 7.1 shows different (τ_1, τ_2) values for this case and the corresponding stability regions are depicted in Figure 7.11. The Figure 7.11 quite evidently shows that size of these stability regions decreases when the magnitude of the delay increases from $|\tau| = 0.5\ s$ to $|\tau| = 1.2\ s$. This results in obtaining smaller set of stabilizing PI controller gains for $\theta = 30^0$. It should be noticed that the angle $\theta = 30^0$ corresponds to the scenario where the delay from the controller to the EVs is smaller than the delay from the controller to the conventional generator, $\tau_2 < \tau_1$.

Moreover, stability regions for $\theta = 45^0$ and 60^0 are obtained. The corresponding stability regions are presented in Figure 7.12 and Figure 7.13, respectively. It should be observed that $\theta = 45^0$ represents the scenario where both the delays are equal $(\tau_1 = \tau_2)$. Comparing the stability regions of Figure 7.12 with that of Figure 7.11, it is evident that the regions computed for $\theta = 45^0$ are smaller than the regions computed for $\theta = 30^0$. This infers that a smaller set of stabilizing controller parameters is obtained when $\tau_1 = \tau_2$ for all $|\tau|$. Figure 7.13 illustrates stability regions for $\theta = 60^0$, which corresponds to the case of $\tau_1 < \tau_2$. It should be noticed that regions get even smaller for $\theta = 60^0$ indicating that an increase in the delay on the EVs side τ_2 significantly affect the size of the regions.

Likewise, the effect of angle θ on the stability regions is investigated. Figure 7.14 depicts the stability regions for $\theta = 30^0$, 45^0 and 60^0 when the delay magnitude $|\tau| = 0.5\text{s}$ is kept constant. The stability regions shrink when θ angle is increased for $\theta \in \left[30^0 - 60^0\right]$. The outermost stability region for $\theta = 30^0$ implies that τ_1 is greater than τ_2. this implies that the effect of delay on the conventional generator side is more on the LFC system than the effect of delay on the EVs side. Besides, the stability region in the center for $\theta = 45^0$ infers that the delay on generator side has an equal impact on the LFC system as that of the delay on EVs side. Whereas, the innermost stability region for $\theta = 60^0$ implies that τ_1 is lesser than τ_2. Such a scenario implies that the effect of delay on EVs side is more significant than the effect of delay on the generator side.

Table 7.1. The value of (τ_1, τ_2) for $\theta = 30^0$

$\lvert\tau\rvert$ sec	Incommensurate Time Delays (*s*)	
	τ_1	τ_2
0.5	0.433	0.25
0.8	0.693	0.4
1.0	0.866	0.5
1.2	1.045	0.6

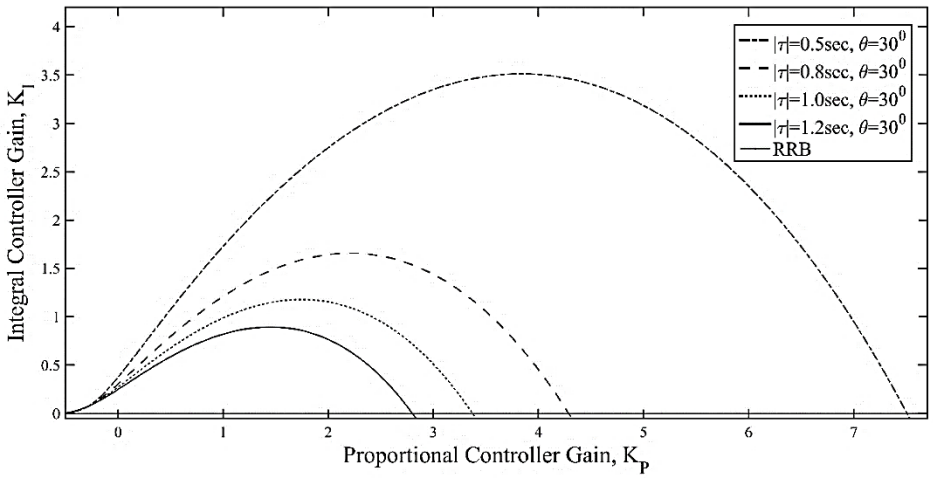

Figure 7.11. Stability regions for different $|\tau|$ values at angle $\theta = 30^0$

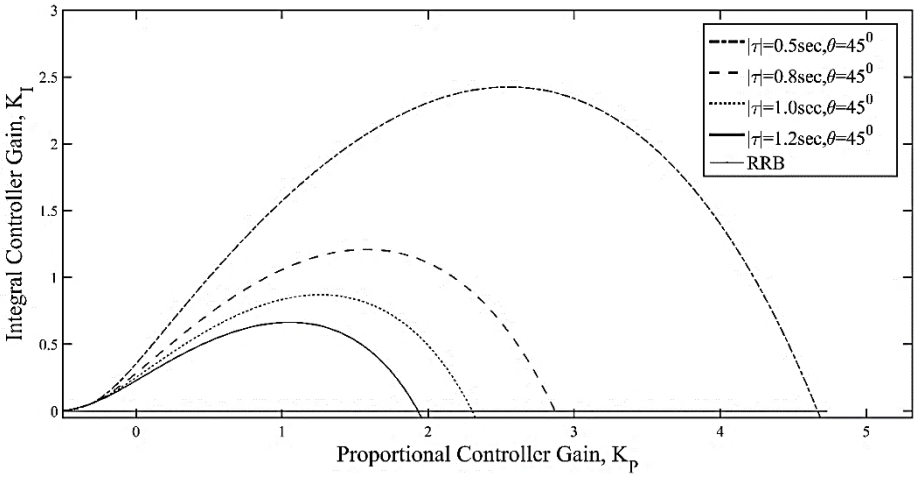

Figure 7.12. Stability regions for different $|\tau|$ values at angle $\theta = 45^0$

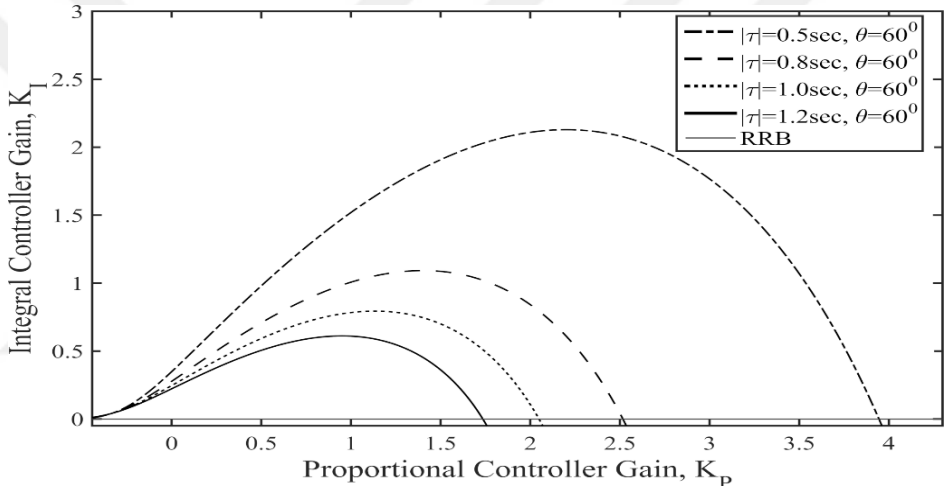

Figure 7.13. Stability regions for different $|\tau|$ values at angle $\theta = 60^0$

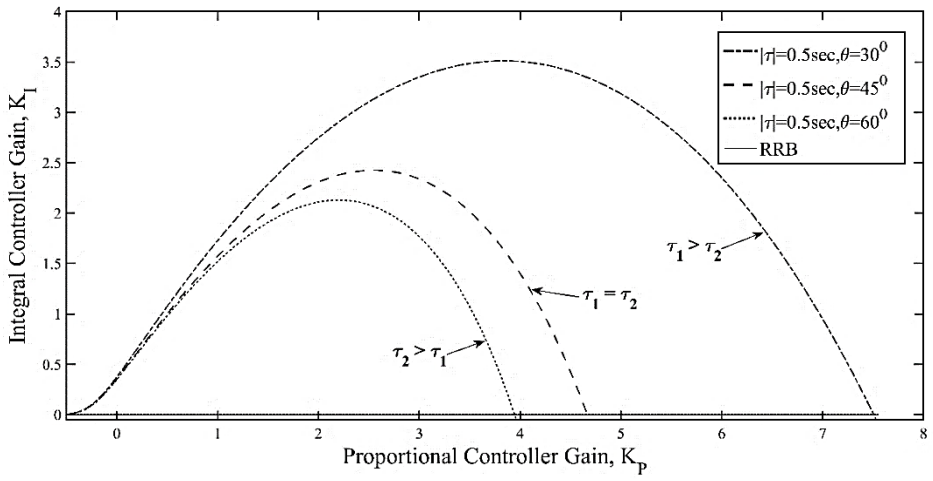

Figure 7.14. Stability regions for the different values angle θ for $|\tau| = 0.5$ sec

7.1.4 Verification of stability regions computed for incommensurate delays case

The accuracy of stability boundary loci CRB and RRB are validated by the time-domain simulations and the QPmR algorithm. For verification studies, the PI controller gains are selected as $(K_P = 3.32, K_I = 3.45)$ on the CRB locus of region shown in Figure 7.11 for $|\tau| = 0.5$ sec and $\theta = 30^0$. Figure 7.15 shows that a complex conjugate roots pair is present on the imaginary axis for $(K_P = 3.32, K_I = 3.45)$ and the LFC-EVs system is marginally stable. Also, sustained oscillations can depicted in the frequency response of Figure 7.15.

The RRB locus is the $K_P -$ axis $(K_I = 0)$ where Equation (7.4) has a root at the origin and the remaining dominant roots are positioned in the left half of $s -$ plane like; $(K_P = 3.00, K_I = 0.00)$. This infers that the Equation (7.4) has a positive real root and the system will become exponentially (non-oscillatory) unstable if PI controller gains are chosen below the $K_P -$ axis. Figure 7.16 clearly shows this case for $(K_P = 3.00, K_I = -0.25)$.

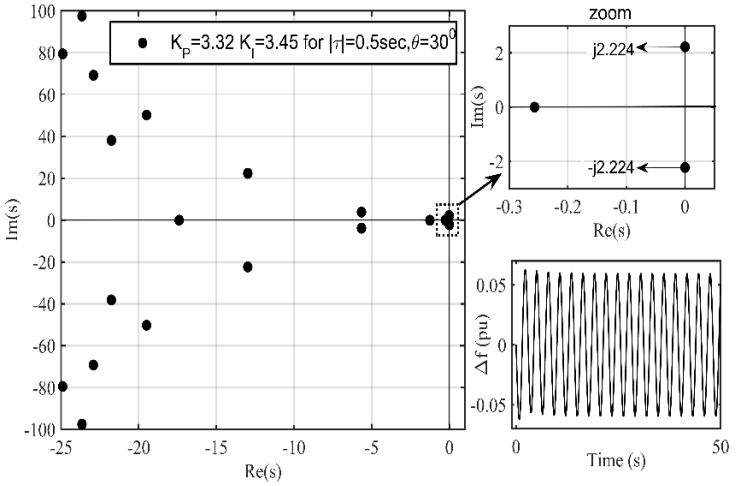

Figure 7.15. Dominant roots distribution on the CRB and frequency response for the marginally stable case

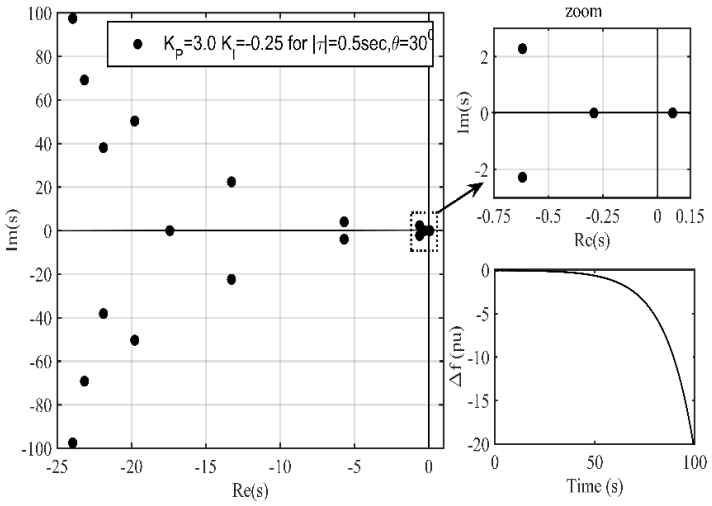

Figure 7.16. Dominant roots distribution below the RRB boundary and frequency response for unstable case

7.1.5 Stability region computation in two-area LFC-EVs system

A step-by-step implementation of the proposed method for identifying the stability regions in the controller parameter space of two-area LFC-EVs system is given below:

Step 1: In order to identify the stability region, it is necessary to obtain the characteristic equation of two-area LFC-EVs system. The characteristic equation given in the form of Equation (3.7) can be easily obtained from the system model shown in Figure 3.2.

Step 2: The characteristic equation of the system for the given parameters $(M_1 = M_2 = 8.8,\quad D_1 = D_2 = 1,\quad T_{g1} = T_{g2} = 0.2s,\quad T_{c1} = T_{c2} = 0.3s,\quad T_{r1} = T_{r2} = 12s,$ $T_{12} = 0.1,\quad F_{P1} = F_{P2} = 1/6,\quad \mathrm{R}_1 = \mathrm{R}_2 = 1/11,\quad \beta_1 = \beta_2 = 21,\quad K_{EV1} = K_{EV2} = 1,$ $T_{EV1} = T_{EV2} = 0.1s)$ is as follows:

$$
\begin{aligned}
\Delta(s,\tau) &= a_0(s) + a_1(s)e^{-\tau s} + a_2(s)e^{-2\tau s} \\
&= \begin{pmatrix} p_{13}s^{13} + p_{12}s^{12} + p_{11}s^{11} + p_{10}s^{10} + p_9 s^9 + p_8 s^8 + \\ p_7 s^7 + p_6 s^6 + p_5 s^5 + p_4 s^4 + p_3 s^3 + p_2 s^2 + p_1 s + p_0 \end{pmatrix} \\
&+ \begin{pmatrix} q_{11}s^{11} + q_{10}s^{10} + q_9 s^9 + q_8 s^8 + q_7 s^7 + \mathrm{q}_6 s^6 + \\ q_5 s^5 + q_4 s^4 + q_3 s^3 + q_2 s^2 + q_1 s + q_0 \end{pmatrix} e^{-\tau s} \\
&+ \begin{pmatrix} r_9 s^9 + r_8 s^8 + r_7 s^7 + r_6 s^6 + r_5 s^5 + \\ r_4 s^4 + r_3 s^3 + r_2 s^2 + r_1 s + r_0 \end{pmatrix} e^{-2\tau s} = 0
\end{aligned}
\tag{7.8}
$$

The coefficients of all the three polynomials $a_0(s)$, $a_1(s)$ and $a_2(s)$ are exactly the same as presented in Appendix A2.

Step 3: The proposed stability boundary locus method requires some modifications for the two-area LFC-EVs system as the coefficients of (7.8) involve some square terms of K_P and K_I controller gains (Sönmez & Ayasun, 2018). The coefficients of $a_0(s)$ polynomial are expressed in terms of PI controller parameters as:

$$
\begin{aligned}
a_0(s) = &\begin{pmatrix} Z_1 s^{13} + Z_2 s^{12} + Z_3 s^{11} + Z_4 s^{10} + Z_6 s^9 + Z_8 s^8 + \\ Z_{10} s^7 + Z_{13} s^6 + Z_{16} s^5 + Z_{19} s^4 + Z_{22} s^3 + Z_{25} s^2 \end{pmatrix} + K_P Z_5 s^{10} + K_P Z_7 s^9 + K_I Z_5 s^9 \\
&+ K_P Z_9 s^8 + K_I Z_7 s^8 + K_P Z_{11} s^7 + {K_P}^2 Z_{12} s^7 + K_I Z_9 s^7 + K_P Z_{14} s^6 + {K_P}^2 Z_{15} s^6 \\
&+ K_I Z_{11} s^6 + 2K_P K_I Z_{12} s^6 + K_P Z_{17} s^5 + {K_P}^2 Z_{18} s^5 + K_I Z_{14} s^5 + 2K_P K_I Z_{15} s^5 \\
&+ {K_I}^2 Z_{12} s^5 + K_P Z_{20} s^4 + {K_P}^2 Z_{21} s^4 + K_I Z_{17} s^4 + 2K_P K_I Z_{18} s^4 + {K_I}^2 Z_{15} s^4 \\
&+ K_P Z_{23} s^3 + {K_P}^2 Z_{24} s^3 + K_I Z_{20} s^3 + 2K_P K_I Z_{21} s^3 + {K_I}^2 Z_{18} s^3 + K_P Z_{26} s^2 + {K_P}^2 Z_{27} s^2 \\
&+ K_I Z_{23} s^2 + 2K_P K_I Z_{24} s^2 + {K_I}^2 Z_{21} s^2 + K_I Z_{26} s + 2K_P K_I Z_{27} s + {K_I}^2 Z_{24} s + {K_I}^2 Z_{27}
\end{aligned}
\tag{7.9}
$$

Where, $Z_1 s^{13}$ corresponds to the coefficient $p_{13}s^{13}$ in Equation (7.8). Similarly, $Z_{25}s^2$ corresponds to the coefficient $p_2 s^2$ given in Equation (7.8) without K_P or K_I terms. Likewise, $Z_{26}s^2$ corresponds to the $p_2 s^2$ coefficient in Equation (7.8) that has K_P terms only. Whereas, $Z_{27}s^2$ corresponds to the $p_2 s^2$ coefficient in Equation (7.8) including ${K_P}^2$ terms only and $Z_{23}s^2$ corresponds to the $p_2 s^2$ coefficient in Equation (7.8) having K_I terms only, $Z_{24}s^2$ corresponds to the $p_2 s^2$ coefficient in Equation (7.8) that includes

the product term of $K_P K_I$ and $Z_{21}s^2$ corresponds to the coefficient $p_2 s^2$ having ${K_I}^2$ terms only. All other coefficients are expressed in a same fashion. Simplifying further yields the following form of $a_0(s)$ polynomial as follows:

$$\begin{aligned} a_0(s) = & \left(\begin{array}{l} Z_1 s^{13} + Z_2 s^{12} + Z_3 s^{11} + Z_4 s^{10} + Z_6 s^9 + Z_8 s^8 + \\ Z_{10} s^7 + Z_{13} s^6 + Z_{16} s^5 + Z_{19} s^4 + Z_{22} s^3 + Z_{25} s^2 \end{array} \right) \\ & + \left(K_P s + K_I \right) \left[Z_5 s^9 + Z_7 s^8 + Z_9 s^7 + Z_{11} s^6 + Z_{14} s^5 + Z_{17} s^4 + Z_{20} s^3 + Z_{23} s^2 + Z_{26} s \right] \\ & + \left(K_P s + K_I \right)^2 \left[Z_{12} s^5 + Z_{15} s^4 + Z_{18} s^3 + Z_{21} s^2 + Z_{24} s + Z_{27} \right] \end{aligned} \tag{7.10}$$

After labeling the terms having $\left(K_P s + K_I \right)^2$ as $Z_b(s)$, the terms having $\left(K_P s + K_I \right)$ as $Z_a(s)$ and the coefficients having neither K_P nor K_I terms as $C(s)$ in (7.10), $a_0(s)$ polynomial can be expressed in a more simpler form as follows:

$$a_0(s) = \left(K_P s + K_I \right)^2 Z_b(s) + \left(K_P s + K_I \right) Z_a(s) + C(s) \tag{7.11}$$

Step 4: The coefficients of $a_1(s)$ polynomial are expressed in terms of PI controller parameters as following:

$$\begin{aligned} a_1(s) = & K_P Y_1 s^{11} + K_P Y_2 s^{10} + K_I Y_1 s^{10} + K_P Y_3 s^9 + K_I Y_2 s^9 + K_P Y_5 s^8 + {K_P}^2 Y_4 s^8 + K_I Y_3 s^8 \\ & + K_P Y_7 s^7 + {K_P}^2 Y_6 s^7 + K_I Y_5 s^7 + 2K_P K_I Y_4 s^7 + K_P Y_9 s^6 + {K_P}^2 Y_8 s^6 + K_I Y_7 s^6 \\ & + 2K_P K_I Y_6 s^6 + {K_I}^2 Y_4 s^6 + K_P Y_{11} s^5 + {K_P}^2 Y_{10} s^5 + K_I Y_9 s^5 + 2K_P K_I Y_8 s^5 + {K_I}^2 Y_6 s^5 \\ & + K_P Y_{13} s^4 + {K_P}^2 Y_{12} s^4 + K_I Y_{11} s^4 + 2K_P K_I Y_{10} s^4 + {K_I}^2 Y_8 s^4 + K_P Y_{15} s^3 + {K_P}^2 Y_{14} s^3 \\ & + K_I Y_{13} s^3 + 2K_P K_I Y_{12} s^3 + {K_I}^2 Y_{10} s^3 + K_P Y_{17} s^2 + {K_P}^2 Y_{16} s^2 + K_I Y_{15} s^2 + 2K_P K_I Y_{14} s^2 \\ & + {K_I}^2 Y_{12} s^2 + K_I Y_{17} s + 2K_P K_I Y_{16} s + {K_I}^2 Y_{14} s + {K_I}^2 Y_{16} \end{aligned} \tag{7.12}$$

Simplifying further yields the following form of $a_1(s)$ polynomial as follows:

$$a_1(s) = \left(K_P s + K_I\right)\left[Y_1 s^{10} + Y_2 s^9 + Y_3 s^8 + Y_5 s^7 + Y_7 s^6 + Y_9 s^5 + Y_{11} s^4 + Y_{13} s^3 + Y_{15} s^2 + Y_{17} s\right] + \left(K_P s + K_I\right)^2\left[Y_4 s^6 + Y_6 s^5 + Y_8 s^4 + Y_{10} s^3 + Y_{12} s^2 + Y_{14} s + Y_{16}\right] \tag{7.13}$$

After labeling the terms having $\left(K_P s + K_I\right)^2$ as $Y_b(s)$ and the terms having $\left(K_P s + K_I\right)$ as $Y_a(s)$ in Equation (7.13), $a_1(s)$ polynomial can be expressed in a more simpler form as following:

$$a_1(s) = \left(K_P s + K_I\right)^2 Y_b(s) + \left(K_P s + K_I\right) Y_a(s) \tag{7.14}$$

Step 4: Likewise, the coefficients of $a_2(s)$ polynomial are expressed in terms of PI controller parameters as follows:

$$\begin{aligned} a_2(s) = {} & K_P{}^2 X_1 s^9 + K_P{}^2 X_2 s^8 + 2K_P K_I X_1 s^8 + K_P{}^2 X_3 s^7 + K_I{}^2 X_1 s^7 + 2K_P K_I X_2 s^7 \\ & + K_P{}^2 X_4 s^6 + K_I{}^2 X_2 s^6 + 2K_P K_I X_3 s^6 + K_P{}^2 X_5 s^5 + K_I{}^2 X_3 s^5 + 2K_P K_I X_4 s^5 \\ & + K_P{}^2 X_6 s^4 + K_I{}^2 X_4 s^4 + 2K_P K_I X_5 s^4 + K_P{}^2 X_7 s^3 + K_I{}^2 X_5 s^3 + 2K_P K_I X_6 s^3 \\ & + K_P{}^2 X_8 s^2 + K_I{}^2 X_6 s^2 + 2K_P K_I X_7 s^2 + K_I{}^2 X_7 s + 2K_P K_I X_8 s + K_I{}^2 X_8 \end{aligned} \tag{7.15}$$

Similar to $a_0(s)$ and $a_1(s)$ polynomials, $a_2(s)$ polynomial is rearranged in terms of $\left(K_P s + K_I\right)$ like; $X_1 s^7\left(K_P s + K_I\right)^2 = K_P{}^2 X_1 s^9 + 2K_P K_I X_1 s^8 + K_I{}^2 X_1 s^7$. Therefore, $a_2(s)$ polynomial is expressed in a more compact form as following:

$$a_2(s) = X_1 s^7\left(K_P s + K_I\right)^2 + X_2 s^6\left(K_P s + K_I\right)^2 + X_3 s^5\left(K_P s + K_I\right)^2 + X_4 s^4\left(K_P s + K_I\right)^2 + X_5 s^3\left(K_P s + K_I\right)^2 + X_6 s^2\left(K_P s + K_I\right)^2 + X_7 s\left(K_P s + K_I\right)^2 + X_8\left(K_P s + K_I\right)^2 \tag{7.16}$$

$$a_2(s) = \left(K_P s + K_I\right)^2\left[X_1 s^7 + X_2 s^6 + X_3 s^5 + X_4 s^4 + X_5 s^3 + X_6 s^2 + X_7 s + X_8\right] \tag{7.17}$$

After labeling the terms having $\left(K_P s + K_I\right)^2$ as $X(s)$ in Equation (7.17), $a_2(s)$ polynomial can be expressed in a more simpler form as following:

$$a_2(s) = \left(K_P s + K_I\right)^2 X\left(s\right) \tag{7.17}$$

Step 5: Using Equations (7.11), (7.14) and (7.17), the characteristic equation (7.8) can be expressed in the following form:

$$\begin{aligned}\Delta\left(s,\tau\right) = a_0(s) + a_1(s)e^{-s\tau} + a_2(s)e^{-2s\tau} = \left(K_P s + K_I\right)Z_a(s) + \left(K_P s + K_I\right)^2 Z_b(s) + C(s) \\ + \left[\left(K_P s + K_I\right)Y_a(s) + \left(K_P s + K_I\right)^2 Y_b(s)\right]e^{-s\tau} + \left[\left(K_P s + K_I\right)^2 X\left(s\right)\right]e^{-2s\tau} = 0\end{aligned} \tag{7.18}$$

Assuming $m = \left(K_P s + K_I\right)$ and rearranging Equation (7.18), it can be expressed in the form of Equatio(7.19) as following:

$$\Delta\left(s,\tau\right) = m\left[Z_a(s) + Y_a(s)e^{-s\tau}\right] + m^2\left[Z_b(s) + Y_b(s)e^{-s\tau} + X\left(s\right)e^{-2s\tau}\right] + C(s) = 0 \tag{7.19}$$

Step 6: Substituting $A(s) = \left[Z_b(s) + Y_b(s)e^{-s\tau} + X\left(s\right)e^{-2s\tau}\right]$, $B(s) = \left[Z_a(s) + Y_a(s)e^{-s\tau}\right]$ in Equation (7.19) yields the following quadratic form of the characteristic equation (7.8):

$$\Delta\left(s,\tau\right) = m^2 A(s) + mB(s) + C(s) = 0 \tag{7.20}$$

The two roots, m_1 and m_2 of (7.20) can be computed using the following Equation (7.21):

$$m_{1,2} = \left(K_P s + K_I\right) = \frac{-B(s) \pm \sqrt{B(s)^2 - 4A(s)C(s)}}{2A(s)} \tag{7.21}$$

Step 7: In order to obtain the stability regions of the two-area LFC-EVs system, $s = j\omega_c$ when $\omega_c > 0$ is substituted into the roots given by (7.21) as following:

$$\left(K_P(j\omega_c) + K_I\right) = \frac{-B(j\omega_c) \pm \sqrt{B(j\omega_c)^2 - 4A(j\omega_c)C(j\omega_c)}}{2A(j\omega_c)} \tag{7.22}$$

$$2A(j\omega_c)\left(jK_P\omega_c + K_I\right) + B(j\omega_c) \mp \sqrt{B(j\omega_c)^2 - 4A(j\omega_c)C(j\omega_c)} = 0 \tag{7.23}$$

Step 8: Substituting $e^{-j\omega_c\tau} = \cos(j\omega_c\tau) - j\sin(j\omega_c\tau)$ into $A(j\omega_c)$ and $B(j\omega_c)$ terms in (7.23) and equating the real $\Re\{\bullet\}$ and imaginary $\Im m\{\bullet\}$ parts of the equation to zero will yield the following set of equations:

$$K_P L_1(\omega_c) + K_I M_1(\omega_c) + N_1(\omega_c) + j\left(K_P L_2(\omega_c) + K_I M_2(\omega_c) + N_2(\omega_c)\right) = 0 \tag{7.24}$$

$$\begin{aligned} K_P L_1(\omega_c) + K_I M_1(\omega_c) + N_1(\omega_c) &= 0 \\ K_P L_2(\omega_c) + K_I M_2(\omega_c) + N_2(\omega_c) &= 0 \end{aligned} \tag{7.25}$$

where $L_1(\omega_c)$ and $M_1(\omega_c)$ belong to the real part of Equation (7.24) including K_P and K_I terms, respectively. Moreover, $L_2(\omega_c)$ and $M_2(\omega_c)$ belong to the imaginary part of Equation (7.24) including K_P and K_I terms, respectively. Also, $N_1(\omega_c)$ and $N_2(\omega_c)$ belong the real and imaginary part of Equation (7.24) neither having K_P nor K_I terms.

Step 9: The set of equations in (7.25) is then solved for K_P and K_I to identify the CRB locus $\ell(K_P, K_I, \omega_c)$ in the $(K_P, K_I)-$plane as following:

$$\begin{aligned} K_P &= \frac{M_1(\omega_c)N_2(\omega_c) - M_2(\omega_c)N_1(\omega_c)}{L_1(\omega_c)M_2(\omega_c) - L_2(\omega_c)M_1(\omega_c)} \\ K_I &= \frac{L_2(\omega_c)N_1(\omega_c) - L_1(\omega_c)N_2(\omega_c)}{L_1(\omega_c)M_2(\omega_c) - L_2(\omega_c)M_1(\omega_c)} \end{aligned} \tag{7.26}$$

In addition to complex root crossing the imaginary axis, some roots of (7.8) may cross the imaginary axis through the origin. It can be observed from (7.25) that such a stability change occurs only for $K_I = 0$ determining the RRB locus. The CRB and RRB loci divide the $(K_P, K_I)-$plane into stable and unstable regions.

It is evident from Equation (7.21) that the two-area LFC-EVs system yields two different

roots m_1 and m_2, which correspond to two different CRBs. Both the CRBs and the RRB are shown in Figure 7.17 when the communication time delay $\tau = 1.0s$. It is observed that both the CRBs for the m_1 and m_2 together yield a marginally stable system. This can be observed from Figure 7.18 that CRB of m_1 shown by solid line and CRB of m_2 represented by dashed line combine to form a stability region when $\tau = 1.0$s.

The impact of participation factors of EVs aggregator $(\alpha_{11} = \alpha_{12} = \alpha_1)$ in both control areas on the stability region is investigated. In order to investigate the impact of both EVs aggregators participation factor on the stability region, three different EVs participation factors are selected, i.e., $\alpha_1 = 0.1,\ 0.2$ and $0.3,$ whereas the time delay is fixed at $\tau = 1.0s$. These participation factors imply that 10%, 20% and 30% of the required control effort are provided by the EVs aggregators with a time delay of $\tau = 1.0s$. Figure 7.19 compares the corresponding stability regions. It is observed that the largest region is computed when EVs participation is least $(\alpha_1 = 0.1)$. More importantly, the size of stability regions decreases as the EVs participation factor increases, whereas the shape of the regions is unchanged. Figure 7.19 clearly illustrates that the stability regions get smaller as the contribution of EVs aggregators to the frequency regulation increases due to the presence of the communication time delays.

Finally, the impact of communication time delays τ is investigated for a selected EVs participation factor. Figure 7.20 illustrates the stability regions for $\tau = 0.5s,\ 0.75s$ and $1.0s,$ when the EVs participation factor is chosen as $\alpha_1 = 0.2$. Figure 7.20 clearly shows that the stability regions shrink as the time delay increases from $\tau = 0.5s$ to $\tau = 1.0s,$ whereas their shapes remain unchanged. The stability regions in Figure 7.19 and Figure 7.20 illustrate that both EVs participation factor and the time delay associated with EVs aggregator have significant adverse effect on the stability regions. These stability regions represent a set of all stabilizing PI controller gains which ensure a stable operation of the LFC-EVs system.

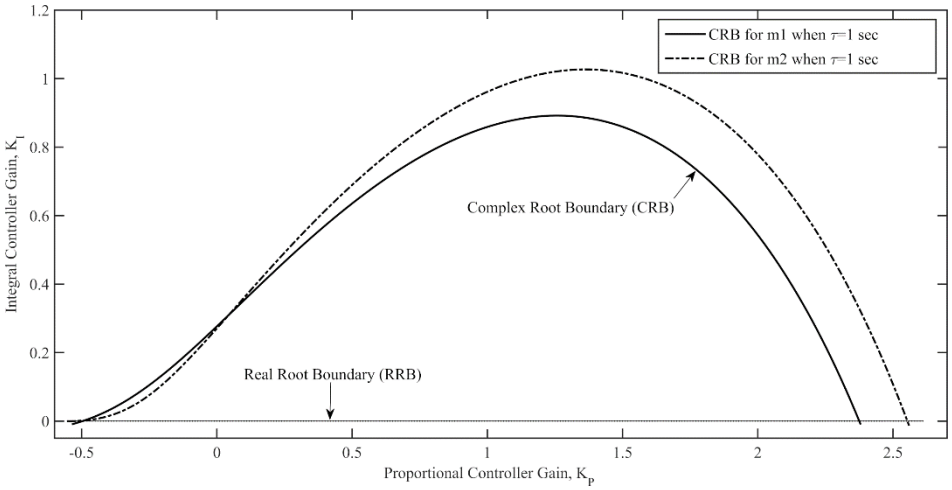

Figure 7.17. CRBs and RRB of m_1 and m_2 when $\tau = 1.0s$

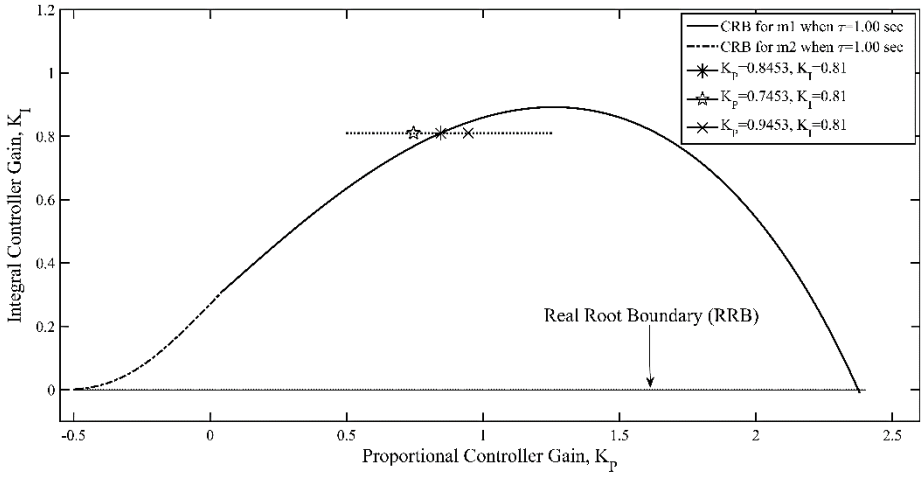

Figure 7.18. Stability region constituted by the combined CRBs of m_1 and m_2

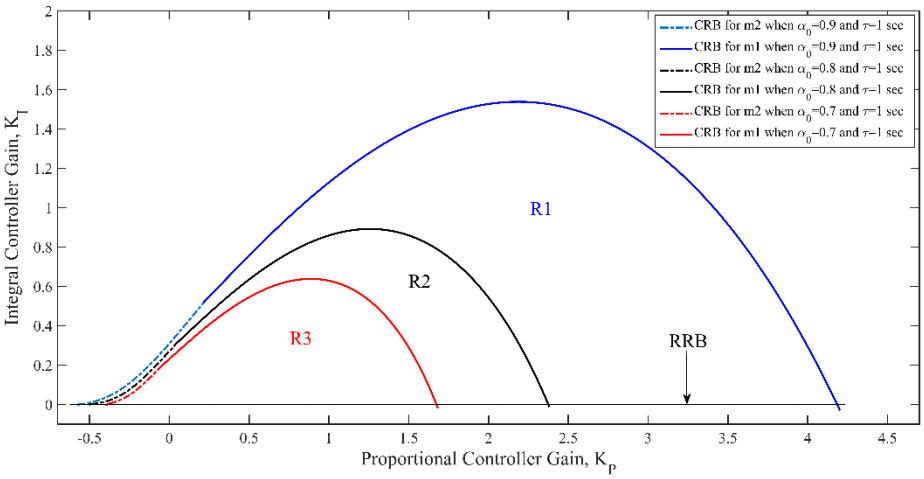

Figure 7.19. Impact of EVs participation factor on stability regions

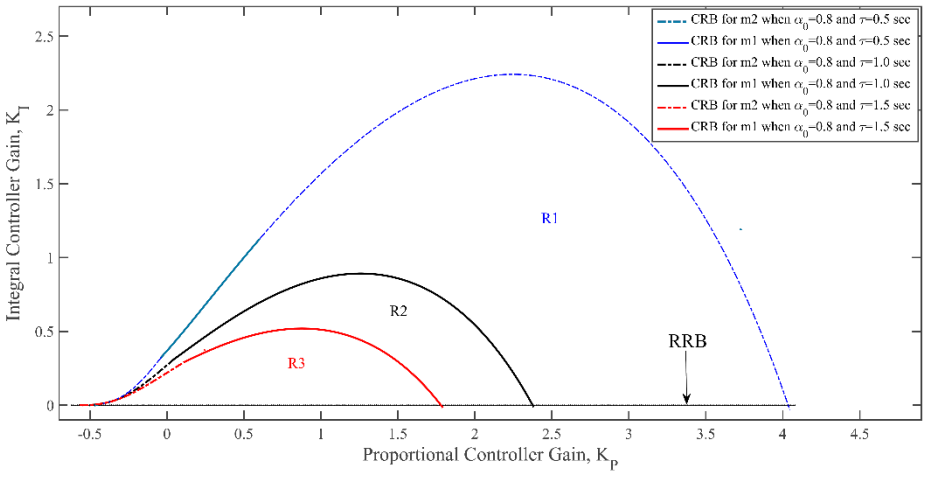

Figure 7.20. Impact of time delay magnitude on stability regions

7.1.6 Verification of stability regions computed for two-area LFC-EVs system

As shown in Figure 7.18, three different test points are selected around the CRB to prove the accuracy of this boundary locus. The integral controller gain value is fixed at $K_I = 0.81$ and the points are selected by choosing different values of K_P. The point inside the region is selected for demonstrating the system response for stable case. Whereas, the point selected exactly on the CRB illustrates marginally stable case and the point outside the region shows system response for unstable case. The time-domain simulation along with the QPmR algorithm based dominant roots distribution and their zoom picture are shown for $(K_P = 0.9453, K_I = 0.81)$ inside the region in Figure 7.21. It should be observed that the dominant roots are located in stable left half of the $s-$plane and a decay in the oscillations of the frequency response can be observed. This indicates that the LFC-EVs system is asymptotic stable. Figure 7.22 shows that the LFC-EVs system is marginally stable due to undamped frequency response because of a complex conjugate roots pair located on the imaginary axis for a point $(K_P = 0.8453, K_I = 0.81)$ selected on the CRB locus. However, the LFC-EVs becomes unstable for any controller gains outside the region. This happens because of a complex roots pair located in the right half of the $s-$plane and the frequency response has growing oscillations as depicted in Figure 7.23 for $(K_P = 0.7453, K_I = 0.81)$.

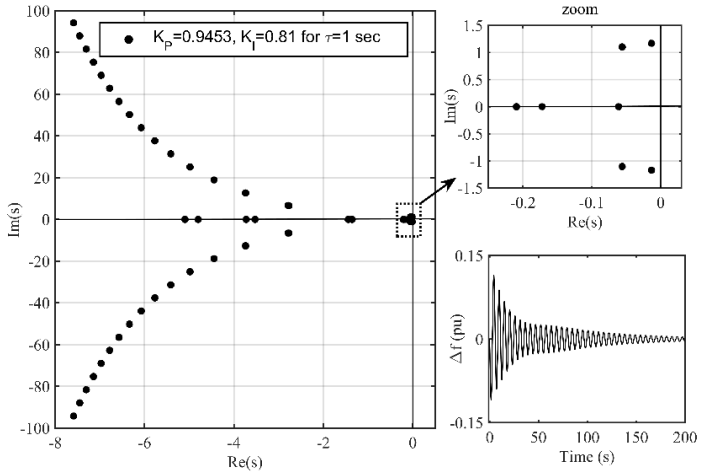

Figure 7.21. Dominant roots distribution and frequency response for stable case

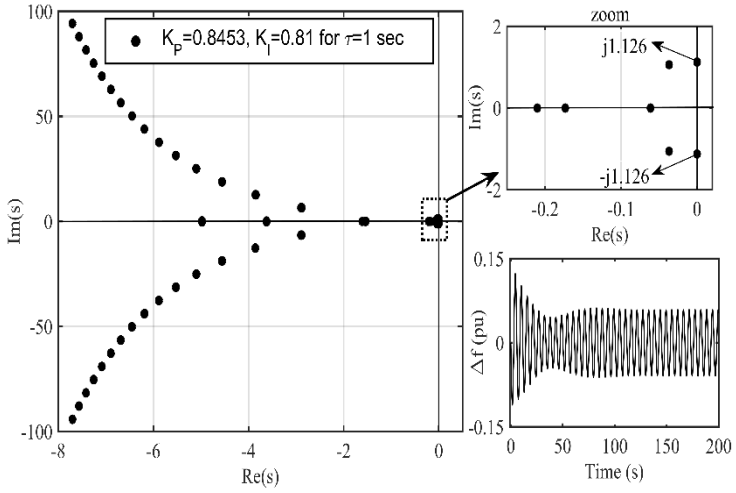

Figure 7.22. Dominant roots distribution and frequency response for marginally stable case

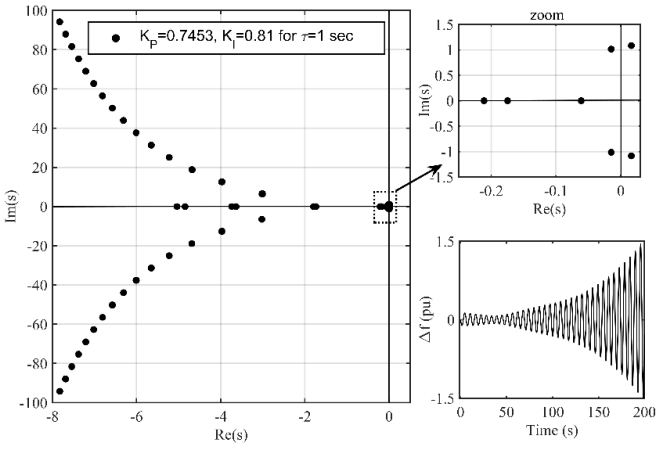

Figure 7.23. Dominant roots distribution and frequency response for unstable case

7.2 Computation of Robust Stability Regions by Kharitonov Theorem

In the modern day complex power systems, the parametric uncertainties are a major issue. Therefore, it is very essential that the control technique being applied to the LFC should be robust toward the parametric uncertainties of the system. Therefore, during the design of a controller, it is important to check whether the controller has the capability to deal with the parameter uncertainties or not. Robust stability regions comprised of stabilizing controller parameters, which assure stable operation of the LFC-EVs system despite of parametric uncertainties are comprehensively investigated in this section.

7.2.1 Robust stability region computation in single-area LFC-EVs system

A step-by-step implementation of the proposed method for identifying the robust stability regions in the controller parameter space for single-area LFC-EVs system is given below:

Step 1: The variations of system parameters under an uncertainty of $\delta = 10\%$ are computed. Also, the time delay and participation factors are selected as $\tau = 0.5s$ and $(\alpha_0 = 0.8, \alpha_1 = 0.2)$, respectively. The computed parameters are given as following:

$M \in [7.92 \quad 9.68]$, $D \in [0.9 \quad 1.1]$, $T_g \in [0.18 \quad 0.22]$, $T_c \in [0.27 \quad 0.33]$,

$T_r \in [10.8 \quad 13.2]$, $F_p \in [0.15 \quad 0.183]$, $R \in [0.0818 \quad 0.1]$, $K_{EV} \in [0.9 \quad 1.1]$,

$T_{EV} \in [0.09 \quad 0.11]$.

Step 2: The upper and lower limit values of the coefficients of characteristic equation (7.1) in terms of system parameters are computed as follows:

$p_6 \in [0.0306 \quad 0.1020]; p_5 \in [0.6299 \quad 1.7200]; p_4 \in [3.9081 \quad 8.7562];$
$p_3''' \in [7.9301 \quad 14.6556]; p_3' \in [0.2004 \quad 0.4472]; p_2''' \in [3.1930 \quad 5.0226];$
$p_2'' \in [0.2004 \quad 0.4472]; p_2' \in [2.3505 \quad 4.2504]; p_1''' \in [1.0736 \quad 1.1100];$
$p_1'' \in [2.3505 \quad 4.2504]; p_1' \in [1.3745 \quad 1.6800]; p_0'' \in [1.3745 \quad 1.6800];$
$q_4' \in [0.1623 \quad 0.4427]; q_3' \in [1.5181 \quad 3.3877]; q_3'' \in [0.1623 \quad 0.4427];$
$q_2' \in [3.4793 \quad 6.3525] q_2'' \in [1.5181 \quad 3.3877]; q_1' \in [0.3093 \quad 0.4620];$
$q_1'' \in [3.4793 \quad 6.3525]; q_0'' \in [0.3093 \quad 0.4620];$

Step 3: The stability regions for each vertex polynomial described in Equation (5.12) are computed with help of Equations (5.6) and (5.7). As a results, intersection of all the four stability regions $\mathrm{G_c}(\omega, \mathrm{K_P}, \mathrm{K_I}) = \bigcap_{\eta=1}^{4} \mathrm{G}_{\mathrm{c}\eta}(\omega, \mathrm{K_P}, \mathrm{K_I})$ is the robust stability region of the single-area LFC-EVs system and the controller gains constituting the robust stability region are the robust controller gains.

A robust stability region computed for the aforementioned parameters, time delay and participation factors is depicted in Figure 7.24. It can be seen that four different stability regions shown by blue, yellow, green and red colors represent the four vertex polynomials. All those regions have an intersectional area filled with grey color. This intersection of all the four stability regions in the parameter space of PI controller gains is the robust stability region of single-area LFC-EVs system. Moreover, the impact of communication time delay for a selected EVs participation factor on single-area LFC-EVs system is investigated. Figure 7.25 illustrates the robust stability regions R3, R2 and R1 computed for corresponding communication delays $\tau = 0.125s$, $\tau = 0.25s$ and $\tau = 0.5s$, respectively. Also, the parametric uncertainties are fixed at $\delta = 10\%$ and the participation factors at $(\alpha_0 = 0.8,\ \alpha_1 = 0.2)$. Figure 7.25 clearly shows that the robust stability regions shrink as the time delay increases from $\tau = 0.125s$ to $\tau = 0.5s$. However, the shapes of each of the three regions show a slight change.

Furthermore, the impact of EVs aggregator participation factor on the stability region is investigated. Three different EVs aggregator participation factors are selected, i.e., $\alpha_1 = 0.1,\ 0.2$ and $0.3,$ whereas the time delay and parametric uncertainties are kept fixed at $\tau = 0.25s$ and $\delta = 10\%$, respectively. These participation factors imply that 10%, 20%

and 30% of the required control effort are provided by the EVs aggregator with a time delay of $\tau = 0.25s$. Figure 7.26 compares the corresponding stability regions A3, A2 and A1. It is observed that the largest region A3 is obtained when EVs participation is minimum ($\alpha_1 = 0.1$). More importantly, the size of stability regions decreases as the EVs participation factor increases. Whereas, the shape of the regions remains unchanged.

Additionally, the impact of parametric uncertainties on the robust stability regions computed in the space of PI controller gains is examined. Figure 7.27 shows robust stability regions T3, T2 and T1 corresponding to the parametric uncertainties $\delta = 5\%$, $\delta = 10\%$, and $\delta = 15\%$, respectively. The time delay and the participation factors are kept fixed at $\tau = 0.25s$ and $(\alpha_0 = 0.8,\ \alpha_1 = 0.2)$, respectively. It can be observed from Figure 7.27 that the largest region T3 is obtained when the parametric uncertainties are minimum $(\delta = 5\%)$. Also, the size of the robust stability regions decreases as the parametric uncertainties increase while the shape of the regions remains unchanged.

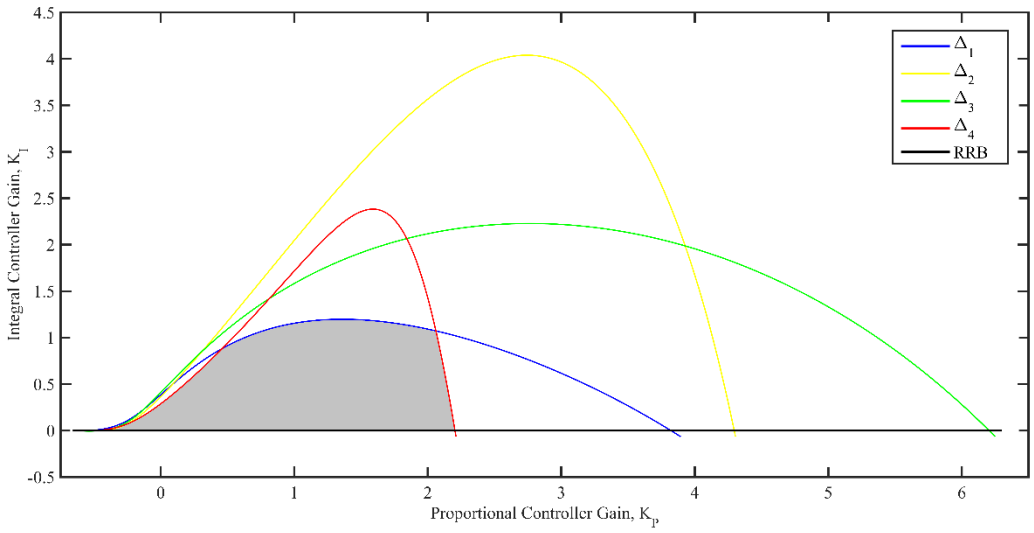

Figure 7.24. Robust stability region for single-area LFC-EVs system when $\tau = 0.5s$, $\delta = 10\%$ and $\alpha_0 = 0.8$

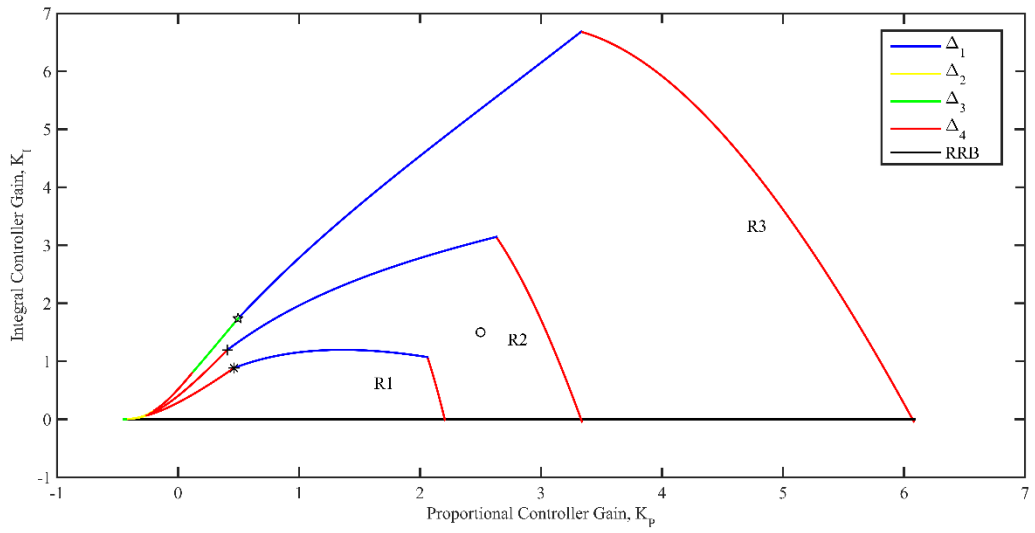

Figure 7.25. Effect of time delay τ on robust stability regions when $\delta = 10\%$ and $\alpha_0 = 0.8$

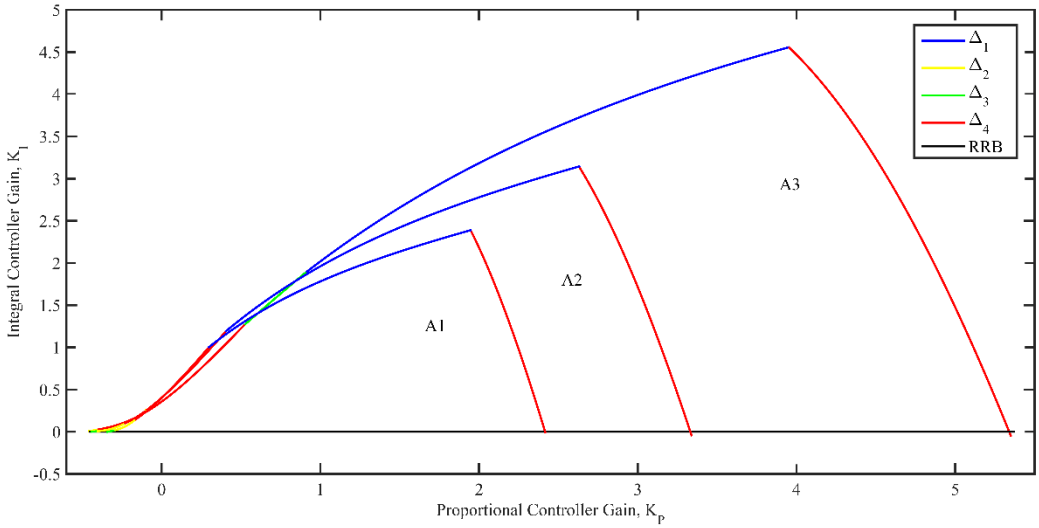

Figure 7.26. Effect of participation ratios α_0 and α_1 on robust stability regions when $\tau = 0.25s$ and $\delta = 10\%$

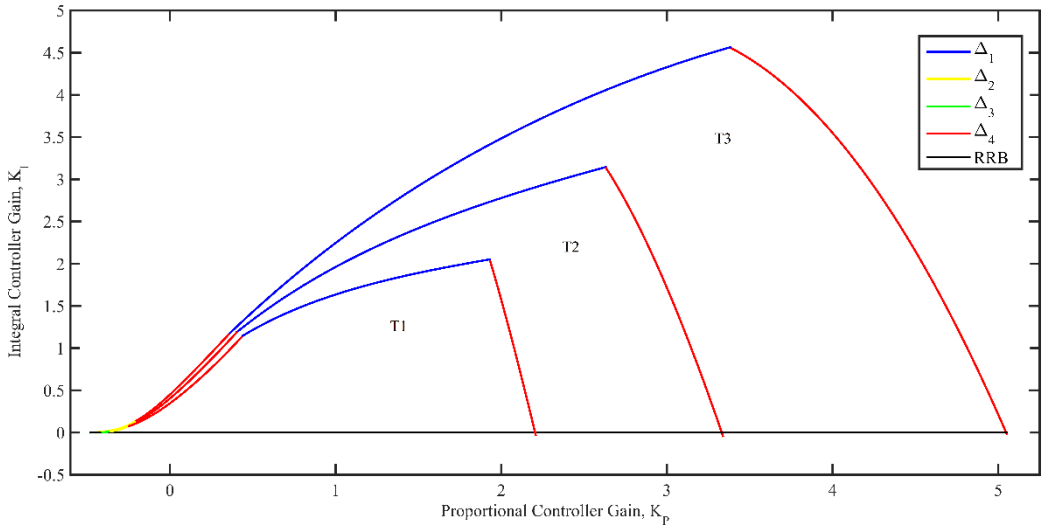

Figure 7.27. Effect of parametric uncertainties δ on robust stability regions when $\tau = 0.25s$ and $\alpha_1 = 0.2$

7.2.2 Verification of robust stability regions computed for single-area LFC-EVs system

The accuracy of the theoretically computed robust stability boundary locus, CRB is validated by the time-domain simulations. Three different points in Figure 7.25 are selected to verify the robustness of each of the stability regions computed in the presence of parametric uncertainties. Those points are given as following; $(K_P = 0.4621, K_I = 0.8837)$ shown by '*' sign on the CRB of R1, $(K_P = 0.4083, K_I = 1.196)$ shown by '×' sign on the CRB of R2 and $(K_P = 0.4966, K_I = 1.738)$ shown by '☆' sign on the CRB of R3. It can be observed from Figure 7.28 that the frequency response of the system at each of the three points is stable hence guaranteeing the stable operation of the system. It is also very important to verify the robustness of the stability regions when the parametric values are randomly selected within the defined intervals. Figure 7.29 shows four different frequency responses of the system at a point $(K_P = 2.5, K_I = 1.5)$ shown by '0' sign inside the region R2 of Figure 7.25 to verify the robustness of the stability region. At first nominal parametric values are selected and the frequency response of the system is analyzed by time domain simulations. The solid line in Figure 7.29 confirms stable operation of the system. Likewise, the dotted and dashed lines also show a stable frequency response for minimum

and maximum parametric values, respectively. Moreover, random parametric values are selected to verify the frequency response of the single-area LFC-EVs system. It can be observed by the dashed-dotted line in Figure 7.29 that the system shows a stable response. Likewise, response of the single-area LFC-EVs system against a large load disturbance shown in Figure 7.30 is analyzed. Three different responses for three different sets of participation ratios $(\alpha_0 = 0.9, \alpha_1 = 0.1)$, $(\alpha_0 = 0.8, \alpha_1 = 0.2)$ and $(\alpha_0 = 0.7, \alpha_1 = 0.3)$ are shown by dotted, solid and dashed lines in Figure 7.31, respectively. It can be observed that the system shows stable frequency responses for the selected robust controller gains under such a large load disturbance, thereby verifying the robustness of stability regions.

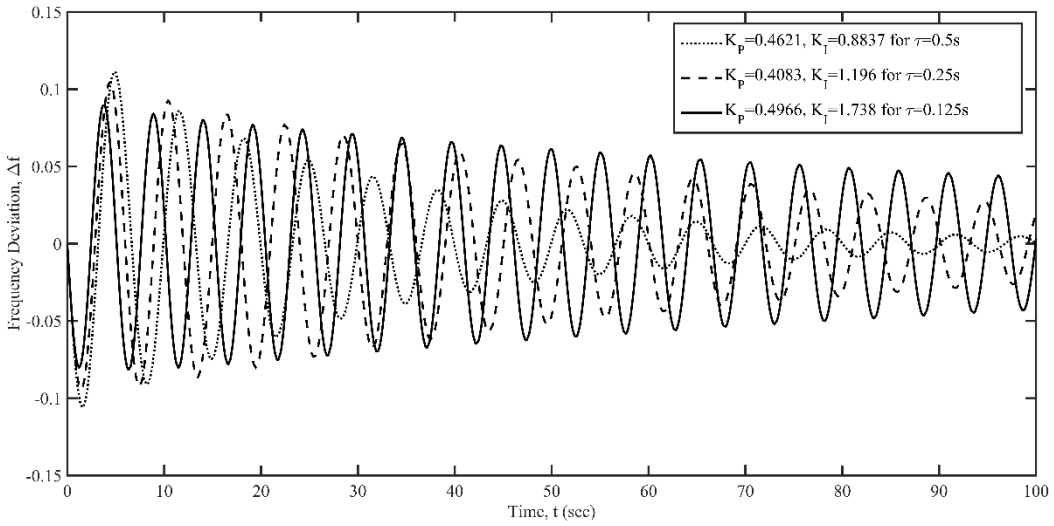

Figure 7.28. Verification of the CRBs of the regions R1, R2 and R3

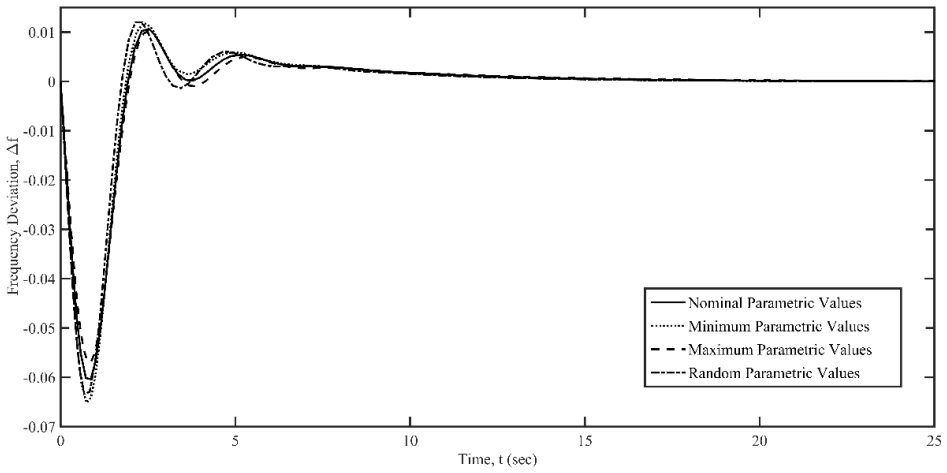

Figure 7.29. Verification of the robust stability region R2 using random parametric values within the defined intervals.

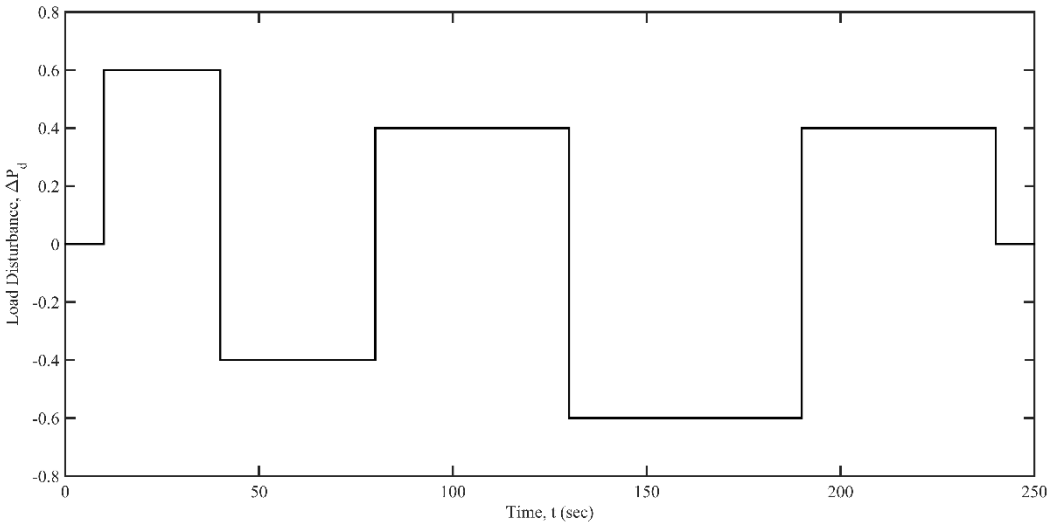

Figure 7.30. A large load disturbance scenario

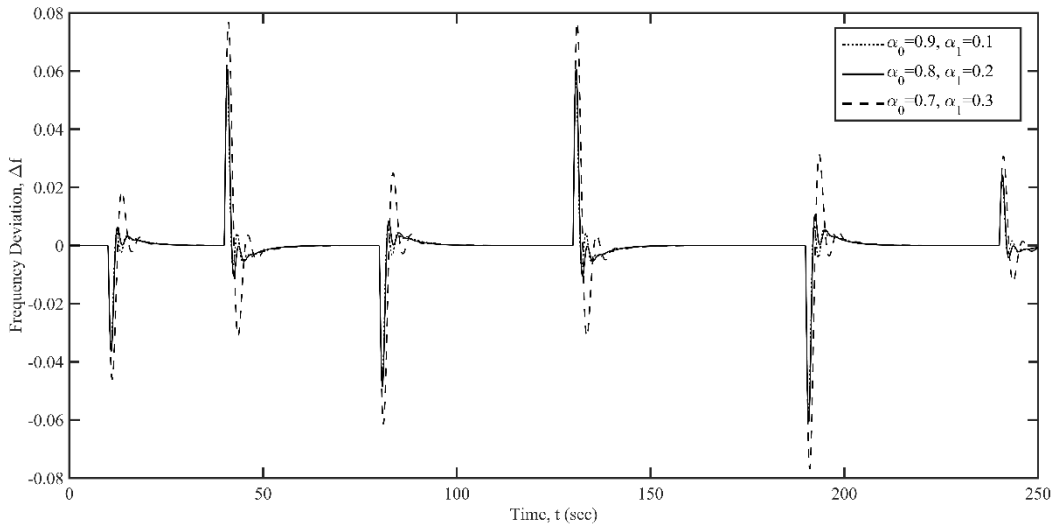

Figure 7.31. Frequency response of the system for the selected robust controller gains under large load disturbance

7.2.3 Robust stability region computation in two-area LFC-EVs system

In this section, robust controller parameters of time-delayed two-area LFC-EVs system shown in Figure 3.2 are computed. It is important to mention here that both the areas are assumed to be weekly coupled and therefore, the tie-line power exchange between both the areas is insignificant to be considered (Lamba *et al.*, 2019). Moreover, the parametric values considered for the first area are exactly the same as those considered for single-area LFC-EVs system (Ko and Sung, 2017a) and its results are already presented in

Section 7.2.1. Whereas, the parametric values considered for the second area are same as that of area 1 reported by (Jiang *et. al* 2011) except for the reheat turbine whose parametric values are considered similar to the one reported by (Ko and Sung, 2017a). A step-by-step implementation of the proposed method for identifying the robust stability regions in the controller parameter space for single-area LFC-EVs system is given below:

Step 1: The variations of system parameters under an uncertainty of $\delta = 10\%$ are computed. Also, the time delay and participation factors are selected as $\tau = 0.25s$ and ($\alpha_0 = 0.8, \alpha_1 = 0.2$), respectively.

$M \in [9 \quad 11]$, $D \in [0.9 \quad 1.1]$, $T_g \in [0.09 \quad 0.11]$, $T_c \in [0.27 \quad 0.33]$, $T_r \in [10.8 \quad 13.2]$,
$F_p \in [0.15 \quad 0.183]$, $R \in [0.045 \quad 0.055]$, $K_{EV} \in [0.9 \quad 1.1]$, $T_{EV} \in [0.09 \quad 0.11]$.

Step 2: The upper and lower limit values of the coefficients of characteristic equation (7.1) in terms of system parameters are computed as follows:

$p_6 \in [0.0096 \quad 0.0319]$; $p_5 \in [0.2498 \quad 0.6820]$; $p_4 \in [2.0162 \quad 4.5114]$;
$p_3''' \in [4.9012 \quad 9.0293]$; $p_3' \in [0.1102 \quad 0.2460]$; $p_2''' \in [2.5706 \quad 3.9669]$;
$p_2'' \in [0.1102 \quad 0.2460]$; $p_2' \in [1.2928 \quad 2.3377]$; $p_1''' \in [1.0405 \quad 1.0605]$;
$p_1'' \in [1.2928 \quad 2.3377]$; $p_1' \in [0.7560 \quad 0.9240]$; $p_0'' \in [0.7560 \quad 0.9240]$;
$q_4' \in [0.0446 \quad 0.1218]$; $q_3' \in [0.6655 \quad 1.4850]$; $q_3'' \in [0.0446 \quad 0.1218]$;
$q_2' \in [1.8983 \quad 3.4659]$; $q_2'' \in [0.6655 \quad 1.4850]$; $q_1' \in [0.1701 \quad 0.2541]$;
$q_1'' \in [1.8983 \quad 3.4659]$; $q_0'' \in [0.1701 \quad 0.2541]$;

Step 3: The stability regions for each vertex polynomial described in Equation (5.12) are computed with help of Equations (5.6) and (5.7). As a results, the intersection of the four stability regions $\mathrm{G_c}(\omega, \mathrm{K_P}, \mathrm{K_I}) = \bigcap_{\eta=1}^{4} \mathrm{G}_{\mathrm{c}\eta}(\omega, \mathrm{K_P}, \mathrm{K_I})$ is the robust stability region of the single-area LFC-EVs system and the controller gains constituting the robust stability region are the robust controller gains.

A robust stability region computed for the second area of two-area LFC-EVs system is depicted in Figure 7.32. It can be observed that there are four different stability regions

shown by blue, yellow, green and red colors that are computed with the help of four vertex polynomials given in Equation (5.12). The intersection of all the four stability regions is shown by grey color Figure 7.32. This intersectional area in the parameter space of PI controller gains is the robust stability region of second area of two-area LFC-EVs system.

Similar to the single-area LFC-EVs system, it is also very important to investigate the impact of communication time delay for a selected EVs participation factor on the given second area of two-area LFC-EVs system. Figure 7.33 illustrates the robust stability regions R3, R2 and R1 computed for different communication time delays; $\tau = 0.125s$, $0.25s$ and $0.5s$. Whereas, the parametric uncertainties are selected as $\delta = 10\%$ and the participation factors are chosen as $(\alpha_0 = 0.8,\ \alpha_1 = 0.2)$. Figure 7.33 shows that the robust stability regions shrink as the time delay increases from $\tau = 0.125s$ to $\tau = 0.5s$. Also, the shapes of each of the three regions show a slight change.

Moreover, the impact of EVs aggregator participation factor on the stability region is also investigated. Three different EVs aggregator participation factors are selected, i.e., $\alpha_1 = 0.1,\ 0.2$ and $0.3,$ whereas the time delay and parametric uncertainties are kept fixed at $\tau = 0.25s$ and $\delta = 10\%,$ respectively. These participation factors imply that 10%, 20% and 30% of the required control effort are provided by the EVs aggregator with a time delay of $\tau = 0.25s$. Figure 7.34 compares the corresponding stability regions A3, A2 and A1. It is observed that the largest region A3 is computed when EVs participation is minimum ($\alpha_1 = 0.1$). More importantly, the size of stability regions decreases as the EVs participation factor increases, whereas the shape of the regions is unchanged.

Furthermore, the impact of parametric uncertainties on the robust stability regions computed in the space of PI controller gains is examined. The time delay and the participation factors are kept fixed at $\tau = 0.25$ sec and ($\alpha_0 = 0.8, \alpha_1 = 0.2$), respectively. Figure 7.35 shows these robust stability regions T3, T2 and T1 corresponding to the parametric uncertainties $\delta = 5\%,\ \delta = 10\%,$ and $\delta = 15\%,$ respectively. It can be seen from Figure 7.35 that the largest region T3 is obtained when the parametric uncertainties are minimum ($\delta = 5\%,$). Also, the size of the robust stability regions decreases as the parametric uncertainties increase, whereas the shape of the regions remains unchanged.

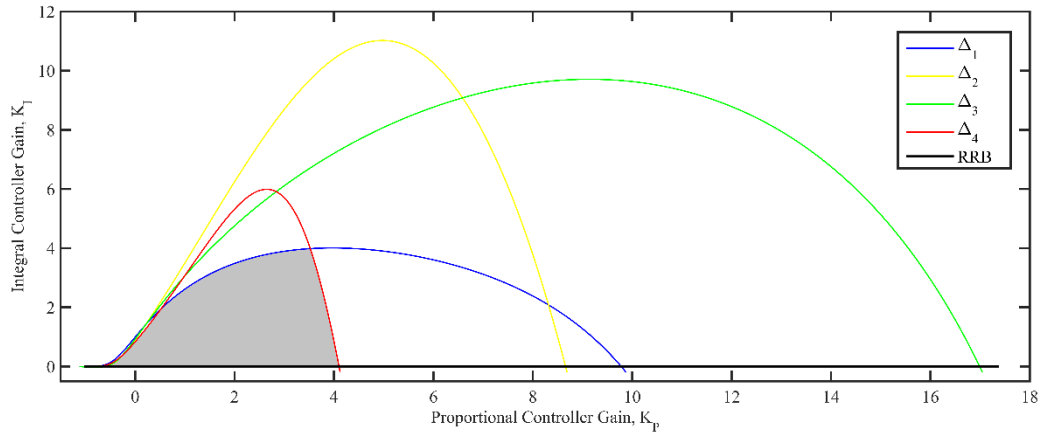

Figure 7.32. Robust stability region for second area when $\tau = 0.25s$, $\delta = 10\%$ and $\alpha_0 = 0.8$

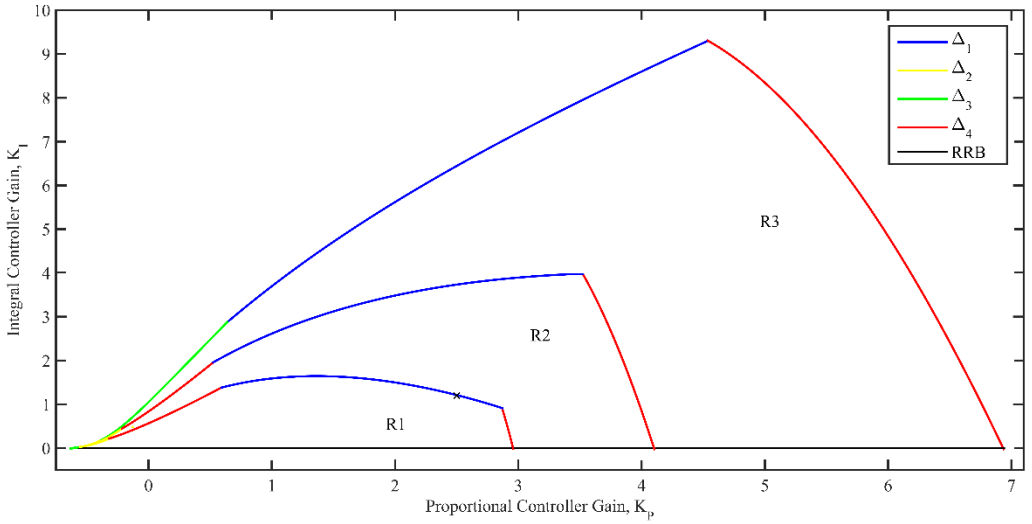

Figure 7.33. Effect of time delay τ on robust stability regions of second area when $\delta = 10\%$ and $\alpha_0 = 0.8$

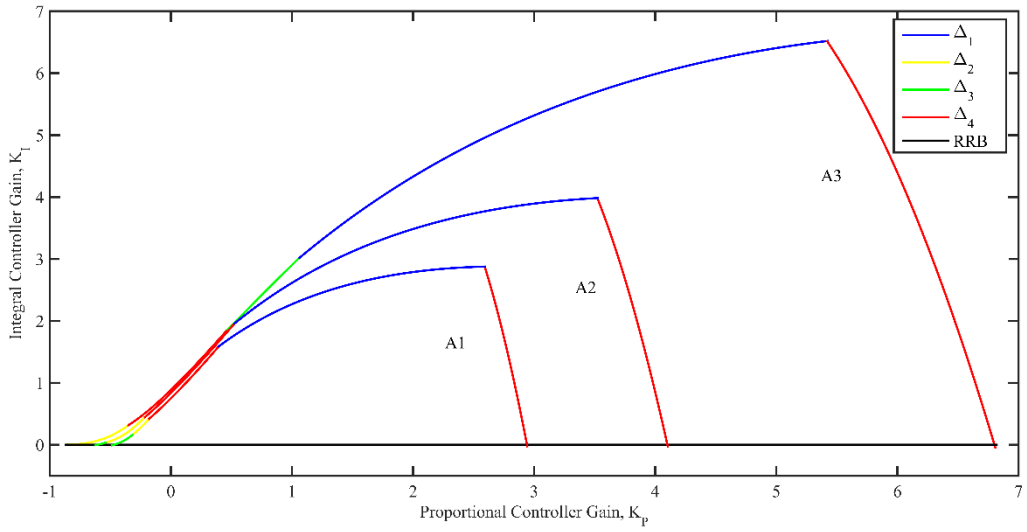

Figure 7.34. Effect of participation ratios α_0 and α_1 on robust stability regions of second area when $\tau = 0.25s$ and $\delta = 10\%$

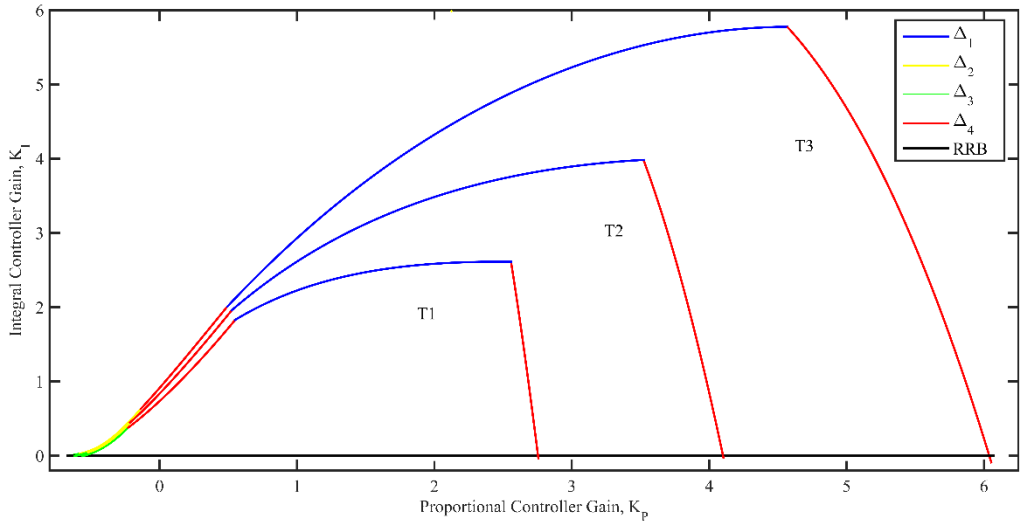

Figure 7.35. Effect of parametric uncertainties δ on robust stability regions of second area when $\tau = 0.25s$ and $\alpha_0 = 0.8$

7.2.4 Verification of Robust Stability Regions Computed for Second Area of Two-Area LFC-EVs System

The accuracy of the theoretically computed robust stability boundary locus, CRB is validated by the time-domain simulations. A set of robust controller gains; $(K_P = 2.5, K_I = 1.2)$ shown by '×' sign on the CRB of R1 in Figure 7.33 is selected to

verify the robustness of the stability region computed in the presence of parametric uncertainties. It can be observed from Figure 7.36 that the frequency response of the system is stable hence guaranteeing the stable operation of the system. Three different responses for three different sets of participation ratios $(\alpha_0 = 0.9, \alpha_1 = 0.1)$, $(\alpha_0 = 0.8, \alpha_1 = 0.2)$ and $(\alpha_0 = 0.7, \alpha_1 = 0.3)$ are shown by dotted, solid and dashed lines in Figure 7.37. It can be observed that the system shows stable frequency responses for the selected robust controller gains under a large load disturbance scenario shown in Figure 7.30. This infers that the obtained robust stability regions provide such controller gains which assure the stable operation of the system.

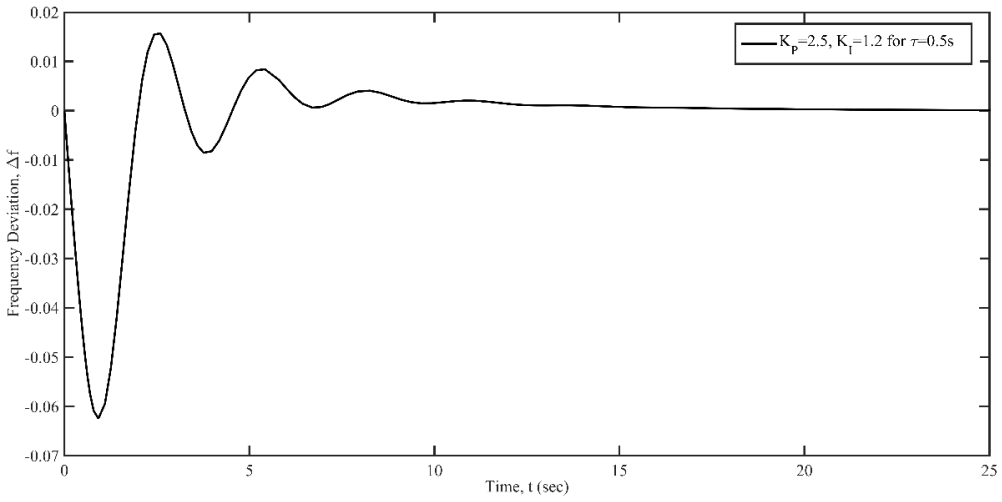

Figure 7.36. Verification of the robust stability region R1 of second area using random parametric values within the defined intervals

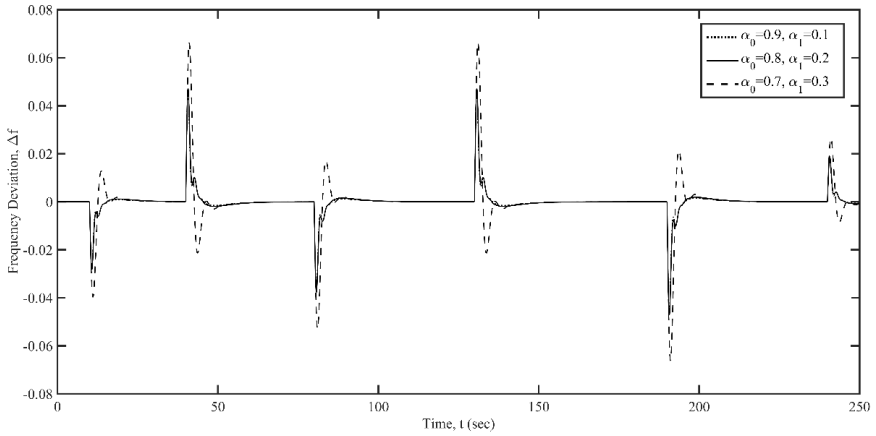

Figure 7.37. Frequency response of second area for the selected robust controller gains under large load disturbance

CHAPTER VIII

CONCLUSIONS

The effect of EVs aggregators integration into the conventional LFC system that causes communication time delays in the system is comprehensively investigated. For a given set of controller gains, system parameters and load sharing schemes, stability margins for both Single and Two-Area LFC-EVs system have been determined using frequency domain direct method and Rekasius substitution method. It has been observed that both the methods provide the same stability margin values for LFC-EVs system. Also, the stability margins become smaller with an increase in the integral gain. For any given set of PI controller gains, an increase in EVs aggregator participation factor results in a decrease in stability margins. It has been concluded that if the PI controller gains and participation factor of EVs are not properly selected, the participation of EVs aggregator with a communication delay may cause instability and degrade the dynamic response of the system. Also, the effect of tie-line power on stability delay margin is observed. The stability delay margins are higher when the power exchange from area 2 to area 1 is lesser and those delay margin values start to decrease with an increase in this power exchange. The observations and comments based on the obtained results are as following: 1) The PI controller gains have significant impact on delay margins. 2) When the proportional controller gain is kept constant, the delay margin decreases as the integral controller gain is increased, indicating a smaller stability margin for LFC systems. 3) The delay margin increases at first and decreases with the increase of the proportional gain when integral controller gain remains unchanged. 4) Stability delay margins results obtained by the proposed method are almost the same as the ones determined by simulations, proving that the proposed method accurately estimate delay margins of LFC systems. 5) QPmR algorithm also validates the stability delay margin results obtained theoretically.

For a given time delay and load sharing scheme, stability regions in the PI controller parameter space for both Single and two-area LFC-EVs system have been determined using stability boundary locus method. It has been observed that stability regions become smaller with an increase in the communication time delay. Also, the size of the stability regions reduces with an increase in EVs aggregator participation factor for any given delay value. It has been concluded that if the PI controller gains and participation factor

of EVs are not properly selected, the participation of EVs aggregator with a communication time delay may cause instability and degrade the dynamic response. The observations and comments based on the obtained results are as following: 1) The participation factors have significant impact on stability regions. 2) The CRBs and RRBs of stability regions obtained by the stability boundary locus method are almost the same as the ones determined by simulations, proving that the proposed method accurately computes stability regions for LFC-EVs systems. 3) QPmR algorithm also validates the stability regions results that are computed theoretically.

Moreover, this work has presented a comprehensive stability analysis to overcome the stability concerns of time delayed LFC-EVs system with uncertain parameters by computing robust stability regions that assure robustness and guarantee stable operation of the system. The robust stability regions in the parameter space of PI controller gains are computed with the help of Kharitonov's theorem and stability boundary locus method. For a given time delay, load sharing scheme and parametric uncertainties, stability regions in the robust controller parametric space for both Single and two-area LFC-EVs system have been determined. It has been observed that robust stability regions become smaller with an increase in the communication time delay. Moreover, for any given delay value, the size of the stability regions reduces with an increase in EVs aggregator participation factor. Also, an increase in the parametric uncertainties decreases the robust stability regions. It has been concluded that if the robust PI controller gains and participation factor of EVs are properly selected, the participation of EVs aggregator with a communication time delay can improve the LFC dynamic performance. The observations and comments based on the obtained results are as following; 1) Communication time delay has significant impact on robust stability regions. 2) The effect of participation factors on robust stability regions is significant. 3) The parametric uncertainties can significantly affect the robust stability regions. 4) Time domain simulations validate the robust stability regions results that are computed theoretically.

It is expected that the obtained results will help in determining communication delay requirements and robust controller design specifications for EVs aggregators participating in frequency regulation service while the system parameters are varying because of the uncertainties. Computation of robust stability regions in the PI controller parametric space for two-area LFC-EVs systems without having weakly coupled control

areas and verification of the accuracy of those theoretical results by simulation studies is placed in future studies. Moreover, computation of stability delay margins considering incommensurate time delays by using frequency-domain methods can be done in future studies. Additionally, modelling of EVs while considering the state of charge of the battery system will be considered in the future prospects.

REFERENCES

Ahn, C., Li, C.T. and Peng, H., "Optimal decentralized charging control algorithm for electrified vehicles connected to smart grid", ***Journal of Power Sources*** 196(23), 10369-10379, 2011.

Alomoush, M.I., "Load frequency control and automatic generation control using fractional-order controllers", ***Electrical Engineering*** 91(7), 357-368, 2010.

Ayasun, S., "Computation of time delay margin for power system small-signal stability", ***European Transactions on Electrical Power*** 19(7), 949-968, 2009.

Ayasun, S. and Nwankpa, C.O., "Stability of a Two-Area Automatic Generation Control System with Communication Delays", ***International Conference on Electrical and Electronics Engineering (ELECO 2009)***, Bursa, Turkey, s. 65-69, 5-8 November, 2009.

Aziz, A., Oo, A.T. and Stojcevski, A., "Frequency regulation capabilities in wind power plant", ***Sustainable Energy Technologies and Assessments*** 26, 47-76, 2018.

Bessa, R.J. and Matos, M.A., "The role of an aggregator agent for EV in the electrical market", ***7th Mediterranean Conference and Exhibition on Power Generation, Transmission, Distribution and Energy Conversion (MedPower 2010),*** Agia Napa, Cyprus, s. 1-19, 7-10 November, 2010.

Bessa, R.J., Matos, M.A. and Soares, F.J., "Framework for the Participation of EV Aggregators in the Electricity Market", ***2014 IEEE International Electric Vehicle Conference (IEVC)***, Florence, Italy, s. 1-8, 17-19 December, 2014.

Bevrani, H., Robust Power System Frequency Control, ***Springer-Verlag***, New York, 2014.

Bevrani, H., Ghosh, A. and Ledwich, G., "Renewable energy sources and frequency regulation: survey and new perspectives", ***IET Renewable Power Generation*** 4(5), 438-457, 2010.

Bhattacharyya, S.P., Chapellat, H. and Keel, L.H., Robust Control: The Parametric Approach, Chapter 5, ***Prentice Hall PTR***, New Jersey, 1995.

Bhowmik, S., Tomsovic, K. and Bose, A., "Communication models for third party load frequency control", ***IEEE Transactions on Power Systems*** 19(1), 543-548, 2004.

Bilh, A., Naik, K. and El-Shatshat, R., "Evaluating electric vehicles' response time to regulation signals in smart grids", ***IEEE Transactions on Industrial Informatics*** 14(3), 1210-1219, 2017.

Carreiroa, A.M., Jorgea, H.M. and Antunesa, C.H., "Energy management systems aggregators: A literature survey", ***Renewable and Sustainable Energy Reviews*** 73, 1160-1172, 2017.

Chen, J., Gu, G. and Nett, C.N., "A new method for computing delay margins for stability of linear delay systems", ***System and Control Letters*** 26(2), 101-117, 1995.

Chen, J. and Latchman, H.A., "Frequency Sweeping Tests for Stability Independent of Delay", ***IEEE Transactions on Automatic Control*** 40, 1640-1645, 1995.

Datta, M., Senjyu, T., Yona, A., Funabashi, T. and Kim, C.H., "A frequency-control approach by photovoltaic generator in a PV-diesel hybrid power system", ***IEEE Transactions on Energy Conversion*** 26(2), 559-571, 2011.

Delille, G., Francois, B. and Malarange, G. "Dynamic frequency control support by energy storage to reduce the impact of wind and solar generation on isolated power system's inertia", ***IEEE Transactions on Sustainable Energy*** 3(4), 931-939, 2012.

Díaz-González, F., Hau, M., Sumper, A. and Gomis-Bellmunt, O., "Participation of wind power plants in system frequency control: review of grid code requirements and control methods", ***Renewable and Sustainable Energy Reviews*** 34, 551-564, 2014.

Dong, C., Jia, H., Xu, Q., Xiao, J., Xu, Y., Tu, P., ... and Wang, P., "Time-delay stability analysis for hybrid energy storage system with hierarchical control in DC microgrids", ***IEEE Transactions on Smart Grid*** 9(6), 6633-6645, 2017.

ENTSO-E, UCTE OH-Policy 1: load-frequency control, ***European Networks of Transmission System Operators for Electricity Report***, 2009.

EPDK, "Elektrik şebeke yönetmeliği", ***Enerji Piyasasi Düzenleme Kurumu,*** https://www.epdk.gov.tr/Detay/Icerik/3-6730/elektrik--sebeke-yonetmeligi-**,** 2020.

Falahati, S., Taher, S.A. and Shahidehpour, M., "A new smart charging method for EVs for frequency control of smart grid", ***Electrical Power and Energy Systems*** 83, 458-469, 2016.

Fan, H., Jiang, L. and Mao, C., "Frequency regulation of multi-area power systems with plug-in electric vehicles considering communication delays", ***IET Generation, Transmission and Distribution*** 10(14), 3481-3491, 2016.

Fazelinia, H., Sipahi, R. and Olgaç, N., "Stability robustness analysis of multiple time delayed systems using "building block" concept", ***IEEE Transactions on Automatic Control*** 52(5), 799-810, 2007.

Fu, P., Niculescu, S.I. and Chen, J., "Stability of linear neutral time-delay systems: exact conditions via matrix pencil solutions", ***IEEE Transactions on Automatic Control*** 51(6), 1063-1069, 2006.

Golshannavaz, S., Khezri, R., Esmaeeli, M. and Siano, P., "A two-stage robust-intelligent controller design for efficient LFC based on Kharitonov theorem and fuzzy logic", ***Journal of Ambient Intelligence and Humanized Computing*** 9(5), 1445-1454, 2018.

Green, R. C., Wang, L. and Alam, M., "The impact of plug-in hybrid electric vehicles on distribution networks: A review and outlook", ***Renewable and Sustainable Energy Reviews*** 15(1), 544-553, 2011.

Gu, K., Kharitonov, V.L. and Chen. J., Stability of Time Delay Systems, ***Birkhauser***, Boston, 2003.

Guille, C. and Gross, G., "A conceptual framework for the vehicle-to-grid (V2G) implementation", ***Energy Policy*** 37(11), 4379-4390, 2009.

Gündüz, H., Sönmez, Ş. and Ayasun, S., "A comprehensive gain and phase margins based stability analysis of micro-grid frequency control system with constant communication time delays", ***IET Generation, Transmission and Distribution*** 11(3), 719-729, 2017.

Güngör, V.C., Şahin, D., Koçak, T., Ergut, S., Buccella, C., Cecati, C. and Hancke, G.P., "A survey on smart grid potential applications and communication requirements", ***IEEE Transactions on Industrial Informatics*** 9(1), 28-41, 2013.

Hamamcı, S.E. and Köksal, M., "Calculation of all stabilizing fractional-order PD controllers for integrating time delays", ***Computers and Mathematics with Applications***, 59(5), 1621-1629, 2010.

Hamamcı, S.E. and Tan, N., "Design of PI controllers for achieving time and frequency domain specifications simultaneously", ***ISA Transactions*** 45(4), 529-543, 2006.

Han, S., Han, S. and Sezaki, K., "Development of an optimal vehicle-to-grid aggregator for frequency regulation", ***IEEE Transactions on Smart Grid*** 1(1), 65-72, 2010.

Hartmann, B., Vokony, I. and Táczi, I., "Effects of decreasing synchronous inertia on power system dynamics—overview of recent experiences and marketization of services", ***International Transactions on Electrical Energy Systems*** 29(12), e12128, 2019.

Ho, M.T., Datta, A. and Bhattackaryya, S.P., “Design of P, PI and PID controllers for interval plants”, ***Proceedings of the 1998 IEEE American Control Conference. ACC (IEEE Cat. No. 98CH36207)***, Philadelphia, USA, s. 2496-2501, 26 June, 1998.

Hund, T. D., Gonzalez, S. and Barrett, K. “Grid-tied PV system energy smoothing”, ***2010 35th IEEE Photovoltaic Specialists Conference (PVSC)***, Honolulu, USA, s. 2762-2766, 20-25 June, 2010.

Jia, H., Li, X., Mu, Y., Xu, C., Jiang, Y., Yu, X., Wu, J. and Dong, C., “Coordinated control for EV aggregators and power plants in frequency regulation considering time-varying delays”, ***Applied Energy*** 1363-1376, 2018.

Jia, H., Yu, X., Yu, Y. and Wang, C. “Power system small signal stability region with time delay”, ***International Journal of Electrical Power & Energy Systems*** 30(1), 16-22, 2008.

Jiang, L., Yao, W., Wu, Q.H., Wen, J.Y. and Cheng, S.J., “Delay-dependent stability for load frequency control with constant and time-varying delays”, ***IEEE Transactions on Power Systems*** 27(2), 932-941, 2012.

Jin, L., Zhang, C.K., He, Y., Jiang, L. and Wu, M., “Delay-dependent stability analysis of multi-area load frequency control with enhanced accuracy and computation efficiency”, ***IEEE Transactions on Power Systems*** 34(5), 3687-3696, 2019.

Kempton, W. and Letendre, S.E., “Electric vehicles as a new power source for electric utilities”, ***Transportation Research Part D: Transport and Environment*** 2(3), 157-175, 1997.

Khalil, A., Rajab, Z., Alfergabi, A. and Mohamed, O. “The impact of the time delay on the load frequency control system in Microgrid with plug-in-electric-vehicles”, ***Sustainable Cities and Society*** 35, 365-367, 2017.

Khalil, A. and Peng, A.S., “Delay margin computation for load frequency control system with plug-in electric vehicles”, ***International Journal of Power and Energy Systems*** 38(3), 1-17, 2018.

Khalil, A. and Peng, A.S. “A New Method for Computing the Delay Margin for the Stability of Load Frequency Control Systems”, ***Energies*** 11(12), 3460, 2018.

Kharitonov, V.L., “Asymptotic stability of an equilibrium position of a family systems of linear differential equations”, ***Differential’nye Uraveniya*** 14, 1483-1485, 1978a.

Kharitonov, V.L., “On a generalization of a stability criterion”, ***Izvestiya Akademii Nauk Kazakhskoi SSR Seriya Fizika Matematika*** 1, 53-57, 1978b.

Khodabakhshian, A., Pour, M.E. and Hooshmand, R., “Design of a robust load frequency control using sequential quadratic programming technique”, ***International Journal of Electrical Power and Energy Systems*** 40(1), 1-8, 2012.

Ko, K.S. and Sung, D.K. “The effect of EV aggregators with time-varying delays on the stability of a load frequency control system”, ***IEEE Transactions on Power Systems*** 33(1), 669-680, 2017a.

Ko, K.S. and Sung, D.K. 2017. “The Effect of Cellular Network-Based Communication Delays in an EV Aggregator’s Domain on Frequency Regulation Service”, ***IEEE Transactions on Smart Grid*** 10(1), 65-73, 2017b.

Krishnan, R., Pragatheeswaran, J. K. and Ray, G., “Robust stability of networked load frequency control systems with time-varying delays”, ***Electric Power Components and Systems*** 45(3), 302-314, 2017.

Kundur, P., Power System Stability and Control, ***McGraw-Hill Inc.,*** New York, 1994.

Kumar, S.S. and Shreesha, C., “Design of robust PID controller for a CSTR plant with interval parametric uncertainty using Kharitonov theorem”, ***2016 IEEE International***

Conference on Computation of Power, Energy Information and Communication (ICCPEIC), Melmaruvathur, India, s. 430-433, 20-21 April, 2016.

Lamba, R., Singla, S.K. and Sondhi, S., "Design of fractional order pid controller for load frequency control in perturbed two area interconnected system", ***Electric Power Components and Systems*** 47(11-12), 998-1011, 2019.

Li, G. and Zhang, X., "Modeling of plug-in hybrid electric vehicle charging demand in probabilistic power flow calculations", ***IEEE Transactions on Smart Grid*** 3(1), 492-499, 2012.

Li, Y.J., Xu, Z., Ngan, H.W. and Wong, S.C., "A novel topology design for integration of offshore wind farm via high-voltage DC transmission", ***Electric Power Components and Systems*** 43(8), 1100-1112, 2015.

Liang, T., Chen, J. and Zhao, H., "Robust stability region of fractional order PIλ controller for fractional order interval plant", ***International journal of systems science*** 44(9), 1762-1773, 2013.

Liu, H., Qi, J., Wang, J., Li, P., Li, C. and Wei, H., "EV dispatch control for supplementary frequency regulation considering the expectation of EV owners", ***IEEE Transactions on Smart Grid*** 1-10, 2016.

Liu, K., Seuret, A., Xia, Y., Gouaisbaut, F. and Ariba, Y., "Bessel–Laguerre inequality and its application to systems with infinite distributed delays", ***Automatica*** 109, 108562, 2019.

Louisell, J., "A matrix method for determining the imaginary axis eigenvalues of a delay system", ***IEEE Transactions on Automatic Control*** 46(12), 2008-2012, 2001.

Luo, X., Xia, S. and Chan, K.W., "A decentralized charging control strategy for plug-in electric vehicles to mitigate wind farm intermittency and enhance frequency regulation", ***Journal of Power Sources*** 248, 604-614, 2014.

Mak, K.H. and Holland, B.L., “Migrating electrical power network SCADA systems to TCP/IP and ethernet networking”, ***Power Engineering Journal*** 16(6), 305–311, 2002.

Masuta, T. and Yokoyama, A., “Supplementary load frequency control by use of a number of both electric vehicles and heat pump water heaters”, ***IEEE Transactions on Smart Grid*** 3, 1253-1262, 2012.

Mu, Y., Wu, J., Ekanayake, J., Jenkins, N. and Jia, H., “Primary frequency response from electric vehicles in the Great Britain power system”, ***IEEE Transactions on Smart Grid*** 4(2), 1142-1150, 2013.

Naduvathuparambil, B., Valenti, M.C. and Feliachi, A., “Communication delays in wide area measurement systems”, ***Proceedings of the Thirty-Fourth Southeastern Symposium on System Theory***, Huntsville, USA, s. 118-122, 19 March, 2002.

Naveed, A., Sönmez, Ş. and Ayasun, S., “Identification of Stability Delay Margin for Load Frequency Control System with Electric Vehicles Aggregator using Rekasius Substitution”, ***2019 IEEE Milan PowerTech,*** Milan, Italy, s. 1-6, 23-27 June, 2019.

Naveed, A., Sönmez, Ş. and Ayasun, S., “Impact of electric vehicle aggregator with communication time delay on stability regions and stability delay margins in load frequency control system”, ***In Journal of Modern Power Systems and Clean Energy*** 2020. https://doi.org/ 10.35833/MPCE.2019.000244.

Nazari, S., Amjadifard, R., Shokoohi, S. and Nateghi, A., “Application of Kharitonov's Theorem in Robust Stability of Voltage and Frequency of an Islanded Microgrid”, ***2018 IEEE Smart Grid Conference (SGC)***, Sanandaj, Iran, s. 1-6, 28-29 November, 2018.

Olgaç, N. and Sipahi, R., “An exact method for the stability analysis of time-delayed linear time invariant (LTI) systems”, ***IEEE Transactions on Automatic Control*** 47(5), 793-797, 2002.

Olgaç, N. and Sipahi, R., “A practical method for analyzing the stability of neutral type LTI-time delayed systems”, ***Automatica*** 40(5), 847-853, 2004.

Pillai, J. and Bak-Jensen, B., "Integration of vehicle-to-grid in the western Danish power system", ***IEEE Transactions on Sustainable Energy*** 2(1), 12-19, 2011.

Pekař, L. and Gao, Q., "Spectrum analysis of LTI continuous-time systems with constant delays: A literature overview of some recent results", ***IEEE Access*** 6, 35457-35491, 2018.

Quinn, C., Zimmerle, D. and Bradley, T.H., "The effect of communication architecture on the availability, reliability, and economics of plug-in hybrid electric vehicle-to-grid ancillary services", ***Journal of Power Sources*** 195(5), 1500-1509, 2010.

Rekasius, Z.V., "A stability test for systems with delays" ***Joint Automatic Control Conference***, San Francisco, USA, Paper No. TP9-A, 1980.

Richardson, P., Flynn, D. and Keane, A., "Optimal charging of electric vehicles in low-voltage distribution systems", ***IEEE Transactions on Power Systems*** 27(1), 268-279, 2012.

Rigatos, G. and Siano, P., "Design of robust electric power system stabilizers using Kharitonov's theorem", ***Mathematics and Computers in Simulation*** 82(1), 181-191, 2011.

Saadat, H., Power System Analysis, ***McGraw-Hill Inc.***, New York, 1999.

Saxena, S. and Hote, Y.V., "Decentralized PID load frequency control for perturbed multi-area power systems", ***Electrical Power and Energy Systems*** 81, 405-415, 2016.

Sekyung, H., Soohee, H. and Sezaki, K., "Development of an optimal vehicle-to-grid aggregator for frequency regulation", ***IEEE Transactions on Smart Grid*** 1, 65-72, 2010.

Seuret, A. and Gouaisbaut, F., "Hierarchy of LMI conditions for the stability analysis of time-delay systems", ***Systems & Control Letters*** 81, 1-7, 2015.

Shimizu, K., Masuta, T., Ota, Y. and Yokoyama, A., “Load frequency control in power system using vehicle-to-grid system considering the customer convenience of electric vehicles”, ***2010 International Conference on Power System Technology (POWERCON)***, Zhejiang, China, s. 1-8, 24-28 October, 2010.

Simulink, Model-Based and System-Based Design, Using Simulink. Natick, ***MathWorks***, MA, USA, 2000.

Sipahi, R. and Olgaç, N., “A comparative survey in determining the imaginary characteristic roots of LTI time delayed systems”, ***16th IFAC World Congress***, Prague, Czech Republic, s. 390-399, 3-8 July, 2005.

Sondhi, S. and Hote, Y.V., “Relative stability test for fractional-order interval systems using kharitonov’s theorem. Journal of Control”, ***Automation and Electrical Systems*** 27(1), 1-9, 2016.

Sönmez, Ş. and Ayasun, S., "Stability region in the parameter space of PI controller for a single-area load frequency control system with time delay", ***IEEE Transactions on Power Systems*** 31(1), 829-830, 2016.

Sönmez, Ş. and Ayasun, S., “Gain and phase margins based delay-dependent stability analysis of single-area load frequency control system with constant communication time delay”, ***Transactions of the Institute of Measurement and Control*** 40(5), 701-710, 2018.

Sönmez, Ş., Ayasun, S. and Eminoğlu, U., “Computation of time delay margins for stability of a single-area load frequency control system with communication delays”, ***WSEAS Transactions on Power Systems*** 9, 67-76, 2014.

Sönmez, Ş., Ayasun, S. and Nwankpa, C.O., "An exact method for computing delay margin for stability of load frequency control systems with constant communication delays", ***IEEE Transactions on Power Systems***, 31(1), 370-377, 2016.

Sönmez, Ş., Eminoğlu U. and Ayasun, S., "An exact method to compute time delay margin for stability of time-delayed generator excitation control system", ***International Research Journal of Engineering and Technology*** 2(8), 276-283, 2015.

Söylemez, M.T., Munro, N. and Baki, H., "Fast calculation of stabilizing PID controllers", ***Automatica*** 39(1), 121-127, 2003.

Tan, N., Kaya, I., Celaleddin, Y. and Atherton, D.P., "Computation of stabilizing PI and PID controllers using the stability boundary locus", ***Energy Conversion and Management*** 47(18-19), 3045-3058, 2006.

Tan, N., Özgüven, Ö.F. and Özyetkin, M.M., "Robust stability analysis of fractional order interval polynomials", ***ISA transactions*** 48(2), 166-172, 2009.

Tan, W., Zhang, H. and Yu, M., "Decentralized load frequency control in deregulated environments", ***International Journal of Electrical Power and Energy Systems*** 41(1), 16-26, 2012.

Thangaiah, J.M. and Parthasarathy, R., "Delay-dependent stability analysis of microgrid with constant and time-varying communication delays", ***Electric Power Components and Systems*** 44(13), 1441-1452, 2016.

Toulabi, M. R., Shiroei, M. and Ranjbar, A.M., "Robust analysis and design of power system load frequency control using the Kharitonov's theorem", ***Electrical Power and Energy Systems*** 55, 51-58, 2014.

Walton, K.E. and Marshall, J.E., "Direct method for TDS stability analysis", ***IEEE Proceeding Part D.*** 134, 101-107, 1987.

Wang, J., Tse, N. and Gao, Z., "Synthesis on-PI-based pitch controller of large wind turbine generator", ***Energy Conversion and Management*** 52(2), 1288-1294, 2011.

Wang, W., Xu, Y., and Khanna, M., "A survey on the communication architectures in smart grid", ***Computer Networks*** 55, 3604-3629, 2011.

Wang, Y.J., “Graphical computation of gain and phase margin specifications-oriented robust PID controllers for uncertain systems with time-varying delay”, ***Journal of Process Control*** 21, 475-488, 2011.

Xu, S.J., Darouach, M. and Schaefers, J., “Expansion of det (a+ b) and robustness analysis of uncertain state space systems”, ***IEEE Transactions on Automatic Control*** 38(11), 1671-1675, 1993.

Xu, Q., Stépán, G. and Wang, Z., “Delay-dependent stability analysis by using delay-independent integral evaluation”, ***Automatica*** 70, 153-157, 2016.

Vyhlídal, T. and Zítek, P., “Mapping based algorithm for large-scale computation of quasi-polynomial zeros”, ***IEEE Transactions Automatic Control*** 2054 (1), 171-177, 2009.

Yan, Y., Qian, Y., Sharif, H. and Tipper, D., “A survey on smart grid communication infrastructures: motivations, requirements and challenges”, ***IEEE Communications Surveys and Tutorials*** 15(1), 5-20, 2013.

Yang, B., Makarov, Y., Desteese, J., Viswanathan, V., Nyeng, P., McManus, B. and Pease, J., “On the use of energy storage technologies for regulation services in electric power systems with significant penetration of wind energy”, ***2008 5th International Conference on the European Electricity Market***, Lisboa, Portugal, s. 1-6, 28-30 May, 2008.

Yang, J., Dong, H., Huang, Y., Cai, L., Gou, F. and He, Z., “Coordinated optimization of vehicle-to-grid control and load frequency control by considering statistical properties of active power imbalance”, ***International Transactions on Electrical Energy Systems*** 29(3), e2750, 2019.

Yao, E., Wong, V. W. and Schober, R., “Robust frequency regulation capacity scheduling algorithm for electric vehicles”, ***IEEE Transactions on Smart Grid*** 8(2), 984-997, 2016.

Yazdizadeh, A., Ramezani, M.H. and Hamedrahmat, E., “Decentralized load frequency control using a new robust optimal miso PID controller”, ***International Journal of Electrical Power and Energy Systems*** 35(1), 57-65, 2012.

Yu, X. and Tomsovic, K., “Application of linear matrix inequalities for load frequency control with communication delays”, ***IEEE transactions on power systems*** 19(3), 1508-1515, 2004.

Yuan, C., Song, S., Gao, Q., Karimi, H.R., Pekar, L. and Guo, S., “A novel frequency-domain approach for the exact range of imaginary spectra and the stability analysis of LTI systems with two delays”, ***IEEE Access*** 8, 36595-36601, 2020.

Zeng, H.B., Zhai, Z.L., He, Y., Teo, K.L. and Wang, W., “New insights on stability of sampled-data systems with time-delay”, ***Applied Mathematics and Computation*** 374, 125041, 2020.

Zeng, H.B., Liu, X.G. and Wang, W., “A generalized free-matrix-based integral inequality for stability analysis of time-varying delay systems”, ***Applied Mathematics and Computation*** 354, 1-8, 2019.

Zhang, C.K., He, Y., Jiang, L., Wu, M. and Zeng, H.B., “Delay-variation-dependent stability of delayed discrete-time systems”, ***IEEE Transactions on Automatic Control*** 61(9), 2663-2669, 2015.

Zhang, C.K., Jiang, L., Wu, Q.H., He, Y. and Wu, M., “Further results on delay-dependent stability of multi-area load frequency control”, ***IEEE Transactions on Power Systems*** 28(4), 4465-4474, 2013.

Zhang, C.K., Long, F., He, Y., Yao, W., Jiang, L. and Wu, M., “A relaxed quadratic function negative-determination lemma and its application to time-delay systems”, ***Automatica*** 113, 108764, 2020.

Zhou, B., Yao, F., Littler, T. and Zhang, H., “An electric vehicle dispatch module for demand-side energy participation”, ***Applied Energy*** 177, 464-474, 2016.

Zhou, S.J., Zeng, H.B. and Xiao, H.Q., “Load Frequency Stability Analysis of Time-Delayed Multi-Area Power Systems with EV Aggregators Based on Bessel-Legendre Inequality and Model Reconstruction Technique”, ***IEEE Access*** 8, 99948-99955, 2020.

APPENDICES

Appendix A1

$$p_6 = MRT_gT_rT_cT_{EV};$$

$$p_5 = DRT_gT_rT_cT_{EV} + MR(T_gT_rT_c + T_rT_cT_{EV} + T_gT_cT_{EV} + T_gT_rT_{EV});$$

$$p_4 = DR(T_gT_rT_c + T_rT_cT_{EV} + T_gT_cT_{EV} + T_gT_rT_{EV}) + MR(T_rT_c + T_gT_c + T_gT_r + T_cT_{EV} + T_rT_{EV} + T_gT_{EV});$$

$$p_3 = DR(T_rT_c + T_gT_c + T_gT_r + T_cT_{EV} + T_rT_{EV} + T_gT_{EV}) + MR(T_c + T_r + T_g + T_{EV}) + F_pT_rT_{EV} + K_p[\alpha_0\beta RF_pT_rT_{EV}];$$

$$p_2 = DR(T_c + T_r + T_g + T_{EV}) + MR + F_pT_r + T_{EV} + K_p[\alpha_0\beta R(T_{EV} + F_pT_r)] + K_I[\alpha_0\beta RF_pT_rT_{EV}];$$

$$p_1 = DR + 1 + K_p[\alpha_0\beta R] + K_I[\alpha_0\beta R(T_{EV} + F_pT_r)]; \quad p_0 = K_I[\alpha_0\beta R];$$

$$q_4 = K_p[\alpha_1\beta RK_{EV}T_gT_rT_c];$$

$$q_3 = K_p[\alpha_1\beta RK_{EV}(T_rT_c + T_gT_c + T_gT_r)] + K_I[\alpha_1\beta RK_{EV}T_gT_rT_c];$$

$$q_2 = K_p[\alpha_1\beta RK_{EV}(T_c + T_r + T_g)] + K_I[\alpha_1\beta RK_{EV}(T_rT_c + T_gT_c + T_gT_r)];$$

$$q_1 = K_p[\alpha_1\beta RK_{EV}] + K_I[\alpha_1\beta RK_{EV}(T_c + T_r + T_g)]; \quad q_0 = K_I[\alpha_1\beta RK_{EV}];$$

Appendix A2

$$p_{13} = M^2R^2T_c^2T_{EV}^2T_g^2T_r^2;$$

$$p_{12} = 2M^2R^2(T_c^2T_{EV}^2T_g^2T_r + T_c^2T_{EV}^2T_gT_r^2 + T_c^2T_{EV}T_g^2T_r^2 + T_cT_{EV}^2T_g^2T_r^2) + 2DMR^2T_c^2T_{EV}^2T_g^2T_r^2;$$

$$p_{11} = D^2R^2T_c^2T_{EV}^2T_g^2T_r^2 + 4DMR^2(T_c^2T_{EV}^2T_g^2T_r + T_c^2T_{EV}^2T_gT_r^2 + T_c^2T_{EV}T_g^2T_r^2 + T_cT_{EV}^2T_g^2T_r^2) + M^2R^2(4T_c^2T_{EV}^2T_gT_r + 4T_c^2T_{EV}T_g^2T_r + 4T_c^2T_{EV}T_gT_r^2 + 4T_cT_{EV}^2T_g^2T_r + 4T_cT_{EV}^2T_gT_r^2 + 4T_cT_{EV}T_g^2T_r^2 + T_c^2T_{EV}^2T_g^2 + T_c^2T_{EV}^2T_r^2 + T_c^2T_g^2T_r^2 + T_{EV}^2T_g^2T_r^2) + 4MR^2T_{12}T_c^2T_{EV}^2T_g^2T_r^2\pi;$$

$$p_{10} = 2F_PMRT_cT_{EV}^2T_gT_r^2 + M^2R^2(2T_cT_{EV}^2T_g^2 + 2T_c^2T_{EV}T_g^2 + 2T_c^2T_{EV}^2T_g + 2T_cT_{EV}^2T_r^2 + 2T_c^2T_{EV}T_r^2 + 2T_c^2T_{EV}^2T_r + 2T_c^2T_gT_r^2 + 2T_c^2T_g^2T_r + 2T_{EV}T_g^2T_r^2 + 2T_{EV}^2T_gT_r^2 + 2T_{EV}^2T_g^2T_r + 8T_cT_{EV}T_gT_r^2 + 8T_cT_{EV}T_g^2T_r + 8T_cT_{EV}^2T_gT_r + 8T_c^2T_{EV}T_gT_r) + 2D^2R^2(T_cT_{EV}^2T_g^2T_r^2 + T_c^2T_{EV}T_g^2T_r^2 + T_c^2T_{EV}^2T_gT_r^2 + T_c^2T_{EV}^2T_g^2T_r) + DMR^2(2T_c^2T_{EV}^2T_g^2 + 2T_c^2T_{EV}^2T_r^2 + 2T_c^2T_g^2T_r^2 + 2T_{EV}^2T_g^2T_r^2 + 8T_cT_{EV}T_g^2T_r^2 + 8T_cT_{EV}^2T_gT_r^2 + 8T_cT_{EV}^2T_g^2T_r + 8T_c^2T_{EV}T_gT_r^2 + 8T_c^2T_{EV}T_g^2T_r + 8T_c^2T_{EV}^2T_gT_r) + 8MR^2T_{12}(T_cT_{EV}^2T_g^2T_r^2\pi + T_c^2T_{EV}T_g^2T_r^2\pi + T_c^2T_{EV}^2T_gT_r^2\pi + T_c^2T_{EV}^2T_g^2T_r\pi) + 4DR^2T_{12}T_c^2T_{EV}^2T_g^2T_r^2\pi + K_P[2F_PMR^2T_cT_{EV}^2T_gT_r^2\alpha_0\beta];$$

$$p_9 = MR(2T_cT_{EV}^2T_gT_r + 2F_PT_cT_{EV}^2T_r^2 + 2F_PT_{EV}^2T_gT_r^2 + 4F_PT_cT_{EV}T_gT_r^2 + 2F_PT_cT_{EV}^2T_gT_r) + 2DF_PRT_cT_{EV}^2T_gT_r^2 + M^2R^2(T_c^2T_{EV}^2 + T_c^2T_g^2 + T_{EV}^2T_g^2 + T_c^2T_r^2 + T_{EV}^2T_r^2 + T_g^2T_r^2 + 4T_cT_{EV}T_g^2 + 4T_cT_{EV}^2T_g + 4T_c^2T_{EV}T_g + 4T_cT_{EV}T_r^2 + 4T_cT_{EV}^2T_r + 4T_c^2T_{EV}T_r + 4T_cT_gT_r^2 + 4T_cT_g^2T_r + 4T_c^2T_gT_r + 4T_{EV}T_gT_r^2 + 4T_{EV}T_g^2T_r + 4T_{EV}^2T_gT_r + 16T_cT_{EV}T_gT_r) + MR^2T_{12}\pi(4T_c^2T_{EV}^2T_g^2 + 4T_c^2T_{EV}^2T_r^2 + 4T_c^2T_g^2T_r^2 + 4T_{EV}^2T_g^2T_r^2 + 16T_cT_{EV}T_g^2T_r^2 + 16T_cT_{EV}^2T_gT_r^2 + 16T_cT_{EV}^2T_g^2T_r + 16T_c^2T_{EV}T_gT_r^2 + 16T_c^2T_{EV}T_g^2T_r + 16T_c^2T_{EV}^2T_gT_r) + D^2R^2(T_c^2T_{EV}^2T_g^2 + T_c^2T_{EV}^2T_r^2 + T_c^2T_g^2T_r^2 + T_{EV}^2T_g^2T_r^2 + 4T_cT_{EV}T_g^2T_r^2 + 4T_cT_{EV}^2T_gT_r^2 + 4T_cT_{EV}^2T_g^2T_r + 4T_c^2T_{EV}T_gT_r^2 + 4T_c^2T_{EV}T_g^2T_r + 4T_c^2T_{EV}^2T_gT_r) + 8DR^2T_{12}\pi(T_cT_{EV}^2T_g^2T_r^2 + T_c^2T_{EV}T_g^2T_r^2 + T_c^2T_{EV}^2T_gT_r^2 + T_c^2T_{EV}^2T_g^2T_r) + DMR^2(4T_cT_{EV}^2T_g^2 + 4T_c^2T_{EV}T_g^2 \ldots$$

$$+4T_c^2T_{EV}^2T_g+4T_cT_{EV}^2T_r^2+4T_c^2T_{EV}T_r^2+4T_c^2T_{EV}^2T_r+4T_cT_g^2T_r^2+4T_c^2T_gT_r^2+4T_c^2T_g^2T_r$$
$$+4T_{EV}T_g^2T_r^2+4T_{EV}^2T_gT_r^2+4T_{EV}^2T_g^2T_r+16T_cT_{EV}T_gT_r^2+16T_cT_{EV}T_g^2T_r+16T_cT_{EV}^2T_gT_r$$
$$+16T_c^2T_{EV}T_gT_r)+K_P[R^2\alpha_0\beta(2MT_cT_{EV}^2T_gT_r+2F_PMT_cT_{EV}^2T_r^2+2F_PMT_{EV}^2T_gT_r^2$$
$$+2F_PMT_cT_{EV}^2T_gT_r+4F_PMT_cT_{EV}T_gT_r^2+2DF_PT_cT_{EV}^2T_gT_r^2)$$
$$+4F_PMR^2T_{12}T_cT_{EV}^2T_gT_r^2\alpha_0\pi]+K_I[2F_PMR^2T_cT_{EV}^2T_gT_r^2\alpha_0\beta];$$

$$p_8=MR(2T_cT_{EV}^2T_g+2T_cT_{EV}^2T_r+2T_{EV}^2T_gT_r+4T_cT_{EV}T_gT_r+4F_PT_cT_{EV}T_r^2+2F_PT_cT_{EV}^2T_r$$
$$+2F_PT_cT_gT_r^2+2F_PT_{EV}^2T_gT_r+2F_PT_{EV}^2T_r^2+4F_PT_{EV}T_gT_r^2+4F_PT_cT_{EV}T_gT_r)$$
$$+4F_PRT_{12}T_cT_{EV}^2T_gT_r^2\pi+DR(2T_cT_{EV}^2T_gT_r+2F_PT_cT_{EV}^2T_r^2+2F_PT_{EV}^2T_gT_r^2$$
$$+2F_PT_cT_{EV}^2T_gT_r+4F_PT_cT_{EV}T_gT_r^2)+M^2R^2(2T_cT_{EV}^2+2T_c^2T_{EV}+2T_cT_g^2+2T_c^2T_g$$
$$+2T_{EV}T_g^2+2T_{EV}^2T_g+2T_cT_r^2+2T_c^2T_r+2T_{EV}T_r^2+2T_{EV}^2T_r+2T_gT_r^2+2T_g^2T_r+8T_cT_{EV}T_g$$
$$+8T_cT_{EV}T_r+8T_cT_gT_r+8T_{EV}T_gT_r)+MR^2T_{12}\pi(8T_cT_{EV}^2T_g^2+8T_c^2T_{EV}T_g^2+8T_c^2T_{EV}^2T_g$$
$$+8T_cT_{EV}^2T_r^2+8T_c^2T_{EV}T_r^2+8T_c^2T_{EV}^2T_r+8T_cT_g^2T_r^2+8T_c^2T_gT_r^2+8T_c^2T_g^2T_r+8T_{EV}T_g^2T_r^2$$
$$+8T_{EV}^2T_gT_r^2+8T_{EV}^2T_g^2T_r+32T_cT_{EV}T_gT_r^2+32T_cT_{EV}T_g^2T_r+32T_cT_{EV}^2T_gT_r+32T_c^2T_{EV}T_gT_r)$$
$$+D^2R^2(2T_cT_{EV}^2T_g^2+2T_c^2T_{EV}T_g^2+2T_c^2T_{EV}^2T_g+2T_cT_{EV}^2T_r^2+2T_c^2T_{EV}T_r^2+2T_c^2T_{EV}^2T_r$$
$$+2T_cT_g^2T_r^2+2T_c^2T_gT_r^2+2T_c^2T_g^2T_r+2T_{EV}T_g^2T_r^2+2T_{EV}^2T_gT_r^2+2T_{EV}^2T_g^2T_r+8T_cT_{EV}T_gT_r^2$$
$$+8T_cT_{EV}T_g^2T_r+8T_cT_{EV}^2T_gT_r+8T_c^2T_{EV}T_gT_r)+DMR^2(2T_c^2T_{EV}^2+2T_c^2T_g^2+2T_{EV}^2T_g^2$$
$$+2T_c^2T_r^2+2T_{EV}^2T_r^2+2T_g^2T_r^2+8T_cT_{EV}T_g^2+8T_cT_{EV}^2T_g+8T_c^2T_{EV}T_g+8T_cT_{EV}T_r^2$$
$$+8T_cT_{EV}^2T_r+8T_c^2T_{EV}T_r+8T_cT_gT_r^2+8T_cT_g^2T_r+8T_c^2T_gT_r+8T_{EV}T_gT_r^2+8T_{EV}T_g^2T_r$$
$$+8T_{EV}^2T_gT_r+32T_cT_{EV}T_gT_r)+DR^2T_{12}\pi(4T_c^2T_{EV}^2T_g^2+4T_c^2T_{EV}^2T_r^2+4T_c^2T_g^2T_r^2$$
$$+4T_{EV}^2T_g^2T_r^2+16T_cT_{EV}T_g^2T_r^2+16T_cT_{EV}^2T_gT_r^2+16T_cT_{EV}^2T_g^2T_r+16T_c^2T_{EV}T_gT_r^2$$
$$+16T_c^2T_{EV}T_g^2T_r+16T_c^2T_{EV}^2T_gT_r)+K_P[MR^2\alpha_0\beta(2T_cT_{EV}^2T_g+2T_cT_{EV}^2T_r+2T_{EV}^2T_gT_r$$
$$+4T_cT_{EV}T_gT_r+2F_PT_{EV}^2T_r^2+2F_PT_cT_{EV}^2T_r+2F_PT_cT_gT_r^2+2F_PT_{EV}^2T_gT_r+4F_PT_cT_{EV}T_r^2$$
$$+4F_PT_{EV}T_gT_r^2+4F_PT_cT_{EV}T_gT_r)+DR^2\alpha_0\beta(2T_cT_{EV}^2T_gT_r+2F_PT_cT_{EV}^2T_r^2+2F_PT_{EV}^2T_gT_r^2$$
$$+2F_PT_cT_{EV}^2T_gT_r+4F_PT_cT_{EV}T_gT_r^2)+R^2T_{12}\alpha_0\pi(4MT_cT_{EV}^2T_gT_r+4F_PMT_cT_{EV}^2T_r^2$$
$$+4F_PMT_{EV}^2T_gT_r^2+8F_PMT_cT_{EV}T_gT_r^2+4F_PMT_cT_{EV}^2T_gT_r+4DF_PT_cT_{EV}^2T_gT_r^2$$
$$+4F_PT_cT_{EV}^2T_gT_r^2\beta)]+K_I[R^2\alpha_0\beta(2MT_cT_{EV}^2T_gT_r+2F_PMT_cT_{EV}^2T_r^2+2F_PMT_{EV}^2T_gT_r^2$$
$$+2F_PMT_cT_{EV}^2T_gT_r+4F_PMT_cT_{EV}T_gT_r^2+2DF_PT_cT_{EV}^2T_gT_r^2)$$
$$+4F_PMR^2T_{12}T_cT_{EV}^2T_gT_r^2\alpha_0\pi];$$

$$
\begin{aligned}
p_7 = {} & 2MR(T_cT_{EV}^2 + T_{EV}^2T_g + T_{EV}^2T_r + T_cT_gT_r) + 4MR(T_cT_{EV}T_g + T_cT_{EV}T_r + T_{EV}T_gT_r) \\
& + 2F_PMR(T_cT_r^2 + T_cT_r^2 + T_{EV}^2T_r + T_gT_r^2 + T_{EV}^2T_r + T_gT_r^2 + T_cT_gT_r) + 4F_PMR(T_{EV}T_r^2 \\
& + T_{EV}T_r^2 + T_cT_{EV}T_r + T_{EV}T_gT_r) + 4RT_{12}\pi(T_cT_{EV}^2T_gT_r + F_PT_cT_{EV}^2T_r^2 + F_PT_{EV}^2T_gT_r^2) \\
& + 2DR(T_cT_{EV}^2T_g + T_cT_{EV}^2T_r + T_{EV}^2T_gT_r + T_cT_{EV}^2T_g + T_cT_{EV}^2T_r + T_{EV}^2T_gT_r + F_PT_{EV}^2T_r^2 \\
& + F_PT_{EV}^2T_r^2 + F_PT_cT_gT_r^2 + F_PT_{EV}^2T_gT_r + F_PT_cT_{EV}^2T_r) + 4DR(T_cT_{EV}T_gT_r + F_PT_cT_{EV}T_r^2 \\
& + F_PT_{EV}T_gT_r^2 + F_PT_cT_{EV}T_gT_r) + F_P^2T_{EV}^2T_r^2 + M^2R^2(T_c^2 + T_{EV}^2 + T_g^2 + T_r^2 + 4T_cT_{EV} \\
& + 4T_cT_g + 4T_{EV}T_g + 4T_cT_r + 4T_{EV}T_r + 4T_gT_r) + D^2R^2(T_c^2T_{EV}^2 + T_c^2T_g^2 + T_{EV}^2T_g^2 + T_c^2T_r^2 \\
& + T_{EV}^2T_r^2 + T_g^2T_r^2 + 4T_cT_{EV}T_g^2 + 4T_cT_{EV}^2T_g + 4T_c^2T_{EV}T_g + 4T_cT_{EV}T_r^2 + 4T_cT_{EV}^2T_r \\
& + 4T_c^2T_{EV}T_r + 4T_cT_gT_r^2 + 4T_cT_g^2T_r + 4T_c^2T_gT_r + 4T_{EV}T_gT_r^2 + 4T_{EV}T_g^2T_r + 4T_{EV}^2T_gT_r \\
& + 16T_cT_{EV}T_gT_r) + DMR^2(4T_cT_{EV}^2 + 4T_c^2T_{EV} + 4T_cT_g^2 + 4T_c^2T_g + 4T_{EV}T_g^2 + 4T_{EV}^2T_g \\
& + 4T_cT_r^2 + 4T_c^2T_r + 4T_{EV}T_r^2 + 4T_{EV}^2T_r + 4T_gT_r^2 + 4T_g^2T_r + 16T_cT_{EV}T_g + 16T_cT_{EV}T_r \\
& + 16T_cT_gT_r + 16T_{EV}T_gT_r) + F_PRT_{12}T_cT_g\pi(4T_{EV}^2T_r + 8T_{EV}T_r^2) + MR^2T_{12}\pi(4T_c^2T_{EV}^2 \\
& + 4T_c^2T_g^2 + 4T_{EV}^2T_g^2 + 4T_c^2T_r^2 + 4T_{EV}^2T_r^2 + 4T_g^2T_r^2 + 16T_cT_{EV}T_g^2 + 16T_cT_{EV}^2T_g + 16T_c^2T_{EV}T_g \\
& + 16T_cT_{EV}T_r^2 + 16T_cT_{EV}^2T_r + 16T_c^2T_{EV}T_r + 16T_cT_gT_r^2 + 16T_cT_g^2T_r + 16T_c^2T_gT_r + 16T_{EV}T_gT_r^2 \\
& + 16T_{EV}T_g^2T_r + 16T_{EV}^2T_gT_r + 64T_cT_{EV}T_gT_r) + DR^2T_{12}\pi(8T_cT_{EV}^2T_g^2 + 8T_c^2T_{EV}T_g^2 \\
& + 8T_c^2T_{EV}^2T_g + 8T_cT_{EV}^2T_r^2 + 8T_c^2T_{EV}T_r^2 + 8T_c^2T_{EV}^2T_r + 8T_cT_g^2T_r^2 + 8T_c^2T_gT_r^2 + 8T_c^2T_g^2T_r \\
& + 8T_{EV}T_g^2T_r^2 + 8T_{EV}^2T_gT_r^2 + 8T_{EV}^2T_g^2T_r + 32T_cT_{EV}T_gT_r^2 + 32T_cT_{EV}T_g^2T_r + 32T_cT_{EV}^2T_gT_r \\
& + 32T_c^2T_{EV}T_gT_r) + K_P[2F_P^2RT_{EV}^2T_r^2\alpha_0\beta + MR^2\alpha_0\beta(2T_cT_{EV}^2 + 2T_{EV}^2T_g + 2T_{EV}^2T_r \\
& + 2T_cT_gT_r + 4T_cT_{EV}T_g + 4T_cT_{EV}T_r + 4T_{EV}T_gT_r + 2F_PT_cT_r^2 + 2F_PT_{EV}^2T_r + 2F_PT_gT_r^2 \\
& + 2F_PT_cT_gT_r + 4F_PT_{EV}T_r^2 + 4F_PT_cT_{EV}T_r + 4F_PT_{EV}T_gT_r) + DR^2\alpha_0\beta(2T_cT_{EV}^2T_g \\
& + 2T_cT_{EV}^2T_r + 2T_{EV}^2T_gT_r + 4T_cT_{EV}T_gT_r + 2F_PT_{EV}^2T_r^2 + 2F_PT_cT_{EV}^2T_r + 2F_PT_cT_gT_r^2 \\
& + 2F_PT_{EV}^2T_gT_r + 4F_PT_cT_{EV}T_r^2 + 4F_PT_{EV}T_gT_r^2 + 4F_PT_cT_{EV}T_gT_r) \\
& + MR^2T_{12}\alpha_0\pi(4F_PT_{EV}^2T_r^2 + 4T_cT_{EV}^2T_g + 4T_cT_{EV}^2T_r + 4T_{EV}^2T_gT_r + 8T_cT_{EV}T_gT_r \\
& + 4F_PT_cT_{EV}^2T_r + 4F_PT_cT_gT_r^2 + 4F_PT_{EV}^2T_gT_r + 8F_PT_cT_{EV}T_r^2 + 8F_PT_{EV}T_gT_r^2 \\
& + 8F_PT_cT_{EV}T_gT_r) + R^2T_{12}\alpha_0\pi(4DT_cT_{EV}^2T_gT_r + 4DF_PT_cT_{EV}^2T_r^2 + 4DF_PT_{EV}^2T_gT_r^2 \\
& + 4DF_PT_cT_{EV}^2T_gT_r + 8DF_PT_cT_{EV}T_gT_r^2 + 4T_cT_{EV}^2T_gT_r\beta + 4F_PT_cT_{EV}^2T_r^2\beta \\
& + 4F_PT_{EV}^2T_gT_r^2\beta + 4F_PT_cT_{EV}^2T_gT_r\beta + 8F_PT_cT_{EV}T_gT_r^2\beta)] + K_P^2[F_P^2R^2T_{EV}^2T_r^2\alpha_0^2\beta^2]...
\end{aligned}
$$

$$+K_I[MR^2\alpha_0\beta(2T_cT_{EV}^2T_g+2T_cT_{EV}^2T_r+2T_{EV}^2T_gT_r+4T_cT_{EV}T_gT_r+2F_PT_{EV}^2T_r^2$$
$$+2F_PT_cT_{EV}^2T_r+2F_PT_cT_gT_r^2+2F_PT_{EV}^2T_gT_r+4F_PT_cT_{EV}T_r^2+4F_PT_{EV}T_gT_r^2$$
$$+4F_PT_cT_{EV}T_gT_r)+DR^2\alpha_0\beta(2T_cT_{EV}^2T_gT_r+2F_PT_cT_{EV}^2T_r^2+2F_PT_{EV}^2T_gT_r^2$$
$$+2F_PT_cT_{EV}^2T_gT_r+4F_PT_cT_{EV}T_gT_r^2)+MR^2T_{12}\alpha_0\pi(4T_cT_{EV}^2T_gT_r+4F_PT_cT_{EV}^2T_r^2$$
$$+4F_PT_{EV}^2T_gT_r^2+4F_PT_cT_{EV}^2T_gT_r+8F_PT_cT_{EV}T_gT_r^2)+4F_PR^2T_{12}T_cT_{EV}^2T_gT_r^2\alpha_0\pi(D+\beta)];$$

$$p_6=2MR(T_cT_g+T_cT_r+T_gT_r+T_{EV}^2)+4MR(T_cT_{EV}+T_{EV}T_g+T_{EV}T_r)+F_PMR(2T_r^2$$
$$+2T_cT_r+2T_gT_r+4T_{EV}T_r)+DR(2T_cT_{EV}^2+2T_{EV}^2T_g+2T_{EV}^2T_r+2T_cT_gT_r+4T_cT_{EV}T_g$$
$$+4T_cT_{EV}T_r+4T_{EV}T_gT_r+2F_PT_cT_gT_r+2F_PT_cT_r^2+2F_PT_{EV}^2T_r+2F_PT_gT_r^2+4F_PT_cT_{EV}T_r$$
$$+4F_PT_{EV}T_gT_r+4F_PT_{EV}T_r^2)+RT_{12}\pi(4T_cT_{EV}^2T_g+4T_cT_{EV}^2T_r+4T_{EV}^2T_gT_r+8T_cT_{EV}T_gT_r)$$
$$+F_PRT_{12}\pi(4T_{EV}^2T_r^2+4T_cT_{EV}^2T_r+4T_cT_gT_r^2+4T_{EV}^2T_gT_r+8T_cT_{EV}T_r^2+8T_{EV}T_gT_r^2$$
$$+8T_cT_{EV}T_gT_r)+2(F_PT_{EV}^2T_r+F_P^2T_{EV}T_r^2)+2M^2R^2(T_c+T_{EV}+T_g+T_r)+2DMR^2(T_c^2$$
$$+T_{EV}^2+T_g^2+T_r^2)+8DMR^2(T_cT_{EV}+T_cT_g+T_{EV}T_g+T_cT_r+T_{EV}T_r+T_gT_r)$$
$$+4F_P^2RT_{12}T_{EV}^2T_r^2\alpha_0\pi+8MR^2T_{12}\pi(T_cT_{EV}^2+T_c^2T_{EV}+T_cT_g^2+T_c^2T_g+T_{EV}T_g^2+T_{EV}^2T_g$$
$$+T_cT_r^2+T_c^2T_r+T_{EV}T_r^2+T_{EV}^2T_r+T_gT_r^2+T_g^2T_r)+32MR^2T_{12}\pi(T_cT_{EV}T_g+T_cT_{EV}T_r$$
$$+T_{EV}T_gT_r+T_cT_gT_r)+2D^2R^2(T_cT_{EV}^2+T_c^2T_{EV}+T_cT_g^2+T_c^2T_g+T_{EV}T_g^2+T_{EV}^2T_g+T_cT_r^2$$
$$+T_c^2T_r+T_{EV}T_r^2+T_{EV}^2T_r+T_gT_r^2+T_g^2T_r)+8D^2R^2(T_cT_{EV}T_g+T_cT_{EV}T_r+T_{EV}T_gT_r$$
$$+T_cT_gT_r)+4DR^2T_{12}\pi(T_g^2T_r^2+T_c^2T_{EV}^2+T_c^2T_g^2+T_{EV}^2T_g^2+T_c^2T_r^2+T_{EV}^2T_r^2)$$
$$+16DR^2T_{12}\pi(T_cT_{EV}T_g^2+T_cT_{EV}^2T_g+T_c^2T_{EV}T_g+T_cT_{EV}T_r^2+T_cT_{EV}^2T_r+T_c^2T_{EV}T_r+T_cT_gT_r^2$$
$$+T_cT_g^2T_r+T_c^2T_gT_r+T_{EV}T_gT_r^2+T_{EV}T_g^2T_r+T_{EV}^2T_gT_r)+64DR^2T_{12}T_cT_{EV}T_gT_r\pi$$
$$+K_P[4R\alpha_0\beta(F_PT_{EV}^2T_r+F_P^2T_{EV}T_r^2)+MR^2\alpha_0\beta(2T_{EV}^2+2T_cT_g+2T_cT_r+2T_gT_r$$
$$+4T_cT_{EV}+4T_{EV}T_g+4T_{EV}T_r+2F_PT_r^2+2F_PT_cT_r+2F_PT_gT_r+4F_PT_{EV}T_r)$$
$$+R^2\alpha_0\beta(2DT_cT_{EV}^2+2DT_{EV}^2T_g+2DT_{EV}^2T_r+2DT_cT_gT_r+4DT_cT_{EV}T_g+4DT_cT_{EV}T_r$$
$$+4DT_{EV}T_gT_r+2DF_PT_cT_r^2+2DF_PT_{EV}^2T_r+2DF_PT_gT_r^2+2DF_PT_cT_gT_r+4DF_PT_{EV}T_r^2$$
$$+4DF_PT_cT_{EV}T_r+4DF_PT_{EV}T_gT_r)+MR^2T_{12}\alpha_0\pi(4T_cT_{EV}^2+4T_{EV}^2T_g+4T_{EV}^2T_r+4T_cT_gT_r$$
$$+8T_cT_{EV}T_g+8T_cT_{EV}T_r+8T_{EV}T_gT_r+4F_PT_cT_r^2+4F_PT_{EV}^2T_r+4F_PT_gT_r^2+4F_PT_cT_gT_r$$
$$+8F_PT_{EV}T_r^2+8F_PT_cT_{EV}T_r+8F_PT_{EV}T_gT_r)+R^2T_{12}\alpha_0\pi(4DT_cT_{EV}^2T_g+4DT_cT_{EV}^2T_r$$
$$+4DT_{EV}^2T_gT_r+8DT_cT_{EV}T_gT_r+4DF_PT_{EV}^2T_r^2+4DF_PT_cT_{EV}^2T_r+4DF_PT_cT_gT_r^2$$
$$+4DF_PT_{EV}^2T_gT_r+8DF_PT_cT_{EV}T_r^2+8DF_PT_{EV}T_gT_r^2+8DF_PT_cT_{EV}T_gT_r+4T_cT_{EV}^2T_g\beta$$
$$+4T_cT_{EV}^2T_r\beta+4T_{EV}^2T_gT_r\beta+8T_cT_{EV}T_gT_r\beta+4F_PT_{EV}^2T_r^2\beta+4F_PT_cT_{EV}^2T_r\beta...$$

$$+4F_PT_cT_gT_r^2\beta+4F_PT_{EV}^2T_gT_r\beta+8F_PT_{EV}T_gT_r^2\beta+8F_PT_cT_{EV}T_gT_r\beta+8F_PT_cT_{EV}T_r^2\beta)]$$
$$+K_P^2[R^2\alpha_0^2(2F_PT_{EV}^2T_r\beta^2+2F_P^2T_{EV}T_r^2\beta^2+4F_P^2T_{12}T_{EV}^2T_r^2\beta\pi)]+K_I[2F_P^2RT_{EV}^2T_r^2\alpha_0\beta$$
$$+MR^2\alpha_0\beta(2T_cT_{EV}^2+2T_{EV}^2T_g+2T_{EV}^2T_r+2T_cT_gT_r+4T_cT_{EV}T_g+4T_cT_{EV}T_r+4T_{EV}T_gT_r$$
$$+2F_PT_cT_r^2+2F_PT_{EV}^2T_r+2F_PT_gT_r^2+2F_PT_cT_gT_r+4F_PT_{EV}T_r^2+4F_PT_cT_{EV}T_r$$
$$+4F_PT_{EV}T_gT_r)+DR^2\alpha_0\beta(2T_cT_{EV}^2T_g+2T_cT_{EV}^2T_r+2T_{EV}^2T_gT_r+4T_cT_{EV}T_gT_r+2F_PT_{EV}^2T_r^2$$
$$+2F_PT_cT_{EV}^2T_r+2F_PT_cT_gT_r^2+2F_PT_{EV}^2T_gT_r+4F_PT_cT_{EV}T_r^2+4F_PT_{EV}T_gT_r^2$$
$$+4F_PT_cT_{EV}T_gT_r)+MR^2T_{12}\alpha_0\pi(4T_cT_{EV}^2T_g+4T_cT_{EV}^2T_r+4T_{EV}^2T_gT_r+8T_cT_{EV}T_gT_r$$
$$+4F_PT_{EV}^2T_r^2+4F_PT_cT_{EV}^2T_r+4F_PT_cT_gT_r^2+4F_PT_{EV}^2T_gT_r+8F_PT_cT_{EV}T_r^2+8F_PT_{EV}T_gT_r^2$$
$$+8F_PT_cT_{EV}T_gT_r)+R^2T_{12}\alpha_0\pi(4DT_cT_{EV}^2T_gT_r+4DF_PT_cT_{EV}^2T_r^2+4DF_PT_{EV}^2T_gT_r^2$$
$$+4DF_PT_cT_{EV}^2T_gT_r+8DF_PT_cT_{EV}T_gT_r^2+4T_cT_{EV}^2T_gT_r\beta+4F_PT_cT_{EV}^2T_r^2\beta+4F_PT_{EV}^2T_gT_r^2\beta$$
$$+4F_PT_cT_{EV}^2T_gT_r\beta+8F_PT_cT_{EV}T_gT_r^2\beta)]+K_IK_P[2F_P^2R^2T_{EV}^2T_r^2\alpha_0^2\beta^2];$$

$$p_5=T_{EV}^2+F_P^2T_r^2+M^2R^2+4F_PT_{EV}T_r+MR(2T_c+2T_g+2T_r+4T_{EV}+2F_PT_r)$$
$$+DR(2T_cT_g+2T_cT_r+2T_gT_r+2T_{EV}^2+4T_cT_{EV}+4T_{EV}T_g+4T_{EV}T_r+2F_PT_r^2+2F_PT_cT_r$$
$$+4F_PT_{EV}T_r+2F_PT_gT_r)+4RT_{12}\pi(T_cT_{EV}^2+T_{EV}^2T_g+T_{EV}^2T_r+T_cT_gT_r)+8RT_{12}\pi(T_cT_{EV}T_g$$
$$+T_cT_{EV}T_r+T_{EV}T_gT_r)+4F_PRT_{12}\pi(T_cT_r^2+T_{EV}^2T_r+T_gT_r^2+T_cT_gT_r)+8F_PRT_{12}\pi(T_{EV}T_r^2$$
$$+T_cT_{EV}T_r+T_{EV}T_gT_r)+D^2R^2(T_c^2+T_{EV}^2+T_g^2+T_r^2)+4D^2R^2(T_cT_{EV}+T_cT_g+T_{EV}T_g$$
$$+T_cT_r+T_{EV}T_r+T_gT_r)+4DMR^2(T_c+T_{EV}+T_g+T_r)+4MR^2T_{12}\pi(T_c^2+T_{EV}^2+T_g^2+T_r^2)$$
$$+16MR^2T_{12}\pi(T_cT_{EV}+T_cT_g+T_{EV}T_g+T_cT_r+T_{EV}T_r+T_gT_r)+8DR^2T_{12}\pi(T_cT_{EV}^2+T_c^2T_{EV}$$
$$+T_cT_g^2+T_c^2T_g+T_{EV}T_g^2+T_{EV}^2T_g+T_cT_r^2+T_c^2T_r+T_{EV}T_r^2+T_{EV}^2T_r+T_gT_r^2+T_g^2T_r)$$
$$+32DR^2T_{12}\pi(T_cT_{EV}T_g+T_cT_{EV}T_r+T_cT_gT_r+T_{EV}T_gT_r)+K_P[R\alpha_0\beta(2T_{EV}^2+2F_P^2T_r^2$$
$$+8F_PT_{EV}T_r)+MR^2\alpha_0\beta(2T_c+2T_g+2T_r+4T_{EV}+2F_PT_r)+DR^2\alpha_0\beta(2T_{EV}^2+2T_cT_g$$
$$+2T_cT_r+2T_gT_r+4T_cT_{EV}+4T_{EV}T_g+4T_{EV}T_r+2F_PT_r^2+2F_PT_cT_r+2F_PT_gT_r$$
$$+4F_PT_{EV}T_r)+8RT_{12}\alpha_0\pi(F_PT_{EV}^2T_r+F_P^2T_{EV}T_r^2)+MR^2T_{12}\alpha_0\pi(4T_{EV}^2+4T_cT_g+4T_cT_r$$
$$+4T_gT_r+8T_cT_{EV}+8T_{EV}T_g+8T_{EV}T_r+4F_PT_r^2+4F_PT_cT_r+4F_PT_gT_r+8F_PT_{EV}T_r)$$
$$+R^2T_{12}\alpha_0\pi(4DT_cT_{EV}^2+4DT_{EV}^2T_g+4DT_{EV}^2T_r+4DT_cT_gT_r+8DT_cT_{EV}T_g+8DT_cT_{EV}T_r$$
$$+8DT_{EV}T_gT_r+4DF_PT_cT_r^2+4DF_PT_{EV}^2T_r+4DF_PT_gT_r^2+4DF_PT_cT_gT_r+8DF_PT_{EV}T_r^2$$
$$+8DF_PT_cT_{EV}T_r+8DF_PT_{EV}T_gT_r+4T_cT_{EV}^2\beta+4T_{EV}^2T_g\beta+4T_{EV}^2T_r\beta+4T_cT_gT_r\beta$$
$$+8T_cT_{EV}T_g\beta+8T_cT_{EV}T_r\beta+8T_{EV}T_gT_r\beta+4F_PT_cT_r^2\beta+4F_PT_{EV}^2T_r\beta+4F_PT_gT_r^2\beta$$
$$+4F_PT_cT_gT_r\beta+8F_PT_{EV}T_r^2\beta+8F_PT_cT_{EV}T_r\beta+8F_PT_{EV}T_gT_r\beta)]...$$

$$+K_P^2[R^2\alpha_0^2\beta^2(T_{EV}^2+F_P^2T_r^2+4F_PT_{EV}T_r)+8R^2T_{12}\alpha_0^2\pi\beta(F_PT_{EV}^2T_r+F_P^2T_{EV}T_r^2)]$$
$$+K_I[4R\alpha_0\beta(F_PT_{EV}^2T_r+F_P^2T_{EV}T_r^2)+MR^2\alpha_0\beta(2T_{EV}^2+2T_cT_g+2T_cT_r+2T_gT_r$$
$$+4T_cT_{EV}+4T_{EV}T_g+4T_{EV}T_r+2F_PT_r^2+2F_PT_cT_r+2F_PT_gT_r+4F_PT_{EV}T_r)$$
$$+DR^2\alpha_0\beta(2T_cT_{EV}^2+2T_{EV}^2T_g+2T_{EV}^2T_r+2T_cT_gT_r+4T_cT_{EV}T_g+4T_cT_{EV}T_r+4T_{EV}T_gT_r$$
$$+2F_PT_cT_r^2+2F_PT_{EV}^2T_r+2F_PT_gT_r^2+2F_PT_cT_gT_r+4F_PT_{EV}T_r^2+4F_PT_cT_{EV}T_r$$
$$+4F_PT_{EV}T_gT_r)+4F_P^2RT_{12}T_{EV}^2T_r^2\alpha_0\pi+MR^2T_{12}\alpha_0\pi(4T_cT_{EV}^2+4T_{EV}^2T_g+4T_{EV}^2T_r$$
$$+4T_cT_gT_r+8T_cT_{EV}T_g+8T_cT_{EV}T_r+8T_{EV}T_gT_r+4F_PT_cT_r^2+4F_PT_{EV}^2T_r+4F_PT_gT_r^2$$
$$+4F_PT_cT_gT_r+8F_PT_{EV}T_r^2+8F_PT_cT_{EV}T_r+8F_PT_{EV}T_gT_r)+R^2T_{12}\alpha_0\pi(4DT_cT_{EV}^2T_g$$
$$+4DT_cT_{EV}^2T_r+4DT_{EV}^2T_gT_r+8DT_cT_{EV}T_gT_r+4DF_PT_{EV}^2T_r^2+4DF_PT_cT_{EV}^2T_r$$
$$+4DF_PT_cT_gT_r^2+4DF_PT_{EV}^2T_gT_r+8DF_PT_cT_{EV}T_r^2+8DF_PT_{EV}T_gT_r^2+8DF_PT_cT_{EV}T_gT_r$$
$$+4T_cT_{EV}^2T_g\beta+4T_cT_{EV}^2T_r\beta+4T_{EV}^2T_gT_r\beta+8T_cT_{EV}T_gT_r\beta+4F_PT_{EV}^2T_r^2\beta+4F_PT_cT_{EV}^2T_r\beta$$
$$+4F_PT_cT_gT_r^2\beta+4F_PT_{EV}^2T_gT_r\beta+8F_PT_cT_{EV}T_r^2\beta+8F_PT_{EV}T_gT_r^2\beta+8F_PT_cT_{EV}T_gT_r\beta]$$
$$+K_I^2[F_P^2R^2T_{EV}^2T_r^2\alpha_0^2\beta^2]+K_IK_P[R^2\alpha_0^2(4F_PT_{EV}^2T_r\beta^2+4F_P^2T_{EV}T_r^2\beta^2$$
$$+8F_P^2T_{12}T_{EV}^2T_r^2\beta\pi)];$$

$$p_4=2(T_{EV}+F_PT_r+MR+DMR^2)+DR(2T_c+2T_g+2T_r+2F_PT_r+4T_{EV})+RT_{12}\pi(4T_{EV}^2$$
$$+4T_cT_g+4T_cT_r+4T_gT_r+8T_cT_{EV}+8T_{EV}T_g+8T_{EV}T_r+4F_PT_cT_r+4F_PT_gT_r+4F_PT_r^2$$
$$+8F_PT_{EV}T_r)+8MR^2T_{12}\pi(T_c+T_{EV}+T_g+T_r)+DR^2T_{12}\pi(4T_c^2+4T_{EV}^2+4T_g^2+4T_r^2$$
$$+16T_cT_{EV}+16T_cT_g+16T_{EV}T_g+16T_cT_r+16T_{EV}T_r+16T_gT_r)+2D^2R^2(T_c+T_{EV}+T_g$$
$$+T_r)+K_P[4R\alpha_0\beta(T_{EV}+F_PT_r)+R^2\alpha_0\beta(2M+2DT_c+2DT_g+2DT_r+4DT_{EV}$$
$$+2DF_PT_r)+RT_{12}\alpha_0\pi(4T_{EV}^2+4F_P^2T_r^2+16F_PT_{EV}T_r)+MR^2T_{12}\alpha_0\pi(4T_c+4T_g+4T_r$$
$$+8T_{EV}+4F_PT_r)+R^2T_{12}\alpha_0\pi(4DT_gT_r+4DT_cT_g+4DT_cT_r+4DT_{EV}^2+8DT_{EV}T_g$$
$$+8DT_{EV}T_r+8DT_cT_{EV}+4DF_PT_r^2+4DF_PT_cT_r+4DF_PT_gT_r+8DF_PT_{12}T_{EV}T_r+4T_{EV}^2\beta$$
$$+4T_cT_g\beta+4T_cT_r\beta+4T_gT_r\beta+8T_cT_{EV}\beta+8T_{EV}T_g\beta+8T_{EV}T_r\beta+4F_PT_r^2\beta+4F_PT_cT_r\beta$$
$$+4F_PT_gT_r\beta+8F_PT_{EV}T_r\beta)]+K_P^2[2R^2\alpha_0^2\beta^2(T_{EV}+F_PT_r)+R^2T_{12}\alpha_0^2\pi\beta(4T_{EV}^2+4F_P^2T_r^2$$
$$+16F_PT_{EV}T_r)]+K_I[R\alpha_0\beta(2T_{EV}^2+2F_P^2T_r^2+8F_PT_{EV}T_r)+MR^2\alpha_0\beta(2T_c+2T_g+2T_r$$
$$+4T_{EV}+2F_PT_r)+DR^2\alpha_0\beta(2T_{EV}^2+2T_cT_g+2T_cT_r+2T_gT_r+4T_cT_{EV}+4T_{EV}T_g+4T_{EV}T_r$$
$$+2F_PT_r^2+2F_PT_cT_r+2F_PT_gT_r+4F_PT_{EV}T_r)+8RT_{12}\alpha_0\pi(F_PT_{EV}^2T_r+F_P^2T_{EV}T_r^2)$$
$$+MR^2T_{12}\alpha_0\pi(4T_{EV}^2+4T_cT_g+4T_cT_r+4T_gT_r+8T_cT_{EV}+8T_{EV}T_g+8T_{EV}T_r+4F_PT_r^2$$
$$+4F_PT_cT_r+4F_PT_gT_r+8F_PT_{EV}T_r)+R^2T_{12}\alpha_0\pi(4DT_cT_{EV}^2+4DT_{EV}^2T_g+4DT_{EV}^2T_r\ldots$$

$$+4DT_cT_gT_r+8DT_cT_{EV}T_g+8DT_cT_{EV}T_r+8DT_{EV}T_gT_r+4DF_PT_cT_r^2+4DF_PT_{EV}^2T_r$$
$$+4DF_PT_gT_r^2+4DF_PT_cT_gT_r+8DF_PT_{EV}T_r^2+8DF_PT_cT_{EV}T_r+8DF_PT_{EV}T_gT_r+4T_cT_{EV}^2\beta$$
$$+4T_{EV}^2T_g\beta+4T_{EV}^2T_r\beta+4T_cT_gT_r\beta+8T_cT_{EV}T_g\beta+8T_cT_{EV}T_r\beta+8T_{EV}T_gT_r\beta+4F_PT_cT_r^2\beta$$
$$+4F_PT_{EV}^2T_r\beta+4F_PT_gT_r^2\beta+4F_PT_cT_gT_r\beta+8F_PT_{EV}T_r^2\beta+8F_PT_cT_{EV}T_r\beta$$
$$+8F_PT_{EV}T_gT_r\beta)]+K_I^2[R^2\alpha_0^2(2F_PT_{EV}^2T_r\beta^2+2F_P^2T_{EV}T_r^2\beta^2+4F_P^2T_{12}T_{EV}^2T_r^2\beta\pi)]$$
$$+K_IK_P[R^2\alpha_0^2\beta^2(2T_{EV}^2+2F_P^2T_r^2+8F_PT_{EV}T_r)+16R^2T_{12}\alpha_0^2\beta\pi(F_PT_{EV}^2T_r+F_P^2T_{EV}T_r^2)];$$

$$p_3=1+2DR+RT_{12}\pi(4T_c+4T_g+4T_r+4F_PT_r+8T_{EV})+R^2(4MT_{12}\pi+D^2)$$
$$+8DR^2T_{12}\pi(T_c+T_{EV}+T_g+T_r)+K_P[2\alpha_0\beta(R+DR^2)+8RT_{12}\alpha_0\pi(T_{EV}+F_PT_r)$$
$$+R^2T_{12}\alpha_0\pi(4M+4DT_c+4DT_g+4DT_r+4DF_PT_r+8DT_{EV}+4T_c\beta+4T_g\beta+4T_r\beta$$
$$+4F_PT_r\beta+8T_{EV}\beta)]+K_P^2[R^2\alpha_0^2(\beta^2+8T_{12}T_{EV}\beta\pi+8F_PT_{12}T_r\beta\pi)]+K_I[4R\alpha_0\beta(T_{EV}$$
$$+F_PT_r)+R^2\alpha_0\beta(2M+2DT_c+2DT_g+2DT_r+2DF_PT_r+4DT_{EV})+RT_{12}\alpha_0\pi(4T_{EV}^2$$
$$+4F_P^2T_r^2+16F_PT_{EV}T_r)+R^2T_{12}\alpha_0\pi(4MT_c+4MT_g+4MT_r+4F_PMT_r+8MT_{EV}$$
$$+4DT_{EV}^2+4DT_cT_g+4DT_cT_r+4DT_gT_r+8DT_cT_{EV}+8DT_{EV}T_g+8DT_{EV}T_r+4DF_PT_r^2$$
$$+4DF_PT_cT_r+4DF_PT_gT_r+8DF_PT_{EV}T_r+4T_{EV}^2\beta+4T_cT_g\beta+4T_cT_r\beta+4T_gT_r\beta$$
$$+8T_cT_{EV}\beta+8T_{EV}T_g\beta+8T_{EV}T_r\beta+4F_PT_r^2\beta+4F_PT_cT_r\beta+4F_PT_gT_r\beta+8F_PT_{EV}T_r\beta)]$$
$$+K_I^2[R^2\alpha_0^2\beta^2(T_{EV}^2+4F_PT_{EV}T_r+F_P^2T_r^2)+8R^2T_{12}\alpha_0^2\pi\beta(F_PT_{EV}^2T_r+F_P^2T_{EV}T_r^2)]$$
$$+K_IK_P[4R^2\alpha_0^2\beta^2(T_{EV}+F_PT_r)+R^2T_{12}\alpha_0^2\pi\beta(8T_{EV}^2+8F_P^2T_r^2+32F_PT_{EV}T_r)];$$

$$p_2=4T_{12}\pi(R+DR^2)+K_P[4T_{12}\alpha_0\pi(R+DR^2+R^2\beta)]+K_P^2[4R^2T_{12}\alpha_0^2\beta\pi]+K_I[2\alpha_0\beta(R$$
$$+DR^2)+8RT_{12}\alpha_0\pi(T_{EV}+F_PT_r)+R^2T_{12}\alpha_0\pi(4M+4DT_c+4DT_g+4DT_r+4DF_PT_r$$
$$+8DT_{EV}+4T_c\beta+8T_{EV}\beta+4T_g\beta+4T_r\beta+4F_PT_r\beta)]+K_I^2[2R^2\alpha_0^2\beta^2(T_{EV}+F_PT_r)$$
$$+R^2T_{12}\alpha_0^2\beta\pi(4T_{EV}^2+4F_P^2T_r^2+16F_PT_{EV}T_r)]+K_IK_P[R^2\alpha_0^2(2\beta^2+16T_{12}T_{EV}\beta\pi$$
$$+16F_PT_{12}T_r\beta\pi)];$$

$$p_1=K_I[4\alpha_0\pi(RT_{12}+DR^2T_{12}+R^2T_{12}\beta)]+K_I^2[R^2\alpha_0^2(\beta^2+8T_{12}T_{EV}\beta\pi+8F_PT_{12}T_r\beta\pi]$$
$$+K_IK_P[8R^2T_{12}\alpha_0^2\beta\pi];$$

$$p_0=K_I^2[4R^2T_{12}\alpha_0^2\beta\pi];$$

$$q_{11} = K_P\left[2K_{EV}MR^2T_{EV}T_c^{\,2}T_g^{\,2}T_r^{\,2}\alpha_1\beta\right];$$

$$\begin{aligned}q_{10} = {} & K_P[K_{EV}R^2\alpha_1(2MT_c^{\,2}T_g^{\,2}T_r^{\,2}\beta + 4MT_{EV}T_cT_g^{\,2}T_r^{\,2}\beta + 4MT_{EV}T_c^{\,2}T_gT_r^{\,2}\beta \\ & + 4MT_{EV}T_c^{\,2}T_g^{\,2}T_r\beta + 2DT_{EV}T_c^{\,2}T_g^{\,2}T_r^{\,2}\beta + 4MT_{12}T_{EV}T_c^{\,2}T_g^{\,2}T_r^{\,2}\pi)] \\ & + K_I[2K_{EV}MR^2T_{EV}T_c^{\,2}T_g^{\,2}T_r^{\,2}\alpha_1\beta];\end{aligned}$$

$$\begin{aligned}q_9 = {} & K_P[K_{EV}R^2\alpha_1\beta(2MT_{EV}T_c^{\,2}T_g^{\,2} + 2MT_{EV}T_c^{\,2}T_r^{\,2} + 2MT_{EV}T_g^{\,2}T_r^{\,2} + 4MT_cT_g^{\,2}T_r^{\,2} \\ & + 4MT_c^{\,2}T_gT_r^{\,2} + 4MT_c^{\,2}T_g^{\,2}T_r + 8MT_{EV}T_cT_gT_r^{\,2} + 8MT_{EV}T_cT_g^{\,2}T_r + 8MT_{EV}T_c^{\,2}T_gT_r \\ & + 2DT_c^{\,2}T_g^{\,2}T_r^{\,2} + 4DT_{EV}T_cT_g^{\,2}T_r^{\,2} + 4DT_{EV}T_c^{\,2}T_gT_r^{\,2} + 4DT_{EV}T_c^{\,2}T_g^{\,2}T_r) \\ & + K_{EV}R^2\alpha_1\pi(4MT_{12}T_c^{\,2}T_g^{\,2}T_r^{\,2} + 4T_{12}T_{EV}T_c^{\,2}T_g^{\,2}T_r^{\,2}\beta + 8MT_{12}T_{EV}T_cT_g^{\,2}T_r^{\,2} \\ & + 8MT_{12}T_{EV}T_c^{\,2}T_gT_r^{\,2} + 8MT_{12}T_{EV}T_c^{\,2}T_g^{\,2}T_r + 4DT_{12}T_{EV}T_c^{\,2}T_g^{\,2}T_r^{\,2})] \\ & + K_I[K_{EV}R^2\alpha_1\beta(2MT_c^{\,2}T_g^{\,2}T_r^{\,2} + 4MT_{EV}T_cT_g^{\,2}T_r^{\,2} + 4MT_{EV}T_c^{\,2}T_gT_r^{\,2} + 4MT_{EV}T_c^{\,2}T_g^{\,2}T_r \\ & + 2DT_{EV}T_c^{\,2}T_g^{\,2}T_r^{\,2}) + 4K_{EV}MR^2T_{12}T_{EV}T_c^{\,2}T_g^{\,2}T_r^{\,2}\alpha_1\pi];\end{aligned}$$

$$\begin{aligned}q_8 = {} & K_P[K_{EV}R^2\alpha_1\beta(2MT_c^{\,2}T_g^{\,2} + 2MT_c^{\,2}T_r^{\,2} + 2MT_g^{\,2}T_r^{\,2} + 4MT_{EV}T_cT_g^{\,2} + 4MT_{EV}T_c^{\,2}T_g \\ & + 4MT_{EV}T_cT_r^{\,2} + 4MT_{EV}T_c^{\,2}T_r + 4MT_{EV}T_gT_r^{\,2} + 4MT_{EV}T_g^{\,2}T_r + 8MT_cT_gT_r^{\,2} + 8MT_cT_g^{\,2}T_r \\ & + 8MT_c^{\,2}T_gT_r + 2DT_{EV}T_c^{\,2}T_g^{\,2} + 2DT_{EV}T_c^{\,2}T_r^{\,2} + 2DT_{EV}T_g^{\,2}T_r^{\,2} + 4DT_cT_g^{\,2}T_r^{\,2} + 4DT_c^{\,2}T_gT_r^{\,2} \\ & + 4DT_c^{\,2}T_g^{\,2}T_r + 16MT_{EV}T_cT_gT_r + 8DT_{EV}T_cT_gT_r^{\,2} + 8DT_{EV}T_cT_g^{\,2}T_r + 8DT_{EV}T_c^{\,2}T_gT_r) \\ & + 2F_PK_{EV}RT_{EV}T_cT_gT_r^{\,2}\alpha_1\beta + K_{EV}R^2\alpha_1\pi(4DT_{12}T_c^{\,2}T_g^{\,2}T_r^{\,2} + 4MT_{12}T_{EV}T_c^{\,2}T_g^{\,2} \\ & + 4MT_{12}T_{EV}T_c^{\,2}T_r^{\,2} + 4MT_{12}T_{EV}T_g^{\,2}T_r^{\,2} + 8MT_{12}T_cT_g^{\,2}T_r^{\,2} + 8MT_{12}T_c^{\,2}T_gT_r^{\,2} \\ & + 8MT_{12}T_c^{\,2}T_g^{\,2}T_r + 8DT_{12}T_{EV}T_cT_g^{\,2}T_r^{\,2} + 8DT_{12}T_{EV}T_c^{\,2}T_gT_r^{\,2} + 8DT_{12}T_{EV}T_c^{\,2}T_g^{\,2}T_r \\ & + 16MT_{12}T_{EV}T_cT_gT_r^{\,2} + 16MT_{12}T_{EV}T_cT_g^{\,2}T_r + 16MT_{12}T_{EV}T_c^{\,2}T_gT_r + 4T_{12}T_c^{\,2}T_g^{\,2}T_r^{\,2}\beta \\ & + 8T_{12}T_{EV}T_cT_g^{\,2}T_r^{\,2}\beta + 8T_{12}T_{EV}T_c^{\,2}T_gT_r^{\,2}\beta + 8T_{12}T_{EV}T_c^{\,2}T_g^{\,2}T_r\beta)] \\ & + K_P^{\,2}[2F_PK_{EV}R^2T_{EV}T_cT_gT_r^{\,2}\alpha_0\alpha_1\beta^2] + K_I[K_{EV}R^2\alpha_1\beta(2MT_{EV}T_c^{\,2}T_g^{\,2} + 2MT_{EV}T_c^{\,2}T_r^{\,2} \\ & + 2MT_{EV}T_g^{\,2}T_r^{\,2} + 4MT_cT_g^{\,2}T_r^{\,2} + 4MT_c^{\,2}T_gT_r^{\,2} + 4MT_c^{\,2}T_g^{\,2}T_r + 2DT_c^{\,2}T_g^{\,2}T_r^{\,2} \\ & + 4DT_{EV}T_cT_g^{\,2}T_r^{\,2} + 4DT_{EV}T_c^{\,2}T_gT_r^{\,2} + 4DT_{EV}T_c^{\,2}T_g^{\,2}T_r + 8MT_{EV}T_cT_gT_r^{\,2} + 8MT_{EV}T_cT_g^{\,2}T_r \\ & + 8MT_{EV}T_c^{\,2}T_gT_r) + K_{EV}R^2\alpha_1\pi(4MT_{12}T_c^{\,2}T_g^{\,2}T_r^{\,2} + 8MT_{12}T_{EV}T_cT_g^{\,2}T_r^{\,2} \\ & + 8MT_{12}T_{EV}T_c^{\,2}T_gT_r^{\,2} + 8MT_{12}T_{EV}T_c^{\,2}T_g^{\,2}T_r + 4DT_{12}T_{EV}T_c^{\,2}T_g^{\,2}T_r^{\,2} + 4T_{12}T_{EV}T_c^{\,2}T_g^{\,2}T_r^{\,2}\beta)];\end{aligned}$$

$$
\begin{aligned}
q_7 = {} & K_P[2K_{EV}R\alpha_1\beta(F_PT_{EV}T_cT_r^2 + F_PT_{EV}T_gT_r^2 + F_PT_cT_gT_r^2 + T_{EV}T_cT_gT_r + F_PT_{EV}T_cT_gT_r) \\
& + K_{EV}R^2\alpha_1\beta(2MT_{EV}T_c^2 + 2MT_{EV}T_g^2 + 2MT_{EV}T_r^2 + 4MT_cT_g^2 + 4MT_c^2T_g + 4MT_cT_r^2 \\
& + 4MT_c^2T_r + 4MT_gT_r^2 + 4MT_g^2T_r + 2DT_c^2T_g^2 + 2DT_c^2T_r^2 + 2DT_g^2T_r^2 + 8MT_{EV}T_cT_g \\
& + 8MT_{EV}T_cT_r + 8MT_{EV}T_gT_r + 16MT_cT_gT_r + 4DT_{EV}T_cT_g^2 + 4DT_{EV}T_c^2T_g + 4DT_{EV}T_cT_r^2 \\
& + 4DT_{EV}T_c^2T_r + 4DT_{EV}T_gT_r^2 + 4DT_{EV}T_g^2T_r + 8DT_cT_gT_r^2 + 8DT_cT_g^2T_r + 8DT_c^2T_gT_r \\
& + 16DT_{EV}T_cT_gT_r) + 4F_PK_{EV}RT_{12}T_{EV}T_cT_gT_r^2\alpha_1\pi + K_{EV}R^2\alpha_1\pi(4MT_{12}T_c^2T_g^2 \\
& + 4MT_{12}T_c^2T_r^2 + 4MT_{12}T_g^2T_r^2 + 8MT_{12}T_{EV}T_cT_g^2 + 8MT_{12}T_{EV}T_c^2T_g + 8MT_{12}T_{EV}T_cT_r^2 \\
& + 8MT_{12}T_{EV}T_c^2T_r + 8MT_{12}T_{EV}T_gT_r^2 + 8MT_{12}T_{EV}T_g^2T_r + 16MT_{12}T_cT_gT_r^2 + 16MT_{12}T_cT_g^2T_r \\
& + 16MT_{12}T_c^2T_gT_r + 4DT_{12}T_{EV}T_c^2T_g^2 + 4DT_{12}T_{EV}T_c^2T_r^2 + 4DT_{12}T_{EV}T_g^2T_r^2 + 8DT_{12}T_cT_g^2T_r^2 \\
& + 8DT_{12}T_c^2T_gT_r^2 + 8DT_{12}T_c^2T_g^2T_r + 32MT_{12}T_{EV}T_cT_gT_r + 16DT_{12}T_{EV}T_cT_gT_r^2 \\
& + 16DT_{12}T_{EV}T_cT_g^2T_r + 16DT_{12}T_{EV}T_c^2T_gT_r + 4T_{12}T_{EV}T_c^2T_g^2\beta + 4T_{12}T_{EV}T_c^2T_r^2\beta \\
& + 4T_{12}T_{EV}T_g^2T_r^2\beta + 8T_{12}T_cT_g^2T_r^2\beta + 8T_{12}T_c^2T_gT_r^2\beta + 8T_{12}T_c^2T_g^2T_r\beta + 16T_{12}T_{EV}T_cT_gT_r^2\beta \\
& + 16T_{12}T_{EV}T_cT_g^2T_r\beta + 16T_{12}T_{EV}T_c^2T_gT_r\beta)] + K_P{}^2[K_{EV}R^2\alpha_0\alpha_1(2T_{EV}T_cT_gT_r\beta^2 \\
& + 2F_PT_{EV}T_cT_r^2\beta^2 + 2F_PT_{EV}T_gT_r^2\beta^2 + 2F_PT_cT_gT_r^2\beta^2 + 2F_PT_{EV}T_cT_gT_r\beta^2 \\
& + 8F_PT_{12}T_{EV}T_cT_gT_r^2\beta\pi)] + K_I[2F_PK_{EV}RT_{EV}T_cT_gT_r^2\alpha_1\beta + K_{EV}R^2\alpha_1\beta(2MT_c^2T_g^2 \\
& + 2MT_c^2T_r^2 + 2MT_g^2T_r^2 + 4MT_{EV}T_cT_g^2 + 4MT_{EV}T_c^2T_g + 4MT_{EV}T_cT_r^2 + 4MT_{EV}T_c^2T_r \\
& + 4MT_{EV}T_gT_r^2 + 4MT_{EV}T_g^2T_r + 8MT_cT_gT_r^2 + 8MT_cT_g^2T_r + 8MT_c^2T_gT_r + 16MT_{EV}T_cT_gT_r \\
& + 2DT_{EV}T_c^2T_g^2 + 2DT_{EV}T_c^2T_r^2 + 2DT_{EV}T_g^2T_r^2 + 4DT_cT_g^2T_r^2 + 4DT_c^2T_gT_r^2 + 4DT_c^2T_g^2T_r \\
& + 8DT_{EV}T_cT_gT_r^2 + 8DT_{EV}T_cT_g^2T_r + 8DT_{EV}T_c^2T_gT_r) + K_{EV}R^2\alpha_1\pi(4MT_{12}T_{EV}T_c^2T_g^2 \\
& + 4MT_{12}T_{EV}T_c^2T_r^2 + 4MT_{12}T_{EV}T_g^2T_r^2 + 8MT_{12}T_cT_g^2T_r^2 + 8MT_{12}T_c^2T_gT_r^2 + 8MT_{12}T_c^2T_g^2T_r \\
& + 16MT_{12}T_{EV}T_cT_gT_r^2 + 16MT_{12}T_{EV}T_cT_g^2T_r + 16MT_{12}T_{EV}T_c^2T_gT_r + 4DT_{12}T_c^2T_g^2T_r^2 \\
& + 8DT_{12}T_{EV}T_cT_g^2T_r^2 + 8DT_{12}T_{EV}T_c^2T_gT_r^2 + 8DT_{12}T_{EV}T_c^2T_g^2T_r + 4T_{12}T_c^2T_g^2T_r^2\beta \\
& + 8T_{12}T_{EV}T_cT_g^2T_r^2\beta + 8T_{12}T_{EV}T_c^2T_gT_r^2\beta + 8T_{12}T_{EV}T_c^2T_g^2T_r\beta)] \\
& + K_IK_P[4F_PK_{EV}R^2T_{EV}T_cT_gT_r^2\alpha_0\alpha_1\beta^2];
\end{aligned}
$$

$$
\begin{aligned}
q_6 = {} & K_P[2K_{EV}R\alpha_1\beta(T_{EV}T_cT_g + T_{EV}T_cT_r + T_{EV}T_gT_r + T_cT_gT_r + F_PT_{EV}T_r^2 + F_PT_cT_r^2 \\
& + F_PT_gT_r^2 + F_PT_{EV}T_cT_r + F_PT_{EV}T_gT_r + F_PT_cT_gT_r) + K_{EV}R^2\alpha_1\beta(2MT_c^2 + 2MT_g^2 \\
& + 2MT_r^2\alpha_1\beta + 4MT_{EV}T_g + 4MT_{EV}T_r + 8MT_cT_g + 8MT_cT_r + 8MT_gT_r + 4MT_{EV}T_c \\
& + 2DT_{EV}T_c^2 + 2DT_{EV}T_g^2 + 2DT_{EV}T_r^2 + 4DT_cT_g^2 + 4DT_c^2T_g + 4DT_cT_r^2 + 4DT_c^2T_r \\
& + 4DT_gT_r^2 + 4DT_g^2T_r + 8DT_{EV}T_cT_g + 8DT_{EV}T_cT_r + 8DT_{EV}T_gT_r + 16DT_cT_gT_r)\ldots
\end{aligned}
$$

$$+4K_{EV}R\alpha_1\pi(F_PT_{12}T_{EV}T_cT_r^2+F_PT_{12}T_{EV}T_gT_r^2+F_PT_{12}T_cT_gT_r^2+T_{12}T_{EV}T_cT_gT_r$$
$$+F_PT_{12}T_{EV}T_cT_gT_r)+K_{EV}R^2\alpha_1\pi(4MT_{12}T_{EV}T_c^2+4MT_{12}T_{EV}T_g^2+4MT_{12}T_{EV}T_r^2$$
$$+8MT_{12}T_cT_g^2+8MT_{12}T_c^2T_g+8MT_{12}T_cT_r^2+8MT_{12}T_c^2T_r+8MT_{12}T_gT_r^2+8MT_{12}T_g^2T_r$$
$$+16MT_{12}T_{EV}T_cT_g+16MT_{12}T_{EV}T_cT_r+16MT_{12}T_{EV}T_gT_r+32MT_{12}T_cT_gT_r+4DT_{12}T_c^2T_g^2$$
$$+4DT_{12}T_c^2T_r^2+4DT_{12}T_g^2T_r^2+8DT_{12}T_{EV}T_cT_g^2+8DT_{12}T_{EV}T_c^2T_g+8DT_{12}T_{EV}T_cT_r^2$$
$$+8DT_{12}T_{EV}T_c^2T_r+8DT_{12}T_{EV}T_gT_r^2+8DT_{12}T_{EV}T_g^2T_r+16DT_{12}T_cT_gT_r^2+16DT_{12}T_cT_g^2T_r$$
$$+16DT_{12}T_c^2T_gT_r+32DT_{12}T_{EV}T_cT_gT_r+4T_{12}T_c^2T_g^2\beta+4T_{12}T_c^2T_r^2\beta+4T_{12}T_g^2T_r^2\beta$$
$$+8T_{12}T_{EV}T_cT_g^2\beta+8T_{12}T_{EV}T_c^2T_g\beta+8T_{12}T_{EV}T_cT_r^2\beta+8T_{12}T_{EV}T_c^2T_r\beta+8T_{12}T_{EV}T_gT_r^2\beta$$
$$+8T_{12}T_{EV}T_g^2T_r\beta+16T_{12}T_cT_gT_r^2\beta+16T_{12}T_cT_g^2T_r\beta+16T_{12}T_c^2T_gT_r\beta+32T_{12}T_{EV}T_cT_gT_r\beta)]$$
$$+K_P{}^2[K_{EV}R^2\alpha_0\alpha_1(2T_{EV}T_cT_g\beta^2+2T_{EV}T_cT_r\beta^2+2T_{EV}T_gT_r\beta^2+2T_cT_gT_r\beta^2$$
$$+2F_PT_{EV}T_r^2\beta^2+2F_PT_cT_r^2\beta^2+2F_PT_gT_r^2\beta^2+2F_PT_{EV}T_cT_r\beta^2+2F_PT_{EV}T_gT_r\beta^2$$
$$+2F_PT_cT_gT_r\beta^2+8F_PT_{12}T_{EV}T_cT_r^2\beta\pi+8F_PT_{12}T_{EV}T_gT_r^2\beta\pi+8F_PT_{12}T_cT_gT_r^2\beta\pi$$
$$+8T_{12}T_{EV}T_cT_gT_r\beta\pi+8F_PT_{12}T_{EV}T_cT_gT_r\beta\pi)]+K_I[2K_{EV}R\alpha_1\beta(F_PT_{EV}T_cT_r^2$$
$$+F_PT_{EV}T_gT_r^2+F_PT_cT_gT_r^2+T_{EV}T_cT_gT_r+F_PT_{EV}T_cT_gT_r)+K_{EV}R^2\alpha_1\beta(2MT_{EV}T_c^2$$
$$+2MT_{EV}T_g^2+2MT_{EV}T_r^2+4MT_cT_g^2+4MT_c^2T_g+4MT_cT_r^2+4MT_c^2T_r+4MT_gT_r^2$$
$$+4MT_g^2T_r+8MT_{EV}T_cT_g+8MT_{EV}T_cT_r+8MT_{EV}T_gT_r+16MT_cT_gT_r+2DT_c^2T_g^2\alpha_1\beta$$
$$+2DT_c^2T_r^2+2DT_g^2T_r^2+4DT_{EV}T_cT_g^2+4DT_{EV}T_c^2T_g+4DT_{EV}T_cT_r^2+4DT_{EV}T_c^2T_r$$
$$+4DT_{EV}T_gT_r^2+4DT_{EV}T_g^2T_r+8DT_cT_gT_r^2+8DT_cT_g^2T_r+8DT_c^2T_gT_r+16DT_{EV}T_cT_gT_r)$$
$$+K_{EV}R^2\alpha_1\pi(4MT_{12}T_c^2T_g^2+4MT_{12}T_c^2T_r^2+4MT_{12}T_g^2T_r^2+8MT_{12}T_{EV}T_cT_g^2$$
$$+8MT_{12}T_{EV}T_c^2T_g+8MT_{12}T_{EV}T_cT_r^2+8MT_{12}T_{EV}T_c^2T_r+8MT_{12}T_{EV}T_gT_r^2+8MT_{12}T_{EV}T_g^2T_r$$
$$+16MT_{12}T_cT_gT_r^2+16MT_{12}T_cT_g^2T_r+16MT_{12}T_c^2T_gT_r+32MT_{12}T_{EV}T_cT_gT_r$$
$$+4F_PT_{12}T_{EV}T_cT_gT_r^2+4DT_{12}T_{EV}T_c^2T_g^2+4DT_{12}T_{EV}T_c^2T_r^2+4DT_{12}T_{EV}T_g^2T_r^2+8DT_{12}T_cT_g^2T_r^2$$
$$+8DT_{12}T_c^2T_gT_r^2+8DT_{12}T_c^2T_g^2T_r+16DT_{12}T_{EV}T_cT_gT_r^2+16DT_{12}T_{EV}T_cT_g^2T_r$$
$$+16DT_{12}T_{EV}T_c^2T_gT_r+4T_{12}T_{EV}T_c^2T_g^2\beta+4T_{12}T_{EV}T_c^2T_r^2\beta+4T_{12}T_{EV}T_g^2T_r^2\beta+8T_{12}T_cT_g^2T_r^2\beta$$
$$+8T_{12}T_c^2T_gT_r^2\beta+8T_{12}T_c^2T_g^2T_r\beta+16T_{12}T_{EV}T_cT_gT_r^2\beta+16T_{12}T_{EV}T_cT_g^2T_r\beta$$
$$+16T_{12}T_{EV}T_c^2T_gT_r\beta)]+K_I{}^2[2F_PK_{EV}R^2T_{EV}T_cT_gT_r^2\alpha_0\alpha_1\beta^2]$$
$$+K_IK_P[K_{EV}R^2\alpha_0\alpha_1(4T_{EV}T_cT_gT_r\beta^2+4F_PT_{EV}T_cT_r^2\beta^2+4F_PT_{EV}T_gT_r^2\beta^2+4F_PT_cT_gT_r^2\beta^2$$
$$+4F_PT_{EV}T_cT_gT_r\beta^2+16F_PT_{12}T_{EV}T_cT_gT_r^2\beta\pi)];$$

$$
\begin{aligned}
q_5 = {} & K_P[2K_{EV}R\alpha_1\beta(T_{EV}T_c + T_{EV}T_g + T_{EV}T_r + T_cT_g + T_cT_r + T_gT_r + F_PT_r^2 + F_PT_{EV}T_r \\
& + F_PK_{EV}T_cT_r + F_PK_{EV}T_gT_r) + K_{EV}R^2\alpha_1\beta(2MT_{EV} + 4MT_c + 4MT_g + 4MT_r + 2DT_c^2 \\
& + 2DT_g^2 + 2DT_r^2 + 4DT_{EV}T_c + 4DT_{EV}T_g + 4DT_{EV}T_r + 8DT_cT_g + 8DT_cT_r + 8DT_gT_r) \\
& + 4K_{EV}R\alpha_1\pi(T_{12}T_{EV}T_cT_g + T_{12}T_{EV}T_cT_r + T_{12}T_{EV}T_gT_r + T_{12}T_cT_gT_r + F_PT_{12}T_{EV}T_r^2 \\
& + F_PT_{12}T_cT_r^2 + F_PT_{12}T_gT_r^2 + F_PT_{12}T_{EV}T_cT_r + F_PT_{12}T_{EV}T_gT_r + F_PT_{12}T_cT_gT_r) \\
& + K_{EV}R^2\alpha_1\pi(4MT_{12}T_c^2 + 4MT_{12}T_g^2 + 4MT_{12}T_r^2 + 8MT_{12}T_{EV}T_c + 8MT_{12}T_{EV}T_g \\
& + 8MT_{12}T_{EV}T_r + 16MT_{12}T_cT_g + 16MT_{12}T_cT_r + 16MT_{12}T_gT_r + 4DT_{12}T_{EV}T_c^2 + 4DT_{12}T_{EV}T_g^2 \\
& + 4DT_{12}T_{EV}T_r^2 + 8DT_{12}T_cT_g^2 + 8DT_{12}T_c^2T_g + 8DT_{12}T_cT_r^2 + 8DT_{12}T_c^2T_r + 8DT_{12}T_gT_r^2 \\
& + 8DT_{12}T_g^2T_r + 16DT_{12}T_{EV}T_cT_g + 16DT_{12}T_{EV}T_cT_r + 16DT_{12}T_{EV}T_gT_r + 32DT_{12}T_cT_gT_r \\
& + 4T_{12}T_{EV}T_c^2\beta + 4T_{12}T_{EV}T_g^2\beta + 4T_{12}T_{EV}T_r^2\beta + 8T_{12}T_cT_g^2\beta + 8T_{12}T_c^2T_g\beta + 8T_{12}T_cT_r^2\beta \\
& + 8T_{12}T_c^2T_r\beta + 8T_{12}T_gT_r^2\beta + 8T_{12}T_g^2T_r\beta + 16T_{12}T_{EV}T_cT_g\beta + 16T_{12}T_{EV}T_cT_r\beta \\
& + 16T_{12}T_{EV}T_gT_r\beta + 32T_{12}T_cT_gT_r\beta)] + K_P{}^2[K_{EV}R^2\alpha_0\alpha_1(2F_PT_r^2\beta^2 + 2T_{EV}T_c\beta^2 \\
& + 2T_{EV}T_g\beta^2 + 2T_{EV}T_r\beta^2 + 2T_cT_g\beta^2 + 2T_cT_r\beta^2 + 2T_gT_r\beta^2 + 2F_PT_{EV}T_r\beta^2 + 2F_PT_cT_r\beta^2 \\
& + 2F_PT_gT_r\beta^2 + 8T_{12}T_{EV}T_cT_g\beta\pi + 8T_{12}T_{EV}T_cT_r\beta\pi + 8T_{12}T_{EV}T_gT_r\beta\pi + 8T_{12}T_cT_gT_r\beta\pi \\
& + 8F_PT_{12}T_{EV}T_r^2\beta\pi + 8F_PT_{12}T_cT_r^2\beta\pi + 8F_PT_{12}T_gT_r^2\beta\pi + 8F_PT_{12}T_{EV}T_cT_r\beta\pi \\
& + 8F_PT_{12}T_{EV}T_gT_r\beta\pi + 8F_PT_{12}T_cT_gT_r\beta\pi)] + K_I[2K_{EV}R\alpha_1\beta(T_{EV}T_cT_g + T_{EV}T_cT_r \\
& + T_{EV}T_gT_r + T_cT_gT_r + F_PT_{EV}T_r^2 + F_PT_cT_r^2 + F_PT_gT_r^2 + F_PT_{EV}T_cT_r + F_PT_{EV}T_gT_r \\
& + F_PT_cT_gT_r) + K_{EV}R^2\alpha_1\beta(2MT_c^2 + 2MT_g^2 + 2MT_r^2 + 4MT_{EV}T_c + 4MT_{EV}T_g \\
& + 4MT_{EV}T_r + 8MT_cT_g + 8MT_cT_r + 8MT_gT_r + 2DT_{EV}T_c^2 + 2DT_{EV}T_g^2 + 2DT_{EV}T_r^2 \\
& + 4DT_cT_g^2 + 4DT_c^2T_g + 4DT_cT_r^2 + 4DT_c^2T_r + 4DT_gT_r^2 + 4DT_g^2T_r + 8DT_{EV}T_cT_g \\
& + 8DT_{EV}T_cT_r + 8DT_{EV}T_gT_r + 16DT_cT_gT_r) + 4K_{EV}R\alpha_1\pi(F_PT_{12}T_{EV}T_cT_r^2 + F_PT_{12}T_{EV}T_gT_r^2 \\
& + F_PT_{12}T_cT_gT_r^2 + T_{12}T_{EV}T_cT_gT_r + F_PT_{12}T_{EV}T_cT_gT_r) + K_{EV}R^2\alpha_1\pi(4MT_{12}T_{EV}T_c^2 \\
& + 4MT_{12}T_{EV}T_g^2 + 4MT_{12}T_{EV}T_r^2 + 8MT_{12}T_cT_g^2 + 8MT_{12}T_c^2T_g + 8MT_{12}T_cT_r^2 + 8MT_{12}T_c^2T_r \\
& + 8MT_{12}T_gT_r^2 + 8MT_{12}T_g^2T_r + 16MT_{12}T_{EV}T_cT_g + 16MT_{12}T_{EV}T_cT_r + 16MT_{12}T_{EV}T_gT_r \\
& + 32MT_{12}T_cT_gT_r + 4DT_{12}T_c^2T_g^2 + 4DT_{12}T_c^2T_r^2 + 4DT_{12}T_g^2T_r^2 + 32DT_{12}T_{EV}T_cT_gT_r \\
& + 4T_{12}T_c^2T_g^2\beta + 4T_{12}T_c^2T_r^2\beta + 4T_{12}T_g^2T_r^2\beta + 8T_{12}T_{EV}T_cT_g^2\beta + 8T_{12}T_{EV}T_c^2T_g\beta \\
& + 8T_{12}T_{EV}T_cT_r^2\beta + 8T_{12}T_{EV}T_c^2T_r\beta + 8T_{12}T_{EV}T_gT_r^2\beta + 8T_{12}T_{EV}T_g^2T_r\beta + 16T_{12}T_cT_gT_r^2\beta \\
& + 16T_{12}T_cT_g^2T_r\beta + 16T_{12}T_c^2T_gT_r\beta + 32T_{12}T_{EV}T_cT_gT_r\beta)]\ldots
\end{aligned}
$$

$$+K_I{}^2[K_{EV}R^2\alpha_1\pi(8DT_{12}T_{EV}T_cT_g^2+8DT_{12}T_{EV}T_c^2T_g+8DT_{12}T_{EV}T_cT_r^2+8DT_{12}T_{EV}T_c^2T_r$$
$$+8DT_{12}T_{EV}T_gT_r^2+8DT_{12}T_{EV}T_g^2T_r+16DT_{12}T_cT_gT_r^2+16DT_{12}T_cT_g^2T_r+16DT_{12}T_c^2T_gT_r)$$
$$+K_{EV}R^2\alpha_0\alpha_1(2T_{EV}T_cT_gT_r\beta^2+2F_PT_{EV}T_cT_r^2\beta^2+2F_PT_{EV}T_gT_r^2\beta^2+2F_PT_cT_gT_r^2\beta^2$$
$$+2F_PT_{EV}T_cT_gT_r\beta^2+8F_PT_{12}T_{EV}T_cT_gT_r^2\beta\pi)]+K_IK_P[K_{EV}R^2\alpha_0\alpha_1(4T_{EV}T_cT_g\beta^2$$
$$+4T_{EV}T_cT_r\beta^2+4T_{EV}T_gT_r\beta^2+4T_cT_gT_r\beta^2+4F_PT_{EV}T_r^2\beta^2+4F_PT_cT_r^2\beta^2$$
$$+4F_PT_gT_r^2\beta^2+4F_PT_{EV}T_cT_r\beta^2+4F_PT_{EV}T_gT_r\beta^2+4F_PT_cT_gT_r\beta^2$$
$$+16F_PT_{12}T_{EV}T_cT_r^2\beta\pi+16F_PT_{12}T_{EV}T_gT_r^2\beta\pi+16F_PT_{12}T_cT_gT_r^2\beta\pi$$
$$+16T_{12}T_{EV}T_cT_gT_r\beta\pi+16F_PT_{12}T_{EV}T_cT_gT_r\beta\pi)];$$

$$q_4=K_P[2K_{EV}R\alpha_1\beta(T_{EV}+T_c+T_g+T_r+F_PT_r)+K_{EV}R^2\alpha_1\beta(2M+2DT_{EV}+4DT_c$$
$$+4DT_g+4DT_r)+4K_{EV}RT_{12}\alpha_1\pi(T_{EV}T_c+T_{EV}T_g+T_{EV}T_r+T_cT_g+T_cT_r+T_gT_r+F_PT_r^2$$
$$+T_{EV}T_c+T_{EV}T_g+T_{EV}T_r+T_cT_g+T_cT_r+T_gT_r+F_PT_r^2+F_PT_{EV}T_r+F_PT_cT_r+F_PT_gT_r)$$
$$+K_{EV}R^2T_{12}\alpha_1\pi(4MT_{EV}+8MT_c+8MT_g+8MT_r+4MT_{EV}+8MT_c+8MT_g+8MT_r$$
$$+4DT_c^2+4DT_g{}^2+4DT_r^2+8DT_{EV}T_c+8DT_{EV}T_g+8DT_{EV}T_r+16DT_cT_g+16DT_cT_r$$
$$+16DT_gT_r+4T_c^2\beta+4T_g{}^2\beta+4T_r^2\beta+4T_c^2\beta+4T_g{}^2\beta+4T_r^2\beta+8T_{EV}T_c\beta+8T_{EV}T_g\beta$$
$$+8T_{EV}T_r\beta+16T_cT_g\beta+16T_cT_r\beta+16T_gT_r\beta)]+K_P{}^2[K_{EV}R^2\alpha_0\alpha_1(2T_{EV}\beta^2+2T_c\beta^2$$
$$+2T_g\beta^2+2T_r\beta^2+2F_PT_r\beta^2+8T_{12}T_{EV}T_c\beta\pi+8T_{12}T_{EV}T_g\beta\pi+8T_{12}T_{EV}T_r\beta\pi$$
$$+8T_{12}T_cT_g\beta\pi+8T_{12}T_cT_r\beta\pi+8T_{12}T_gT_r\beta\pi+8F_PT_{12}T_r^2\beta\pi+8F_PT_{12}T_{EV}T_r\beta\pi$$
$$+8F_PT_{12}T_cT_r\beta\pi+8F_PT_{12}T_gT_r\beta\pi]+K_I[2K_{EV}R\alpha_1\beta(T_{EV}T_c+T_{EV}T_g+T_{EV}T_r+T_cT_g$$
$$+T_cT_r+T_gT_r+F_PT_r^2+F_PT_{EV}T_r+F_PT_cT_r+F_PT_gT_r+K_{EV}R^2\alpha_1\beta(2MT_{EV}+4MT_c$$
$$+4MT_g+4MT_r+2DT_c^2+2DT_g{}^2+2DT_r^2+4DT_{EV}T_c+4DT_{EV}T_g+4DT_{EV}T_r$$
$$+8DT_cT_g+8DT_cT_r+8DT_gT_r)+4K_{EV}RT_{12}\alpha_1\pi(T_{EV}T_cT_g+T_{EV}T_cT_r+T_{EV}T_gT_r$$
$$+T_cT_gT_r+F_PT_{EV}T_r^2+F_PT_cT_r^2+F_PT_gT_r^2+F_PT_{EV}T_cT_r+F_PT_{EV}T_gT_r+F_PT_cT_gT_r)$$
$$+K_{EV}R^2T_{12}\alpha_1\pi(4MT_c^2+4MT_g{}^2+4MT_r^2+8MT_{EV}T_c+8MT_{EV}T_g+8MT_{EV}T_r$$
$$+16MT_cT_g+16MT_cT_r+16MT_gT_r+4DT_{EV}T_c^2+4DT_{EV}T_g{}^2+4DT_{EV}T_r^2+8DT_cT_g{}^2$$
$$+8DT_c^2T_g+8DT_cT_r^2+8DT_c^2T_r+8DT_gT_r^2+8DT_g{}^2T_r+16DT_{EV}T_cT_g+16DT_{EV}T_cT_r$$
$$+16DT_{EV}T_gT_r+32DT_cT_gT_r+4T_{EV}T_c^2\beta+4T_{EV}T_g{}^2\beta+4T_{EV}T_r^2\beta+8T_cT_g{}^2\beta+8T_c^2T_g\beta$$
$$+8T_cT_r^2\beta+8T_c^2T_r\beta+8T_gT_r^2\beta+8T_g{}^2T_r\beta+16T_{EV}T_cT_g\beta+16T_{EV}T_cT_r\beta+16T_{EV}T_gT_r\beta$$
$$+32T_cT_gT_r\beta)]...$$

$$+K_I{}^2[K_{EV}R^2\alpha_0\alpha_1(2T_{EV}T_cT_g\beta^2+2T_{EV}T_cT_r\beta^2+2T_{EV}T_gT_r\beta^2+2T_cT_gT_r\beta^2$$
$$+2F_PT_{EV}T_r^2\beta^2+2F_PT_cT_r^2\beta^2+2F_PT_gT_r^2\beta^2+2F_PT_{EV}T_cT_r\beta^2+2F_PT_{EV}T_gT_r\beta^2$$
$$+2F_PT_cT_gT_r\beta^2+8F_PT_{12}T_{EV}T_cT_r^2\beta\pi+8F_PT_{12}T_{EV}T_gT_r^2\beta\pi+8F_PT_{12}T_cT_gT_r^2\beta\pi$$
$$+8T_{12}T_{EV}T_cT_gT_r\beta\pi+8F_PT_{12}T_{EV}T_cT_gT_r\beta\pi)]+K_IK_P[K_{EV}R^2\alpha_0\alpha_1(4F_PT_r^2\beta^2$$
$$+4T_{EV}T_c\beta^2+4T_{EV}T_g\beta^2+4T_{EV}T_r\beta^2+4T_cT_g\beta^2+4T_cT_r\beta^2+4T_gT_r\beta^2$$
$$+4F_PT_{EV}T_r\beta^2+4F_PT_cT_r\beta^2+4F_PT_gT_r\beta^2+16T_{12}T_{EV}T_cT_g\beta\pi+16T_{12}T_{EV}T_cT_r\beta\pi$$
$$+16T_{12}T_{EV}T_gT_r\beta\pi+16T_{12}T_cT_gT_r\beta\pi+16F_PT_{12}T_{EV}T_r^2\beta\pi+16F_PT_{12}T_cT_r^2\beta\pi$$
$$+16F_PT_{12}T_gT_r^2\beta\pi+16F_PT_{12}T_{EV}T_cT_r\beta\pi+16F_PT_{12}T_{EV}T_gT_r\beta\pi+16F_PT_{12}T_cT_gT_r\beta\pi)];$$

$$q_3=K_P[2K_{EV}\alpha_1\beta(R+DR^2)+4K_{EV}R\alpha_1\pi(T_{12}T_{EV}+T_{12}T_c+T_{12}T_g+T_{12}T_r+F_PT_{12}T_r)$$
$$+K_{EV}R^2\alpha_1\pi(4MT_{12}+4DT_{12}T_{EV}+8DT_{12}T_c+8DT_{12}T_g+8DT_{12}T_r+4T_{12}T_{EV}\beta+8T_{12}T_c\beta$$
$$+8T_{12}T_g\beta+8T_{12}T_r\beta)]+K_P{}^2[K_{EV}R^2\alpha_0\alpha_1(2\beta^2+8T_{12}T_{EV}\beta\pi+8T_{12}T_c\beta\pi+8T_{12}T_g\beta\pi$$
$$+8T_{12}T_r\beta\pi+8F_PT_{12}T_r\beta\pi)]+K_I[2K_{EV}R\alpha_1\beta(T_{EV}+T_c+T_g+T_r+F_PT_r)$$
$$+K_{EV}R^2\alpha_1\beta(2M+2DT_{EV}+4DT_c+4DT_g+4DT_r)+4K_{EV}RT_{12}\alpha_1\pi(T_{EV}T_c+T_{EV}T_g$$
$$+T_{EV}T_r+T_cT_g+T_cT_r+T_gT_r+F_PT_r^2+F_PT_{EV}T_r+F_PT_cT_r+F_PT_gT_r)$$
$$+K_{EV}R^2T_{12}\alpha_1\pi(4MT_{EV}+8MT_c+8MT_g+8MT_r+4DT_c^2+4DT_g^2+4DT_r^2+8DT_{EV}T_c$$
$$+8DT_{EV}T_g+8DT_{EV}T_r+16DT_cT_g+16DT_cT_r+16DT_gT_r+4T_c^2\beta+4T_g^2\beta+4T_r^2\beta$$
$$+8T_{EV}T_c\beta+8T_{EV}T_g\beta+8T_{EV}T_r\beta+16T_cT_g\beta+16T_cT_r\beta+16T_gT_r\beta)]$$
$$+K_I{}^2[K_{EV}R^2\alpha_0\alpha_1(2F_PT_r^2\beta^2+2T_{EV}T_c\beta^2+2T_{EV}T_g\beta^2+2T_{EV}T_r\beta^2+2T_cT_g\beta^2$$
$$+2T_cT_r\beta^2+2T_gT_r\beta^2+2F_PT_{EV}T_r\beta^2+2F_PT_cT_r\beta^2+2F_PT_gT_r\beta^2+8T_{12}T_{EV}T_cT_g\beta\pi$$
$$+8T_{12}T_{EV}T_cT_r\beta\pi+8T_{12}T_{EV}T_gT_r\beta\pi+8T_{12}T_cT_gT_r\beta\pi+8F_PT_{12}T_{EV}T_r^2\beta\pi+8F_PT_{12}T_cT_r^2\beta\pi$$
$$+8F_PT_{12}T_gT_r^2\beta\pi+8F_PT_{12}T_{EV}T_cT_r\beta\pi+8F_PT_{12}T_{EV}T_gT_r\beta\pi+8F_PT_{12}T_cT_gT_r\beta\pi)]$$
$$+K_IK_P[K_{EV}R^2\alpha_0\alpha_1(4T_{EV}\beta^2+4T_c\beta^2+4T_g\beta^2+4T_r\beta^2+4F_PT_r\beta^2+16T_{12}T_{EV}T_c\beta\pi$$
$$+16T_{12}T_{EV}T_g\beta\pi+16T_{12}T_{EV}T_r\beta\pi+16T_{12}T_cT_g\beta\pi+16T_{12}T_cT_r\beta\pi+16T_{12}T_gT_r\beta\pi$$
$$+16F_PT_{12}T_r^2\beta\pi+16F_PT_{12}T_{EV}T_r\beta\pi+16F_PT_{12}T_cT_r\beta\pi+16F_PT_{12}T_gT_r\beta\pi)];$$

$$q_2 = K_P[4K_{EV}T_{12}\alpha_1\pi(R+R^2\beta+DR^2)]+K_P{}^2[8K_{EV}R^2T_{12}\alpha_0\alpha_1\beta\pi]+K_I[2K_{EV}\alpha_1\beta(R$$
$$+DR^2)+4K_{EV}RT_{12}\alpha_1\pi(T_{EV}+T_c+T_g+T_r+F_PT_r)+K_{EV}R^2T_{12}\alpha_1\pi(4DT_{EV}+8DT_c$$
$$+8DT_g+8DT_r+4M+4T_{EV}\beta+8T_c\beta+8T_g\beta+8T_r\beta)]+K_I{}^2[K_{EV}R^2\alpha_0\alpha_1(2T_{EV}\beta^2$$
$$+2T_c\beta^2+2T_g\beta^2+2T_r\beta^2+2F_PT_r\beta^2+8T_{12}T_{EV}T_c\beta\pi+8T_{12}T_{EV}T_g\beta\pi+8T_{12}T_{EV}T_r\beta\pi$$
$$+8T_{12}T_cT_g\beta\pi+8T_{12}T_cT_r\beta\pi+8T_{12}T_gT_r\beta\pi+8F_PT_{12}T_{EV}T_r\beta\pi+8F_PT_{12}T_cT_r\beta\pi$$
$$+8F_PT_{12}T_gT_r\beta\pi+8F_PT_{12}T_r{}^2\beta\pi)]+K_IK_P[K_{EV}R^2\alpha_0\alpha_1(4\beta^2+16T_{12}T_{EV}\beta\pi$$
$$+16T_{12}T_c\beta\pi+16T_{12}T_g\beta\pi+16T_{12}T_r\beta\pi+16F_PT_{12}T_r\beta\pi)];$$

$$q_1 = K_I[4K_{EV}\alpha_1\pi(RT_{12}+R^2T_{12}\beta+DR^2T_{12})]+K_I{}^2[K_{EV}R^2\alpha_0\alpha_1(2\beta^2+8T_{12}T_{EV}\beta\pi$$
$$+8T_{12}T_c\beta\pi+8T_{12}T_g\beta\pi+8T_{12}T_r\beta\pi+8F_PT_{12}T_r\beta\pi)]+K_IK_P[16K_{EV}R^2T_{12}\alpha_0\alpha_1\beta\pi];$$

$$q_0 = K_I{}^2\left[8\pi K_{EV}R^2T_{12}\alpha_0\alpha_1\beta\right];$$

$$r_9 = K_P{}^2[K_{EV}{}^2R^2\alpha_1^2\beta^2T_c{}^2T_g{}^2T_r{}^2];$$

$$r_8 = K_P{}^2[2K_{EV}{}^2R^2\alpha_1^2\beta^2(T_cT_g{}^2T_r{}^2+T_c{}^2T_gT_r{}^2+T_c{}^2T_g{}^2T_r)$$
$$+4K_{EV}{}^2R^2T_{12}\alpha_1^2\beta\pi T_c{}^2T_g{}^2T_r{}^2]+K_IK_P[2K_{EV}{}^2R^2\alpha_1^2\beta^2T_c{}^2T_g{}^2T_r{}^2];$$

$$r_7 = K_P{}^2[K_{EV}{}^2R^2\alpha_1^2\beta^2(T_c{}^2T_g{}^2+T_c{}^2T_r{}^2+T_g{}^2T_r{}^2+4T_cT_gT_r{}^2$$
$$+4T_cT_g{}^2T_r+4T_c{}^2T_gT_r)+8K_{EV}{}^2R^2T_{12}\alpha_1^2\beta\pi(T_cT_g{}^2T_r{}^2+T_c{}^2T_gT_r{}^2+T_c{}^2T_g{}^2T_r)]$$
$$+K_I{}^2[K_{EV}{}^2R^2\alpha_1^2\beta^2T_c{}^2T_g{}^2T_r{}^2]+K_IK_P[4K_{EV}{}^2R^2\alpha_1^2\beta^2(T_cT_g{}^2T_r{}^2+T_c{}^2T_gT_r{}^2$$
$$+T_c{}^2T_g{}^2T_r)+8K_{EV}{}^2R^2T_{12}\alpha_1^2\beta\pi T_c{}^2T_g{}^2T_r{}^2];$$

$$r_6 = K_P{}^2[K_{EV}{}^2R^2\alpha_1^2\beta^2(2T_cT_g{}^2+2T_c{}^2T_g+2T_cT_r{}^2+2T_c{}^2T_r+2T_gT_r{}^2+2T_g{}^2T_r+8T_cT_gT_r)$$
$$+K_{EV}{}^2R^2T_{12}\alpha_1^2\beta\pi(4T_c{}^2T_g{}^2+4T_c{}^2T_r{}^2+4T_g{}^2T_r{}^2+16T_cT_gT_r{}^2+16T_cT_g{}^2T_r+16T_c{}^2T_gT_r)]$$
$$+K_I{}^2[2K_{EV}{}^2R^2\alpha_1^2\beta^2(T_cT_g{}^2T_r{}^2+T_c{}^2T_gT_r{}^2+T_c{}^2T_g{}^2T_r)+4K_{EV}{}^2R^2T_{12}\alpha_1^2\beta\pi T_c{}^2T_g{}^2T_r{}^2]$$
$$+K_IK_P[K_{EV}{}^2R^2\alpha_1^2\beta^2(2T_c{}^2T_g{}^2+2T_c{}^2T_r{}^2+2T_g{}^2T_r{}^2+8T_cT_gT_r{}^2+8T_cT_g{}^2T_r+8T_c{}^2T_gT_r)$$
$$+16K_{EV}{}^2R^2T_{12}\alpha_1^2\beta\pi(T_cT_g{}^2T_r{}^2+T_c{}^2T_gT_r+T_c{}^2T_g{}^2T_r)];$$

$$r_5 = K_P^{\,2}[K_{EV}^{\,2}R^2\alpha_1^2\beta^2(T_c^{\,2}+T_g^{\,2}+T_r^{\,2}+4T_cT_g+4T_cT_r+4T_gT_r)+K_{EV}^{\,2}R^2T_{12}\alpha_1^2\beta\pi(8T_cT_g^{\,2}$$
$$+8T_c^{\,2}T_g+8T_cT_r^{\,2}+8T_c^{\,2}T_r+8T_gT_r^{\,2}+8T_g^{\,2}T_r+32T_cT_gT_r)]+K_I^{\,2}[K_{EV}^{\,2}R^2\alpha_1^2\beta^2(T_c^{\,2}T_g^{\,2}$$
$$+T_c^{\,2}T_r^{\,2}+T_g^{\,2}T_r^{\,2}+4T_cT_gT_r^{\,2}+4T_cT_g^{\,2}T_r+4T_c^{\,2}T_gT_r)+8K_{EV}^{\,2}R^2T_{12}\alpha_1^2\beta\pi(T_cT_g^{\,2}T_r^{\,2}$$
$$+T_c^{\,2}T_gT_r^{\,2}+T_c^{\,2}T_g^{\,2}T_r)]+K_IK_P[4K_{EV}^{\,2}R^2\alpha_1^2\beta^2(T_cT_g^{\,2}+T_c^{\,2}T_g+T_cT_r^{\,2}+T_c^{\,2}T_r+T_gT_r^{\,2}$$
$$+T_g^{\,2}T_r)+8K_{EV}^{\,2}R^2T_{12}\alpha_1^2\beta\pi(8T_c^{\,2}T_g^{\,2}+8T_c^{\,2}T_r^{\,2}+8T_g^{\,2}T_r^{\,2})+16K_{EV}^{\,2}R^2\alpha_1^2\beta^2T_cT_gT_r$$
$$+32K_{EV}^{\,2}R^2T_{12}\alpha_1^2\beta\pi(T_cT_gT_r^{\,2}+T_cT_g^{\,2}T_r+T_c^{\,2}T_gT_r)];$$

$$r_4 = K_P^{\,2}[2K_{EV}^{\,2}R^2\alpha_1^2\beta^2(T_c+T_g+T_r)+K_{EV}^{\,2}R^2T_{12}\alpha_1^2\beta\pi(4T_c^{\,2}+4T_g^{\,2}+4T_r^{\,2}+16T_cT_g$$
$$+16T_cT_r+16T_gT_r)]+K_I^{\,2}[2K_{EV}^{\,2}R^2\alpha_1^2\beta^2(T_cT_g^{\,2}+T_c^{\,2}T_g+T_cT_r^{\,2}+T_c^{\,2}T_r+T_gT_r^{\,2}+T_g^{\,2}T_r)$$
$$+K_{EV}^{\,2}R^2T_{12}\alpha_1^2\beta\pi(4T_c^{\,2}T_g^{\,2}+4T_c^{\,2}T_r^{\,2}+4T_g^{\,2}T_r^{\,2}+8T_cT_gT_r+16T_cT_gT_r^{\,2}+16T_cT_g^{\,2}T_r$$
$$+16T_c^{\,2}T_gT_r)]+K_IK_P[K_{EV}^{\,2}R^2\alpha_1^2\beta^2(2T_c^{\,2}+2T_g^{\,2}+2T_r^{\,2}+8T_cT_g+8T_cT_r+8T_gT_r)$$
$$+K_{EV}^{\,2}R^2T_{12}\alpha_1^2\beta\pi(16T_cT_g^{\,2}+16T_c^{\,2}T_g+16T_cT_r^{\,2}+16T_c^{\,2}T_r+16T_gT_r^{\,2}+16T_g^{\,2}T_r$$
$$+64T_cT_gT_r)];$$

$$r_3 = K_P^{\,2}[K_{EV}^{\,2}R^2\alpha_1^2\beta^2+8K_{EV}^{\,2}R^2T_{12}\alpha_1^2\beta\pi(T_c+T_g+T_r)+K_I^{\,2}[K_{EV}^{\,2}R^2\alpha_1^2\beta^2(T_c^{\,2}$$
$$+T_g^{\,2}+T_r^{\,2}+4T_cT_g+4T_cT_r+4T_gT_r)+K_{EV}^{\,2}R^2T_{12}\alpha_1^2\beta\pi(8T_cT_g^{\,2}+8T_c^{\,2}T_g+8T_cT_r^{\,2}$$
$$+8T_c^{\,2}T_r+8T_gT_r^{\,2}+8T_g^{\,2}T_r+32T_cT_gT_r)]+K_IK_P[4K_{EV}^{\,2}R^2\alpha_1^2\beta^2(T_c+T_g+T_r)$$
$$+K_{EV}^{\,2}R^2T_{12}\alpha_1^2\beta\pi(8T_c^{\,2}+8T_g^{\,2}+8T_r^{\,2}+32T_cT_g+32T_cT_r+32T_gT_r)];$$

$$r_2 = K_P^{\,2}[4K_{EV}^{\,2}R^2T_{12}\alpha_1^2\beta\pi]+K_I^{\,2}[2K_{EV}^{\,2}R^2\alpha_1^2\beta^2(T_c+T_g+T_r)$$
$$+K_{EV}^{\,2}R^2T_{12}\alpha_1^2\beta\pi(4T_c^{\,2}+4T_g^{\,2}+4T_r^{\,2}+16T_cT_g+16T_cT_r+16T_gT_r)$$
$$+K_IK_P[2K_{EV}^{\,2}R^2\alpha_1^2\beta^2+16K_{EV}^{\,2}R^2T_{12}\alpha_1^2\beta\pi(T_c+T_g+T_r)];$$

$$r_1 = K_I^{\,2}[K_{EV}^{\,2}R^2\alpha_1^2\beta^2+8K_{EV}^{\,2}R^2T_{12}\alpha_1^2\beta\pi(T_c+T_g+T_r)]+K_IK_P[8K_{EV}^{\,2}R^2T_{12}\alpha_1^2\beta\pi];$$

$$r_0 = K_I^{\,2}[4K_{EV}^{\,2}R^2T_{12}\alpha_1^2\beta\pi];$$

CURRICULUM VITAE

Ausnain NAVEED was born on January 22nd, 1989 in Muzaffarabad, Azad Kashmir, Pakistan. He got his early education from Army Public School, Muzaffarabad. Later, he started receiving his secondary education at Cadet College Palandri, Azad Kasmir and secured a distinction in SSC examination of 2005. He completed his higher secondary education from the same college in 2007. Then, he got enrolled in Bahria University Islamabad for his undergraduate studies. He received his B.E. (Electrical) degree from Department of Electrical Engineering, Bahria University Islamabad in year 2012. He then moved on to England for his postgraduate studies where he completed his M.Sc. (Advanced Electrical and Electronic Engineering) from University of Leicester, Leicestershire, UK in year 2014. Subsequently, he joined the faculty of Electrical Engineering in The University of Azad Jammu & Kashmir as lecturer in year 2016. Eventually, he got admission in Graduate School of Natural and Applied Sciences, Department of Electrical and Electronic Engineering at Niğde Ömer Halisdemir University, Niğde, Turkey in September 2016. He pursued his PhD under the supervision of Prof. Dr. Saffet AYASUN. During his PhD thesis research, he worked on delay-dependent stability analysis of load frequency control systems with electric vehicles and robust controller design. He knows English, Urdu, Hindku and Turkish languages.

PUBLICATIONS PRODUCED FROM PhD RESEARCH

Covering the scope of this thesis, 5 (five) international article were published/produced. Additionally, this research work has been presented at 6 (six) international conferences and congresses. The detail is presented below:

Publications in SCI /SCI-E indexed journals

1. Naveed, A., Sönmez, Ş. and Ayasun, S., "Impact of electric vehicle aggregator with communication time delay on stability regions and stability delay margins in load frequency control system", ***In Journal of Modern Power Systems and Clean Energy*** 2020. https://doi.org/ 10.35833/MPCE.2019.000244.

2. Naveed, A., Sönmez, Ş. and Ayasun, S., "Impact of Load Sharing Schemes on the Stability Delay Margins Computed by Rekasius Substitution Method in Load Frequency Control System with Electric Vehicles Aggregator", ***In International Transactions on Electrical Energy Systems*** 2021. https://doi.org/10.1002/2050-7038.12884

3. Naveed, A., Sönmez, Ş. and Ayasun, S., "Impact of Electric Vehicles Aggregators with Communication Delays on Stability Delay Margins of Two-Area Load Frequency Control System", ***In Transactions of the Institute of Measurement and Control*** 2021.

4. Katipoğlu, D., Sönmez, Ş., Ayasun, S., and Naveed, A., "The effect of demand response control on stability delay margins of load frequency control systems with communication time delays", ***In Turkish Journal of Electrical Engineering & Computer Sciences*** 2020. https://doi.org/ 10.3906/elk-2006-165.

Publication in peer reviewed journal other than SCI /SCI-E indexed journals

1. Naveed, A., Sönmez, Ş. and Ayasun, S., "Determination of Stability Margins in Single Area Load Frequency Control System having Incommensurate Communication Delays due to Plug-in Electric Vehicles", ***Eurasian Journal of Science Engineering and Technology*** 1(1), 11-19, 2020.

Work presented in International Conferences and Congresses

1. Naveed, A., Sönmez, Ş. and Ayasun, S., "Stability regions in the parameter space of PI controller for LFC system with EVs aggregator and incommensurate time delays", ***2019 IEEE 1st Global Power, Energy and Communication Conference (GPECOM)***, Nevsehir, Turkey, s. 461-466, 12-15 June, 2019.

2. Naveed, A., Sönmez, Ş. and Ayasun, S., "Stability Analysis of a Single-Area Load Frequency Control System with Electric Vehicles Group and Communication Time Delays", ***In Proceedings of International Turkic World Congress on Science and Engineering (UTUFEM)***, Niğde, Turkey, s. 897-905, 17-18 June, 2019.

3. Naveed, A., Sönmez, Ş. and Ayasun, S., "Identification of Stability Delay Margin for Load Frequency Control System with Electric Vehicles Aggregator using Rekasius Substitution", ***2019 IEEE Milan PowerTech***, Milan, Italy, s. 1-6, 23-27 June, 2019.

4. Naveed, A., Zerdali, E., Sönmez, Ş. and Ayasun, S., "Optimization of PI Controller Gains using Genetic Algorithm for Time-Delayed Load Frequency Control Systems with Electric Vehicles Aggregator", ***2019 IEEE 11th International Conference on Electrical and Electronics Engineering (ELECO)***, Bursa, Turkey, s. 76-80, 28-30 November 2019.

5. Naveed, A., Sönmez, Ş. and Ayasun, S., "Damping Based Relative Stability Regions in Load Frequency Control System with Plug-in Electric Vehicles and Communication Delays", ***2020 IEEE 2nd Global Power, Energy and***

Communication Conference (GPECOM), Izmir, Turkey, s. 202-207, 20-23 October, 2020.

6. Naveed, A., Katipoğlu, D., Sönmez, Ş. and Ayasun, S., "Delay-dependent stability analysis of a single-area load frequency control system enhanced by electric vehicles aggregator and demand response control", ***In Proceedings of TURK-COSE 2020: 2. International Turkic World Congress on Science and Engineering***, Nur-Sultan (Astana), Kazakhistan, s. 546-554, 14-15 November, 2020.